

**Investigating possible role of a Golgi resident
PtdIns4P effector, an oncogenic homolog
in Golgi size control mechanism**

By

**Prasanna R Iyer
[LIFE09201104017]**

**ACTREC-TATA MEMORIAL CENTRE
Mumbai**

*A thesis submitted to the
Board of Studies in Life Sciences*

*In partial fulfillment of requirements
For the Degree of*

**DOCTOR OF PHILOSOPHY
Of
HOMI BHABHA NATIONAL INSTITUTE**



April, 2019

STATEMENT BY AUTHOR

This dissertation has been submitted in partial fulfillment of requirements for an advanced degree at Homi Bhabha National Institute (HBNI) and is deposited in the Library to be made available to borrowers under rules of the HBNI.

Brief quotations from this dissertation are allowable without special permission, provided that accurate acknowledgement of source is made. Requests for permission for extended quotation from or reproduction of this manuscript in whole or in part may be granted by the Competent Authority of HBNI when in his or her judgment the proposed use of the material is in the interests of scholarship. In all other instances, however, permission must be obtained from the author.

Prasanna R Iyer

DECLARATION

I, hereby declare that the investigation presented in the thesis has been carried out by me. This work is original and has not been submitted earlier as a whole or in part for a degree / diploma at this or any other Institution / University.

Prasanna R Iyer

List of Publications arising from the thesis

Publications from the thesis:

A. Published:

1) **Prasanna Iyer**, Madhura Bhave, Bhawik Kumar Jain, Sudeshna Roy Chowdhury, Dibyendu Bhattacharyya. Vps74p controls Golgi size in Arf1-dependent manner. FEBS Letters. 2018 October. PMID: 30291722. Article DOI: 10.1002/1873-3468.13266

B. To be submitted:

- 1) **Iyer P**, Sutradhar S, Paul R, Bhattacharyya D. A novel combinatorial approach of quantitative microscopy and in silico modeling deciphers arf1 dependent Golgi size regulation.
- 2) **Iyer P**, Bhattacharjee C, Bhattacharyya D. GOLPH3, GOLPH3L, and ARF1 regulate Golgi shape by adjusting the ratio of amounts of tubules and vesicles.

Chapter in books and lectures notes- NIL

Conferences

1. Won **3rd prize** for Poster presentation on topic “ Genome wide screening of yeast mutants of altered organelle Size” in **Global Cancer Genomics Consortium symposium** 2011, held at ACTREC- TMC, India
2. Poster presentation on topic “**Role of PtdIn4P effector- Vps74/ GOLPH3 in Golgi size control mechanism and in Cancer**” in international symposium on Conceptual Advances in Cellular Homeostasis regulated by Proteases and Chaperons 2013, in ACTREC-TMC, India [Poster presentation]
3. Poster presentation on topic Role of “**PtdIn4P effector- Vps74/ GOLPH3 in Golgi size control mechanism**” in **Biophysics Paschim Meet** 2014, ACTREC- TMC, India

4. Presented poster on topic “**Study of PtdIns4P effector- Vps74/GOLPH3 in Golgi size control mechanism**” in International conference **American society of Cell Biology conference (ASCB-2015)** - December 2015, San Diego, U.S.
5. Presented poster on topic “**PtdIns4P effector- Vps74/GOLPH3 affects Golgi size**” in **Optics within Life Science conference (OWLS)** - March 2016, TIFR, Mumbai, India.
6. Won **2nd prize** for Oral presentation on topic “**Does PtdIns4P effector- Vps74/GOLPH3, an oncogene affect Golgi size?**” in **National Research Scholars Meet in Life Science**, ACTREC- TMC, India – December 2016.
7. Presented Poster on topic “**How a Yeast homologue and mammalian oncogene – Vps74/GOLPH3 maintain Golgi size and shape?**” in International conference of Cell biology (ICCB) held at CCMB, Hyderabad – January 2018

Participation in Workshops:

- ∞ Attended Cancer Informatics Workshop, ACTREC-TMC, Mumbai, India in Jan 2013.
- ∞ Attended STED workshop in IISER Pune, India – June 2015.

Other Publications

Published:

- 1) Bhawe M[#], Papanikou E[#], **Iyer P**, Pandya K, Jain BK, Ganguly A, Sharma C, Pawar K, Austin J II, Day KJ, Rossanese OW, Glick BS, Bhattacharyya D. Golgi enlargement in Arf-depleted yeast cells is due to altered dynamics of cisternal maturation. *J Cell Sci.* 2014 Jan 1; 127(Pt 1):250-7. PMID: 24190882

Prasanna R Iyer

*Dedicated
To*

*Amma (Mrs. Uma radhakrishnan Iyer),
Appa (Mr. K. Radhakrishnan Iyer),*

Prasad (Anna),

My beloved Late. Tatappa & Late. Ammamma

Acknowledgment

Undertaking this Ph.D. has been a truly life-changing experience for me and it would not have been possible to do without the support and guidance that I received from many people. I would like to express my sincere gratitude to all of them. I would like to first say a very big thank you to my supervisor Dr. Dibyendu Bhattacharyya for introducing me to one of the wonderful work lines in membrane trafficking in Golgi. He has tried to make available all the upcoming advances in microscopy and trained not only me but also the entire lab fellows at his own best level. His enthusiasm for doing science has always envisioned me to be a good researcher. I promise to be one of the good researchers in the future. I have learned a lot in my Ph.D. degree because of the freedom he gave me to learn in my own way. Thank you for supporting and helping me throughout.

I am thankful to Dr. S. V. Chiplunkar (Director, ACTREC), Dr. Rajiv Sarin (Ex-Director, ACTREC) and Dr. Surekha Zingde (Ex-Deputy Director, ACTREC) for the academic support and the facilities provided to carry out the research work at the Institute. I sincerely thank Dr. S.V. Chiplunkar to provide financial support through the Institute for a period of 3 months to cover up my expenses after I underwent my ACL surgery. I gratefully acknowledge the funding received towards my Ph.D. through ACTREC-DAE, India. I am thankful to TMC for funding my project. My sincere thanks to the funding agencies, Sam-mystery, and HBNI for sponsoring international travel; hence I could present my work at an international conference.

I am grateful to all my Doctoral committee Chairpersons Dr. Rita Mulherkar (Ex-Chairperson), Dr. Milind Vaidya (Ex-Chairperson), Dr. V. Prasanna (Chairperson) and members Dr. Sanjay Gupta, Dr. Sorab N Dalal and Late Dr. Rajiv Kalaraiya for serving as my committee members

even at hardship. I thank all of you for their encouragement, insightful comments, and hard questions. It incited me to widen my research from various perspectives.

I greatly appreciate the support received from the collaborative work under the guidance of Dr. Raja Paul at Indian Association for the Cultivation of Science (IACS), Kolkata. Thank you to Raja Sir, for the training provided to learn C-language. On each day of my training, I was made to write new codes as per the levels of modulation required. I really enjoyed working with him. I really started thinking to work in inter-disciplinary sciences due to the training acquired in Paul Lab.

I thank all the Bhattacharyya lab members (Diblets). I thank Mansi to procure all the requirements in the lab via indenting and other administrative procedures involved. I thank the lab technician Sanjay dada to help us and provide all the glass wares and miscellaneous required for carrying out the daily experiments. I thank my fellow labmates Dr. Madhura Bhave, Dr. Abira Ganguly, Kaushal, Bhawik, Ketakee, Dr. Chumki Bhattacharjee, Pravin, Sudeshna, Naini, Shreosi and Roma for the brainstorming discussions, for the sleepless nights we were working together before deadlines, and for all the fun we have had. It was great sharing laboratory with all of you. Thanks for all your encouragement and financial help provided at the time of crisis. I would like to thank my trainee Rashmi Varghese.

I would like to thank following institute staff: Dandekar Sir, Vaishali, Tanuja, Shyamal, Aruna, Seema, Maya, Chitra, Prema for their unfailing support and assistance.

I thank the Institute to provide medical assistance through BARC, due to which I could undergo my ACL surgery in the terminal year of my Ph.D. tenure. I thank orthopedic surgeon, Dr. Nandan Kamath. I thank the Physiotherapist Dr. Shruti and Dr. Krishna Kumar for the corrective

treatment given on time to enable the full range of my knee movement. It was indeed a painful process to provide flexibility to new graft implanted. Thank you for all the kindness and cooperation. I also thank the TMH patient bus driver John to shuttle me to BARC and back to ACTREC during my physiotherapy sessions.

I extend my thanks to Dr. Rupa Mishra, Rajashree, Dr. Pratik Chaudhary, Dr. Richa Tiwari, Saim, Asmita, Dr. Sonali Vishal for helping and training me in new experiments carried out which were not my forte. I thank my friends Dr. Rubina Shaikh, Renam, Anupama, Dr. Rasika Hudlikar and Venkatesh for the fun times we shared. I thank my best friends Rasika Hudlikar, Swati Pandey and Sumedha Korgaonkar to be during all the thick and thin times. I thank my entire Ph.D. batch 2011. I thank the ACTREC student community for their support in either organizing any scientific event or towards any other sort of scientific help. Throughout my tough and tight schedule of Doctoral research, two activities that had always eased my journey is Swimming and Cycling. I thank YMCA - Learn to swim training sessions and also my friend Rasika to teach me cycling. Thank you, Dr. Lumbini Yadav to lend your cycle to learn cycling.

A special thanks to Amma, Appa, late grandparents (Tattappa & Ammamma), Prasad (brother) and Shubangi (sister-in-law) for all the sacrifices that you have made on my behalf. Your prayer for me was what sustained me thus far. I would also like to thank all of my relatives, friends, and cousins who supported and incited me to strive towards my goal.

Above all, I owe it all to Almighty God for granting me the wisdom, health, and strength to undertake this research task and enabling me to its completion.

Table of contents	
Synopsis	1
List of Figures	18
List of Table	25
Abbreviation	26
Chapter 1 - Introduction	
1.1: Background of the work	33
1.2: Layout of the thesis	33
Chapter 2- Review of Literature	
2.1 Cell and its organelle	36
2.2 Organelle size matters	36
2.3 The mechanisms that control the organelle size	37
2.4 Organelle size study and its application	37
2.5 The early secretory pathway and its associated components	38
2.5.1- Endoplasmic Reticulum – ER	38
2.5.2- COPI	39
2.5.3- COPII	40
2.5.4- Golgi	42
A) Functions of Golgi:	42
B) Morphology of Golgi:	42
C) Model system of Golgi:	43
D) Alteration in Golgi size	46
2.5.5- Functionally same but differs in organization:	47
A) Yeast Golgi	47
B) Mammalian Golgi	48
2.5.6- Significance of stacked ribbon-shaped Golgi over unstacked Golgi	49

2.6 Different Golgi markers	50
A) Gea2	50
B) Vrg4	50
C) Rer1	51
D) Sec7	51
2.7 Proteins/Lipids maintain membrane shape and help in bending	51
2.8 Function of PtdIns4P at the Golgi:	55
2.9 GOLPH3 (Golgi associated phosphoprotein-3)	56
2.10 Vps74	58
2.11 Function of Vps74 and GOLPH3	60
2.12 Functional similarity and difference of Vps74, GOLPH3, and GOLPH3L proteins	61
2.13 Golgi size and its regulation	64
2.14 Golgi size regulation is important	65
Chapter 3- Aims & Objectives	
3.1: Statement of the problem:	68
3.2: Hypothesis:	68
3.3: Objectives:	69
3.3.1: Detailed Objectives:	69
3.4: Work done	69
Chapter 4- Materials & Method	
4.1: Molecular cloning and bacterial culture	72
4.1.1: Preparation of ultra-competent E. coli	72
4.1.2.: Preparation of competent DCM-DAM- cells:	73
4.1.3: Bacterial Transformation	74
4.1.4: Plasmid DNA isolation	74
4.1.4.1: QIAprep Spin Miniprep method	74
4.1.4.2: Plasmid DNA isolation using TELT buffer	75

4.1.4.3: Plasmid DNA isolation by Cesium Chloride (CsCl) equilibrium density gradient centrifugation:	76
4.1.5: Agarose gel electrophoresis	77
4.1.6: Polymerase chain reaction (PCR)	78
4.1.7: Quick change mutagenesis	80
4.1.8: Gene Cloning	82
4.1.8.1: Restriction Digestion	82
4.1.8.2: Purification of restriction digested DNA or PCR product	83
4.1.8.3: Purification of DNA fragments from agarose gel	84
4.1.8.4: Ligation reaction	85
4.1.8.5: Screening of recombinant bacterial clones	86
4.2: Basic Yeast Techniques	87
4.2.1: Retrieving strains from the yeast collection	87
4.2.2: Growing yeast log phase culture	88
4.2.3: Freezing Yeast	88
4.2.4: Yeast transformation	89
4.2.5: Replica plating for screening transformants	90
4.2.6: Genomic DNA isolation	91
4.2.7: Checking fluorescence signal in upright microscope for screening	91
4.2.8: Manipulating Yeast Genome	92
4.2.9: PCR based gene deletion strategy	92
4.2.10: 5-FOA plates for popping out URA based plasmid	93
4.2.11.: Removal of Kanamycin cassette from deletion strain by Cre induction	94
4.2.12: Yeast Live Cell Imaging	95
4.2.13: Microscopy setting for Yeast culture	95
4.2.14.: Image analysis	96
4.2.15.: Quantitative analysis of maturation parameters	97
4.2.16.: Colocalization analysis	97
4.2.17.: Statistical measurement	97
4.3: Mathematical simulation:	98
4.3.1.: Assumptions for in-silico cell:	98
4.3.2.: K_{early} and K_{late} rate determines resident protein density:	98

4.3.3.: Random force calculation between vesicles	99
4.3.4.: Density of proteins in newly emerged cisterna	100
4.3.5.: Input parameters value range adjustment	101
4.3.6.: 4D imaging for velocity calculation	102
4.3.7.: Cisterna velocity calculation <i>in vivo</i>	103
4.4: Mammalian Cell Culture Techniques	103
4.4.1. Daily Observations of Cell Culture of following	103
4.4.2: Reviving Cells from Frozen Stock	104
4.4.3: Cell passaging	105
4.4.4: Freezing of cell line	106
4.4.5: Transfection of DNA in different cell lines	107
4.4.6. Kill curve for puromycin selection	107
4.4.7.: Stable clone preparation	108
4.4.8.: G-DNA preparation of mammalian cell line	109
4.4.9.: T7 micronuclease assay:	109
4.4.10: Mammalian Live Cell Imaging	111
4.4.11: Microscopy settings for mammalian cell line	111
Chapter 5-Study regulation of Golgi cisterna size by VPS74 in budding yeast <i>S. cerevisiae</i>	
5.1: Introduction	113
5.2: Results	116
5.2.1 Development of fluorescently tagged - Ras2p, Vps74p and Rer1p	116
A) Development of membrane marker mCherry- Ras2:	117
B) Fluorescent labeling of Vps74p	118
C) Cloning of 3X-iGFP Rer1	119
5.2.2 Homotypic fusion frequency based on temporal scale of maturation	119
5.2.3: Deletion and/or over expression of gene <i>VPS74</i> and <i>ARF1</i> and its effect on Golgi size	123

A) Knock out of <i>VPS74</i> gene	123
B) Cloning to over express <i>VPS74</i> :	129
C) <i>VPS74</i> interacts with protein ARF1 and COPI	130
D) Double knock out <i>ARF1</i> and <i>VPS74</i>	132
E) Effect of over expression of <i>Arf1p</i> in <i>vps74</i> null mutant	134
F) Effect of over expression of <i>Vps74p</i> in <i>arf1</i> null mutant	135
G) <i>Arf1p</i> over expression in WT does not alter Golgi cisterna size	137
H) <i>Vps74</i> over expression in WT alters late Golgi cisterna size	138
I) Over expression of <i>Arf1p</i> and <i>Vps74p</i> in wild type dual color strain <i>Rer1-Sec7</i>	140
5.2.4: How the cisterna maturation parameters differ for WT, null mutants and overexpressing strain?	142
5.2.5: <i>ARF1</i> deletion can alter the <i>Vps74</i> gradient	144
5.2.6: PI4P gradient is disturbed in Golgi compartments of <i>vps74</i> and <i>arf1</i> null mutants	146
5.2.7: Effect of <i>pik1^{ts}</i> mutation on Golgi cisterna	150
5.3: Discussion	151
Chapter 6- Study Golgi size regulation in budding yeast <i>S. cerevisia</i> by Mathematical simulation	
6.1: Introduction:	159
6.1.1 Rationale for the in-silico study	161
6.2: Results	165
6.2.1 The cisterna volume is conserved before and after fusion	165
6.2.2 Tuning of parameters	166
6.2.2A. The rates K_{early} and K_{late} parameter studied with respect to Golgi vesicle size and number	167
6.2.2B. The parameter $Size_{denovo}$ and K_{denovo} studied with respect to Golgi	168

vesicle size and number	
6.2.3 Magnitude of force exerted is tuned to match velocity of cisterna	171
6.2.4 Tabulation of parameters for simulating different strains	173
6.2.5 Rationale for parameters values used in different strains	174
6.2.6 Comparative plot for experiment and simulation	176
6.3: Discussion	181
Chapter 7- CRISPR mediated gene knock out in mammalian cells	
7.1: Introduction	185
7.2: Results	187
7.2.1 Transient knock out of GOLPH3, GOLPH3L and ARF1	187
7.2.2 Stable clone development for ARF1, GOLPH3 and GOLPH3L knock out	189
7.2.3 Sequence analysis of knock out clones	190
7.2.4: T7 endonuclease test	192
7.2.5 Quantitative measure of the Golgi morphology changes in the stable GOLPH3L KO	195
7.3: Discussion	196
Chapter 8-Summary	
Chapter 9- Bibliography	
Chapter 10- Appendix	
Appendix 10.1: Cloning strategy for mCherry- Ras2	212
Appendix 10.2: Cloning strategy for 3X-iGFP Vps74	216
Appendix 10.3: Cloning strategy for 3X-iGFP Rer1	219
Appendix 10.4: Cloning strategy for YEplac195 Vps74:	221
Appendix 10.5: Making gene disruption cassette for deleting Vps74 gene:	223
Appendix 10.6: Making gene disruption cassette for deleting 67-345 region of Vps74 gene	225
Appendix 10.7: Annealing of complementary oligonucleotide guide sequence	226

Appendix 10.8: Ligation reaction of inserting guide sequence with CRISPR vector	227
Appendix 10.9: PCR for checking integration of guide sequence in CRISPR vector	228
Publication	232

**Homi Bhabha National Institute****Ph.D. PROGRAMME**

- 1. Name of the Student:** Ms. Prasanna R Iyer
- 2. Name of the Constituent Institution:** TMC-ACTREC
- 3. Enrolment No.:** LIFE09201104017
- 4. Title of the Thesis:** “Investigating possible role of a Golgi resident PtdIns4P effector, an oncogenic homolog in Golgi size control mechanism”
- 5. Board of Studies:** Life Sciences

SYNOPSIS**1. Introduction:**

The cell presumably has the machinery to sense and maintain intracellular objects ranging from macromolecules to organelles [1]. We are interested to know the mechanism that controls and maintains the size and shape of intracellular organelles, such as Golgi apparatus, the dynamic organelle essential for protein sorting and transport. Cargo from the ER exit sites (ERES) traverses the stack from the ‘cis’ cisternae to the ‘trans’ cisternae. Golgi has varying cisterna number in different species; for example, budding yeast *Pichia pastoris* has 3-5 stack cisterna, protist *Euglena* has twenty-seven. There is variation in cisterna number and also size. Within species, the size and shape of Golgi apparatus change during different differentiation stages or

pathological conditions. Golgi Enlargement is reported during viral infections and some cancers. This observation implies to understand the Golgi size regulation and characterize the genes involved to maintain it. The Golgi apparatus occupies a central position in the secretory pathway, playing defined roles in glycoprotein maturation and the sorting of proteins into vesicles for exocytosis or delivery to the endomembrane system. However, very minimal interface with cancer biology so far has been discovered for this well-known organelle. A genome-wide copy number analyses [2] of human cancers identified a frequent 5p13 amplification in several solid tumor types, including lung (56%), ovarian (38%), breast (32%), prostate (37%) and melanoma (32%). A Golgi associated protein, GOLPH3 a potent oncogene is validated as a target of 5p13 amplification. GOLPH3 is an effector of phosphatidylinositol 4-phosphate (PtdIns4P), a predominant phospholipid of Golgi. Phosphatidylinositol 4-kinases (PI4Ks) regulate vesicle-mediated export from the Golgi apparatus via PtdIns4P binding effector proteins that control budding vesicle reactions and regulate membrane dynamics [3]. It monitors network that ensures an appropriate membrane composition established before a transport vesicle buds from the Golgi. The effectors orchestrate membrane transformation events facilitating vesicle formation and targeting [3]. GOLPH3 knockdown alters the Golgi morphology and blocks the anterograde transport [4]. GOLPH3 regulates cell-cell interaction and hence plays a role in metastasis [5]. GOLPH3 is overexpressed in many human tumors [2, 6]. GOLPH3 has been implicated in Golgi size control, but that is not corroborated in the yeast system. The yeast homolog *VPS74* act as an adaptor linking certain Golgi associated glycosyltransferases to COPI vesicles thereby mediating their retrograde transport[7, 8]. Role of yeast

homolog *VPS74* in Golgi size regulation is not elucidated. However, GOLPH3 can partially substitute for Vps74 when expressed in yeast, so it is possible that Vps74 and GOLPH3 serve a similar, as yet unidentified function. It is therefore essential to study the true nature of the role of Vps74 in maintaining Golgi size. Study of GOLPH3 in cisterna maturation is difficult with mammalian cells due to stacked ribbon-shaped Golgi. The dispersed Golgi phenotype of *S.cerevisiae* allows the characterization of Vps74 in cisterna maturation and kinetics.

2. Objectives:

I] Investigation of possible role in Golgi size by functional characterization of *VPS74*, an oncogene homologue and Golgi resident PtdIns4P effector molecule.

II] Investigation of possible role in Golgi size by Mathematical simulation.

3. Work Plan:

I] Investigation of possible role in Golgi size by functional characterization of *VPS74*, an oncogene homologue and Golgi resident PtdIns4P effector molecule.

A. Development of cell membrane marker to measure cell size and volume.

B. Study the role of Vps74 and its interactome protein on Golgi size control mechanism.

C. CRISPR mediated knock out of GOLPH3 (mammalian homolog of Vps74), GOLPH3L and ARF1.

II] Investigation of possible role in Golgi size by Mathematical simulation.

A. Development of coarse grain simulation model for the Golgi system of *S.cerevisiae*.

B. zOptimization of four parameters $Size_{denovo}$, K_{denovo} , K_{early} , and K_{late} .

4. Results:

I] Investigation of possible role in Golgi size by functional characterization of *VPS74*, an oncogene homologue, and Golgi resident PtdIns4P effector molecule:-

A. Development of cell membrane marker to measure cell size and volume:-

Golgi cisternae were labeled with Sec7 6X GFP. This epitope tagging enabled the calculation of the average volume of Golgi cisternae in various mutants. It has been seen that organelle size changes with respect to cell size. So for a better comparison, it is necessary to compare any organelle volume change with respect to cell volume. Ras2 was used to label the cell membrane in yeast *S.cerevisiae* [9, 10]. Ras2p was epitope tagged with mCherry at N-terminus to make a fluorescent fusion mCherry-Ras2 protein. This fusion protein was cloned under strong promoter TPI (Triose phosphate isomerase). The final plasmid YIPlac204-T_C mCherry-Ras2 was integrated into endogenous tryptophan locus in all organelle size mutants (Golgi or nucleus associated) to measure cell volume change with respect to alteration in the organelle studied in the lab.

B. Study the role of *VPS74* and its interactome protein on Golgi size control mechanism:-

Deletion of *VPS74* gene: - Endogenous *VPS74* was replaced with Kan- Max cassette by classical knockdown strategy [11, 12] to verify the effect on Golgi size. Yeast cell

with the desired deletion was confirmed by replica plating on YPD and YPD-G418 plates simultaneously. Further, PCR confirmed the gene deletion. Using this strategy *VPS74* is deleted in two-color maturation wild-type strain JK9 GFP-Vrg4 (cis) Sec7 Ds-Red (trans). The dispersed Golgi cisterna of *S.cerevisiae* will enable to monitor the effect of *VPS74* deletion on cisternae maturation kinetics. *VPS74* deletion has increased the Sec7 or trans cisternal volume by twice the amount observed in wild-type. *VPS74* deletion affected the GFP-Vrg4 (early cisterna protein) localization. It seems on *VPS74* deletion Vrg4 protein (cis marker) aggregates together and gives a phenotype very different than that seen in wild-type. To know the effect of *VPS74* deletion on early cisterna, gene deletion was carried out in another two-color wild-type strain with Rer1 3X GFP as an early marker and Sec7 Ds-Red as a late marker. The average diameter and volume of late cisterna had increased, while alteration of early cisterna (marked with Rer1 3X GFP) average volume and diameter was not observed. The fluorescent signal of Rer1 3X GFP was weak for live cell imaging, and to calculate maturation parameters. Hence we chose another early marker Gea2. Maturation of Gea2 cisterna to the early compartment containing Vrg4 was demonstrated, and it validates Gea2 as an early marker. The fluorescent signal of Gea2 3X- GFP was stable. *VPS74* deletion was carried out in Gea2- Sec7 two-color system, and it also showed effect only on late cisterna (Sec7) size. There is a significant reduction in the number of late cisternae. Persistence time of early and late cisterna did not alter in the *vps74* null mutant. However, the parameter, maturation frequency (rate of conversion of early to late cisterna) and homotypic late cisterna fusion event also increased.

Role of Vps74 interacting protein on Golgi size control: - *VPS74* has domain 67-345 region interacting with Arf1 and arginine residue at 6-8 position interacts with COPI [13]. We overexpressed the mutant form of Vps74 protein with alanine residues at position 6-8 in *vps74* null mutant to interrupt the interaction of Vps74 with COPI. It showed a partial reduction in the volume of late cisterna. However, the enlarged Golgi phenotype existed. The Arf1 interacting domain of Vps74, region 67-345 was deleted and replaced with Ura cassette in the dual epitope tag strain Gea2-Sec7. The late cisterna showed an increase in volume and diameter after the deletion of Arf1 interacting region of Vps74. It is evident that amongst the two interacting partners, Arf1 interacting region is more prominent in changing Golgi size. *ARF1* deletion alters cisterna maturation kinetics is reported [14].

Null mutants of *arf1* or *vps74* alter cisterna size. Arf1 has a role in recruiting COPI coat to trans Golgi, while for sorting certain COPI associated Golgi resident proteins Vps74 is required. It led us to find the cumulative function of Arf1 and Vps74 proteins in regulating Golgi cisterna size and maturation. Double knock out of *VPS74* and *ARF1* gene caused two-fold increased late Golgi volume compared to *vps74* null mutant. We overexpressed Vps74 in the $\Delta arf1$ and Arf1 in the $\Delta vps74$ and monitored the effect on Golgi size. *VPS74* overexpression in *arf1* deletion strain did not rescue the Golgi phenotype to the wild-type. However, *ARF1* overexpression in *vps74* deletion strain rescued the enlarged Golgi phenotype to wild-type.

Simultaneously it was essential to know the effect of overexpression of either Arf1 or Vps74 in the wild-type strain. *ARF1* overexpression in wild-type did not affect

the Golgi size, probably might be there is a saturation level of the protein to be functional. However, *VPS74* overexpression in wild-type caused a slight decrease in the trans-Golgi cisterna volume and size. There was a 25% reduction in volume compared to WT. Since Vps74 is involved in budding reaction from trans cisterna [7], we hypothesized that deletion of the gene reduces the vesicle budding mechanism leading to increased Golgi volume. Overexpression of *VPS74* might enhance the budding vesicle reaction causing a reduction in Golgi volume.

We have shown Vps74 is a downstream effector of Arf1 because *ARF1* deletion altered the distribution of Vps74. We have also demonstrated a deletion of either *ARF1* or *VPS74* can change the PI4P gradient across the Golgi compartment.

Vps74 distribution is higher towards early cisterna while lower towards late cisterna [7]. We have demonstrated that in the absence of Arf1, Vps74 prominently colocalize with late cisterna Sec7. Thereby, it verifies Vps74 is an effector of Arf1 and regulates Golgi cisterna size in Arf1 dependent manner. Golgi pool of PI4P has a gradient opposite to Vps74. We have demonstrated the colocalization of PI4P along the Golgi compartment in case of $\Delta arf1$ or $\Delta vps74$ mutants. Average Pearson's coefficient of PI4P increases with late cisterna Sec7 while it slightly decreases with early cisterna Gea2 in null mutants of *arf1* or *vps74*. Along with alteration of cisterna size and maturation parameters in null mutants we have also shown the change of the gradient of PI4P. Arf1 overexpression can rescue the enlarged phenotype of $\Delta vps74$, also implies the function of Vps74 in Golgi size regulation is Arf1 dependent.

Pik1 kinase maintains PI4P levels in Golgi. The *pik1^{ts}* mutation affects secretion and Golgi integrity [15, 16]. We have shown that the conditional mutation of *pik1-83^{ts}* in non-permissive condition alters the early cisterna Vrg4 while there is no such prominent alteration in the Sec7 cisterna.

C. CRISPR mediated knock out of GOLPH3 (mammalian homolog of Vps74), GOLPH3L and ARF1: -

Golgi in the mammalian cell is stacked and ribbon-shaped perinuclear in position. We carried out CRISPR/Cas9 knock out of genes GOLPH3, GOLPH3L and ARF1 [17-20]. We designed guide sequence such that the Cas9 targets an initial region of Exon 1 of these genes. Though all cell types constitutively express GOLPH3 and ARF1, GOLPH3L is expressed only in the secretive type of cells [21]. U2-OS cell line expresses GOLPH3L. Hence we used this cell line to knock out these three genes individually. We transfected CRISPR BFP vectors targeting guide sequence along with Golgi marker GalNacT2-GFP post 24 hr seeding and imaging was done post 48 hr transfection. In the case of GOLPH3 KO, we observed the Golgi has become compact while in the case of GOLPH3L and ARF1 KO the Golgi became dispersed. However, we could not sort the monoclonal population of knock out positive cells. Few transfection-positive cells showed normal ribbon-shaped Golgi. We made CRISPR based stable knock out clones using puromycin selection.

Stable Knock out clone: - Cloned guide sequence in another CRISPR vector PX459-Puro. We could make a stable clone knock out for GOLPH3L and ARF1. Isolated Genomic DNA for these clones, and the gene was sequenced. T7 endonuclease

treatment confirmed the mutation in the exon region of the knock out strains. All cells showed dispersed Golgi phenotype. We calculated total Golgi volume and no. of fragmented Golgi surfaces. There is a significant increase in the no. of fragmented surfaces in GOLPH3L KO compared to control U2-OS cells. Sequencing and the T7 assay were used to confirm ARF1 KO stable clone. ARF1 KO cells generated by CRISPR/Cas9 method showed fragmented and bulky Golgi compared to control cells. The number of fragmented Golgi surfaces is similar to the U2-OS cells (control). However, the ARF1 KO cells show increased total Golgi volume compared to control cells. Though each different gene KO show dispersed Golgi phenotype, GOLPH3L KO results in an increased number of fragmented Golgi surfaces while ARF1 KO result into increase in total Golgi volume.

II] Investigation of possible role in Golgi size by Mathematical simulation:-

We formulated a simple mathematical, empirical equation, the average number of cisterna is equal to the product of maturation frequency and the persistence time of cisterna [14]. This, however, did not match with our experimental observation. We could not incorporate homotypic fusion frequency in the proposed equation. Hence we resorted developing a mathematical simulation to mimic the cisterna maturation of *S.cerevisiae*. This model will then be further utilized to study the kinetics in different mutants as well.

A. Development of coarse grain simulation model for the Golgi system of *S.cerevisiae*: - Developed a coarse grain model replicating in vivo Golgi apparatus of *S.cerevisiae* considering 50-100nm vesicles emerging from ER. Since membrane

trafficking is a complex mechanism involving many coat proteins, GTPases, SNARE proteins; inclusion of all fine details would complicate the simulation. Hence coarse grain simulation would allow only large scale events. We had tried to implicate the effect of these different proteins in terms of rates [22]. An ellipsoidal volume of the unbudded cell with an origin (0,0,0) along x,y, z-axes contains spherical Golgi cisterna, and placed $1\mu\text{m}$ radii nucleus randomly. A repulsive force considered prevents the fall back of Golgi cisterna outside the cell. The density of early proteins marked by rate $K_{\text{early}}=1$ makes the cisterna cis/early, while the $K_{\text{late}}=1$ scores the cisterna as trans/late. Considered homotypic fusion among similar nature of cisterna. Golgi vesicles move intermittently with random force (F_{random}). Assumed a repulsive potential ($F_{\text{repulsion}}$) between late and early cisterna preventing their fusion. Matched this random force with the velocity of cisterna obtained in experimental data. Considered volume conservation during fusion is validated in experiments.

B. Optimization of four parameters $\text{Size}_{\text{denovo}}$, K_{denovo} , K_{early} , and K_{late} : - We have considered four settings to tune our *insilico* model. Golgi vesicles which are attaining average size $\text{Size}_{\text{denovo}}$ exit with rate K_{denovo} from ER exit sites and are distributed randomly throughout the cytoplasm. K_{early} and K_{late} are the rates at which early or late Golgi resident proteins decay or accumulate respectively. This rate in turn also monitors the persistence time of cisterna, thereby indirectly affecting maturation dynamics. Initially for an early cisterna $K_{\text{early}}=1$ and $K_{\text{late}}=0$, gradually when the cisterna matures as late, K_{early} value tends to 0 due to the biochemical process [23] while K_{late} value increases and becomes 1. The values for these parameters varied for different strains as per the role of genes known. We did mathematical simulation for the *arf1* null mutant.

Based on the assumptions for the four parameters the model was run for 15 minutes to attain stable state and then simulated for 30 minutes to collect data for maturation parameters like cisterna number and size, persistence time, maturation frequency and homotypic fusion frequency. In sync with experimental data, we have counted vesicles only above 250nm and recorded the model data after every 4 seconds. Our *in silico* prediction corroborated well with the experimental results when homotypic fusion was accounted. The experiment and *insilico* data for few parameters varied, but their respective change in simulation and experimental values were similar.

5. Summary and Conclusion:

This study has demonstrated the role of *VPS74*, a yeast homolog of mammalian oncogene *GOLPH3* on trans Golgi size and other cisterna maturation parameters. We could also study the role of *Vps74* on Golgi maturation dynamics. *Arf1* alters Golgi size by changing cisterna maturation was previously reviewed [14]. We showed *Arf1* overexpression in Wild-type did not alter the Golgi Size. However, *Arf1* overexpression in *vps74* null background rescued the enlarged Golgi phenotype to the wild-type. Clathrin adaptor recruitment on TGN is *Arf1* and PI4P dependent process. *Arf1* required for clathrin coat assembly from the TGN membrane is PI4P dependent process [24-29]. Assembly of clathrin adaptors in $\Delta arf1$ was delayed [26]. Probably *Arf1* overexpression in $\Delta vps74$ might have increased this process of clathrin-associated budding dynamics which in turn may rescue the large late cisterna size phenotype of $\Delta vps74$. Thus *VPS74* regulates Golgi cisterna size in an *ARF1* dependent manner. However, fewer and larger Golgi cisternae observed in $\Delta arf1$ phenotype is dominant [14, 30] and probably for that

reason overexpression of Vps74 in $\Delta arf1$ fails to rescue $\Delta arf1$ phenotype. Vps74 overexpression in wild-type caused a slight reduction in the late cisterna size. We hypothesize absence of *VPS74* might cause a reduced budding reaction leading to increased late cisterna size while overexpressing Vps74 in WT cause increased vesicle budding reaction leading to a slight reduction in late cisterna size. We have demonstrated Arf1, and Vps74 are mechanistically linked to monitor other maturation kinetics and thereby affect the Golgi cisterna size. *ARF1* deletion alters cisterna size, by increasing the persistence time and homotypic fusion frequency of early cisterna, and reduces the maturation frequency. While *VPS74* deletion increases maturation frequency, providing late cisterna available for homotypic fusion and the increased late cisterna fusion frequency has resulted in increased late cisterna size. In the absence of *ARF1*, overexpression of *VPS74* is not sufficient to rescue the enlarged phenotype. *ARF1* or *VPS74* overexpression in WT alters the cisterna persistence time. We, therefore, hypothesize that Arf1 and Vps74 are two sides of the same coin to change cisterna size. Vps74 might act as a switch for maturation event while Arf1 tightly regulate the persistence time of cisterna and indirectly modify maturation event. *VPS74* regulation of maturation kinetics and cisterna size is an *ARF1* dependent phenomenon.

We have also shown Vps74 gradient is altered in the absence of Arf1 and they colocalize more with late cisterna Sec7. Thus Vps74 is a downstream effector of Arf1. In null mutant of *arf1* or *vps74*, the gradient of PI4P is altered along the Golgi compartment. In the null mutants, PI4P colocalizes more prominently to late Golgi compartment Sec7 while it also shows a slight reduction in the association with early cisterna compartment Gea2. In $\Delta vps74$, functional Vps74 is absent for the reported

retrograde transport of COPI coated vesicles along with phospholipid PI4P. While in case of $\Delta arf1$, the delay in the budding of clathrin-coated anterograde transport and the accumulation of effector Vps74 in late Golgi compartment result in increased PI4P in late Golgi compartment Sec7. Thus there is not only size and maturation parameter alteration of Golgi compartment but also disturbance in the gradient of PI4P across the Golgi compartment. Vps74 regulate cisterna size by maintaining PI4P gradient. Pik1 maintains PI4P gradient at trans while it is dephosphorylated by Vps74-Sac1 complex at early cisterna. Uncomplexed Vps74 mediates PI4P recruitment to COPI vesicle. The balance of complexed (with Sac1) and uncomplexed form of Vps74 maintains the PI4P gradient and thereby affect the retrograde fission.

In the case of the mammalian system using CRISPR/Cas9 technology, we showed ARF1 or GOLPH3L KO resulted in dispersed Golgi phenotype and altered the 3D measured parameters in their specific way. ARF1 KO causes scattered and bulky Golgi affecting total Golgi volume, while GOLPH3L KO caused increased fragmented Golgi surfaces.

We did *insilico* simulation for wild-type strain and $\Delta arf1$ with markers GFP-Vrg4 and Sec7 -6X DsRed. We demonstrated a match of experimental and *insilico* obtained cisterna maturation parameters for WT and $\Delta arf1$. This prediction model could be used in the future to further develop *insilico* workflow for other null mutants and overexpressing strains. It would be used as a classic kinetic study of genes associated with the transport block from ER-Cis, intra- Golgi and Golgi-endosomes.

6. References

1. Marshall, W., *Size control in dynamic organelles*. Trends Cell Biol, 2002. **12**(9): p. 414-9.
2. Scott, K.L., et al., *GOLPH3 modulates mTOR signalling and rapamycin sensitivity in cancer*. Nature, 2009. **459**(7250): p. 1085-90.
3. Graham, T.R. and C.G. Burd, *Coordination of Golgi functions by phosphatidylinositol 4-kinases*. Trends Cell Biol, 2011. **21**(2): p. 113-21.
4. Dippold, H.C., et al., *GOLPH3 bridges phosphatidylinositol-4-phosphate and actomyosin to stretch and shape the Golgi to promote budding*. Cell, 2009. **139**(2): p. 337-51.
5. Ali, M.F., et al., *Golgi phosphoprotein 3 determines cell binding properties under dynamic flow by controlling Golgi localization of core 2 N-acetylglucosaminyltransferase 1*. J Biol Chem, 2012. **287**(47): p. 39564-77.
6. Abraham, R.T., *GOLPH3 links the Golgi network to mTOR signaling and human cancer*. Pigment Cell Melanoma Res, 2009. **22**(4): p. 378-9.
7. Wood, C.S., et al., *PtdIns4P recognition by Vps74/GOLPH3 links PtdIns 4-kinase signaling to retrograde Golgi trafficking*. J Cell Biol, 2009. **187**(7): p. 967-75.
8. Tu, L., et al., *Signal-mediated dynamic retention of glycosyltransferases in the Golgi*. Science, 2008. **321**(5887): p. 404-7.
9. Shaner, N.C., et al., *Improved monomeric red, orange and yellow fluorescent proteins derived from Discosoma sp. red fluorescent protein*. Nat Biotechnol, 2004. **22**(12): p. 1567-72.
10. Losev, E., et al., *Golgi maturation visualized in living yeast*. Nature, 2006. **441**(7096): p. 1002-6.
11. Guldener, U., et al., *A new efficient gene disruption cassette for repeated use in budding yeast*. Nucleic Acids Res, 1996. **24**(13): p. 2519-24.
12. Gueldener, U., et al., *A second set of loxP marker cassettes for Cre-mediated multiple gene knockouts in budding yeast*. Nucleic Acids Res, 2002. **30**(6): p. e23.
13. Tu, L., L. Chen, and D.K. Banfield, *A conserved N-terminal arginine-motif in GOLPH3-family proteins mediates binding to coatomer*. Traffic, 2012. **13**(11): p. 1496-507.
14. Bhave, M., et al., *Golgi enlargement in Arf-depleted yeast cells is due to altered dynamics of cisternal maturation*. J Cell Sci, 2014. **127**(Pt 1): p. 250-7.
15. Audhya, A., M. Foti, and S.D. Emr, *Distinct roles for the yeast phosphatidylinositol 4-kinases, Stt4p and Pik1p, in secretion, cell growth, and organelle membrane dynamics*. Mol Biol Cell, 2000. **11**(8): p. 2673-89.
16. Walch-Solimena, C. and P. Novick, *The yeast phosphatidylinositol-4-OH kinase pik1 regulates secretion at the Golgi*. Nat Cell Biol, 1999. **1**(8): p. 523-5.
17. Zhou, Y., H. Zhang, and W. Wei, *Simultaneous generation of multi-gene knockouts in human cells*. FEBS Lett, 2016. **590**(23): p. 4343-4353.
18. Zhang, Y., et al., *Efficient and transgene-free genome editing in wheat through transient expression of CRISPR/Cas9 DNA or RNA*. Nat Commun, 2016. **7**: p. 12617.
19. Yang, L., et al., *CRISPR/Cas9-Directed Genome Editing of Cultured Cells*. Curr Protoc Mol Biol, 2014. **107**: p. 31 1 1-17.
20. Yang, L., et al., *CRISPR-Cas-mediated targeted genome editing in human cells*. Methods Mol Biol, 2014. **1114**: p. 245-67.
21. Ng, M.M., et al., *GOLPH3L antagonizes GOLPH3 to determine Golgi morphology*. Mol Biol Cell, 2013. **24**(6): p. 796-808.
22. Kuhnle, J., et al., *A modeling approach to the self-assembly of the Golgi apparatus*. Biophys J, 2010. **98**(12): p. 2839-47.

23. Wooding, S. and H.R. Pelham, *The dynamics of golgi protein traffic visualized in living yeast cells*. Mol Biol Cell, 1998. **9**(9): p. 2667-80.
24. Bonifacino, J.S., *The GGA proteins: adaptors on the move*. Nat Rev Mol Cell Biol, 2004. **5**(1): p. 23-32.
25. Carlton, J.G. and P.J. Cullen, *Coincidence detection in phosphoinositide signaling*. Trends Cell Biol, 2005. **15**(10): p. 540-7.
26. Daboussi, L., G. Costaguta, and G.S. Payne, *Phosphoinositide-mediated clathrin adaptor progression at the trans-Golgi network*. Nat Cell Biol, 2012. **14**(3): p. 239-48.
27. Demmel, L., et al., *The clathrin adaptor Gga2p is a phosphatidylinositol 4-phosphate effector at the Golgi exit*. Mol Biol Cell, 2008. **19**(5): p. 1991-2002.
28. Traub, L.M., *Common principles in clathrin-mediated sorting at the Golgi and the plasma membrane*. Biochim Biophys Acta, 2005. **1744**(3): p. 415-37.
29. Wang, J., et al., *PI4P promotes the recruitment of the GGA adaptor proteins to the trans-Golgi network and regulates their recognition of the ubiquitin sorting signal*. Mol Biol Cell, 2007. **18**(7): p. 2646-55.
30. Gaynor, E.C., et al., *ARF is required for maintenance of yeast Golgi and endosome structure and function*. Mol Biol Cell, 1998. **9**(3): p. 653-70.

7. Publications in Refereed Journals:

a. Published:

1) Prasanna Iyer, Madhura Bhave, Bhawik Kumar Jain, Sudeshna Roy Chowdhury, Dibyendu Bhattacharyya. Vps74p controls Golgi size in Arf1-dependent manner. FEBS Letters. 2018 October. Article DOI: 10.1002/1873-3468.13266

b. Accepted:

c. Communicated: -

d. To be submitted:

- 1) **Iyer P**, Sutradhar S, Paul R, Bhattacharyya D. 'A novel combinatorial approach of quantitative microscopy and in silico modeling deciphers arf1 dependent Golgi size regulation.
- 2) **Iyer P**, Bhattacharjee C, Bhattacharyya D. GOLPH3, GOLPH3L, and ARF1 regulate Golgi shape by adjusting the ratio of amounts of tubules and vesicles.

e. Other Publications:

- 1) Bhave M[#], Papanikou E[#], **Iyer P**, Pandya K, Jain BK, Ganguly A, Sharma C, Pawar K, Austin J II, Day KJ, Rossanese OW, Glick BS, Bhattacharyya D. Golgi enlargement in Arf-depleted yeast cells is due to altered dynamics of cisternal maturation. J Cell Sci. 2014 Jan 1; 127(Pt 1):250-7. PMID: 24190882

I. Book/ Book Chapter: Nil

II. Poster/ Oral Presentation

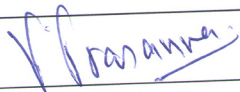
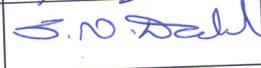
1. Won the **3rd prize** for Poster presentation on topic “ Genome-wide screening of yeast mutants of altered organelle Size” in **Global Cancer Genomics Consortium symposium 2011**, held at ACTREC- TMC, India
2. Poster presentation on topic “Role of Ptdln4P effector- Vps74/ GOLPH3 in Golgi size control mechanism and in Cancer” in an international symposium on **Conceptual Advances in Cellular Homeostasis regulated by Proteases and Chaperons 2013**, in ACTREC-TMC, India [Poster presentation]
3. Poster presentation on topic Role of “**Ptdln4P effector- Vps74/ GOLPH3 in Golgi size control mechanism**” in **Biophysics Paschim Meet 2014**, ACTREC-TMC, India
4. Presented poster on topic “**Study of Ptdlns4P effector- Vps74/GOLPH3 in Golgi size control mechanism**” in International conference **American society of Cell Biology conference (ASCB-2015)** - December 2015, San Diego, U.S.

5. Presented poster on topic "**PtdIns4P effector- Vps74/GOLPH3 affects Golgi size**" in **Optics within Life Science conference (OWLS)** - March 2016, TIFR, Mumbai, India.
6. Won the **2nd prize** for Oral presentation on the topic "**Does PtdIns4P effector- Vps74/GOLPH3, an oncogene affect Golgi size?**" in **National Research Scholars Meet in Life Science**, ACTREC- TMC, India – December 2016.
7. Presented Poster on the topic "**How a Yeast homologue and mammalian oncogene – Vps74/GOLPH3 maintain Golgi size and shape?**" in International conference of Cell Biology (ICCB) held at CCMB, Hyderabad – January 2018

Signature of Student:

Date:

Doctoral Committee

Sr. No.	Name	Designation	Signature	Date
1	Dr. V. Prasanna	Chairperson		10/10/18
2	Dr. Dibyendu Bhattacharyya	Guide		10/10/18
3.	Dr. Sanjay Gupta	Member		10/10/18
4.	Dr. Sorab N. Dalal	Member		10/10/18

Forwarded Through:



Dr. S.V. Chiplunkar
 Director, ACTREC
 Chairperson,
 Academic & training Program, ACTREC



Dr. S.D. Banavali
 Director, Academics
 T.M.C.

Prof. S. D. Banavali
 Director - Academics, TMC
 Mumbai - 400012.

Dr. S. V. Chiplunkar
 Director
 Advanced Centre for Treatment, Research &
 Education in Cancer (ACTREC)
 Tata Memorial Centre
 Kharghar, Navi Mumbai-410210.

Sr. no.	Figure number and Title	Pg. no.
Chapter 2		
1	2.1: Electron microscopy image of Rough Endoplasmic reticulum and smooth Endoplasmic reticulum.	38
2	2.2: COPI coat formation	40
3	2.3: COPII coat formation	41
4	2.4: Vps74 helps in retrograde transport of certain Golgi resident transferase	59
5	2.5: Organelle size regulation based therapy	66
Chapter 5		
6	5.1: JK9 wild type strain with late cisterna marked with Sec7- 6X GFP and the cell membrane labeled with mCherry- Ras2	117
7	5.2: JK9 wild type strain with 3X-iGFP Vps74 (green) and Sec7- 6X Ds-Red (red)	118
8	5.3: Representative two color strain Gea2 DsRed- GFP-Vrg4	120
9	5.4: Time point of 4D imaging of two color strain Gea2 DsRed- GFP-Vrg4 represent Gea2 (red) matures to Vrg4 (green)	120
10	5.5: Gea2 (green) matures to late marker Sec7 (red)	120
11	5.6: Gea2 (red) does not co-localize with well established trans marker Drs2 (green)	121
12	5.7: Homotypic fusion frequency on the temporal scale of maturation	121
13	5.8: Homotypic fusion for 3X-iGFP Rer1	122
14	5.9: Homotypic fusion for Gea2 3X-mEGFP	122
15	5.10: Homotypic fusion for GFP-Vrg4	122
16	5.11: Homotypic fusion for Sec7- 6X DsRed	122
17	5.12: Homotypic fusion frequency for markers Rer1, Gea2, Vrg4 and Sec7, N=10 movies. Student t-test. **p=0.0047, ****p<0.0001	123
18	5.13 Gene knock out strategy	124
19	5.14: JK9 wild-type and the vps74Δ mutant with GFP-Vrg4 (early marker) and Sec7- 6X Ds-Red (late marker)	125

20	5.15: JK9 wild-type and the <i>vps74Δ</i> mutant with Gea2-3X mEGFP (early marker) and Sec7- 6X Ds-Red (late marker)	126
21	5.16: JK9 wild-type and the <i>vps74Δ</i> mutant with Rer1- 3X iGFP (early marker) and Sec7- 6X Ds-Red (late marker)	126
22	5.17: Cisterna maturation parameter graphs for average cisterna volume, average diameter (Upper 2 graphs), average number maturation frequency, homotypic fusion frequency and persistence time (lower 4 graphs) is represented. Student t-test. S.E.M (Standard Error Mean). **p=0.0024 (Sec7 average volume) 0.0086 (maturation frequency graph) 0.0090 (Sec7 homotypic fusion frequency), ***p<0.0001, ****p<0.0001.	128
23	5.18: Cisterna maturation parameter graphs for average cisterna volume (N=60 cells) and average diameter (N=10 cells) is represented. . Student t-test. S.E.M (Standard Error Mean). **p=0.0014, ***p<0.0001	129
24	5.19: Panel shows wild-type, <i>vps74Δ</i> and <i>vps74 67-345Δ</i> with Gea2 and Sec7 marker	130
25	5.20: Graphical plot for average cisterna volume (N= 60 cells) and diameter (N=10 cells) for wild-type, <i>vps74Δ</i> and <i>vps74 67-345Δ</i> with Gea2 (early) and Sec7 (late) marker. Student t-test. S.E.M (Standard Error Mean). **p=0.0022, ****p<0.0001	131
26	5.21: Panel shows wild-type, <i>vps74Δ</i> and <i>vps74Δ/ 6AAA⁸ Vps74 OE</i> with Gea2 and Sec7 marker	132
27	5.22: Graphical plot for average cisterna volume (N= 60 cells) and diameter (N=10 cells) wild-type, <i>vps74Δ</i> and <i>vps74Δ/ 6AAA⁸ Vps74 OE</i> with Gea2 (early) and Sec7 (late) marker. Student t-test. S.E.M (Standard Error Mean). **p=0.0059, ****p<0.0001.	132
28	5.23: Panel shows wild-type, <i>vps74Δ</i> and <i>arf1Δ vps74Δ</i> with Gea2 and Sec7 marker	133
29	5.24: Graphical plot for average cisterna volume (N=60 cells) and diameter (N=10 cells) for wild-type, <i>vps74Δ</i> and <i>arf1Δ vps74Δ</i> with Gea2 (early) and Sec7 (late) marker. Student t-test. *p=0.0225, **p=0.0024, ***p=0.005, ****p<0.0001	133
30	5.25: Panel shows wild-type, <i>Δvps74</i> and <i>Δvps74 / ARF1 OE</i> with Gea2 and Sec7 marker	134

31	5.26: Graphical plot for average cisterna volume (N=60 cells) and diameter (N=10 cells) for wild-type, $\Delta vps74$, and $\Delta vps74 / ARF1 OE$. Student t-test. **** $p < 0.0001$, ** $p = 0.0024$	135
32	5.27: Panel shows wild-type, $\Delta arf1$ and $\Delta arf1 / VPS74 OE$ with Gea2 and Sec7 marker	136
33	5.28: Graphical plot for average cisterna volume (N=60 cells) and diameter (N=10 cells) for wild-type, $\Delta arf1$, and $\Delta arf1 / VPS74 OE$. Student t-test. * $p = 0.0173$, *** $p = 0.0005$, **** $p < 0.0001$	136
34	5.29: Panel shows wild-type, WT/ Arf1 OE with Gea2 and Sec7 marker	137
35	5.30: Graphical plot for average cisterna volume (N=60 cells) and diameter (N=10 cells) for wild-type and WT/ $ARF1 OE$. Analysed statistically using Student t-test.	138
36	5.31: Panel shows wild-type, WT/ $Vps74 OE$ with Gea2 and Sec7 marked	139
37	5.32: Graphical plot for average cisterna volume (N=60 cells) and diameter (N=10 cells) for wild-type and WT/ $VPS74 OE$. Analysed statistically using Student t-test. * $p = 0.0268$, ** $p = 0.0024$.	139
38	5.33: Graphical plot for percent fold change of average cisterna volume for wild-type and WT/ $Vps74 OE$	139
39	5.34: Panel shows wild-type and WT/ Arf1 OE with Rer1 and Sec7 marker	140
40	5.35: Panel shows wild-type and WT/ $VPS74 OE$ with Rer1 and Sec7 marker	140
41	5.36: Graphical plot for average cisterna volume (N=60 cells) and diameter (N= 10 cells) for wild-type and WT/ $ARF1 OE$ with Rer1 and Sec7 marker. Statistically non-significant. Used Student t-test.	141
42	5.37: Graphical plot for average cisterna volume (N=60 cells) and diameter (N=10 cells) for wild-type and WT/ $VPS74 OE$ with Rer1 and Sec7 marker. Performed Student-t test. * $p = 0.0372$ (average volume), * $p = 0.0116$ (average diameter)	141

43	5.38: Cisterna maturation parameter comparison for WT, $\Delta vps74$, $\Delta vps74 / ARF1 OE$ and WT / $VPS74 OE$. Performed Student-t test. **** $p < 0.0001$, ** $p = 0.0090$ (homotypic fusion frequency graph, ** $p = 0.0027$ (persistence time graph) and ** $p = 0.0086$ (maturation frequency graph). Error bar represents S.E.M (Standard error mean).	138
44	5.39: Cisterna maturation parameter comparison for WT, $\Delta arf1$, $arf1\Delta / Vps74 OE$ and WT / $Arf1 OE$. Performed Student-t test. **** $p < 0.0001$, *** $p < 0.0001$ (cisterna number graph), ** $p = 0.0012$ (homotypic fusion frequency graph), *** $p = 0.0002$ (homotypic fusion frequency graph), *** $p = 0.0007$ and 0.0004 (Persistence time graph), ** $p = 0.0028$ (persistence time graph) * $p = 0.225$ (persistence time graph). Error bar represents S.E.M (Standard error mean).	143
45	5.40: Representative image of localization of Vps74 in $\Delta arf1$	145
46	5.41: Average Pearson's coefficient plot obtained for colocalization of Vps74 with Sec7 cisterna in wild-type and $\Delta arf1$. (N=25 cells). Student t-test. **** $p < 0.0001$	145
47	5.42: Figure panel represents localization of PI4P marker GFP- PH^{OSH1} along late Golgi cisterna Sec7-6XmCherry in wild-type, $\Delta vps74$, $\Delta vps74/ARF1OE$, $\Delta arf1$, $\Delta arf1 / VPS74 OE$	147
48	5.43: Figure panel represents localization of PI4P marker mCherry- PH^{OSH1} along early Golgi cisterna Gea2-3X GFP in wild-type, $\Delta vps74$, $\Delta vps74/ARF1OE$, $\Delta arf1$, $\Delta arf1 / VPS74 OE$	148
49	5.44: Average Pearson's coefficient plot showing colocalization of PI4P with Sec7 Golgi cisterna. (N=30 cells). Student t-test. S.E.M (Standard Error Mean). **** $p < 0.0001$	149
50	5.45: Average Pearson's coefficient plot showing colocalization of PI4P with Gea2 Golgi cisterna. (N=30 cells). Student t-test. S.E.M (Standard Error Mean). **** $p < 0.0001$	149
51	5.46: The graph represents the percent fold change of average Pearson's coefficient in mutants compared to wild-type. Wild-type is considered as 100	150
52	5.47: Representative image of the effect of $pik1-83^{ts}$ on Vrg4 and Sec7 Golgi cisterna at the permissive and non-permissive condition	151

53	5.48: Hypothetical model explaining the role of Vps74 in Golgi size regulation	153
Chapter 6		
55	6.1: Illustration diagram of mathematical empirical equation	161
56	6.2: The table shows maturation parameters for wild-type and <i>arf1Δ</i> cells. The red rectangular box marks the parameter value obtained for cisterna number and product of maturation frequency and persistence time	162
57	6.3: Graph representing the concentration of early and late proteins with respect to time	163
58	6.4: Fusion between similar types of vesicles was only allowed	164
59	6.5: Volume of cisterna before and after fusion	166
60	6.6: Heatmap plot for distribution of number and size of cisterna based on parameter space K_{early} and K_{late}	168
61	6.7: Heatmap plot for distribution of number and size of cisterna based on parameter space K_{denovo} and $Size_{denovo}$	169
62	6.8: The cisterna size distribution probability plots for experimental (dark grey shaded bar) and simulation data (light grey shaded bar) of wild type showed a matching overlap for early marker Vrg4 and late marker Sec7	170
63	6.9: Plot for random Force (simulation) and velocity of cisterna (experiment)	172
64	6.10: Experiment and simulation comparison of cisterna maturation parameters for wild type Vrg4-Sec7 strain	177
65	6.11: Experiment and simulation comparison of cisterna maturation parameters for <i>arf1Δ</i> Vrg4-Sec7 strain	177
66	6.12: Experiment and simulation comparison of cisterna maturation parameters for wild-type Gea2-Sec7 strain	178
67	6.13: Experiment and simulation comparison of cisterna maturation parameters for <i>arf1Δ</i> Gea2-Sec7 strain	178
68	6.14: Experiment and simulation comparison of cisterna maturation	179

	parameters for <i>vps74Δ</i> Gea2-Sec7 strain	
69	6.15: Experiment and simulation comparison of cisterna maturation parameters for <i>vps74Δ/ ARF1</i> OE Gea2-Sec7 strain	179
70	6.16: Experiment and simulation comparison of cisterna maturation parameters for <i>arf1Δ/ VPS74</i> OE Gea2-Sec7 strain	179
71	6.17: Experiment and simulation comparison of cisterna maturation parameters for WT/ <i>ARF1</i> OE Gea2-Sec7 strain	180
72	6.18: Experiment and simulation comparison of cisterna maturation parameters for WT/ <i>VPS74</i> OE Gea2-Sec7 strain	180
Chapter 7		
73	7.1: Guide sequence for GOLPH3, GOLPH3L, and ARF1 designed in exon1	188
74	7.2: Representative U2OS cell line with the CRISPR BFP plasmid having guide sequence targeting GOLPH3, GOLPH3L, and ARF1 genes	189
75	7.3: Representative Golgi morphology in control, GOLPH3L, and ARF1 KO cells	190
76	7.4: The upper two panels compare the nucleotide and protein sequence for GOLPH3L KO with control while the bottom two sequence alignments are for ARF1 KO with control	190
77	7.5: Blast sequence comparison for GOLPH3 in the clones and control	191
78	7.6: T7 micronuclease assay for the stable clone of U2OS GOLPH3L knock out	192
79	7.7: T7 micronuclease assay for the stable clone of U2OS ARF1 knock out	193
80	7.8: T7 micronuclease assay for the stable clone of U2OS GOLPH3 knock out	194
81	7.9: Graph for parameter total Golgi volume and no. of disconnected Golgi surfaces is compared for GOLPH3L knock out strains with control cells	195

82	7.10: Hypothetical diagram explaining membrane undergoing vesiculation and tabulation at different conditions	198
Chapter 10		
83	10.1A Ras2 PCR	215
84	10.1B HindIII and XbaI digestion of YCplac33 Ras2 plasmid	215
85	10.1C mCherry PCR	215
86	10.1D BamHI and NcoI digestion of 204-T_C mCherry Ras2	215
87	10.2A Vps74 PCR	218
88	10.2B BspEI digestion of YIplac211 Vps74	218
89	10.2C Diagnosis of clone YIplac211 Vps74 N term BamHI- NheI	218
90	10.2D Yiplac211 3X- iGFP Vps74 linearised with AgeI and HpaI separately	218
91	10.3 BamHI and NheI digestion of Yiplac211- 3X-iGFP Rer1	220
92	10.4A Vps74 PCR	222
93	10.4B Diagnosis of YEplac195 Vps74	222
94	10.5A Vps74 gene disruption cassette PCR	224
95	10.5B Vps74 deletion check for Gea2-Sec7 strain	224
96	10.5C Vps74 deletion check for Vrg4-Sec7 strain	224
97	10.5D Vps74 deletion check for Rer1- Sec7 strain	224
98	10.6 Vps74 67-345 region deletion check for Gea2- Sec7 strain	225
99	10.9A Guide sequence for GOLPH3 confirmed in PX458 BFP mut vector	228
100	10.9B GOLPH3L guide sequence confirmed in PX458 BFP mut	228
101	10.9C GOLPH3 guide sequence confirmed in PX459 vector	228
102	10.9D GOLPH3L guide sequence confirmed in PX459 vector	228

Sr. no.	Table no. and title	Pg. no.
Chapter 2		
1	2.1: PIP binding domains	53
2	2.2: Details of protein Vps74, GOLPH3, and GOLPH3L	61
Chapter 4		
3	4.1: Contents of a PCR reaction	79
4	4.2: Cycling conditions for PCR using Phusion DNA polymerase	80
5	4.3: Contents of PCR reaction for site-directed mutagenesis	81
6	4.4: Cycling conditions for PCR for site-directed mutagenesis by Pfu turbo polymerase	81
7	4.5: Reaction mix for restriction digestion	82
8	4.6 The Components of Ligation Reaction	86
9	4.7: PCR Cycling condition to prepare deletion cassette	93
10	4.8: Cell lines used	104
11	4.9: T7 reaction set up	110
Chapter 6		
12	6.1: Parameter value for different strains	173
Chapter 10		
13	10.1: Ras2 gene PCR cycle	213
14	10.2: Annealing protocol for guide sequence	226
15	10.3: Ligation set of annealed guide sequence with CRISPR vector	225
16	10.4: List of primers	229
17	10.5: List of strains	230

Abbreviation

VPS74	Vacuolar protein sorting 74
GOLPH3	Golgi associated phosphoprotein 3
GOLPH3L	Golgi associated phosphoprotein 3 like
ARF1	ADP ribosylating factor 1
CRISPR	Clustered Regularly Interspaced Short Palindromic Repeats
ER	Endoplasmic reticulum
COPI	Coat protein I
COPII	Coat protein II
PtdIns4P/ PI4P	Phosphatidylinositol 4 Phosphate
NE	Nuclear envelope
RER	Rough Endoplasmic Reticulum
SER	Smooth Endoplasmic Reticulum
BAR	Bin/Amphiphysin/Rvs
PA	Phosphatidic acid
tER	transitional ER

GEF	Guanine exchange factor
GTP	Guanine Triphosphate
GAP	GTPase activating protein
Sec7	Secretory 7
YIP1	Ypt interacting protein
Sed4	Suppressor of Erd2 Deletion
ERGIC	ER- Golgi intermediate compartment
VTC	Vesicular tubular complex
VSV-G	Vesicular Stomatitis Virus Glycoprotein
TGN	Trans Golgi network
mTOR	mammalian target of rapamycin
PKD	Phospho kinase D
Och1	Outer chain elongation 1
Mnn9	Mannosyltransferase 9
RER1	Retention in the Endoplasmic reticulum 1
Vrg4	Vandate Resistance glycosylation 4
Gos1	Golgi Snare 1

Kex2	Killer Expression defective 2
Sys1	Suppressor of Ypt6 1
GRASP	Golgi reassembly stacking protein
Gea2	Guanine nucleotide exchange on Arf1-2
YOP1	YIP one partner 1
DAG	Diacyl glycerol
PIP	Phosphoinositide phosphate
PI	Phosphoinositide
ANTH	AP180 N terminal homology
ENTH	Epsin N terminal homology
FERM	F for 4.1 protein, E for ezrin, R for radixin and M for moesin
KA1	Kinase-associated domain 1
PH	Pleckstrin homology
PTB	Phosphotyrosine binding
PX	Phox homologous domain
Drs2	Deficiency of Ribosomal subunits 2

YPT32	Yeast protein two 32
MYO18A	Myosin VIIIa
MIDAS	mitochondrial DNA absence sensitive factor
NSCLC	Non small cell lung carcinoma
C2GnT1	Core2 N acetylglucosaminyltransferase 1
Kre2	Killer Toxin resistant 2
Ktr6	Kre two related 6
Bos1	Bet one suppressor 1
Cdc34	cell division cycle 34
PM	Plasma membrane
GT	Glycosyltransferases
Thr	Threonine
LB	Luria Broth
SOB	Super-optimal broth
CsCl	Cesium chloride
EtBr	Ethidium bromide
SB	Sodium borate

PCR	Polymerase chain reaction
ddH ₂ O	double distilled water
AP	Alkaline phosphatase
RPM	rotation per minute
YPD	Yeast peptone dextrose
SD	Synthetic Dextrose
LiAc	Lithium acetate
PEG	Polyethylene glycol
TE	Tris EDTA
5 FOA	5 Fluoro orotic acid
Con A	Concanavalin A
SNARE	Soluble N ethylmaleimide sensitive factor attachment protein receptor
WT	Wild type
DMEM	Dulbecco's' modified Eagle medium
CM	Complete medium
DMSO	Dimethyl sulphoxide

PBS	Phosphate buffered saline
PEI	Poly ethylenimine
GalNacT2	N acetyl Galactosaminyltransferase 2
WT	Wild-type
Pik1	Phosphatidylinositol kinase 1

Chapter 1

Introduction

1.1: Background of the work:

Golgi size alters during abundant need of protein secretion, like in mammary glands during parturition. It is critical to know the role of Golgi size in regulating proteins and their mode of altering maturation dynamics. Altered Golgi morphology is associated with glycosylation defects and in cancer [1-3]. GOLPH3, a first Golgi resident protein is reported to be an oncogene [4]. Overexpression of GOLPH3 is detected as a prognostic marker in several cancers like ovarian, breast, and oral. GOLPH3 is also reported to alter the Golgi morphology and anterograde transport [5]. Vps74 is the yeast homolog of GOLPH3 involved in retrograde transport of specific Golgi resident proteins [6, 7]. There is no detailed study of Vps74 in Golgi size regulation. However, GOLPH3 can rescue the function in *vps74* null mutants [7]. This data suggests that there is functional conservation amongst the two proteins. The thesis is mainly divided into two parts. One is to focus on understanding the role of Vps74 in Golgi size regulation using *S.cerevisiae* as the model organism while the other is to study the Golgi size regulation in *S.cerevisiae* using mathematical simulation. The thesis also incorporates CRISPR mediated knock out of genes GOLPH3, GOLPH3L, and ARF1 separately in chapter 7 wherein the altered Golgi morphology obtained in the knock out cells are classified using parameters like volume and no. of fragmented Golgi surfaces.

1.2: Layout of the thesis:

The thesis starts with the review of the literature, chapter 2, describing in brief, the introduction of organelle size study, ER and Golgi in membrane trafficking, general factors involved in protein secretion like COPI, COPII, and model system of Golgi. Details are provided about Phosphatidylinositol-4- Phosphate (PI4P), its domain, and its effector molecules. One of its

effector *VPS74* (in yeast) and *GOLPH3* (in mammals), and its role in Golgi size regulation is outlined. ‘Aims and Objectives’ are described in Chapter 3. A description of various methodologies and reagents are described in chapter 4 as ‘Materials and Methods.’ The findings of the work are presented and discussed in Chapter 5, 6 and 7. Each chapter is subdivided into the Introduction, Results, and Discussion segments. Chapter 5 deals with the study of *Vps74* in Golgi size regulation using *S.cerevisiae* model system. Chapter 6 deals with the study of Golgi size regulation and maturation kinetics by mathematical simulation. Chapter 7 deals with CRISPR mediated knock out of genes in the mammalian system. The summary of the thesis is presented in chapter 8. The references are compiled towards the end of the bibliography in chapter 9.

Chapter 2

Review of literature

2.1 Cell and its organelle

"Everywhere Nature works true to scale, and everything has its proper size accordingly."

-D'Arcy Wentworth.

The regulation of the size of biological organisms and their substructures is unclear. On a similar background, if we focus on the cellular level, the cell and its organelle size regulation are not much explored. Organelles have different shapes- linear and cylindrical in case of microtubules, spheroid nucleus, ER and mitochondria have a complex network, spherical and dispersed Golgi in budding yeast but stacked in higher eukaryotes, vacuole/ lysosome exist as round in structure and more in number, and multiple copies of round- vesicle-like peroxisomes. It is essential to know the genes and the mechanism involved in size regulation of cell and its organelles.

2.2 Organelle size matters

Each membrane-bound organelle holds a different set of biochemical reactions. The organelle size presumably needs to be modulated to accommodate an increased number of reactions as per the cell requirement. The surface area of organelle can limit the rate of influx and efflux; while the volume of the organelle altered can affect the number of molecules, it can hold [8]. Organelle size of certain specialized cells enlarges on functional demand. For example, Golgi size increases as per increased protein secretion in mammary glands during parturition [9] while the respiratory state limits the abundance of mitochondria.

As per evolution, almost similar organelles are present in a simple eukaryote to a complex mammalian cell. However, if one assumes the size aspect of an individual organelle in a simple to a complex cell, it varies. Cell size scales as per the organelle size .

2.3 The mechanisms that control the organelle size

- a. Limiting precursor: Blocking of the component biogenesis can control the organelle size can . Organelle size is inversely proportional to organelle number [8].
- b. The growth rate of the organelle varies as per the cell size.
- c. Sensor molecules act as a measure of organelle size. For example, linear molecules like microtubules are made up of tubulin.
- d. Organelle size varies as per the functional need.
- e. The rate of assembly and disassembly governs few bio-structure sizes. Similarly, the fusion and fission process regulates the size of membrane-bound organelles.

2.4 Organelle size study and its application

Enlarged nuclei observation is still a preliminary diagnostic marker for cancer. Metabolic alterations that are hallmarks of cancer are one of the critical reasons for the altered intracellular morphology. Organelle size reprogramming for cancer cells is hypothesized to be one of the therapy [8]. If the organelle size due to modified metabolism in pathological conditions could be reprogrammed using small molecules, then mismatch of the organelle size and the metabolic state might cause cell death. In other cases, if the organelle size alteration is due to signaling pathway, then a small molecule target could rescue the organelle size to normal range.

Even metabolic engineering could utilize reprogramming of organelle size to enhance metabolite production like biodiesel.

The importance of organelle size regulation is emphasized and the present study outlined would focus more on the secretory hub of the cell: Golgi and its size regulation.

2.5 The early secretory pathway and its associated components

2.5.1- Endoplasmic Reticulum – ER

ER is the critical dynamic organelle of the secretory pathway. It is a continuous membrane system with distinct domains like the nuclear envelope (NE), rough and smooth ER and the regions that contact other organelles. The interphase ER is divided into nuclear and peripheral ER. The NE surrounds the nucleus while peripheral ER extends throughout cell cytoplasm. In *S.cerevisiae*, the peripheral ER is present underneath the plasma membrane and with dozens of large tubules connecting it to NE [10, 11]. The ultra-structure difference between ribosome studded ER and smooth ER was visualized by electron microscopy (Fawcett 1996).

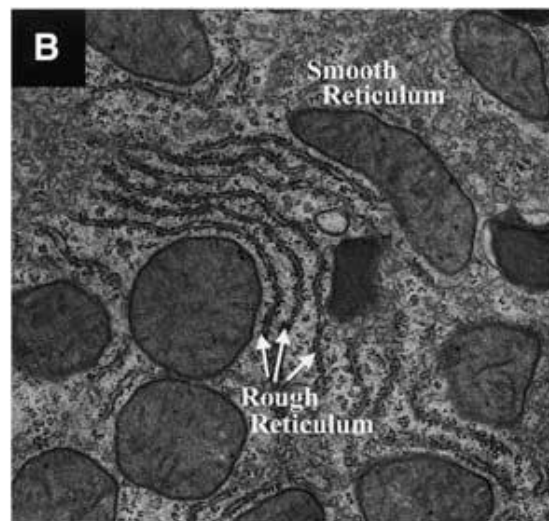


Figure 2.1: Electron microscopy image of Rough Endoplasmic reticulum and smooth Endoplasmic reticulum.

RER has a tubular appearance and granular texture while SER is often more dilated and convoluted. The relative abundance of RER and SER varies in cell types. Cells secreting a large amount of protein have abundant RER. SER is abundant in steroid synthesizing cells like liver, neuron, and muscle with diverse functions. In liver they help in detoxifying hydrophobic substances, it is the site of many of the steroid synthesis steps; it is involved in calcium release and uptake for muscle contraction, and probably for calcium handling in neurons. One type of SER, transitional ER is found in all cells [12]. This tER is involved in protein packaging and transport from ER to Golgi [13]. ER is required in the folding and modification of proteins. ER domain is very intimate to trans-Golgi. ER is closely associated with organelles like plasma membrane, Golgi, vacuoles, mitochondria, peroxisomes, late endosomes and lysosomes [14].

ER is in close proximity to other organelles. One of the main reasons is organelles need lipids, and close contact with the ER makes the direct transfer easier. It also contributes to calcium signaling and regulation.

2.5.2- COPI

Coatomer protein I, associated with vesicular transport was found to bind to di-lysine based motif of cargo proteins [15]. There is evidence that this binding led to the retrograde transport from Golgi to ER. Perturbations of coatomer subunits directly affected the retrograde transport [16, 17]. In the cisterna progression model, maturation process regulates the active intra-Golgi transport. This process would, in turn, allow the escape of many transmembrane and peripheral Golgi glycosylation enzymes. The biochemical approaches found that COPI helps in retrograde intra Golgi transport. This coatomer contained small GTPase ADP Ribosylation factor 1 [18, 19]. Arf1 activation by its binding of GTP recruited coatomer β - COP from the cytosol onto Golgi

membrane initiates COPI vesicle formation [20]. Coatomer consists of sub-units α , β , β' , γ , ϵ , and ζ . These subunits organize similarly to the clathrin coat complex [21]. COPI recognizes two distinct types of di-basic sequences: di-lysine signal located near carboxyl terminal and di-arginine signal located near the amino terminus of cargo proteins.

Following diagram illustrates COPI formation-

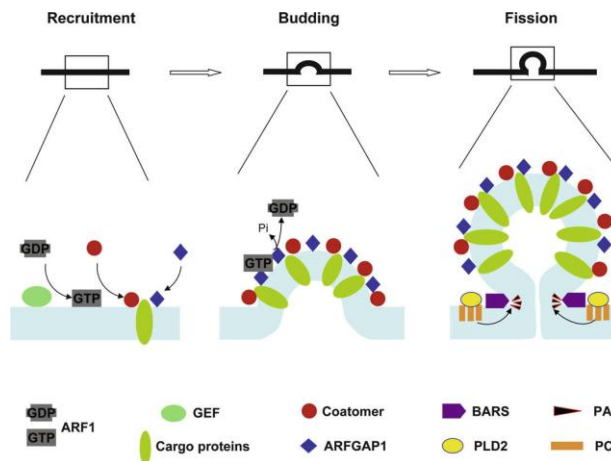


Figure 2.2: COPI coat formation

GBF1 (GEF) activates Arf1 and facilitates interaction with coatomer and cargo proteins. ARFGAP1 deactivates Arf1 and thereby drives budding of vesicles. As budding progresses, Arf1 incorporates cargo proteins. Proteins with BAR domain along with PA help in the fission of the vesicles.

2.5.3- COPII

COPII vesicles are produced near transitional ER (tER) sites. COPII coatomer mediates ER-Golgi transport of cargo proteins. It comprises of Sar1- GTPase, Sec23/24, Sec13/31 and Sec12-

GEF. Sec12 mediates GTP binding and activation of Sar1. Sar1- GTP binds to Sec23 and recruits Sec23- Sec24 heterodimer complex to form a pre-budding complex. Sec23 acts as a GAP for Sar1. However, Sec12 counteracts the GTPase- stimulating the activity of Sec23 by continually activating Sar1 with GTP. Later Sec13-Sec31 complex is recruited, causing membrane deformation to form COPII vesicles 60-70nm in size.

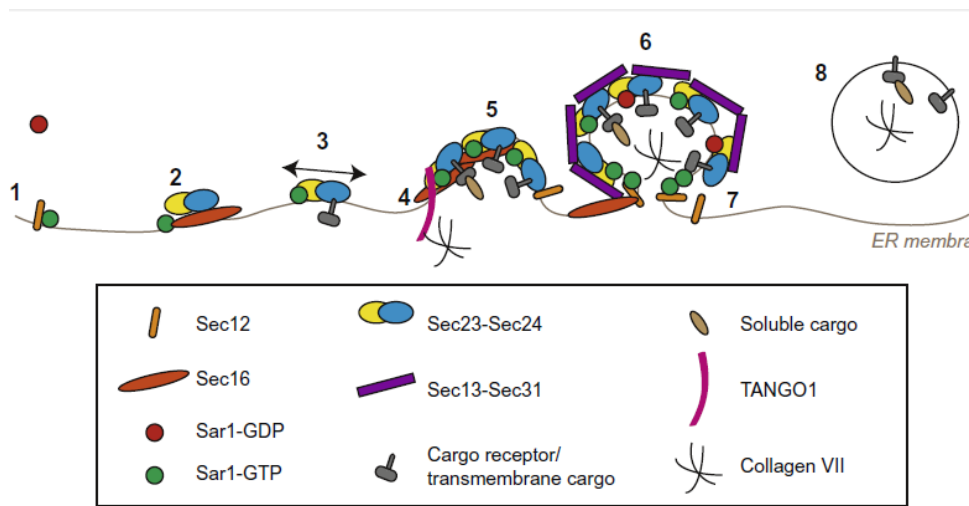


Figure 2.3: COPII coat formation

Some other proteins Sec16, Sed4, and Yip1 are also known to assist the COPII coat formation. Sec24 assists in the selection of cargo molecules. There are different ER export signals, for example- di-acidic (D/E)X(D/E) with x as any amino acid residue, and di-hydrophobic (FF, YY, LL or FY) motifs. However, various Sec24 family proteins bind to Sec23 [22, 23], which enables capture of multiple other cargoes. The N-terminal helix of the Sar1 play vital role in vesicle scission. Sar1 GTP hydrolysis occurs during vesicle fission [24]. Sar1 GTPase cycle eliminates unassembled cargo proteins from budding COPII vesicles [25]. COPII

vesicles shed their coat and fuse to form intermediates such as ER-Golgi intermediate compartment (ERGIC) and vesicular tubular complex (VTC).

2.5.4- Golgi

Golgi is one of the pivotal membrane-bound organelle regulating protein modification-secretion and membrane biogenesis. Golgi being small in size can control such a complex function. Elongation of the Golgi ribbon is observed during mitosis and differentiation for up-regulated secretion. Golgi has its structure maintained by a constant influx and efflux of cargoes and resident proteins through vesicle coat complex COPI and COPII.

A) Functions of Golgi:

- 1) Processing of proteins and lipids. It includes glycosylation, sulfation, and proteolytic processing.
- 2) Sorting of proteins and lipids to other membrane-bound organelles.
- 3) Retrieval of ER and, Golgi proteins.
- 4) Maintains surface area and composition of plasma membrane.
- 5) Ion homeostasis.
- 6) It also serves as a platform for various signaling pathways.

B) Morphology of Golgi:

Most eukaryotic cells have stacked Golgi. Each stack contains three flattened membrane compartments: cis, medial and trans [26]. This compartmentalization is based on the resident enzymes that modify the cargo coming from the ER. Tubular contacts laterally connect adjacent

stacks . Several mini stacks are joined laterally to form the Golgi ribbon. The number of a stack in a Golgi varies from species to species and also based on function or cell type (Eg: differentiation, mitosis). For example, a mammalian Golgi complex has 5-8 cisternae per stack, salivary Brunner's gland have 9-11 cisternae per stack, while 2-3 are present in epithelial cells of seminal vesicles. 20 cisternae per stack are present in certain green algae. The number of stacks is more in secretory cells that enable proper protein processing. Trans Golgi network acts as a specialized compartment for packaging of cargo into the carrier membrane [27]. In case of a Eukaryote, *P. pastoris* the Golgi is stacked, and are 3-4 in number per cell. However, in *S.cerevisiae*, protists and some insect cells, Golgi compartments are dispersed throughout cytosol randomly. In a wild-type, around 7-8 cis and 8-10 trans cisterna vesicles are observed. The cis matures into trans. The nature of this cisterna is stable or dynamic. Time-lapse 3D fluorescence microscopy of *S. cerevisiae* proved that cisterna matures at a constant rate [28].

C) The Model system of Golgi:

- 1) Vesicular transport model- Golgi has stable compartments [29-32]: cis, medial and trans with its respective glycosylating enzymes. The new cargoes from ER enter the cis compartment in COPII vesicles; while intra-Golgi transport of these cargoes takes place in COPI coated vesicles [33]. It was assumed that resident glycosylating enzymes remain associated with the specific Golgi compartment. Later the model was upgraded stating COPI vesicles move in bi-direction. The one moving in anterograde fashion carries cargo while the one moving in retrograde manner carries the Golgi resident proteins [34, 35].

Drawbacks of the model: COPI vesicles have to be huge in number for transport of many cargoes. Instead, some studies show COPI vesicles are less in number. Some have disproved finding of any cargoes in COPI vesicles [36-38]. COPI vesicles could not transport large cargoes like collagen.

- 2) Cisterna progression/ Maturation model: Here each Golgi compartments are transient and dynamic. COPII vesicles carrying cargoes bud from ER and fuse with each other forming new cis- cisternae [39, 40]. Newly formed cis- cisternae mature to medial and then trans, by acquiring the glycosylating enzymes from the COPI vesicles that hop in the retrograde direction [41, 42].

The drawback of the model: It could not explain the existence of heterotypic tubular connections between cisterna and the rapid exit of secretory cargoes. There was no clear evidence of COPI vesicles containing Golgi glycosylating enzymes.

- 3) Cisterna progression/ Maturation with heterotypic tubular transport: With an extension to the cisternal progression model, it includes an idea of vertical heterotypic tubular connections [26, 43, 44]. Presence of tubular connection was shown by some electron tomographic studies [45, 46]. It was proposed that such connections allow rapid anterograde transport of cargoes or retrograde transport of Golgi resident proteins or both [47].

Drawbacks of the model: There was no clear explanation for rapid transport of large cargoes like collagen. The existence of tubular connections in mammals is still in debate while there is no experimental evidence of its presence in fungal and plant system.

Further, the question arises is the maintenance of compartments in the presence of tubular connections.

- 4) Rapid partitioning in a mixed Golgi: Here Golgi exists as a single compartment with domains for processing and exit. The cargoes processed in Golgi exit stochastically to reach their final destination. This model then favored the exponential exit of cargoes. The VSV-G protein was observed to be partially segregated from glycosylating enzymes that gave the concept of separate domains in Golgi [48]. This model could explain the movement of large cargoes and exponential exit of cargoes.

The drawback of the model: This fails to explain the existence of discrete cisternae, Golgi compartments, the polarized distribution of glycosylating enzymes and the transient nature of yeast Golgi cisternae. It does not explain the role of COPI vesicles. This model does not explain the orderly processing of oligosaccharides [49]. Selective partitioning of Golgi domains could be described by simulation for VSV-G [48], but this was not valid for slowly moving cargoes like collagen [46, 50, 51]. This model explains micron scale lipid raft domains that have not been observed in cells [52].

- 5) Stable compartments as cisternal progenitors: This model consists of stable Golgi compartments with domains marked by Rab GTPases. Rab domain would pinch off from Golgi to form mega-vesicle that fuses with later cisternae of adjacent or same cisternae and allows anterograde transfer of cargo. This theory could well explain the polarity of Golgi compartments, transport of large cargoes, heterotypic tubular connections and rapid transportation of small secretory cargoes.

The drawback of the model: It could not explain the transient nature of yeast Golgi cisternae. Role of COPI vesicles is not mentioned. This model is apt for animal cells having stacked Golgi, linked laterally [53, 54] but plants, algae, and fungi have individual stacked Golgi [55-57], while *S.cerevisiae* have discrete cisternae that mature as individual structures [28, 58].

D) Alteration in Golgi size :

- 1) Mitosis: Golgi complex doubles in size as the cell enters the proliferative phase. This increase in size ensures the trafficking of proteins and lipids synthesized during mitosis.
- 2) Golgi complex expansion is observed in cells with increased processing demand. Based on increased cargo load, Golgi resident enzymes are also up-regulated for modification.
- 3) Enhanced sorting and signaling: Sorting involves packaging of cargoes in transport carriers from TGN. The surface area of TGN expands based on increased sorting demands [59]. Golgi membrane also serves as a hub for specific signaling molecules like Ras, PtIns4-P, components of the mTOR pathway. Enhanced signaling via these small molecules may also alter Golgi surface area.
- 4) Golgi influx and efflux: Exit from ER and TGN is an integral part of the secretory pathway that maintains the net flow to Golgi and also its size. Any block in this exit can alter the Golgi size. Cargo molecules drive input to and exit from Golgi complex. However, Golgi resident proteins are recycled back to Golgi. Increased expression of Golgi resident proteins also alters the Golgi complex size.

- 5) Transport factors required for vesicle formation also alter the Golgi complex size. For example, protein kinase D helps in the exit of cargo from TGN. PKD recruits phosphatidylinositol-4-phosphate which then recruits factors required for exit of cargo from TGN. Inhibition of PtdIns4-P leads to expanded Golgi [60, 61](Wang et al. 2003). Src family of kinases is involved in intra-Golgi and Golgi-ER transport.
- 6) Secretory cells show enlarged stacked Golgi. For example, prolactin-secreting cells show enlarged Golgi on stimulation. Up-regulated secretion of immunoglobulin in B cells shows increased Golgi complex size.
- 7) Neuron and muscle cells on differentiation, show altered Golgi organization. Neurons have somal Golgi near the juxtannuclear region. At the dendritic branch points, there is additional Golgi namely, Golgi outpost. Muscle cell differentiates to form syncytia wherein Golgi forms a circumnuclear organization. Later in myotubule, Golgi exists as dispersed ministacks.

2.5.5- Functionally same but differs in the organization:

A) Yeast Golgi

Yeast secretory pathway is simpler and has been used as a model organism for elucidating problems of protein secretion and membrane traffic. Two budding yeast are more extensively studied- *Saccharomyces. cerevisiae* and *Pichia. pastoris*. A typical cell consists of 20 cisternae, functionally divided into early (cis), medial and late (trans). The Golgi apparatus in *S.cerevisiae* consists of individual scattered Golgi cisterna due to delocalized tER, while in

P.pastoris the discrete tER sites generate stacked Golgi similar to higher eukaryotes [62]. Individual compartments have peculiar distinct peripheral or transmembrane proteins which are required to be retained for post-translational modification of different secretory proteins. Cis region comprises of proteins like Och1, Mnn9, Emp47, Rer1, Vrg4. Medial comprises Gos1, Gtn1 while trans comprises Kex2, Sec7, Sys1. The dispersed individual cisterna enables following each cisterna under optical microscopes easily as compared to the stacked. Cisterna Golgi maturation was visualized in *S. cerevisiae* [28, 63]. The time taken for intra Golgi transport of cargo is approximately 5-6 min.

B) Mammalian Golgi

Golgi is stacked and is interconnected laterally to form a ribbon-like structure in the perinuclear area. It appears as a lacy structure that occupies 5-7 um in length, 1-2um in width and 3-5um in depth [64]. The number of stacks varies as per cell type- for example; 9-11 are present in salivary Brunner's gland, while 2-3 are present in the epithelial cell of seminal vesicles. GRASP65 and GRASP55 localized to cis and medial respectively contribute to Golgi stacking [65, 66]. Depletion of either protein disrupts ribbon formation [67-70]. Depletion of both GRASPs disrupt stacking and ribbon formation [70]. Simpler eukaryotes have a single GRASP. There is another group of proteins termed golgins for Golgi stacking [71, 72]. In the case of *S. cerevisiae*, the Golgi is neither stacked nor ribbon.

The organization of Golgi in simple and higher eukaryotes is different, but the function is maintained. Further, in advanced cell type like neurons, we see a miniature form of Golgi namely, Golgi outposts in the dendritic region other than the stacked Golgi ribbon found in the cell body.

2.5.6- Significance of stacked ribbon-shaped Golgi over unstacked Golgi

The morphological organization of Golgi is different between cell types and species. It is dispersed in certain parasitic protists, *S.cerevisiae*; dispersed stack are found in individual plants, invertebrates, fungi like *S.pombe* and *P.pastoris*, protozoans; while they are stacked and linked to form ribbon shape in higher vertebrates. Dispersed Golgi does not compromise Golgi function like secretion, glycosylation. In spite, membrane trafficking occurs with the same kinetics in dispersed or stacked Golgi. Secretion is also functional in dispersed Golgi. Continuous ribbon allows the lateral diffusion of glycosylating enzymes. This ribbon-like linkage required for glycosylation functions perhaps needs some analysis. Such a complex arrangement was favored in the evolutionary history. It seems cell polarization favors ribbon-shaped Golgi . The perinuclear localization of Golgi is essential for specific specialized cells for functions like cell migration, apical-basal axis determination of epithelial cells, helps secretion of lytic granules in cytotoxic T cells and regulates the dendritic growth of neurons. It also provides the signal to a specific domain of cell surface. Destroying ribbon linkage by altering microtubule cytoskeleton or Golgi localized proteins affects cell migration and show polarization defects. Prevention of ribbon unlinking blocks the cell in G2/M phase; thereby disassembly of Golgi promotes mitotic entry. This explains the existence of Golgi-based checkpoints that works parallel to cell-cycle checkpoints. However, the mechanism by which cell cycle machinery senses the altered Golgi morphology is not clear (Wei and Seemann 2014).

2.6 Different Golgi markers

A) Gea2

The systemic name is YEL022W in *S. cerevisiae* database. Gea2 is a Sec7 domain guanine nucleotide exchange factor for ADP ribosylation factors (ARFs). ARFs are the GTPases that regulate the formation of coated vesicles in intracellular trafficking. It is involved in vesicular transport between Golgi and ER. Gea1 is a paralog of Gea2, which arose from whole genome duplication. In yeast, Gea1 and Gea2 can replace each other functionally. However, at least one is required for viability. Temperature sensitive *gea* mutants show defects in ER- Golgi and intra-Golgi transport. Gea1 and Gea2 along with Arf3 play a vital role in the organization of actin cytoskeleton. We had observed Golgi maturation using different early markers like Gea2 and Vrg4.

B) Vrg4

The systemic name is YGL225W in *S.cerevisiae* database. It is a Golgi membrane protein with multiple transmembrane domains and a GDP-mannose transporter. It regulates glycosylation in Golgi. Name description of the gene reads as Vandate Resistance Glycosylation. The protein secreted by *vrg4* mutants lacks outer chain glycosylation. The Vrg4 mutation affects N-linked and O-linked protein glycoprotein modification and mannosylation of sphingolipids. The C-terminal hydrophilic peptide of Vrg4 binds to Ret2p, a subunit of the COPI coat.

C) Rer1

The systemic name is YCL001W in *S.cerevisiae* database. It is Golgi-localized . Name description reads as Retention in the Endoplasmic Reticulum. It functions as a retrieval receptor in returning membrane proteins to the ER. It is a non-essential gene. Null mutants mislocalize membrane proteins to Golgi or vacuole. RER1 is required for the retention of Sec12p [73, 74]. Sec12 is a GEF for Sar1, a constituent of COPII vesicle. Functionally mutant RER1 strain show mislocalized Sec71 and Sec63 [75].

D) Sec7

The systemic name is YDR170C in *S.cerevisiae* database. It is a well-known trans-Golgi marker. It is a GEF for ADP ribosylation factors. It is an essential gene. Conditional mutants accumulate Berkeley bodies and are defective in protein secretion and autophagy. Yeast and many other species show conserved catalytic domain of Sec7 . DCB/HUS domain of Sec7 activates Arf1 on the membrane surface by facilitating membrane insertion of Arf1 amphipathic helix [76]. BIG1 and BIG2 are the mammalian homologs of Sec7.

2.7 Proteins / Lipids maintain membrane shape and help in bending –

Lipids and membrane dynamics:

Role of proteins in deforming and shaping the membranes of organelles is well studied. ER continuous with the nuclear envelope is tubules that are highly curved in cross-section with relatively flat sheets. Depletion of scaffolding proteins DP1/ Yop1p results in the conversion of tubules to sheets while overexpression leads to the formation of the long tubule. However,

lipids are also equally important in the maintenance of cellular membranes. Lipids with negative membrane curvature along with membrane proteins assist membrane bending. A curved membrane can be achieved in the following ways:

- 1) Alter types or number of lipid in either or both layer.
- 2) Inserting hydrophobic or amphipathic region of the protein
- 3) Applying external scaffolding forces
- 4) Other mechanisms include line extension generated at the boundaries of lipid patches.

Lipids that are hexagonal or cone-shaped fit more aptly in the bilayer curvature favoring energetic cost, e.g., diacylglycerol, phosphatidylethanolamine. DAG maintains organelle shape and helps in membrane fusion in vivo. DAG levels lowered in sea urchin oocytes and eggs by microinjecting enzymes to reduce its pre-cursor or convert it to phosphatidic acid caused delayed or inhibited membrane fusion leading to the formation of the nuclear envelope and forming extended ER sheet. Proteins and lipids both are pre-requisite for bending of the membranes and shape maintenance.

Phospholipids act as a signaling molecule for many downstream effectors- which includes protein for shape and size maintenance of organelles. Phosphoinositides (PIPs) are family of anionic lipids low in abundance; have binding domains for cationic cluster region of certain proteins. There are seven different PIPs based on the number and positioning of phosphorylation. Monophosphorylated – PI(3)P, PI(4)P and PI(5)P; bisphosphorylated – PI(3,4)P₂, PI(3,5)P₂ and PI(4,5)P₂; and triphosphorylated PI(3,4,5)P₆.

PIP- binding domain includes ANTH, BAR, C2, ENTH, FERM, FYVE, GOLPH, KA1, PDZ, PH, PROPPINS, PTB, PX and TUBBY.

Table 2.1: PIP binding domains

<u>Sr. no.</u>	<u>Domain</u>	<u>PIP selectivity</u>
1	ANTH	PI(4,5)P2 and PI(3,4,5)P6. PI(3,4)P2 for some
2	BAR	PI(4,5)P2, PI(4)P
3	C2	PI(4,5)P2 as well as other PIPs
4	ENTH	PI(4,5)P2
5	FERM	PI(4,5)P2
6	FYVE	Majorly PI(3)P. Protrudin FYVE: PI(4,5)P2, PI(3,4)P2, and PI(3,4,5)P3
7	GOLPH	PI(4)P
8	KA1	Anionic lipids

9	PDZ	PI(4,5)P2 for some, but many are non-selective
10	PH	PI(3,4,5)P3, PI(4,5)P2, PI(3,4)P2, PI(3,5)P2, PI(3)P, PI(4)P. Some are selective for one PIP while others are non-selective
11	PROPPINS	PI(3,5)P2 and PI(3)P
12	PTB	PI(4,5)P2
13	PX	Mostly PI(3)P Some: PI(4)P, PI(4,5)P2, PI(3,4,5)P3, or PI(3,4)P2
14	TUBBY	PI(4,5)P2

These phospholipids are distributed spatially in different organelles that enable communicating with target proteins and regulating membrane trafficking, lipid transfer proteins, enzymes, ion channels, and endocytic and exocytic machinery. PI (4, 5) P2 and PI(4)P are abundant in the plasma membrane and Golgi respectively. PI(3)P is found abundantly in early endosomes while PI(3,5)P2 is abundant in late endosomes/ lysosome.

Organelle-specific protein is recruited based on PIP binding domain along with other organelle-specific features. PI(4)P at the Golgi has many downstream effectors. PI is phosphorylated at the D-4 position by two classes of phosphatidylinositol 4-kinases (PI4Ks). The human genome encodes two types- Type II PI4Ks (PI4KII α and PI4KII β) and Type III (PI4KIII α and PI4KIII β) kinases; while *Saccharomyces.cerevisiae* has one Type II PI4K (Lsb6) and two Type III PI4Ks (Stt4 and Pik1). In the mammalian system PI4KII α associates with Golgi membrane by palmitoylation while PI4KIII β binds NCS-1 and Arf1 for Golgi localization. NCS-1 homolog Frq1 in yeast assists Pik1 localization to TGN. These kinases maintain the concentration of PtdIns4P in trans-Golgi. Sac1 dephosphorylate PtdIns4P pools in the early Golgi compartment . Thus PI4K and Sac1 help in retaining a concentration gradient across the Golgi. Increased Sac1 activity, a PtdIns4P phosphatase reduced cell-cell adhesion and increases cell migration. While increased PI4KIII β , kinase increased cell-cell adhesion and reduced cell invasion [77]. PtdIns4P is higher in TGN and gradually decreases from medial to cis. PtdIns4P in the trans-Golgi enriches PI4K effectors that regulate vesicle budding and membrane dynamics. Protein kinase D regulates PI4K activity. PtdIns4P effectors include Vps74/GOLPH3, a phospholipid flippase-Drs2, and a Rab guanine nucleotide exchange factor (GEF) – Sec2.

2.8 Function of PtdIns4P at the Golgi:

- 1) Membrane biogenesis and lipid homeostasis: PtdIns4P and DAG control the sphingolipid and sterol content of trans compartment via regulators- OSBP1, FAPP2, and CERT. The co-ordinated production of DAG adds on negative curvature to the membrane that enables bending during fission of vesicles from the TGN. In yeast PITPs- Sec14 and Nir2

maintain the DAG pool in Golgi while OSBPs- Kes1 and OSBP1 modulate sterol content and thereby promoting vesicle formation. Thus PtdIns4P effectors control the TGN lipid content and initiate export of cargo from TGN.

- 2) Vesicle-mediated trafficking: In yeast, a multiprotein complex exocyst is recruited in the Golgi derived vesicles that are targeted to the plasma membrane. Sec2 first binds to PtdIns4P along with Ypt32 during vesicle budding. The presence of PtdIns4P does not allow binding with Sec15. Sec2 is a GEF for Sec4 on newly forming vesicles. Once vesicle has budded from Golgi, diminished PtdIns4P levels alters the conformation of Sec5. Sec2 activates Sec4, and both proteins bind Sec15, an exocyst subunit and enables vesicle formation.

2.9 GOLPH3 (Golgi associated phosphoprotein-3)

GOLPH3 is an effector of PtdIns4P in mammalian cells. It is required for an efficient anterograde pathway from Golgi to PM. In cultured human cells, RNAi mediated knockdown of GOLPH3 results in compact Golgi, and the anterograde transport is affected [5]. GOLPH3 maintains the flattened structure of Golgi by interacting with myosin MYO18A. Overexpression of GOLPH3 causes dispersed Golgi [78] and increased anterograde transport [79]. GOLPH3 also known as MIDAS (mitochondrial DNA absence sensitive factor) is enhanced in the absence of mtDNA. MIDAS is overexpressed in mitochondrial diseases associated with dysfunctional muscle fibers,. MIDAS regulates the total mitochondrial mass through biogenesis of phospholipid, cardiolipin.

GOLPH3 is identified as first Golgi associated oncoprotein, a target of 5p13 amplification. GOLPH3 overexpression was found in diverse tumor types like NSCLC, ovarian carcinoma, prostate cancer, breast, and melanoma. GOLPH3 knockdown in CRL-5889, Sbc12 and SK-MEL-5 cells with 5p13 amplification led to the loss of anchorage-independent growth. It led to the potent suppression of soft-agar growth and inhibition of proliferation [4]. Ectopic expression of GOLPH3 was capable of causing malignant transformation in both primary non-transformed mouse and human cells. GOLPH3 has a potent transforming activity. GOLPH3 is localized to trans-Golgi.

The mechanistic pathway of GOLPH3 causing cancer is linked to mTOR pathway. Vps35 was found to be GOLPH3 interacting by the yeast two-hybrid system and Co-IP studies further confirmed it. VPS35 and GOLPH3 co-localize at the endosome-like structure. VPS35 and VPS29 deletion altered sensitivity to rapamycin; led to postulate that GOLPH3 regulates mTOR pathway. Human tumor specimen showing over-expressed GOLPH3 showed increased mTOR expression and increased phosphorylation of mTOR substrate S6 kinase and AKT; thereby affecting mTOR signaling through specific substrates. It is also possible that interaction with VPS35 causes an increase in the abundance of RTKs on the PM and thus enhances the signaling.

Golgi is involved in different post-translational modifications of proteins and lipids. Processes like protein folding, cell-cell interaction, cell movement, cellular signaling, and others depend on Glycosylation. GOLPH3 regulates Golgi glycosylation. GOLPH3 controls cell-cell interaction essential for metastasis, through Golgi localization of C2GnT1 (Core2- N- acetylglucosaminyltransferase-1) [80]. This enzyme is required for

synthesis of Core2 associated sialyl Lewis X antigen; a ligand involved in selectin-mediated leukocyte trafficking and cancer metastasis. Cell migration, sialylation of N-glycans and Akt signaling are affected in GOLPH3 knockdown cells [81]. Overexpression of ST6Gal1 restored the function. GOLPH3 has been shown to behave as a coatmer adaptor for localization of certain Golgi glycosyltransferases like C2GnT1 and ST6Gal1 [82].

2.10 Vps74

Vps74 is yeast homolog protein for GOLPH3 and also an effector of PtdIns4P. Systemic name in the *Saccharomyces* genome database is YDR372C. It is made of 345 amino acids and has molecular weight 39275.2 KD. It is an effector of Phosphatidylinositol-4-phosphate (PtdIns4P). PtdIns4P have a concentration gradient, higher at trans cisterna which gradually lowers in medial and then cis. The concentration gradient of Vps74 is opposite to that of PtdIns4P [6]. It is required for the retention of certain Golgi associated glycosyltransferases. Cytoplasmic N-terminal tail of certain glycosyltransferases (GT) like Kre2, Mnn9, Mnn2 and Ktr6 lack COPI binding motif [7]. Vps74 acts as an adaptor to incorporate these enzymes to COPI coated vesicles and thereby help in their retrograde transport.

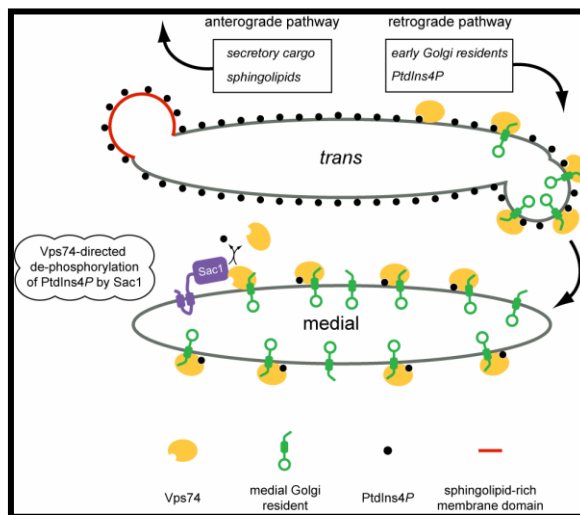


Figure 2.4: Vps74 helps in retrograde transport of certain Golgi resident transferase

$\Delta vps74$ is viable. On deletion of Vps74, these GT enzymes were mislocalized either to vesicle-like haze (Mnn9p) or to the lumen of the vacuole (Mnn2p, Kre2p, and Ktr6p) [7]. Vps74 binds to conserved consensus sequence (F/L)-(L/I/V)-X-X-(R/K) present on yeast Golgi resident GT. Overexpression of Vps74 shifted the distribution of Kre2p from Golgi to ER [7].

Vps74 interacts genetically with Bos1 and Sec23 (mutants defective in ER-Golgi trafficking). A genetic screen identified Vps74 as an essential gene required in the absence of YPT6, a Rab GTPase that regulates intra-Golgi and endosome-Golgi traffic. N and O-linked glycosylation defect is seen in $\Delta vps74$ strain [83]. Vps74 exist as a tetramer in solution and the crystal structure. B hairpin region 197-208 of Vps74 helps in tetramerization, and its deletion mislocalizes Vps77. COPI subunit mutants Sec21-1 and Sec27-1 led to mislocalization of Kre2p to the vacuole ($\Delta vps74$ phenotype) [83]. The N-terminal of Vps74 is not required for its localization to Golgi membrane but necessary for

retention of glycosyltransferases [84]. Cdc34-2 showed elongated cell morphology. However, $\Delta vps74$ in cdc34-2 cells reversed the phenotype [84]. Vps74 arginine residue at position 6th to 8th binds COPI coatomer. Region 67-345 of Vps74 binds Arf1, an interaction that is one of the essential ones for Golgi membrane localization of Vps74 [85].

2.11 Function of Vps74 and GOLPH3

GOLPH3 is required for anterograde transport from Golgi to PM, while Vps74 helps in retrograde transport of certain Golgi resident GT from trans to medial or cis Golgi. GOLPH3 knockdown result in compact Golgi and its overexpression cause dispersed Golgi. However, no clear reports are stated for the effect of $\Delta vps74$ in Golgi size or shape[86]. This findings highlights the functional difference. However, structurally the two proteins of two different species have conserved domains- the arginine motif for COPI binding, conserved residue for PtdIns4P binding and β - hairpin loop for oligomerization. GOLPH3 can rescue the functionality in $\Delta vps74$ strain [7]. These similarities emphasize that the two proteins are functionally conserved. In the mammalian system, there is another paralog of GOLPH3- GOLPH3L. GOLPH3 is present constitutively in all cell types. However, GOLPH3L is abundant only in secretive cells like the salivary gland, intestinal cells. GOLPH3L has a reversal effect on Golgi size. Knockdown of GOLPH3L cause dispersed Golgi while overexpression causes compact Golgi.

2.12 Functional similarity and difference of Vps74, GOLPH3, and GOLPH3L proteins

Table 2.2: Details of protein Vps74, GOLPH3, and GOLPH3L

<u>Protein</u>	Vps74 (Vacuolar protein sorting-associated protein 74) ORF name: YDR372C	GOLPH3 (Golgi Phosphoprotein 3) Alternative name: Coat protein GPP34, MIDAS (Mitochondrial DNA absence factor)	GOLPH3L
<u>Amino acid length/ Mol wt</u>	345/ 39,287 Da	298/33,811 Da	285/ 32,767 Da
<u>Function</u>	The PI4P binding protein may also bind to the coatomer to regulate Golgi membrane trafficking, retrograde transport of specific Golgi resident enzymes, cis and medial Golgi localization of mannosyltransferases through direct binding of their cytosolic domains, Involved in vacuolar protein sorting.	PI4P binding protein links Golgi membranes to the cytoskeleton and may participate in the tensile force required for vesicle budding from the Golgi. It may also bind to the coatomer to regulate Golgi membrane trafficking, anterograde transport from the Golgi to the plasma membrane and regulate secretion, control of the localization of Golgi enzymes through interaction with their cytoplasmic part,	a phosphatidylinositol-4-phosphate-binding protein that may antagonize the action of GOLPH3 does not interact with MYO18A, may interact with Arf1

		indirect role in cell migration, modulation of mTOR signaling, involved in the regulation of mitochondrial lipids biosynthesis	
<u>Subunit structure</u>	Homotetramer	Homodimer	Homooligomer
<u>Subcellular location</u>	Golgi apparatus › Golgi stack membrane; Peripheral membrane protein; Cytoplasmic side	Golgi apparatus › trans Golgi network membrane; Peripheral membrane protein; Cytoplasmic side. Mitochondrion intermembrane space. Cell membrane, Endosome	Golgi apparatus › trans-Golgi network membrane; Peripheral membrane protein; Cytoplasmic side.
<u>Post translational Modification</u>	Phosphorylation	Phosphorylation	
<u>Sequence features</u>	197-208 : Beta hairpin required for oligomerization, Binding site for PtdIn4P: 88,97,178,181 Sac1 interacting sites: L170 & I176. (Yiying Cai et.al 2014).	190-201 : Beta hairpin required for oligomerization, Binding site for PtdIn4P: 81,90,171, 177.	176-187 : Beta hairpin required for oligomerization, Binding site for PtdIn4P: 67, 76, 157,160

<u>Amino acid modification</u>	Phosphoserine at 14 & 19	Phosphoserine at 36, 84 < -> 108 Disulphide bond formation	
<u>Mutagenesis experimental info</u>	<p>6-8: RRR → AAA: Loss of coatomer-binding,</p> <p>19- S → A: Alters phosphorylation but has no effect on Golgi enzymes localization</p> <p>88: W → A: Abolishes phosphoinositide binding and Golgi localization; when associated with A-97.</p> <p>97: R → A: Abolishes phosphoinositide binding and Golgi localization; when associated with A-88</p> <p>178: K → A: Abolishes phosphoinositide binding and Golgi localization; when associated with A-181</p> <p>181: R → A: Abolishes phosphoinositide binding and Golgi localization; when associated with A-</p>	<p>7: R → A: Altered binding to coatomer,</p> <p>14-15: RR → AA: Loss of binding to coatomer</p> <p>81: W → A: Abolishes phosphoinositide binding and localization to the Golgi apparatus; when associated with A-90,</p> <p>90: R → A: Abolishes phosphoinositide binding and localization to the Golgi apparatus; when associated with A-81,</p> <p>90: R → L: Loss of function in vesicle budding, abolishes phosphoinositide binding and localization to the Golgi apparatus</p> <p>171: R → A or L: Abolishes phosphoinositide binding and localization to the</p>	7-10: RARR → AAAA: Loss of binding to coatomer

	178.	Golgi apparatus; when associated with A-174, 174: R → A: Abolishes phosphoinositide binding and localization to the Golgi apparatus; when associated with A-171 or L-171	
<u>Query score from BLAST</u>	Vps74 – GOLPH3 = 67% Vps74 – GOLPH3 L= 64%	Vps74 – GOLPH3 = 67%	Vps74 – GOLPH3 L= 64%
<u>Identity Score from BLAST</u>	Vps74 – GOLPH3 = 47%, Vps74 – GOLPH3L = 48%	Vps74 – GOLPH3 = 47%	Vps74 – GOLPH3L = 48%

2.13 Golgi size and its regulation:

Golgi is the prime organelle of the secretory pathway. If organelle is considered to be a reaction vessel, its size alters to accommodate the increased metabolons as per cells' requirement [8]. Increased Golgi size is observed during increased protein secretion and also in diseased conditions. Genes regulating Golgi size are vital. Discovering such genes

can be helpful to understand if any of its mutants alter the Golgi size and is involved directly or indirectly in any diseased condition. GOLPH3 affects Golgi size [5]. There is no such clear study for the role of Vps74 (yeast homolog) in Golgi size. GOLPH3 is a potent oncogene, associated with Golgi. GOLPH3 is involved in deregulating mTOR pathway or the uptake of RTK receptors. Golgi size regulation might have a link with cancer. Functional similarity and differences of GOLPH3 and Vps74 discussed embarks on studying Golgi size aspect with respect to Vps74 in yeast. *Saccharomyces cerevisiae* is an easy model to study the function of genes. Our lab has also done a detailed study of Arf1 and its role in Golgi size. Arf1 deletion causes enlarged trans Golgi phenotype and altered cisterna maturation kinetics [87]. Bhattacharyya lab has shown that the cisterna maturation is also delayed on Arf1 deletion. Vps74 interacts with Arf1 [85]. This interaction might have a role in Golgi size regulation. We speculate Vps74 also regulates Golgi size.

2.14 Golgi size regulation is important

Wallace Marshall has hypothesized two ways in which organelle size changes in diseased condition. It is described pictorially below. The top panel depicts organelle size change as a consequence of mutation causing the alteration in cell signaling and metabolism. The bottom panel depicts the mutation that alters cell signaling effects organelle size, which then changes metabolism. Organelle size reversion might change the diseased cell to the non-pathological state.

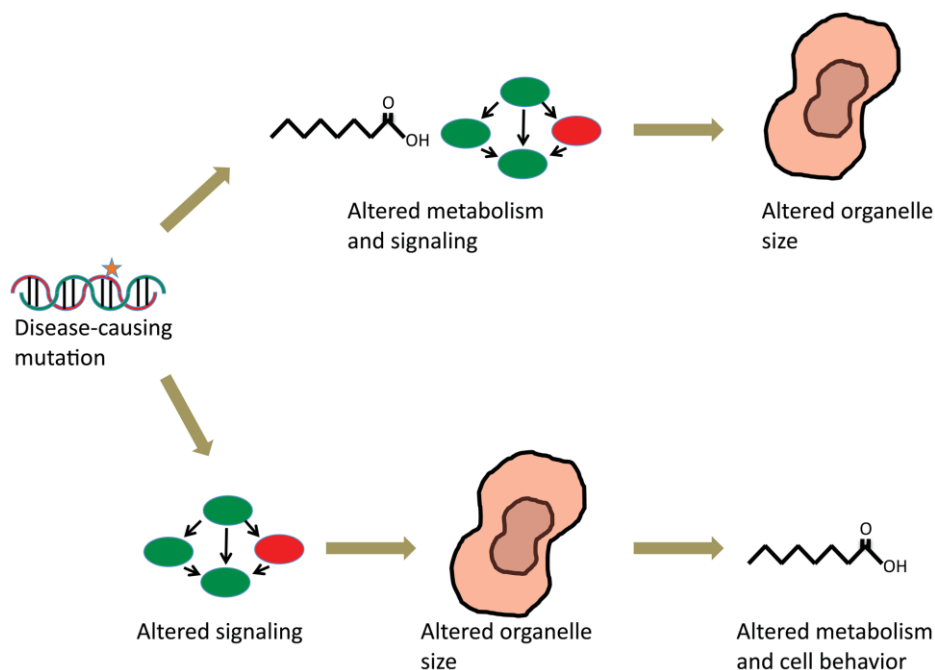


Figure 2.5: Organelle size regulation based therapy

GOLPH3 is the first Golgi associated oncoprotein. DNA damage causes DNA-PK to phosphorylate GOLPH3 on Thr143 and Thr148 that increases interaction with MYO18A and leads to Golgi dispersal [88]. Defects in DNA damage is a hallmark of cancer. Down-regulation of GOLPH3 makes the Golgi compact, while overexpression leads to dispersed Golgi [78]. Cancer cells also exhibit altered Golgi morphology [1]. Before entry into mitosis, the cell undergoes Golgi fragmentation in G2 phase. Increased growth of cancer cells is correlated with increased Golgi fragmentation [89]. Golgi fragmentation may be linked to tumor development and maintenance [2]. These imply the role of Golgi fragmentation in cancer cell biology. There is a prerequisite in understanding the genes that regulate Golgi morphology.

Chapter 3

Aims & Objectives

3.1: Statement of the problem:

Protein secretion maintains Golgi size . During parturition Golgi size increases in mammary glands due to high protein secretion. Golgi size also alters in diseased conditions. There exist regulators for controlling the Golgi size as per the cell requirement. Previously from our lab, we have detailed that Arf1 protein affects cisternal size in *S. cerevisiae* by altering maturation kinetics. There exist even other Golgi size regulators that are not studied. GOLPH3, a mammalian oncogene affects Golgi morphology and anterograde transport. Vps74, the yeast homolog of GOLPH3 is not reported to alter Golgi morphology, and it is functional in retrograde transport.

3.2: Hypothesis:

This observation describes functional discrepancy among the homologous proteins Vps74 (yeast) and GOLPH3 (mammalian). However reports are explaining GOLPH3 can rescue the function when expressed in *vps74* null mutants. Thus Vps74 may probably alter the Golgi size or maturation kinetics. Role of Vps74 in Golgi size regulation is studied using budding yeast *S. cerevisiae* as a model organism. Study of maturation dynamics in the mammalian system is difficult due to the resolution limit of stacked ribbon-shaped Golgi. However, dispersed Golgi cisterna in *S.cerevisiae* makes the maturation study feasible. We have demonstrated a link between Vps74 and Arf1 in Golgi size regulation and in maintaining the PI4P gradient along the Golgi stack.

3.3: Objectives:

I] Investigation of the possible role in Golgi size by functional characterization of *VPS74*, an oncogene homolog and Golgi resident PtdIns4P effector molecule.

II] Investigation of the possible role in Golgi size by Mathematical simulation.

3.3.1: Detailed Objectives:

I] Investigation of the possible role in Golgi size by functional characterization of *VPS74*, an oncogene homolog and Golgi resident PtdIns4P effector molecule.

A. Development of cell membrane marker to measure cell size and volume.

B. Study the role of *Vps74* and its interactome protein on Golgi size control mechanism.

C. CRISPR mediated knock out of *GOLPH3* (mammalian homolog of *Vps74*), *GOLPH3L* and *ARF1*.

II] Investigation of the possible role in Golgi size by Mathematical simulation.

A. Development of coarse grain simulation model for the Golgi system of *S. cerevisiae*.

B. Optimization of four parameters $Size_{denovo}$, K_{denovo} , K_{early} , and K_{late} .

3.4: Work done

The results and discussion of the work carried out under the objectives mentioned above are presented as three chapters with the following heading:

Chapter 5

Study the regulation of Golgi cisternal size by *VPS74* in budding yeast *S. cerevisiae*.

Chapter 6

Study Golgi size regulation in budding yeast *S. cerevisiae* by Mathematical simulation.

Chapter 7

CRISPR mediated gene knock out in mammalian cells.

Each chapter is composed of an introduction, results, and discussion section separately.

Chapter 4

Materials & Methods

4.1: Molecular cloning and bacterial culture

Host strain: E. coli DH5 α

Media and reagents essentially required to maintain bacterial culture:

Luria-Bertani (LB) (HiMedia) medium: Dissolve 20g powdered Luria Broth in 800 ml deionized milliQ (D/W) and adjust the volume to 1 liter with milliQ. For making LB-agar plates, 20g bacteriological grade agar powder was dissolved in 1L of LB broth and sterilized by autoclaving.

Antibiotics: Final Concentrations for ampicillin and kanamycin are 50 $\mu\text{g/ml}$ and 30 $\mu\text{g/ml}$ respectively. Add antibiotics as per the working concentration in LB broth or agar.

Super optimal broth (SOB): Dissolve all the following ingredients in milliQ, 2% Bactopeptone (HiMedia), 0.5% yeast extract(Himedia), 10mM NaCl(Merck), 5.5mM KCL(Merck), 10mM MgCl₂, 10mM MgSO₄ and autoclave to sterilize.

SOC media: To 98ml of sterile SOB, add filter sterilized 2M glucose and autoclaved 2M Mg. Store SOC media at 4°C.

Transformation buffer (TB): To 100 ml of D/W; 10 mM PIPES(Sigma), 15 mM CaCl₂, 250 mM KCl are added, adjust pH to 6.7 with 5N KOH, add 55 mM MnCl₅. Finally, the solution is filter sterilized through a 0.2 μ membrane. This buffer was freshly prepared, chilled and used.

4.1.1: Preparation of ultra-competent E. coli

For efficient transformation high competent bacterial cells are essential. DH5 α was made ultra-competent for the transformation of recombinant/routine plasmid vectors.

Method:

Streak *E. coli* DH5 α cells on LB agar plate and incubate overnight at 37°C. Inoculate single colony in 250 ml SOB medium and incubate on refrigerated shaker incubator with 200 RPM at 18°C until OD₆₀₀ reaches to 0.45 to 0.55. Incubate the flask on ice for 10 minutes and spin the culture at 2500g (3500 RPM) for 10 minutes at 4°C. Resuspend the cells very gently in 80 ml of cold transformation buffer and again keep on ice for another 10 minutes. Spin the mixture at 2500 x g (3500 RPM) for 10 minutes at 4°C. Resuspend the cells gently in 20 ml of cold transformation buffer. Incubate on ice for 10 minutes. Add 7% (1.4 ml) DMSO to a final concentration and mix by pipetting up and down. Aliquot 100 μ l cells in a tube and freeze the vial in liquid nitrogen and stored at -80°C. Use these cells within 2 -3 months.

4.1.2.: Preparation of competent DCM-DAM- cells:

These cells were used to change the methylation status of a few plasmids used in the study.

Pick a single colony of ER2252 from a freshly revived LB plate and inoculate in a 5ml LB broth. Maintain it at 37°C for 16-20hrs. Inoculate this fully grown culture of 5ml in 100ml LB/ SOB broth contained in the 500ml flask. Incubate at 37°C/ 200RPM for 3hrs. Monitor the growth of culture by checking O.D 600 every 30 minutes. Harvest cells at optimal density 0.45-0.55. Aseptically transfer the cells to cold 50ml propylene tubes. Cool the culture to 0°C by storing the tubes on ice for 10 minutes. Recover the cells by centrifugation at 4000rpm for 10 min at 4°C. Decan the media from cell pellets and allow the last drop also to drain away. Resuspend the pellet in 10ml ice-cold 0.1M CaCl₂ and store on ice for 20 minutes. Recover the cells by centrifugation at 4000 rpm for 10 minutes at 4°C and decan the entire fluid from the cell pellets. Resuspend each pellet in 0.6 ml 50% glycerol and 1.4 ml 0.1M CaCl₂ for each 50ml original culture. Aliquot of 100ul cells was done in cold eppendorf and thrown in liquid nitrogen.

Preserve cells in- 80°C. Note that this could be used for the the1-month duration as the transformation efficiency deteriorates.

4.1.3: Bacterial Transformation [90]

Take out 100µL aliquots of ultra-competent cells from -80°C and thaw by keeping in ice. Add 10 µl (50-100 ng) of DNA to 100µl thawed competent cells (avoid disturbing cells by pipetting rather tap the tube gently). Incubate on ice for 30 minutes. Give heat shock to the vial by keeping in 42°C water-bath for 45 seconds. Place on ice immediately for 5 minutes. Add 200µl of cold SOC medium to the vial aseptically. Incubate 37°C with shaking at 180 RPM for 60 minutes. Plate the cells on appropriate antibiotic-containing LB agar plate. Incubate at 37°C for 12-16 hours to appear colony.

4.1.4: Plasmid DNA isolation

Various methods of plasmid DNA isolation.

4.1.4.1: QIAprep Spin Miniprep method

Kit used- Qiagen miniprep kit.

As per manufacturers protocol, QIAprep Spin Columns contains a unique silica membrane that binds up to 20 µg DNA in the presence of a high concentration of chaotropic salt and allows elution in a small volume of low-salt buffer.

Inoculate a single colony in10ml of selection media LB-amp/ LB-kan and incubate at 37°C for 12-16 hours at 180 RPM bacterial shaker incubator. Transfer the bacterial culture in a 15 ml tube and spin at room temperature for 5 minutes at 6000 RPM. Vortex the pellet briefly and then resuspend in 250µl of Buffer P1 and transfer to a microcentrifuge tube (Ensure RNase A has

been added to Buffer P1). Add 250µl of buffer P2 and invert the tube 4–6 times. Immediately add 350µl of buffer N3 and again invert the tube 4–6 times. Spin the lysate at 13,000 RPM for 10 minutes. Add the clear supernatant very carefully to the QIAprep spin column. Spin the column for 30–60 seconds and discard the flow-through. Add 600µl of buffer PE to wash the QIAprep spin column and again spin for 30–60 seconds. Discard the flow through. Wipe the column from outside to remove any residual buffer PE. Then place the column in a dry tube and spin at 13000 RPM for 2 minutes to remove any residual wash buffer. Now, put the QIAprep column in a clean 1.5 ml microcentrifuge tube. Add 50µl Buffer EB (pre-warmed at 50°C) to the center of the QIAprep spin column, let it stand for 2 minutes. Centrifuge for 2 minutes at 14000 RPM to elute Plasmid DNA.

4.1.4.2: Plasmid DNA isolation using TELT buffer

This method was used for regular screening for positive clones in all the cloning experiments.

It is a quick and cost-effective protocol for preparing plasmid DNA. It involves a special buffer - TELT buffer [50mM Tris-HCL (Sigma) pH 4.5, 65.5mM EDTA (Fischer Scientific) pH-8, 0.4% Triton X100(Sigma), 5.5M LiCl (Sigma)]. The other ingredients required are Lysozyme (Sigma) (50mg/ml), 70% ethanol, Absolute alcohol (Merck) and TE buffer.

Inoculate bacterial culture in 1.5ml LB-antibiotic (Amp/ Kan) media and incubate at 37°C, for 12-16 hours at 200 RPM. Spin cells at 14000 RPM for 1 minute at 4°C to pellet down cells. Discard the supernatant; resuspend the pellet in 150µl TELT buffer and vortex briefly. Add 5µl lysozyme (Stock 50mg/ml) to the same and mix well. Incubate the vial on ice for 1 minute. Incubate the vial in boiling water bath for 1 minute. Immediately place the vial on ice for 10 minutes. Spin at 4°C at 15000 RPM for 10 minutes and collect supernatant in a new vial. Add 330µl absolute chilled alcohol and incubate at -20°C for 30 minutes or -80°C for 5 minutes. Spin

at 4°C at 15000 RPM for 10 minutes. Add 200µl chilled 70% ethanol for washing the DNA pellet and again centrifuge at 15000 RPM at 4°C for 5min. Dry the pellet to remove all remaining alcohol and re-suspend in 20µl TE buffer.

4.1.4.3: Plasmid DNA isolation by Cesium Chloride (CsCl) equilibrium density gradient centrifugation:

It is essential to get high-quality plasmid DNA to transfect the mammalian cells with high efficiency. CsCl equilibrium density gradient centrifugation yields very pure plasmid DNA. It is entirely free from salts, broken fragments.

Materials: Solution I: 50 mM Glucose (Sigma), 25 mM Tris.Cl (pH 8.0), 10 mM EDTA.2H₂O; D/W to make up the total volume;

Solution II: freshly prepared 0.2 N NaOH (Sigma), 1% SDS (Sigma); D/W to make up the total volume;

Solution III: 5M Potassium Acetate (Sigma) 60 ml, Glacial acetic acid (Merck)11.5 ml, D/W 28.5 ml; Tris/EDTA (TE) pH 8.0; Cesium chloride (Himedia): 1 g/ml in TE buffer; isopropanol (Merck),

Ethidium bromide (Himedia): 10 mg/ml in D/W

Method:

Spin 500 ml culture at 5000 rpm for 10 minutes in a sorvall centrifuge GS-3 at 4°C. Discard the supernatant and re-suspend the pellet in 18 ml of solution I, keep vortexing. Add 2 ml of lysozyme solution and mix properly. Add 40 ml of freshly prepared solution II, mix slowly by inverting followed by incubation at room temperature for 10 minutes. Add 40 ml of ice chilled

solution III, mix by inversion and store on ice for 10 minutes. Spin the tubes at 5000 RPM for 15 minutes at 4°C in (rotor- sorvall SS-34). In the meantime, prepare TE buffer. Filter the supernatant into HS 50 tubes by passing through gauze (4 fold). Add 0.8X volume of isopropanol to each tube. Incubate at room temperature for 10 minutes, and then spin at 8000 RPM for 15 minutes (rotor-SS-34 sorvall). Wash the pellet with 70 % alcohol (5 ml in each tube). Spin at 8000 RPM for 10 minutes at 4°C. Dissolve the properly in 8.5 ml of 1X TE buffer. Add 8.5 grams of cesium chloride (CsCl) to each tube. (Dissolve CsCl properly). Add 0.25 ml (Stock 10mg/ ml) of ethidium bromide mix properly. Spin at 8000 RPM for 5 minutes at 4°C. Load the mixture in ultracentrifuge tubes, sealed and balanced. Ultra-centrifuge for 22 hours, at speed 60, 000 RPM. After the run ends, prick the tube on top of the tube by 23 G needle very carefully. Using 18 G needle, pull the band of covalently closed circular DNA. Release the band from in a 15 ml tube. Add an equal volume of water-saturated butanol and vortex briefly. Spin at 3000 RPM for 2 minutes. Repeat this step, until pink color completely goes away; also both layers should be completely colorless. Add 2 volume of sterile dH₂O and 6 volume of 100% alcohol to DNA solution (2ml DNA solution + 4ml dH₂O + 12ml 100 % ethanol) in new T50. Incubate at 4°C for 30 minutes to 1 hour followed by Spin at 8000 RPM for 20 minutes at 4°C. Wash the DNA pellet with 70% alcohol and spin at 8000 RPM for 15 minutes at 4°C. Discard the supernatant and invert the tube on tissue paper. (Dry the pellet completely until no alcohol smell remains). Dissolve the DNA pellet in ~500µl of TE.

4.1.5: Agarose gel electrophoresis

Agarose gel electrophoresis is a routinely used method for the analysis and screening of the plasmids prepared after cloning. Various size DNA fragments can be separated on agarose gels using different concentrations of agarose. The requirements for the preparation of agarose gel is

Ethidium bromide 0.5 µg/ml, 6X Gel loading dye: 1.2ml glycerol, 1.2ml 0.3mM EDTA, 300µl of 20% SDS, 160 µl of 0.5% Bromophenol blue stock, nuclease-free water to make volume to 10ml.

Sodium Borate (SB) buffer: 10mM NaOH pH 8.5 adjusted with boric acid for 1X SB buffer.

Method-

Weigh agarose powder as per requirement of percentage of gels (depends on the size of DNA fragments), for example, to make a 0.8% agarose gel, add 0.48g of agarose powder in a conical flask, to which add 60ml of 1X sodium borate (SB) buffer. Microwave the mixture for 2 minutes, so that agarose powder melts and gets dissolved. Allow the boiling mixture to cool down to add ethidium bromide (to visualize DNA) at a final concentration of 0.5µg/ml (stock 10mg/ml). Mix well without creating bubbles and pour the mixture into the gel tray, place comb to develop wells. Remove the comb after the gel is solidified. Pour 1X SB buffer (running buffer) to the tank containing agarose gel. Dilute DNA sample (Plasmid DNA, PCR fragments, restriction digestion fragments or ligated DNA) with 6X gel loading dye (to make a final concentration 1X). Standard 1Kb or 100bp ladders were run in parallel to understand the size of DNA fragments . Visualise DNA bands using a gel documentation system.

4.1.6: Polymerase chain reaction (PCR)

The PCR technique provides specific DNA amplification of the sequence of interest from a template (yeast genomic DNA / plasmid DNA /cDNA) with the help of two oligonucleotide primers that bind to opposite strands in a sequence-specific manner. A thermostable DNA polymerase is used for extension of the primers at 3' end. Phusion high fidelity DNA polymerase was used for PCR amplification.

A typical mixture of a PCR reaction includes the following additives:

Table 4.1: Contents of a PCR reaction

	Components	Final concentration
1	H ₂ O	To make up the volume
2	5X buffer HF/GC*	1X
3	10mM dNTP mixture	200 μ M
4	Forward primer	0.5 μ M
5	Reverse primer	0.5 μ M
6	Template DNA	50ng (Plasmid DNA) 100ng (Genomic DNA or cDNA)
7	DNA polymerases	0.02 U/ μ l

*- (Depending on GC content)

Thaw all the samples on ice and add all the reagents as per the order stated in the table above followed by short spin the PCR tube after addition of all the components. Transfer quickly to the thermocycler preheated to the denaturation temperature (98°C) to start the reaction.

Table 4.2: Cycling conditions for PCR using Phusion DNA polymerase

Cycle step	Temperature	Time	Cycles
Initial denaturation	98°C	3 minutes	1
Denaturation	98°C	30 seconds	30-34
Annealing	Lower T _m +3	30seconds	
Extension	72°C	60 seconds /Kb	
Final extension	72°C	8minutes	1
Final hole	4°C	Forever	

Check the PCR product on the agarose gel.

4.1.7: Quick change mutagenesis [91]

Quick change mutagenesis was used to introduce either point mutation or insertion or deletion of few bases in a gene of interest with the help of high fidelity Pfu Turbo polymerase.

Prepare oligo mix by mixing 5µl of each forward and reverse primer (from 100µM stock) and 40µl of ddH₂O (1:10 dilution). Template concentration should be between 40-60 ng/µl.

The reaction set up:

Table 4.3: Contents of PCR reaction for site-directed mutagenesis

Components	Volume (μ l)
H ₂ O	15.3
10X buffer for Pfu Turbo	2
10mM dNTPs	0.4
Primer mix (1:10 dilution)	0.4
Template DNA (40ng/ μ l)	1
Pfu Turbo polymerases	0.4 (20U)

Table 4.4: Cycling conditions for PCR for site-directed mutagenesis

by Pfu turbo polymerase

Cycle step	Temperature	Time	Cycles
Initial denaturation	95°C	30s	1
Denaturation	95°C	30s	30
Annealing	55°C	60s	
Extension	68°C	2min/Kb	
Final extension	68°C	8min	1

4.1.8: Gene Cloning [92]

In gene cloning, plasmid DNA is cleaved with one or more RE to get blunt/cohesive ends and then foreign DNA fragment of variable sizes with compatible ends are ligated. The ligated heterogeneous mix is then transformed into a suitable bacterial host to propagate the clones. The resulting transformed recombinant clones are then screened by RE digestion to confirm the recombinant clone. Different strategies are used to clone a fragment of DNA in a plasmid vector, for example, PCR based cloning, sticky end based directional cloning, etc.

4.1.8.1: Restriction Digestion

Restriction enzymes or restriction endonucleases cut at a specific site in the template DNA. The components of preparative and analytical restriction digestion reaction were as follows:

Table 4.5: Reaction mix for restriction digestion

Components	Preparative	Analytical
Plasmid DNA	1 µg	100ng
H ₂ O	To make up the volume to 50µl	To make up the volume to 10µl
10X buffer	5µl	1µl
BSA	If required	If required
Enzyme	5U (1µl)	1U (0.2µl)

Add all the components in a microcentrifuge tube. Add the enzyme in the end. Briefly vortex the tube followed by short spinning the tube. Incubate the tube at 37°C for 2-4 hours in a water bath

(or, at any other temperature if explicitly mentioned for a particular enzyme). For any vector preparation in a cloning method, add 1 µl alkaline phosphatase (FastAP) (NEB) in the reaction tube and incubate for another 1 hour (Alkaline Phosphatase removes the 5'-phosphate groups of DNA from both the termini of the digested vector so as to avoid the self-ligation of the vector). Analyze the digested DNA fragment on an agarose gel.

4.1.8.2: Purification of restriction digested DNA or PCR product

For cloning of digested DNA fragments (either vector or insert), it is very important to purify them to remove nucleotides, primers, enzymes, mineral oil, salts, agarose, ethidium bromide, and other impurities from DNA samples before setting up ligation reaction.

Nucleotide removal kit (Qiagen), Gel extraction kit (Sigma)

QIAquick Nucleotide Removal Kit was used to remove DNA impurities during all cloning procedures. Columns contain a silica membrane assembly for binding of DNA in high-salt buffer and elution with pre-warmed water. The protocol is as follows-

Add 5 volumes of Buffer PN to 1 volume of the reaction sample and mix them homogeneously. Transfer the mixture in a QIA quick spin column, placed in 2 ml collection tube. Centrifuge the tube for 1 min at 6000 RPM, discard the flow-through. Add 600µl of buffer PE to the column and centrifuge for 1 min at 6000 RPM. Discard the flow through. Wipe the column from outside to remove any residual buffer PE. Then place the column in a dry tube and spin at 13000 RPM for 2 minutes to remove any residual wash buffer. Now, put the column in a clean 1.5 ml microcentrifuge tube. Add 50µl pre-warmed (at 50°C) autoclaved water to the center of the

column, let it stand for 2 minutes, and centrifuge for 2 minutes at 14000 RPM to elute pure DNA.

[To increase the concentration of the pure DNA, freeze the DNA by keeping the eppendorf tube at -80°C for 20 minutes, once frozen, then concentrate the DNA in a Speed-Vac at 4°C until the volume reduces]

4.1.8.3: Purification of DNA fragments from agarose gel

For cloning of digested DNA fragments (either vector or insert) or to get any pure PCR product, sometimes DNA bands of specific size had to be cut from agarose gel followed by removal of agarose from DNA samples before setting up ligation reaction. GenElute Gel Extraction Kit (Sigma) was used to purify DNA fragment from agarose gels.

Place the agarose gel containing DNA band of interest in a gel doc machine under UV light to visualize DNA. Cut the DNA band from the gel using sharp scalpel pre-sterilized with 70% alcohol. (Remove excess agarose to increase the yield). Make small pieces of the DNA band and place them in an eppendorf. Add 3 volume of the Gel Solubilisation Solution to the gel slice. (For every 100mg of agarose gel, added 300 ml of Gel Solubilisation Solution). Incubate the gel mixture at 60°C for 10-15 minutes with intermittent vortexing. In the meantime, add 500 ml of the column preparation solution to the binding column and centrifuged for 1 minute. Discard the flow through. Add 1 gel volume of 100% isopropanol and mix homogeneously. The solubilized gel solution mixture was then added to the binding column and centrifuged for 1 minute at 6000rpm. Discard the flow-through liquid . Add 600µl of buffer PE to the column and centrifuge for 1 min at 6000 RPM. Discard the flow through, Wipe the column from outside to remove any residual buffer PE. Place the column in a dry tube and spin at 13000 RPM for 2 minutes to

remove any residual wash buffer. Now, place the QIAprep column in a clean 1.5 ml microcentrifuge tube. Add 50µl pre-warmed (at 50°C) autoclaved water to the center of the column, let it stand for 2 minutes, and centrifuge for 2 minutes at 14000 RPM to elute pure DNA.

[To increase the concentration of the purified DNA, freeze the DNA by keeping the eppendorf tube at -80°C for 20 minutes, once frozen, then concentrate the DNA in a SpeedVac at 4°C until the volume reduces]

4.1.8.4: Ligation reaction

DNA ligase enzyme creates a phosphodiester bond between a 5'- phosphate termini and a 3'- hydroxyl group of two different DNA fragments and ligates the vector and insert DNA.

Method-

Measure the concentration of purified vector and insert DNA fragments. The typical ratio of vector: insert used was 1:3 which can vary depends on the size of either vector or insert. Calculate the amount of vector and insert fragment required to achieve a 1:3 molar ratio as per the following table in any *insilico* ligation calculator.

Always set up a positive control (any plasmid DNA of same concentration without vector and insert, to check if transformation worked) and negative control (another ligation mixture without insert fragment). Incubate the reactions at 22°C for 2-4 hours or at 16°C for overnight. Transform all the three reaction mixture in E. coli cells and check for positive clones.

Add the components of the ligation reaction as mentioned in the following table-

Table 4.6 the Components of Ligation Reaction

Components of the ligation reaction	Total volume (10 μ L)
Nuclease-free water	To make up the volume
10X T4 DNA ligase buffer	1 μ L
Vector	As calculated
Insert	As calculated from the above table
T4 DNA Ligase	200U

4.1.8.5: Screening of recombinant bacterial clones

Screen clones for the presence of the specific insert. If the test plate contains more colonies compare to the negative control plate, then only proceed for clone screening. Ideally, in the negative control plate, there should not be any colonies.

Method-

1. Replica plate transformants on LB-Amp or LB-Kan plates and inoculate in 1.5ml antibiotic containing LB broth.
5. Incubate eppendorf tubes at 37⁰C for 12-16 hours at 200 RPM. (Each clone was given a specific miniprep number for documentation).

6. Following day, isolate plasmid DNA using TELT buffer protocol.
4. Set up restriction digestion for the clones along with vector control DNA in which one restriction enzyme present in the vector DNA and another enzyme is present in the insert DNA to confirm the presence of the insert in the final clone.
5. Analyze the digested fragment in agarose gel electrophoresis.

4.2: Basic Yeast Techniques[93]

Yeast strain: *Saccharomyces cerevisiae* strain JK9-3d. Genotype: leu2-3,112 ura3-52 rme1 trp1 his4

Media preparation: Prepare media as indicated on the bottles by dissolving the powder in distilled water & autoclaved for sterilization. Drop out media were prepared for selection of clones after transformation. Prepare drop out media by adding yeast nitrogen base, glucose, CSM without a particular amino acid for selection and ammonium sulphate in a proportion as indicated on media bottles. They were sterilized by autoclaving. (YPD ready mix powder, synthetic complete media powder SD, Yeast nitrogen base, glucose, complete supplementary mixture, CSM without URA/ TRP/ LEU)

4.2.1: Retrieving strains from the yeast collection

UV sterilizes the laminar hood. Open Filemaker database → Yeast freeze down collection. Note down location number for a particular strain and auxotrophic marker. Identify the appropriate vial (Labeled location number) from -80°C. Remove vial from -80°C and place in ice. Using a

sterile pipette tip, take a small amount of the frozen cell and streak on YPD plate or auxotrophic dropout plate (only for strains containing episomal plasmids). Incubate at 30°C (wild-type) / 25°C (thermo-sensitive mutants) incubator.

4.2.2: Growing yeast log phase culture

Inoculate single colony from plates in 5 mL YPD medium/ auxotrophic dropout medium in a pre-culture tube (This tubes with loose lids allow proper aeration). Incubate cells at 30°C (wild-type) / 25°C (thermo-sensitive mutants) at 200 RPM for 48 hours for a saturated pre-culture (After cells settle in the bottom of the tube, the whole bottom of the tube should fill with cells). Inoculate 0.1% from saturated pre-culture for a log phase culture in the baffled flask (No other than this flask to maintain proper aeration and further good results). OD₆₀₀ of the culture should be 0.5 for any further experiment (if not mentioned otherwise).

4.2.3: Freezing Yeast

15% glycerol was prepared in distilled water & was sterilized by autoclaving

Method-

Inoculate yeast cells in pre-culture tube overnight until the culture is saturated. Plate 400µl cell suspension from saturated pre-culture on 2 YPD plates or plates of selection medium. Plates were incubated at the appropriate temperature until lawn growth appeared. For each strain, prepare two cryovials by placing 1.5ml sterile 15% Glycerol in each vial. Obtain a location number for freeze down of the strain by making a new entry in the Filemaker yeast database of the lab. Label each vial with this location number on the top. Write the details of the strain on the side of cryovials. About a third of the lawn (YPD plates) or an entire lawn (selective plates) was

scraped off and re-suspend in one of the vials using a small sterilized tip. Repeat the procedure for the second vial. The vials were placed in respective yeast freeze down box in the -80°C freezer. Place one vial in standard collection, and an identical vial in the backup collection. Enter complete information about the strain in the Filemaker yeast database of the lab.

4.2.4: Yeast transformation [94]

High-Efficiency Yeast Transformation with LiAc was used for transforming integrating, centromeric, episomal plasmids as well as PCR products in yeast cells.

1M Lithium acetate: 10.2 g of lithium acetate dihydrate was dissolved in 100 ml sterile. Distilled H₂O & sterilized by filtration through 0.22 μ filter.

50% Polyethylene glycol: 50g of PEG 3350 was weighed & added in a 150-ml beaker. Distilled H₂O was added slowly to this beaker. The mixture was stirred with a magnetic stirrer until the PEG dissolved completely. Adjust the volume to 100 ml with distilled H₂O. The solution was filter sterilized through the 0.22μ filter and stored in a tightly capped bottle at room temperature.

Method-

From a saturated pre-culture inoculate cells in 50ml YPD media (grow as described earlier) to an OD₆₀₀ of 0.5. Prepare a fresh 0.1 M LiAc solution (100μL 1M LiAc + 900μL sterile distilled H₂O). A fresh solution of PEG/LiAc was prepared by mixing (100μL 1M LiAc + 100μL sterile distilled H₂O+ 800μL sterile 50% PEG [Polyethylene glycol]), give a brief vortex to get a uniform mixture. Check optical density at 600 and start when it reaches 0.5, take the culture in T50 tube. Spin cells for 3 minutes at 3000 RPM at room temperature in a tabletop centrifuge. (If the proper pellet is not forming or it is getting mixed, increase the time for centrifugation from 3

minutes to 10 minutes). Resuspend the pellet in 20 ml sterile distilled H₂O (To remove excess media). Spin again for 3 minutes at 3000 RPM at room temperature, discard the supernatant. Resuspend in 0.5 ml 0.1M LiAc and transfer cell suspension in a microcentrifuge tube. Incubate the cell suspension for 15 min at 30°C in a water bath. Meanwhile, boil an aliquot of single-stranded carrier DNA at 99°C for 10 minutes in a thermo-mixer or boiling water, then cooled by placing vial on ice. Add 5 µl boiled carrier DNA and approximately 100ng transforming DNA (in 5 µl or less) for each transformation at room temperature inside the hood. For each transformation, include a negative control (only carrier DNA) & a positive control (DNA of same auxotrophic marker as in test). Add 50 µl cells to each transformation tube, give a brief vortex. Add 300 µl PEG/LiAc solution and mix by repeated gentle pipetting with a 1ml pipette (to obtain a uniform mixture). Incubate cell suspension and DNA-PEG/ LiAc mixture for 30 min at 30°C. Give heat shock for 15 minutes at 42°C. (In case of temperature sensitive cells, first incubation is at 25°C, and heat shock is at 30°C to avoid cell death). Spin the cells at high speed for 10 seconds in a microcentrifuge. Discard the PEG/LiAc supernatant. Resuspend cells gently in 200µl sterile distilled H₂O. Spread cells using sterile glass beads on a selective plate. Incubate plates at the appropriate temperature until colonies appeared.

4.2.5: Replica plating for screening transformants

Make grids and lines in a fresh plate and put numbers on the plate. Replica plate colonies from transformation plate (after colony appears) in a new plate to screen for positive transformants. Incubate at the 30°C incubator for 24 hours.

4.2.6: Genomic DNA isolation [95, 96]

Breaking buffer: 2 % (v/v) Triton X-100, 1% (v/v) SDS, 100 mM NaCl, 10 mM Tris-Cl, pH 8.0.
1 mM EDTA, pH 8.0, Distilled H₂O(sterile)

Method-

Inoculate colony from replica plate in preculture tube (5-6 ml)/ Eppendorf tube (1ml). Grow culture overnight at 30°C 200 RPM. Spin for 5minute at 3000 RPM in room temperature. Remove supernatant and wash pellet (resuspend, spin and discard the supernatant) with 0.5mL MQ. Vortex pellet briefly, add 200µl of freshly prepared breaking buffer and resuspend cells. Add 0.3 g (200 µl in vol.) small glass beads and 200 µl phenol (cold)/chloroform. Vortex at highest speed for 3min and lyse cells. Add 200 µl 1X TE buffer and give a brief vortex. Centrifuge at highest speed for 5 min, at room temperature. Transfer the aqueous layer to a fresh tube and add 1ml 100% ethanol (cold), mix by inverting tubes. Incubate tubes at -20°C for 1 hour for DNA precipitation. Centrifuge tubes for 5-10 minutes at highest speed at room temperature. Remove the supernatant and resuspend pellet in 0.4 ml in 1X TE Buffer. Add 3µl RNaseA (Stock 10 mg/ml), mix and incubate for 5 min at 37°C to remove RNA contamination. Add 10 µl of 4M Ammonium acetate and 1ml of 100% ethanol mix by inversion, and incubate at -20°C for 1 hour. Centrifuge tube at room temperature for 10-15 min at 14000 RPM. Discard supernatant and air dry pellet. Resuspend DNA pellet in 20µl TE buffer. Store at -20°C.

4.2.7: Checking fluorescence signal in an upright microscope for screening

Take little amount of colony from replica plate and resuspend in 20µl of SD media. Clean the slides & coverslips with Colin& air-dried. Add 5µl of cell suspension on the slide and place the

coverslip from the top on this suspension. Press the inverted slide gently on tissue paper to remove excess cell suspension. Seal the coverslip with transparent nail polish. Add a drop of immersion oil on the coverslip and place slide on the microscope stage for viewing. Cells were focused in the bright field & then fluorescence was checked by selecting an appropriate fluorescent filter.

4.2.8: Manipulating Yeast Genome

Gene targeting by homologous recombination is one of the most powerful and important techniques available for studies in yeast. A gene at its normal chromosomal location can be removed or replaced with an allele created in vitro, such that the only genetic difference between the initial strain and the final strain is that particular allele. Therefore, phenotypes conferred by null mutations or any other types of mutations can be analyzed. Genes can also be modified to be fused to the coding sequence for fluorescent proteins, such as green fluorescent protein (GFP). Because the epitope tag or fusion is made in the genomic context, the tagged gene is subject to native regulation. The properties of a strain containing the epitope tag or fusion can be compared to an isogenic wild-type strain that lacks the tag to study gene function, localization and regulation.

4.2.9: PCR based gene deletion strategy [97, 98]

Principle

Deletion of an entire open-reading frame (ORF) of a gene deletion creates a null mutation, allowing for the analysis of loss-of-function phenotypes. To generate a deletion, the gene sequence from start to stop codon is removed and is generally replaced with a selectable marker

(Kanmax/ URA3). The vectors used for gene deletion were pUG6 (KanMX marker) and pUG72 (URA3 marker).

PCR amplify the deletion cassette using either pUG6 or pUG72 plasmids as template. (Primers would contain 5' and 3' flanking region homologous to the ORF of interest.). PCR mixture is the same as described in 6.4. (Template concentration 50 ng). PCR cycle for creating deletion cassettes is as follows:

Table 4.7: PCR Cycle condition to prepare deletion cassette

Cycle step	Temperature	Time	Cycles
Initial denaturation	98°C	3 minutes	1
Denaturation	98°C	30s	34
Annealing	Lower T _m + 3	60s	
Extension	72°C	2 minutes	
Final extension	72 °C	8 minutes	1

Purify the amplicon using Qiaquick nucleotide removal kit. Transform the purified amplicon in the background yeast strain. Check integration of the deletion cassette in the transformant strain by PCR.

4.2.10: 5-FOA plates for popping out URA based plasmid [99]

Yeast cells expressing URA3⁺ are unable to grow on media containing 5-Fluoro-orotic acid (5FOA) (a pyrimidine analog), but mutant yeast strains containing ura3⁻ mutants usually grow.

This method gives the advantage of selecting yeast cells which lack wild-type URA3 allele. By this method, it is possible to take out the URA3 expressing plasmid out of cells.

Preparation of FOA plates:

Contents for making 250ml SD media were mixed in 125ml distilled water; 250mg of 5FOA powder was added to this mixture & sterilized by filtering through the 0.22 μ filter. In 125ml distilled water, add 5g agar. Autoclave for dissolving agar & for sterilization. Later this autoclaved agar solution & sterilized medium with 5-FOA were mixed well & poured in plates. The final concentration of 5-FOA was 1mg/ml.

4.2.11.: Removal of Kanamycin cassette from deletion strain by Cre induction

This method was used to remove the Kanamycin cassette. Transform pSH47 (Ura⁺) Cre recombinase containing plasmid in Kanamycin positive deletion strain. Replica plate Cre⁻ transformed colony on Sd Ura⁻ plate. Inoculate in 5ml SD Ura⁻ broth and grow for 15-20hrs until saturated growth appears. Inoculate from this saturated culture to synthetic raffinose Ura⁻ media, and allow growing till 0.8 O.D is attained. Add 2% Galactose and grow it further for 3hrs. Make serial dilutions of this culture and plate 1: 1000 and 1: 10,000 dilutions on YPD plate to get at least 50 isolated colonies. Make a patch of 50 colonies on SD Ura⁻ G418 plate and SD Ura⁻ simultaneously. Select the clone which grows on SD Ura⁻ and does not grow on SD Ura⁻ G418. Due to Galactose induction, Cre recombinase is activated, which will allow recombination between lox-P sites. Lox-P site flanks the Kanamycin cassette. Thereby recombination allows removal of Kanamycin cassette, and another round of gene deletion can be done using Kanamycin marker. Cure Cre plasmid of the strain by plating on SD FOA plates.

4.2.12: Yeast Live Cell Imaging

For Yeast cell imaging: Dissolve Concanavalin A in distilled water to the concentration of 2mg/ml & 100µl aliquots were made & stored at -20°C

Method-

Clean the glass bottom plate with Colin. Treat the glass bottom plate with a 200µl aliquot of concanavalin-A for 30 minutes. Remove the concanavalin-A using a pipette, and rinse the plate with milli-Q water. Air dry the dish completely. Add 200µl log phase yeast culture (OD₆₀₀ 0.5-0.6) to Con-A coated glass surface and incubate for 12 minutes at room temperature. Remove the culture and wash gently with SD media to remove all unattached cells. Later 1.5 ml of SD media was added for imaging.

4.2.13: Microscopy setting for a Yeast culture

Leica SP8 or Zeiss LSM 780 confocal microscopes were used for different experimental need.

Microscope setting involved

1. 63X 1.4NA oil immersion objective
5. 256 x 150 format for 3D imaging, 512 x 128 format for 4D imaging (movie)
6. 1 airy-unit pinhole for Leica SP8
4. Z step size 0.3µm

Special measures in Leica-STED

1. Averaging - 2
5. HyD detectors
6. Bidirectional scans on
4. Galvo flow always on
5. Zoom – 10 (63X objective), 6.5 (100X objective) for 3D imaging, while Zoom is kept 5 for 4D imaging (movie).
6. Scan speed- 700 Hz for 3D imaging 1400 Hz for 4D imaging (movie)
4. Pixel size 70nm

4.2.14.: Image analysis

Volume- Rendered the 3D surface for early and late cisterna using Imaris software by surface fill tool. The average diameter of $0.5\mu\text{m}$, the filter of radius $0.07\mu\text{m}$ for smoothing, and enabled $0.5\mu\text{m}$ split for touching surfaces. This settings enabled to quantify the volume of cisterna. 20 cells were imaged in a triplicate set and quantified.

Diameter- The major X-Y plane of each early and late cisterna were measured in surpass mode of Imaris for randomly 10 cells of all strains.

4D images were opened in Image J and passed through the plug-in 3D hybrid median filter-Vytas. Enable tight mean to correct background noise. After bleach correction, it was opened in Imaris to observe maturation parameters.

4.2.15.: Quantitative analysis of maturation parameters

All the quantification of maturation parameters were done using 10 movies each of wild-type and mutants with Gea2 3x-mGFP and Sec7 6X Ds-Red marker. The analysis was carried out for the mother cell. The movie captured for all the strains had one optical Z section captured in 4-5 seconds.

- 1) Cisterna number was calculated for 10 frames in a movie and then averaged.
- 2) Monitored homotypic fusion frequency for the 2-minute frame from 1 to 3 min of movie and event occurrence was converted to per minute.
- 3) For persistence time calculation the time point from which green signal appears marks the birth of a new early cisterna and was chased until it partially converts to the red signal, which is the formation of new late cisterna, and red eventually disappears. Exclude cisterna undergoing fusion while calculating persistence time. Further, the late cisterna was chased until it disappears from the cell.
- 4) The number of maturation events for the 3-minute frame from 1-4 minute was converted to the event occurring per minute.

4.2.16.: Colocalization analysis: Use Coloc tool of Imaris software for colocalization study. In the Coloc tool, the threshold method enabled, gave a statistic detail of Pearson's coefficient for the analyzed image.

4.2.17.: Statistical measurement: Statistical analysis was done using unpaired student t-Test. All graphs are plotted using Graph Pad Prism.

4.3: Mathematical simulation:

The theoretical framework of the model:

It is useful to adapt a coarse-grained model that smears out molecular processes on fine scales while still allowing capturing the large-scale events. In other words, molecules like COP proteins, lipids, different SNARE proteins, and accessory regulators are not modeled explicitly; instead, rates how they appear/disappear efficiently in specific events have been taken into account.

4.3.1.: Assumptions for in-silico cell:

We assume Golgi cisternae as discrete spherical objects. An ellipsoidal volume centered at the origin with semi-major axes a_{cell} , b_{cell} , c_{cell} along the x, y and z-axes respectively, mimics the cellular volume of the budding yeast (unbudded). Placed nucleus as a spherical object of radius $1 \mu\text{m}$ at a random position within the cell. Steric forces between the Golgi cisterna and the cellular and nuclear periphery keeps the cisterna within the cytoplasm. Nascent Golgi vesicles of average size $\text{Size}_{\text{denovo}}$ appear in the cytoplasm from the Endoplasmic reticulum (ER) exit sites with rate K_{denovo} distributed throughout the cytoplasm [100].

4.3.2.: K_{early} and K_{late} rate determines resident protein density:

These nascent Golgi vesicles, released from ER, contain the early resident proteins at the maximum density (1) and devoid of any late resident proteins (0). The density of early resident proteins decays with a constant rate K_{early} following various biochemical pathways, while, at the same time, the density of late resident proteins increase at a constant rate K_{late} . The density of the early proteins higher than the density of late proteins marked the cisterna as early Golgi cisterna. While the density of late proteins dominating over the density of the early proteins labeled the

cisterna as late Golgi. Once the densities of early and late resident proteins become 0 and 1 respectively, matured Golgi disappears through fission. K_{early} and K_{late} characterize the persistence time of the Golgi cisterna and relate to the retrograde flow of the resident proteins. For the sake of simplicity, the fission process considered is an instantaneous event in the model. Upon encounter, two Golgi cisternae fuse forming larger cisterna. The fusion is restricted between homotypic cisterna only, i.e., two early or two late Golgi cisternae can merge [28, 87].

4.3.3.: Random force calculation between vesicles:

Apart from the thermal noise, an active random force acting on the vesicles arising from the interactions between Golgi membrane and cytoskeletal filaments move Golgi cisterna intermittently over short distances through the cytoplasm [101]. Magnitude and distribution of the random force are tuned to match the velocity distribution of the vesicles obtained from our experimental measurements. We simplify the movement of Golgi cisterna following Brownian dynamics, i.e., the position of i^{th} cisterna updated after time δt according to:

$$\vec{X}_i(t + \delta t) = \vec{X}_i(t) + \vec{\beta}_i + \vec{F}_i^{\text{conserved}} \delta t / \xi \quad \text{Eq.1}$$

$\vec{X}_i(t)$ is the position vector of the i^{th} cisterna in the 3-dimensional time t . $\vec{\beta}_i$ represents the displacement due to active force plus thermal noise and is drawn from a Gaussian distribution with 0 mean and variance $2D\delta t$. Here D ($\sim 0.25 \mu\text{m}^2/\text{s}$) is the diffusion constant and $\vec{F}_i^{\text{conserved}}$ is the conserved force on the i^{th} cisterna due to repulsion from other heterotypic cisternae (Fig 2B), nucleus and cell membrane; ξ represents the viscous drag and δt ($\sim 10 \text{ ms}$) is the time increment in the simulation.

Steric repulsion avoids overlap between early and late Golgi cisterna. If R_{ij} denotes the center-to-center distance between i^{th} (early) and j^{th} (late)cisterna and \vec{e}_{ij} denotes the unit vector pointing from i to j , the repulsive force on i^{th} cisterna is given by:

$$\vec{F}_i^{\text{rep}} = F^0 \vec{e}_{ij} (1 - R_{ij}/(R_i + R_j)), \text{ if } R_{ij} < (R_i + R_j) \quad \text{Eq.2}$$

Where F^0 is the maximal repulsion force and R_i and R_j are the radii of the i^{th} and j^{th} cisterna. A similar expression for the repulsive force between Golgi vesicles and cell or nuclear periphery is considered. Integrating all repulsive forces, one can obtain the total conserved force $\underline{F}_i^{\text{conserved}}$.

4.3.4.: The density of proteins in newly emerged cisterna:

Following a homotypic fusion, the following scheme calculates the density of proteins (early and late) in the newly emerged cisterna:

$$D_{\text{new}} = (D_i V_i + D_j V_j) / V_{\text{new}} \quad \text{Eq.3}$$

Here D 's and V 's represent densities and volumes of the two merging Golgi cisterna respectively. We assumed volume conservation during fusion, supported by our experimental measurement. Collecting Equations 1, 2 and 3, into our computational model, simulations carried out using parameters listed in TABLE 1.

As per Equations 1, 2 and 3, vesicles distinguish from each other following the level of early or late Golgi resident proteins, as discussed earlier. While, the remaining three free parameters are chosen wisely as follows: scanning the parameter-space of K_{denovo} , K_{early} , K_{late} fix optimized values for which known experimental data is reproduced satisfactorily. Identifying the right set of parameters, we compute various quantities such as vesicle number, persistence time, maturation frequency, etc. and find them corroborate well with our experimentally observed values for the Wild-Type cell. Altering parameters obtained for the WT scenario, we establish new sets of

parameters predicting Golgi phenotypes with different types of perturbations of potential regulators (such as *arf1* deletion). While updating the list of parameters, we extrapolated the WT values guided by the existing knowledge about the regulators and their known functions in the Golgi maturation kinetics. A positive match between simulation and experimental data will validate the assumptions made and provide insight into the regulatory mechanism. To test our model with added complexity, we used *ARF1* as the regulator, and changed the parameters as per mutant.

4.3.5.: Input parameters value range adjustment

The four parameter-values set for wild-type Vrg4-Sec7 strain is mentioned in the Table1. Several reports indicate that *ARF1* clusters facilitate positive curvature at the required for budding of COPI vesicles [102-107] and we assumed the enhanced size of early cisterna ($\text{Size}_{\text{denovo}}$) in *arf1* Δ . We further believe that *arf1* Δ also reduces the retrograde flow different resident proteins by decreasing the nucleation of small vesicles that carry the resident-proteins and hence affecting the rates (K_{early} and K_{late}) at which resident protein of a cisterna mature [103-105, 108]. Therefore, in the model we considered that the presence of *ARF1* maintains:

- i. The rate of budding from the late Golgi and
- ii. Retrograde flow of different resident proteins to facilitate faithful maturation dynamics.

These statements further support the reduced K_{denovo} , increased K_{early} and K_{late} and in turn, would alter the persistence time of cisterna. Since our experiment suggests enlarged cisterna in *arf1* Δ , initial $\text{Size}_{\text{denovo}}$ is considered larger than the WT.

The computational model built on these inputs aimed to quantify the number of early and late Golgi cisterna, maturation frequency, the size distribution of the Golgi cisterna, persistence time

and homotypic fusion frequency of early and late Golgi for both wild-type and $\Delta arf1$ cells. Our *insilico* prediction corroborated well with the experimental results when homotypic fusion was accounted.

Coordinated with the experiment, the model considers the following while doing the measurement:

- 1) Counted cisterna, which is above the microscopic resolution (~250 nm).
- 2) Recorded model outputs at every 4 s (same as experiments) counting the number of cisterna, persistence time, maturation frequency, etc.
- 3) Before recording the data, we simulated the model for ~15 min to reach the initial steady state. Following this, the system evolved through a ~30 min simulation, and measured the parameters. We have simulated 50 independent samples for each measurement.

Clarity of the model is justified by the ability to incorporate experimental input in terms of the trajectories of the early Golgi particles and predict outcome as a function of two effective rates. Based on the heatmap diagram for tuning rates K_{denovo} , K_{early} , and K_{late} governing the size and number of cisterna, we could simulate *insilico* Golgi cisterna maturation process of *S.cerevisiae* and arrive at the proximity of experimental key parameters measured.

4.3.6.: 4D imaging for velocity calculation:

Separate 3-minute movie for Vrg4 and Sec7 marker was taken in Zeiss LSM-780 with minimum 1.5 -2s for single Z optical section. Scan mode frame 512 X 128 enabled, with 4X zoom, 63X objective, 0.372 optical sections and averaging 5. Speed 13 with piezo-stage enabled.

4.3.7.: Cisterna velocity calculation *in vivo*:

Marked Central pixel of the cisterna initially and the distance traveled in each time frame was measured using the measurement tool in Imaris. Around 9 movies, each for Vrg4 and Sec7 was used for analysis. Chased path of cisterna showing bright cisterna until it merges with other cisterna or disappears. Based on this, a total of 75 Vrg4 cisternae and 46 Sec7 cisternae was monitored. Distance covered in consecutive time frame was divided by difference in the time frame to evaluate the velocity of the cisterna. These experimentally evaluated velocity obtained was used for tuning the random force exerted on Golgi vesicles in the mathematical simulation.

4.4: Mammalian Cell Culture Techniques

4.4. Methods used in mammalian cell line studies:

4.4.1. Daily Observations of Cell Culture of following

Cell morphology, pH of the media, incubator setting, and water level in the tank inside the incubator, and levels of CO₂, and temperature were monitored frequently on a daily basis.

When to Subculture Cells?

Cells covered the entire surface available for growth. Cells should attain 80-90% confluency.

Origin of the cells – All are established cell lines (No primary culture)

Precautions while handling any Cell Culture work:-

Never culture two cell types at the same time. Keep the media clearly labeled with the – Name, Date and if specific for any particular cell line. Pre-warm all media in the 37°C water bath. Wipe

all surfaces and bottles with 70% alcohol before starting. UV sterilize laminar hood every time before and after the use of cell culture. Always wear gloves.

Table 4.8: Cell lines used

Name	Tissue origin	Medium
U2-OS	Bone osteosarcoma cell line	DMEM

4.4.2: Reviving Cells from Frozen Stock

Dulbecco’s Modified Eagle Medium (DMEM): 16.5g powdered medium was dissolved in ~900 ml autoclaved distilled water, supplemented further with 6.7 g sodium bicarbonate (NaHCO₃). Adjust pH to 4.1-4.2 with concentrated HCl, or 0.5N NaOH and volume made up to 1 L. Filter the medium through a 0.22 μ sterile filter and stored at 4°C.

Complete medium (CM): DMEM supplemented with 10% FBS and 1% antibiotics [Anti-bacterial Anti-mycotic (Gibco)], was prepared as needed.

Method-

Thawing and recovery of cells from liquid nitrogen must be done quickly. Media are pre-warmed by keeping at 37°C. Cryovial is removed from liquid nitrogen and immediately placed in 37°C water bath. (Note: Be very careful while removing cryovial from the cylinder, the box should be removed very slowly, remove individual vial by using forceps, wait until the fumes from vial are completely gone, then place the vial in the incubator. Otherwise vials sometimes burst). Transfer the vial into the laminar hood. Before opening, wipe outside of the vial with 70% ethanol. Transfer the thawed cell in pre-warmed 10ml medium (DMEM + 10% FBS + 1% Antibiotic) kept in 90mm petri dish. Gently add the cells (aliquot entire vial content in a plate at high density

to optimize recovery) and incubate at 37°C in a CO₂ incubator. After 12 hours, ensure cells are attached. Change culture media to remove non-adherent cells and replenish nutrients. Changing the culture media will also remove any DMSO residues. In case of puromycin stable clones, revive them in complete media. Once cell attains 80-90% confluency, cells were sub-cultured and maintained in complete media containing desired puromycin concentration.

4.4.3: Cell passaging

Phosphate buffered saline (PBS): NaCl-8.0g, KCl-0.2g, KH₂PO₄-0.24g, Na₂HPO₄·2H₂O-1.44g dissolved in 1L distilled water; pH was adjusted to 7.4 and sterilized by autoclaving.

Trypsin-EDTA: EDTA disodium salt-0.01g, D-glucose-0.1g, KCl-0.04g, NaCl-0.8g, NaHCO₃-0.058g, Trypsin-0.025g, adjust pH to 7.2 and volume made up to 100ml, Sterilized by passing through 0.22µ sterile filter and stored at 4°C.

Method-

Place plates or T25 flasks in the hood from the incubator. Attach an aspirating pipette to the tube attached to a vacuum. Turn on the vacuum system by opening the vacuum valve in the hood. Using the aspirator, liquid media covering the cells is sucked out. Add 5 ml of 1X PBS to cells and wash cells very gently by swirling the flask gently followed by aspirating PBS. Add 2 ml trypsin-EDTA to cells. Incubate flask at the 37°C incubator for 2-5 minutes. (Trypsin is highly active, relatively non-specific, used in concentration of 0.05 to 0.25 %, cleaves proteins on the cell surface and extracellular matrix, removes adhesion molecules, EDTA is added to enhance the activity of trypsin, Ca²⁺ chelator removes calcium and causes cell rounding, cell adhesion through cadherins and selectins is calcium dependent, low calcium causes cells to internalize adhesion molecules, rounding or detachment). Check cells under a microscope to confirm that

cells are detached from the surface. Add 10 ml of complete media (Supplemented with serum) to deactivate trypsin. Carefully re-suspend cells. Transfer cell suspension in 15 ml centrifuge tube. (Important: Label tube). Centrifuge cells for 4 min at 500 RPM. In the meantime, appropriately pipette volume of fresh media into new T flasks or plates as needed. Label with name, date, cell type, passage number and passage dilution (Very important). After centrifugation, aspirate supernatant. Cell pellet should remain at the base of the tube. Resuspend cells in 1 ml media. Aliquot appropriate volume of cell suspension into freshly prepared T flasks with media. Swirl media and cells to mix and keep the flask/plates in the 37°C CO₂ incubator. Dispose of liquid and solid biohazards waste properly. Clean hood with ethanol.

4.4.4: Freezing of cell line

Freezing Medium- 90% Serum + 10% DMSO

Method- Before starting with cell harvesting properly label the cryovial and arrange in the hood. Seed the cells in T75 flask and harvest when cells are 80% confluent. (Cells should be healthy, and over 90% cells should be viable). Pellet down cells as mentioned in the previous section at step 10. Remove supernatant and resuspend the cells in cold 5.7ml serum. Make a single cell suspension (1×10^6 cells per ml). Just before adding to cryovial, add 300µl of DMSO to the cell suspension and pipette up and down gently to ensure single cell suspension. (DMSO is toxic to cells, so should not be exposed to the cells at room temperature for any longer than necessary, from this step to step 6 should be completed as soon as possible). Make aliquots of 1 ml of the cell suspension into each cryovial. From one T75 flask with 80% cell confluency, make 3 freezedown vials. Place the cryovials in an isopropanol chamber chiller and store them at -80°C

for overnight. Next day, transfer frozen cells to liquid nitrogen cylinder in a properly labeled box. (Maintain a record of cryovials for each cell line, kept inside the liquid nitrogen cylinder)

4.4.5: Transfection of DNA in different cell lines

PEI reagent was used for all the transfection.

We seeded cells in 50-60% confluency to achieve healthy and well-spread cells for imaging experiments.

Seed cells in glass bottom chamber (35mm dish) the day before, for all the imaging experiments. Dilute required DNA and transfection reagents in 2 different tubes containing 100 μ l of incomplete media (DMEM medium without serum and antibiotic) each. PEI transfection reagent was used in 1:3 DNA to transfection reagent ratio. Incubate two tubes separately for 5-10 min at room temperature. Mix both the diluted DNA and transfection reagent together from two different tubes and incubate for another 1hr. Add 200 μ l of the mixture to the glass bottom chamber dropwise. Mix gently. Imaging was done 48hrs post transfection. All the CRISPR associated plasmids were transfected in the concentration of 2 μ g while Golgi marker GalNacT2-GFP was used in a concentration of 200ng

4.4.6. Kill curve for puromycin selection:

U2-OS cell line was subjected to an increasing amount of puromycin concentration. The minimum concentration of puromycin needed to kill all cells over the course of one week was determined. Plate cells in 1ml complete media in a 12 well plate each. Ideally, cells should reach 60-80% confluency on the day of introducing antibiotic. After 24 hr of seeding cells, antibiotic was added in an increasing concentration of 150, 250,350,450,550,650,750,850,950 and 1050

ng/ml. This experiment was done in duplicate. One well with cells and no antibiotic was introduced as a control well. Every day the culture was examined for visual toxicity over 1 week. Change the media every 2 days. At a low dose, we could see minimal visual toxicity even after 7 days while at high dose all cells were dead within 2-3 days of antibiotic selection. The optimal concentration at which all cells were dead after one week of puromycin selection was 750-850ng/ml. We chose the concentration 800ng for making puromycin selective, stable cell lines.

4.4.7.: Stable clone preparation:

The optimum concentration of puromycin used for U2-OS cell line was 800ng/ml. After 24 hr of seeding U2-OS cells (50-60% confluent) in a 35 mm plate, transfect the cells with the CRISPR plasmid targeting the desired gene (GOLPH3, GOLPH3L or ARF1). The transfection reagent Polyethyleneimine (PEI) was used. For a 1 μ g concentration of CRISPR DNA about 3 μ l PEI reagent was used. We used 2 μ g DNA for transfection. After 24 hr the transfected cells were trypsinized and seeded onto 90mm plate with 10 ml complete media. Further after 24 hr, replace the complete media with complete media containing 800ng/ml puromycin (optimal concentration obtained from kill curve analysis). After every 2 days, change the media. Continue this until some large colonies were visible that could be spot trypsinized (using 8-16 μ l trypsin) and plated onto 12 well plates for the single pure colony. Once the cells in 12 well were 80-90% confluent, they were trypsinized and seeded onto 60 mm plate in duplicate. 80-90% confluent cells from 60 mm plate were used to make freeze down, and preserve the vials in liquid nitrogen containing tank. Meanwhile, use one of the 35mm plate containing the desired clone for genomic DNA preparation. Note that throughout the experiment from selection to making freeze down of single clone cells were maintained in complete media containing 800ng/ml puromycin.

4.4.8.: G-DNA preparation of mammalian cell line:

Stock solutions to be prepared: 1M Tris-HCl, pH-9, 0.5M EDTA, pH-8, 20% SDS, 8M potassium acetate, Isopropanol, 70% ethanol and 1X TE, pH-8 containing RNase.

Method- After the cells grown are 80-90% confluent they can be harvested for genomic DNA preparation. Discard the medium from the plate and give one wash of 1X PBS. Wipe off any drop of PBS left. Add 1ml of Solution A. Swirl the solution all over the plate by tilting the plate. Pull it together with a pipette tip. Transfer the extract directly into eppendorf tube (preferably without pipetting). Immediately transfer the tube to 72°C heating block. Incubate at 72°C for 30 min. Add 140µl of 8M Potassium acetate for each 1ml of the extract (70µl for 0.5ml) Mix by shaking the tube vigorously (Do not use vortex mixer). Leave the tube on ice for 30 minutes. Centrifuge 20C at 12000 RPM for 20 minutes. Transfer the supernatant to a fresh tube carefully without taking the white precipitate. Precipitate the DNA by adding 0.5ml of isopropanol at room temperature for 5-10 minute. Mix the solutions only by shaking the tube vigorously. Do not vortex. Centrifuge at room temperature at 12000rpm for 15 minutes. Pour off the supernatant. Add 1ml 70% ethanol. Invert the tube 3-4 times to let the salt dissolve. Centrifuge RT at 10000rpm for 5min. Pour off the ethanol. Keep the tube inverted on the tissue paper for drying. Dissolve the DNA in 50 µl 1X TE pH 8 containing RNase, incubate at 37°C for 1hr. Store DNA at 4°C.

4.4.9.: T7 micronuclease assay:

Most of the guide sequence targeted for knock out was mostly present in the exon 1 of the gene. To check the indels in the desired region, we had done PCR to include the target andflanking

region at 5' and 3'. The desired PCR length was almost less than 1kb. Based on the protocol used for PCR using Phusion DNA polymerase or Dynazyme Taq polymerase obtain the desired amplicon. If the target region has indels, we could determine by using T7 endonuclease, which will cut even if single nucleotide deletion or insertion is present.

Initially, the PCR for the desired region was done using template genomic DNA of the control U2OS cells and the samples for ARF1 KO clones. Then the components given in the table were mixed to make a volume of 20 μ l and incubated at 99°C for 5 min in a boiling water bath, and it was allowed to cool to room temperature gradually. Ramp down strategy will enable the mixing of control and mutant PCR product randomly.

Table 4.9: T7 reaction set up

Contents	Control	Mutant
PCR from control	5 μ l	5 μ l
PCR from mutant	-	5 μ l
Buffer 2	2 μ l	2 μ l
MiliQ	13 μ l	8 μ l

Then to the 10 μ l of this mix 0.2 μ l, the T7 enzyme was added in both control and mutant Ramp down PCR mix. It was incubated for 6hr at 37°C and stored at 4°C. Even if a single nucleotide deletion or insertion is present T7 endonuclease will cleave and generate two bands release smaller than the entire length amplicon. Visualise T7 treated and untreated sample alongside in agarose gel.

4.4.10: Mammalian Live Cell Imaging[109]

DMEM without Phenol Red, 1X PBS

Preparation of Mammalian Sample-

Seed cells in glass bottom chamber plate or coverslips (0.15 mm thickness). After transfection live cell imaging can be done at different time points based on experimental need. In most of our experiments, we did imaging 48 hours post-transfection. Before starting imaging, turn on the microscope incubation chamber (37°C and 5% CO₂).

4.4.11: Microscopy settings for mammalian cell line

Leica SP8 confocal microscopes were used for different experimental need.

Microscope setting involved

1. 63X 1.4NA oil immersion objective
2. 512 X 512 format
3. 1 airy-unit pinhole
4. Z step size 0.35µm

Special measures in Leica-STED

1. Averaging - 2
2. HyD detectors
3. Bidirectional scans on
4. Galvo flow always on
5. Zoom – 2
6. Scan speed- 700 Hz

Chapter 5

**Study the regulation of Golgi cisternal size by
VPS74 in budding yeast *S. cerevisiae***

5.1: Introduction

Vps74 (Vacuolar protein sorting -74) is a Golgi associated peripheral protein; it is the yeast homolog of mammalian oncogene GOLPH3. The Mammalian homolog has been shown to affect Golgi morphology [5]. Knockdown of GOLPH3 makes Golgi compact while overexpression causes Golgi to be dispersed [78]. Role of Vps74 in Golgi size regulation is not studied. Few different functions of these homologous proteins have been reported, GOLPH3 is involved in anterograde transport [5] while Vps74 in retrograde transport [7]. GOLPH3 can rescue the function of Vps74 in its null mutant [7]. This also shows functional conservation of the protein in two species. Arf1 is reported to alter the Golgi size. Interaction of Vps74 with Arf1 also gives a hint that Vps74 has some role in regulating Golgi size. Hence there is the necessity of functional study of Vps74 in Golgi size.

The mammalian system has stacked Golgi, which does not enable to distinguish early and late compartment in live cell imaging. The dispersed Golgi cisterna in *S. cerevisiae* allows the study of any protein in cisternal maturation. Functional study of Vps74 was done, not only concerning Golgi size regulation but also concerning cisternal maturation. When *VPS74* was deleted in two-color system JK9 Vrg4- Sec7, it resulted in enlarged late Golgi phenotype and mislocalization of the marker, GFP-Vrg4 (Fig 5.13). Since we could not infer the effect of Vps74 deletion on early Golgi size with Vrg4 marker, deletion of *VPS74* was also done in another two-color system JK9 Rer1- Sec7. *VPS74* deletion resulted in enlarged late Golgi size (Sec7 6X DsRed) but did not alter the early Golgi size (Rer1 -3X iGFP) (Fig 5.14). The fluorescent signal of Rer1 3X iGFP was

feeble for live cell imaging. Hence we chose another early marker Gea2 which is earlier in maturation time scale than Vrg4. Gea2 labeled cisterna matures into Vrg4 labeled cisterna (Fig: 5.4) and thereby Gea2 can be used as an early marker. We deleted *VPS74* in JK9 Gea2-Sec7 strain (Fig 5.15). We observed *VPS74* deletion alters only late cisternal size (Sec7).

VPS74 has two important domains that interact with COPI (Coatomer protein I) and Arf1 (ADP- Ribosylation Factor) [85]. To identify if through these interactions Vps74 regulates the Golgi size, we created an Arf1 interacting domain deleted strain (Vps74 67-345 Δ) and mutated the arginine residue at 6-8 position (COPI interacting residues) of *VPS74* with alanine residues. Overexpression of mutant *VPS74* with altered COPI interacting residues (R replaced with A at 6th to 8th position) in *vps74 Δ* strain resulted in an enlarged late cisterna (Fig 5.20). We got the same enhanced late cisterna phenotype on deletion of Arf1 interacting domain – *VPS74* 67-345 region (Fig 5.19). We also reported the role of *ARF1* deletion in JK9 Gea2- Sec7 strain.

Arf1 and Vps74 are functional at trans cisterna. *ARF1* regulates COPI association in membrane trafficking while *VPS74* governs the transport of certain COPI associated Golgi resident mannosyltransferases. We speculated that Arf1- Vps74 interaction has some critical role in regulating Golgi size. We have studied the cisternal size in a double knock out of Vps74 and Arf1. We checked whether Arf1 overexpression in Δ vps74 or vice versa has any phenotype rescue. We also verified the effect of overexpression of Arf1 or Vps74 on Golgi cisternal size.

In brief, we have studied the role of Vps74 in the regulation of Golgi cisternal size and also tried to understand other maturation parameters. It helped us to know the link of proteins, Vps74, and Arf1 on Golgi cisternal size and maturation regulation.

We tried to understand the mechanism by which the Golgi cisterna size is altered in *vps74* and *arf1* null mutants. In Δ *arf1* strain, Vps74 had accumulated to the Sec7 compartment. This Vps74 is maintained in a gradient manner, higher at early Golgi cisterna compartment and lower towards the late cisterna, while PI4P phospholipid abundant in Golgi has an opposite gradient higher towards late Golgi cisterna. The PI4P brought along with Vps74 mediated COPI coated vesicles in the early Golgi compartment is dephosphorylated by Sac1. The PI4P gradient was monitored along the Golgi compartment in wild-type versus different null mutants.

We demonstrated altered PI4P gradient pattern in null mutants. Further, we also studied the role of degradation of PI4P levels on Golgi morphology. The Pik1 kinase is present at late Golgi compartment and helps in phosphorylation of phosphatidylinositol and thereby forms higher amounts of PI4P. PIK1 is an essential gene, and a conditional mutant of *pik1^{ts}* has reduced the PI4P level. We checked the effect on Golgi cisterna in case of *pik1^{ts}* at permissive (22°C) and non-permissive conditions (37°C). This gave a detailed picture of altered Golgi cisterna in *pik1^{ts}* mutants explained in the result section.

5.2: Results

This section includes seven segments. The first section (5.2.1) describes the cloning strategy of epitope tagging *RAS2* (plasma membrane protein), *Vps74* and *Rer1* (early Golgi protein). The second part (5.2.2) describes homotypic fusion frequency based on a temporal scale of maturation. The third part (5.2.3) explains the role of deleting or overexpressing protein *Vps74* or *Arf1* on the regulation of Golgi size. The fourth part (5.2.4) emphasizes on the overall altered maturation parameters in different null and overexpressing mutants. Section 5.2.5 explains *Arf1* can alter the distribution of *Vps74*. Section 5.2.6 describes the PI4P gradient along the Golgi compartment in null mutants. Section 5.2.7 explains effect of *Pik1^{ts}* on Golgi cisterna. Thus this section demonstrates the plausible combined role of *Vps74* and *Arf1* on Golgi size regulation in case of simple model organism *S. cerevisiae*.

5.2.1 Development of fluorescently tagged - Ras2p, Vps74, and Rer1

Ras2p is abundant in the plasma membrane, and it is epitope tagged at N-termini to make a potent cell membrane marker. Made mCherry-Ras2 for labeling the plasma membrane. *Vps74* studied in detail in this project also is epitope tagged at N-termini with 3X-GFP to locate its association with the Golgi compartment. We examined the effect of *VPS74* deletion on early Golgi cisterna using widely used *Vrg4p* (Vandate Resistance Glycosylation) marker, *Rer1* (Retention in the Endoplasmic reticulum) and another early cisterna marker *Gea2*. *Rer1* is epitope tagged at its N-termini with three tandem copy of GFP.

A) Development of membrane marker mCherry- Ras2:

In all cells, the organelle size is maintained concerning the cell size. This gives us the comparative term karyoplasmic ratio for the nucleus. Similarly, to check out any organelle size alteration concerning cell size in *S.cerevisiae*, a cell membrane marker was developed. Ras2p a GTP binding protein is majorly localized to the plasma membrane. We tagged N-terminal of the *RAS2* gene with mCherry. Various cloning strategy was used to replace the endogenous copy of *RAS2* with mCherry-*RAS2*. However, the final construct that worked was mCherry-Ras2 expressed under the control of strong TPI promoter at Tryptophan locus. Appendix section 10.1 describes the cloning strategy for mCherry-Ras2 . This construct was further used to mark the cell membrane and thereby quantify the cell volume concerning any organelle size studied in our lab for wild-type strain and other mutants. The image represents the cell periphery marked with mCherry-Ras2 (Fig 5.1).

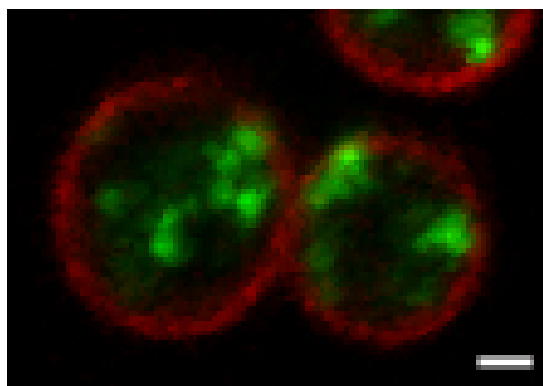


Figure 5.1: JK9 wild-type strain with late cisterna marked with Sec7- 6X GFP and the cell membrane labeled with mCherry- Ras2

B) Fluorescent labeling of Vps74:

Vps74 is a known functional trans peripheral protein with a concentration gradient higher towards the early Golgi compartment. It was essential to tag Vps74 with a fluorescent marker and to check its localization to Golgi. We tried to tag C-termini of endogenous *VPS74* with GFP. We could not see the punctate like pattern as in case of Vps74-GFP. C terminal of Vps74 has active sites important for interaction with PI4P, Sac1 and Arf1. Probable C-termini tagging affects these interaction and Vps74 protein is affected. GFP-Vps74 is functional [110]. Later Vps74 was tagged at its N-termini. Amongst different strategy, tagging of three tandem copies of GFP at N-terminus of *VPS74* gene gave a precise, distinct localization of Vps74. Appendix section 10.5 details the cloning strategy for the same. The below image represents the localization of Vps74 (green puncta) concerning trans-Golgi marker Sec7 (red) (Fig: 5.2).

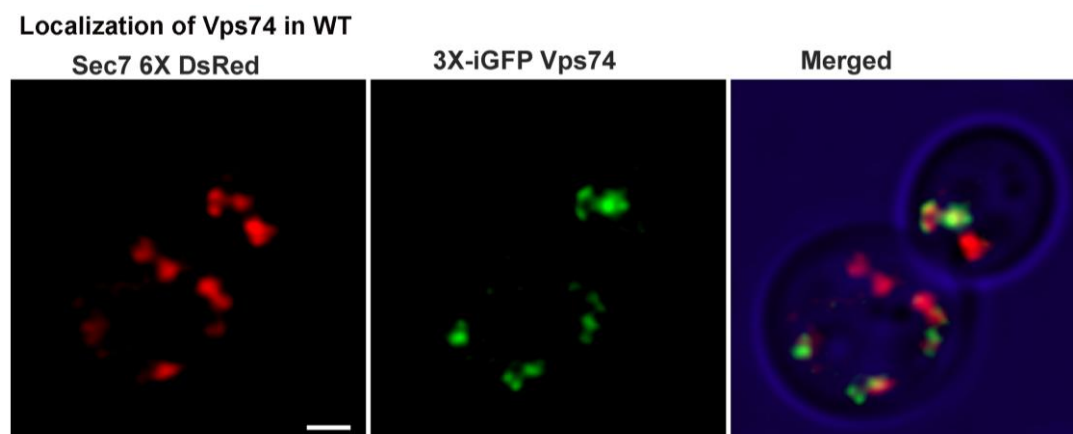


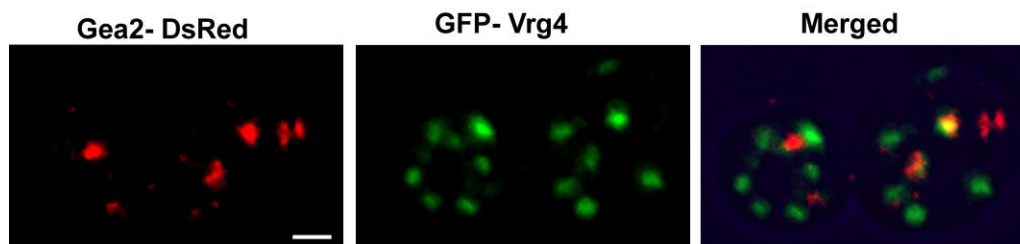
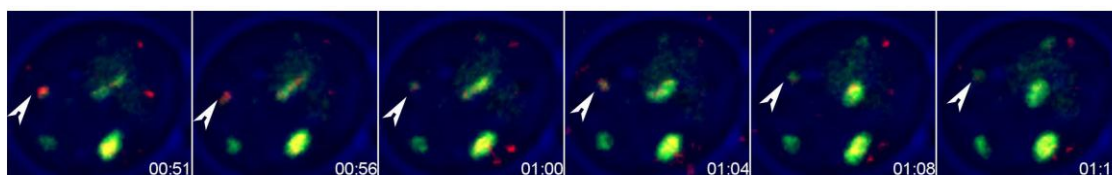
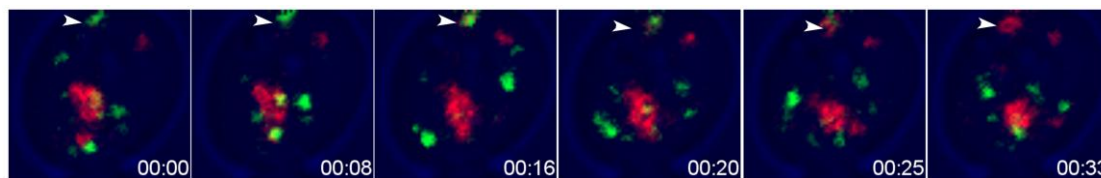
Figure 5.2: JK9 wild-type strain with 3X-iGFP Vps74 (green) and Sec7- 6X Ds-Red (red)

C) Cloning of 3X-iGFP Rer1:

To verify the effect of deletion of genes on early cisterna, we had used early cisterna markers Vrg4 and Gea2. On deleting *VPS74* gene, Vrg4 localization was affected (Fig 5.13). Rer1 was chosen as another early cisterna marker to validate the effect of *VPS74* deletion. Appendix section 10.6 demonstrates the cloning step for 3X iGFP Rer1. The final plasmid was linearized with restriction enzyme PstI and then transformed into the desired yeast strain. We made another two-color strain in *S.cerevisiae* with early marker 3X-iGFP Rer1, and late cisterna marked with Sec7- 6X DsRed (Fig 5.15).

5.2.2 Homotypic fusion frequency based on the temporal scale of maturation

The fusion of similar Golgi cisterna, i.e., two early or two late cisternae is termed as homotypic fusion. We observed decidedly less homotypic fusion frequency with markers Vrg4 or Sec7 [87]. We speculated that the rate of homotypic fusion would be more if we chose a Golgi tag earlier to Vrg4 . To prove fusion frequency is high for temporally earlier placed cisterna markers, two other early markers Gea2 and Rer1 was used. Fig 5.3 shows Vrg4 and Gea2 localization . We observed that Gea2 (red) matures into Vrg4 (green) and thereby proved Gea2 protein falls temporally ahead of Vrg4 (Fig 5.4).

Figure 5.3: Representative two color strain Gea2 DsRed- GFP-Vrg4**Figure 5.4:** Time point of 4D imaging of two color strain Gea2 DsRed- GFP-Vrg4 represent Gea2 (red) matures to Vrg4 (green)**Figure 5.5:** Gea2 (green) matures to late marker Sec7 (red)

We also observed that in JK9 Gea2- Sec7 strain, Gea2 matures into Sec7 (Fig 5.5). Both the observation of Gea2 maturing into another early marker Vrg4 and also Gea2 maturation to late marker Sec7 validates the positioning of Gea2 before Vrg4 and Sec7 on the temporal maturation scale of Golgi markers. Fig 5.6 represents the localization of Gea2 (red) marker concerning trans marker Drs2p (green).

Figure 5.6: Gea2 (red) does not co-localize with well established trans marker Drs2 (green)

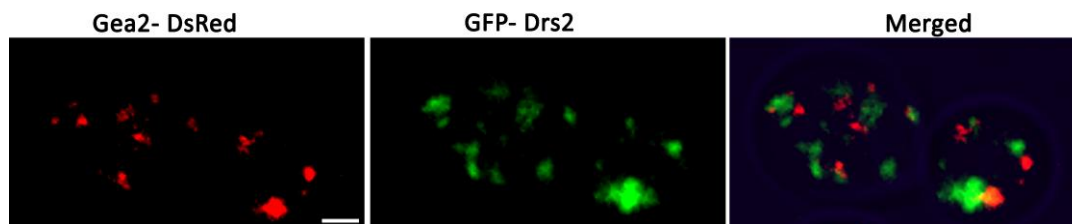
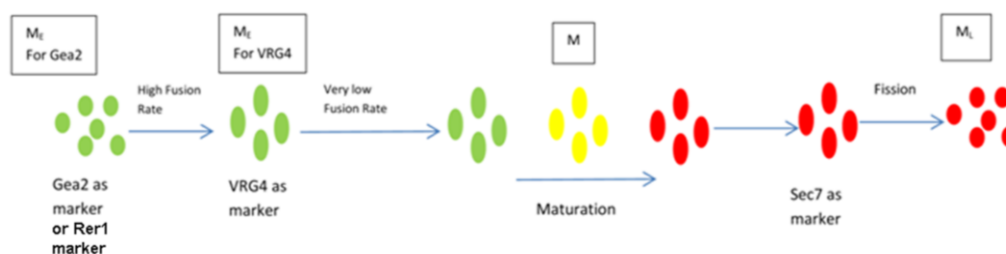


Figure 5.7: Homotypic fusion frequency on the temporal scale of maturation



We hypothesized that the markers falling earlier on the temporal scale of maturation would show increased homotypic fusion events (Fig 5.7). To validate this hypothesis; we used cisterna markers Rer1, Gea2, Vrg4, and Sec7. Amongst this Rer1, Gea2 and Vrg4 are early Golgi cisterna markers while Sec7 is late Golgi cisterna marker. We constructed two color strain – JK9 Gea2- 3X GFP/Sec7- 6X DsRed and JK9 Rer1-3X iGFP/ Sec7- 6X DsRed. We did 4D imaging of the two color strain constructed. Captured 5-minute movies, and analyzed ten such movies for each strain. Fig 5.8, 5.9, 5.10 & 5.11 represents the homotypic fusion event for different Golgi marker. We calculated homotypic fusion events for the two-minute frame from 1- 3 minutes and converted it to an event per minute. We analyzed the fusion events for marker Rer1, Gea2, and Sec7 markers.

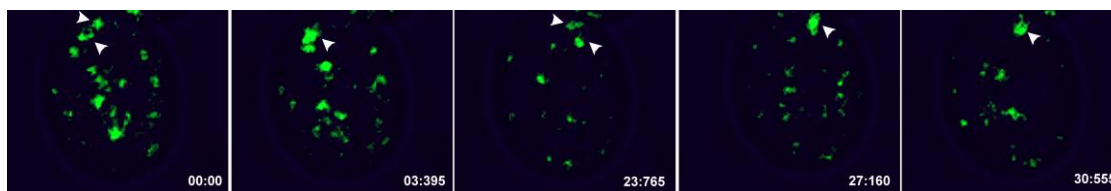
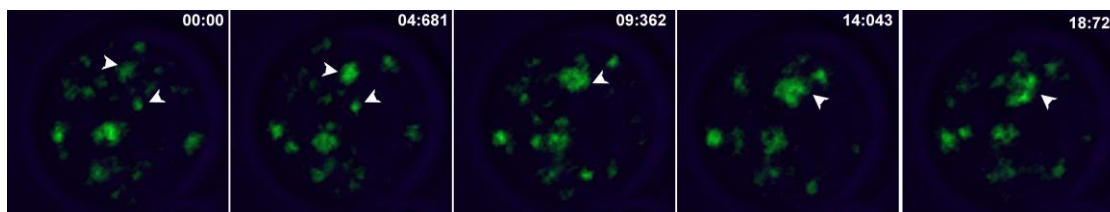
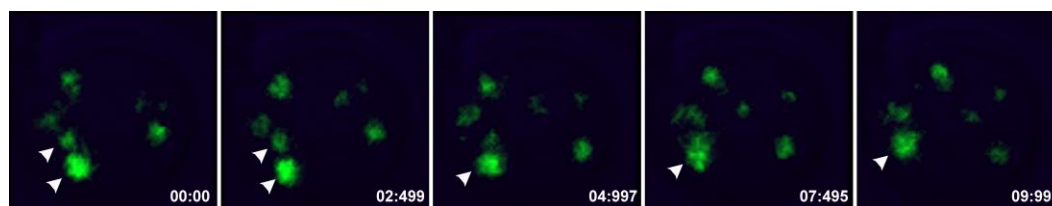
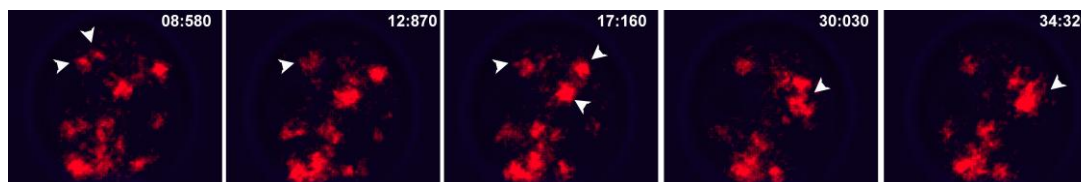
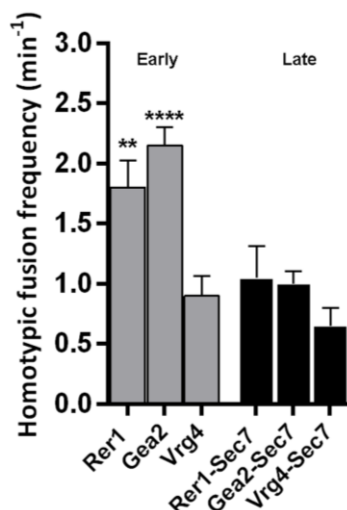
Figure 5.8: Homotypic fusion for 3X-iGFP Rer1**Figure 5.9:** Homotypic fusion for Gea2 3X-mEGFP**Figure 5.10:** Homotypic fusion for GFP-Vrg4**Figure 5.11:** Homotypic fusion for Sec7- 6X DsRed

Figure 5.12: Homotypic fusion frequency for markers Rer1, Gea2, Vrg4 and Sec7, N=10 movies.

Student t-test. **p=0.0047, ****p<0.0001



From the graph plotted (Fig 5.12), we observed that the fusion events with early marker Rer1 and Gea2 are higher as compared to early marker Vrg4 and late marker Sec7. Rer1 and Gea2 fall earlier in the temporal scale of maturation markers used. Thus we demonstrated high fusion frequency for the very early markers like Rer1 and Gea2 than Vrg4 and Sec7. Therefore the fusion events are more evident amongst the earliest marker on the temporal scale, and we had experimentally shown fusion events with different early Golgi proteins.

5.2.3 Deletion and overexpression of gene *VPS74* and *ARF1* and its effect on the Golgi size

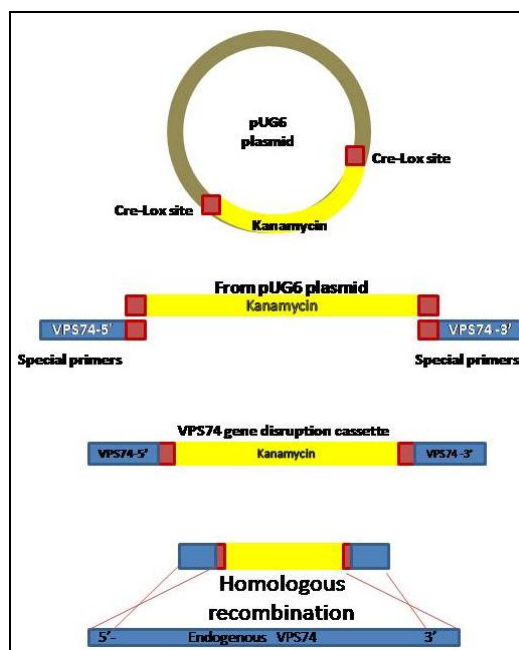
A) Knock out of *VPS74* gene:

Knock out of *VPS74* gene was done by homologous recombination using a gene disruption cassette against it [97, 98]. The gene disruption cassette had the cre-lox flanking site with centrally placed kanamycin cassette and 5' and 3' overhangs

homologous to *VPS74*. This cassette was amplified using template plasmid pUG6 (Kan+).

However, for enabling homologous recombination of gene disruption cassette with the endogenous copy of *VPS74*, homology site was generated at the 5' and 3' end of the kanamycin gene disruption cassette using special primers (Fig: 5.13). These primers had 50bp sequence homology to *VPS74* at 5'-end and 19-20 bp sequence of vector pUG6 at 3'-end. Using primers Vps74-Kan-Fw and Vps74-Kan-Rv (Refer Table 10.4 for the sequence of primers) gene disruption cassette with *VPS74* homology was created (Appendix section 10.5).

Figure 5.13 Gene knockout strategy



Transformed gene disruption cassette into the two-color system of *S.cerevisiae*. By homologous recombination, Kanamycin cassette having cre-lox flanking end replaced

VPS74. The deletion of endogenous *VPS74* was confirmed by PCR (Appendix section 10.5). We had even used Uracil cassette for removal of *VPS74* or specific domains of *VPS74* when any strain had its kanamycin marker unavailable. Used the template plasmid pUG72 with uracil as selection marker.

Deletion of *VPS74* gene from the two color system JK9 Vrg4 -Sec7, severely hampered the localization of GFP-Vrg4 (early cisterna) while the trans marked cisterna Sec7 6X Ds-Red was seen to be enlarged (Fig 5.14).

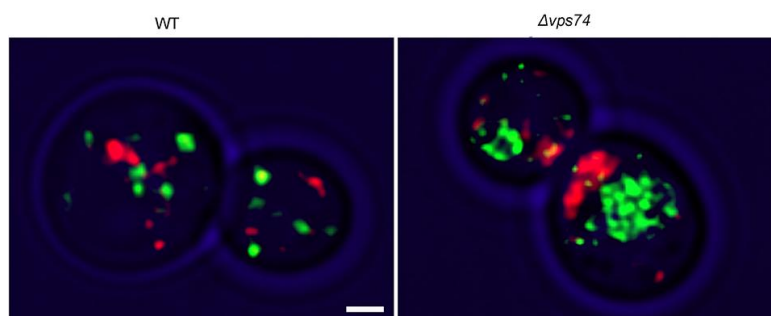


Figure 5.14: JK9 wild-type and the $\Delta vps74$ mutant with GFP-Vrg4 (early marker) and Sec7- 6X Ds-Red (late marker)

It could not clearly explain the effect of $\Delta vps74$ on early cisterna. Hence we knocked out *VPS74* in two-color system JK9 Gea2 – Sec7. Wherein there was no alteration of early Golgi cisterna, but it had resulted in enlargement of trans-Golgi cisterna (Fig 5.15). To further validate the effect of *VPS74* deletion in early cisterna we used two color strain JK9 Rer1- Sec7. This observation also made us infer that *VPS74* deletion had no effect on early Golgi cisterna but had enlarged the trans-Golgi cisterna (Fig 5.16).

Figure 5.15: JK9 wild-type and the $\Delta vps74$ mutant with Gea2-3X mEGFP (early marker) and Sec7- 6X Ds-Red (late marker)

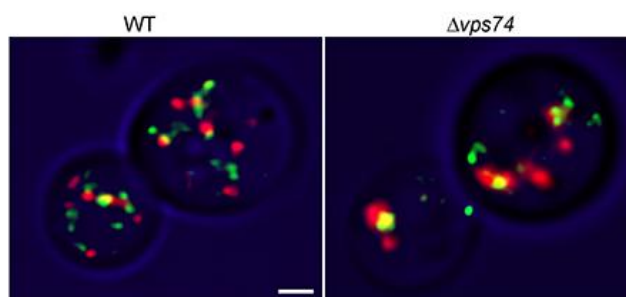
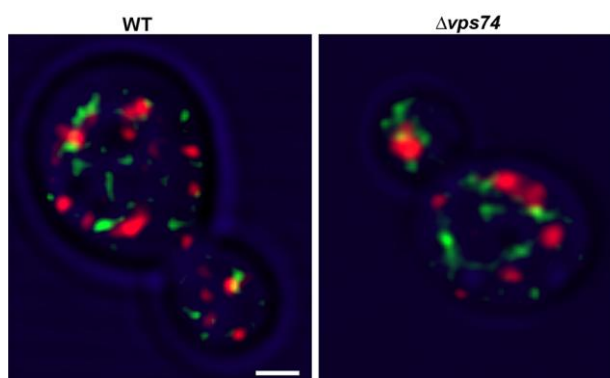


Figure 5.16: JK9 wild-type and the $\Delta vps74$ mutant with Rer1- 3X iGFP (early marker) and Sec7- 6X Ds-Red (late marker)



We did quantify all cisterna maturation parameters like the number, average volume, average diameter, homotypic fusion frequency, maturation frequency, and persistence time for WT and $\Delta vps74$ in Gea2-Sec7 epitope-tagged background. Parameters volume and diameter of cisterna were measured from images while for quantifying other parameters with time dimension we did 4D imaging.

Details of parameter measurement-

Calculated the following parameters from 4D movies. The sample analysis of 10 movies is maintained for measuring cisterna number, homotypic fusion frequency, maturation frequency and persistence time

- 1) The number of cisternae (early or late) for ten-time frames was averaged to obtain the cisterna number.
- 2) Two small cisternae (early or late) fuses to form a big cisterna. It is called homotypic fusion. Such fusion event frequency was calculated from period 1-3 minutes and converted to the event per minute.
- 3) Maturation is the event of the transformation of early cisterna (green) to late (red) (Fig: 5.5). Maturation frequency occurring for period 1-4 minutes was converted to the event per minute.
- 4) An early cisterna once appeared in the cell slowly disintegrates and matures into late cisterna which marks the period or persistence time of early cisterna. While the late cisterna after appearing in the maturing cisterna stays for a while and then disintegrates and disappears from the cell, marks the persistence time of late cisterna.

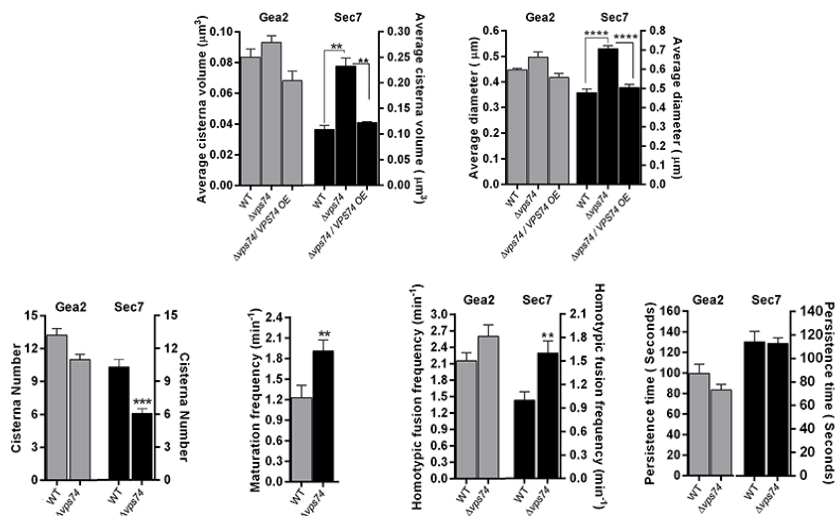


Figure 5.17: Cisterna maturation parameter graphs for average cisternal volume, average diameter (Upper 2 graphs), average number, maturation frequency, homotypic fusion frequency and persistence time (lower four graphs) is represented. Student t-test. S.E.M (Standard Error Mean). **p=0.0024 (Sec7 average volume) 0.0086 (maturation frequency graph) 0.0090 (Sec7 homotypic fusion frequency), ***p<0.0001, ****p<0.0001.

The average volume (N=60 cells) and diameter (N= 10 cells) were calculated from three independent experiments. The early and late punctae quantified in each cell was approximately more than 8 in wild type. The graph (Fig 5.17) represents that the increase in the average volume of late cisterna in $\Delta vps74$ is statistically significant. Even the late cisterna diameter (Fig 5.17) also showed a considerable increase in $\Delta vps74$ as compared to wild-type, while the number of late Golgi cisterna had reduced in $\Delta vps74$ as compared to wild-type (Fig 5.17). All the statistical analysis is carried out using Graph Pad Prism 5. Student's t-test was performed for all the parameters analyzed.

Homotypic fusion frequency in late cisterna had increased in $\Delta vps74$ (Fig 5.17). Due to the increased late cisterna fusion frequency, there was a reduction in number, while an increase in the volume of late cisterna. Maturation frequency in $\Delta vps74$ had increased as compared to WT (Fig 5.17). However, the persistence time of early and late cisterna in $\Delta vps74$ did not alter as compared to WT (Fig 5.17).

The following Fig 5.18 is the graphical plot for volume and diameter changes of Golgi cisterna in WT and $\Delta vps74$ with two-color Rer1-Sec7 epitope tag background. It explains that the early cisterna size is not altered.

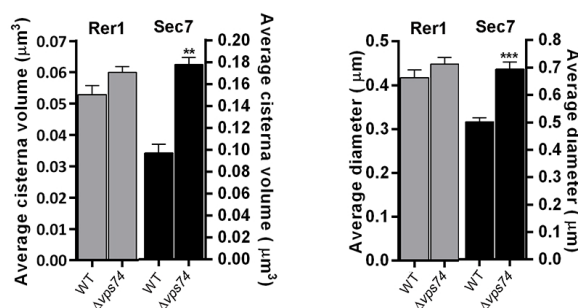


Figure 5.18: Cisterna maturation parameter graphs for average cisterna volume (N=60 cells) and the average diameter (N=10 cells) is represented. Student t-test. S.E.M (Standard Error Mean).

p=0.0014, *p<0.0001

B) Cloning to overexpress *VPS74*:

We have endogenous cloned *VPS74* with its promoter in YEplac195 vector. Appendix section 10.4 explains the cloning strategy. Used the construct YEplac195 *VPS74* for phenotype rescue experiment in $\Delta vps74$ strain (Fig 5.17). It was also used to see the effect of *Vps74* overexpression in WT, described in a later part of the result section.

C) Vps74 interacts with protein Arf1 and COPI [85]:

Vps74, an effector of PI4P, co-packages specific Golgi associated proteins with COPI coated vesicles. Thus Vps74 helps in sorting COPI cargos, while COPI function requires Arf1, and Arf1 and COPI are known to regulate cisternal maturation. Based on this we speculated that Vps74 and Arf1 might function in coordination to control cisterna maturation rate as well as the Golgi size.

Deletion of Arf1 interacting region of VPS74 (region 67-345) alters cisterna size

The region 67-345 of VPS74 interacts with Arf1 [85]. The Arf1 interacting region of VPS74 was replaced with Uracil containing gene disruption cassette. Primers Vps74-67-Leu Del- F and Vps74-Kan-Rv were used with template pUG72 to amplify the gene disruption cassette. PCR confirmed the deletion (Appendix section 10.6). In JK9 *Vps74* 67-345 Δ Gea2- Sec7, enlarged late cisterna was demonstrated (Fig 5.19) by quantifying its volume and size (Fig 5.20).

Figure 5.19: Panel shows wild-type, $\Delta vps74$ and *vps74* 67-345 Δ with Gea2 and Sec7 marker

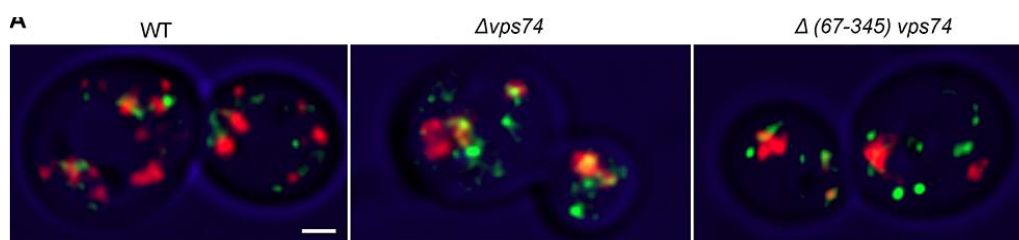
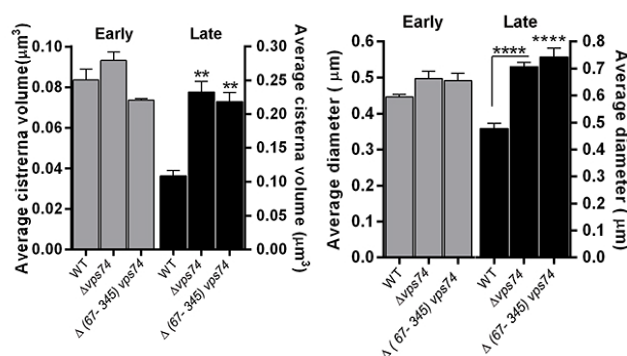


Figure 5.20: Graphical plot for average cisterna volume (N=60 cells) and diameter (N=10 cells) for wild-type, $\Delta vps74$ and $\Delta(67-345) vps74$ with Gea2 (early) and Sec7 (late) marker. Student t-test. S.E.M (Standard Error Mean). **p=0.0022, ****p<0.0001



Cloning to mutate COPI interacting residue of VPS74:

Vps74 interacts with COPI. Arginine residues at the 6-8 position of VPS74 bind COPI [85]. We tried mutating the arginine residues of endogenous VPS74 to alanine at the 6-8 position. We could not make an endogenous mutation. Hence we resorted cloning VPS74 with the alanine mutation (that would remove the COPI interacting residue arginine) at the 6-8 position in an overexpressing plasmid backbone YEplac195. The desired mutation was done by quick change mutagenesis in the YEplac195 VPS74 vector (earlier mentioned in B sub-point). Primers used were Vps74 6-AAA-8 up- and Vps74 6-AAA-8 bottom. Appendix section 10.4 describes the cloning strategy. **Thus COPI interacting domain of VPS74 was altered to see the effect on Golgi cisterna size.** Transformed YEplac195 6AAA8 VPS74 plasmid in $\Delta vps74$. We did not observe any phenotype rescue (Fig 5.21), rather cisterna was enlarged. The average volume and size for cisterna were quantified (Fig 5.22).

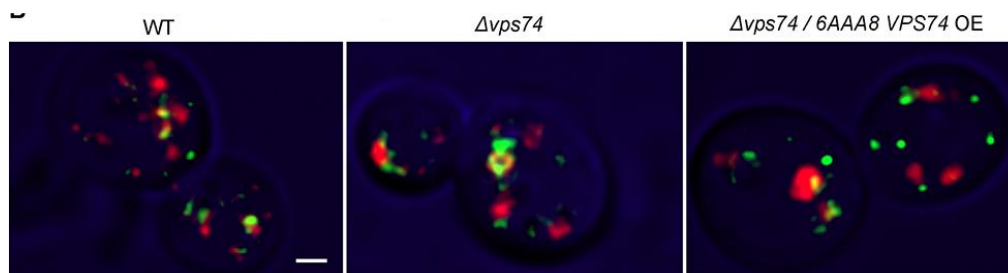


Figure 5.21: Panel shows wild-type, $\Delta vps74$ and $\Delta vps74/6AAA^8 Vps74$ OE with Gea2 and Sec7

marker

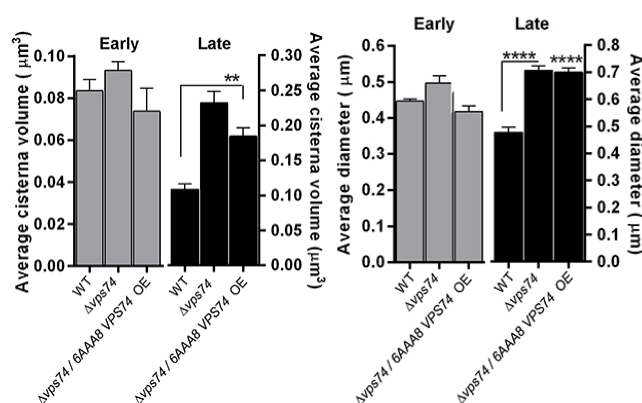


Figure 5.22: Graphical plot for average cisterna volume (N=60 cells) and diameter (N=10 cells)

wild-type, $\Delta vps74$ and $\Delta vps74/6AAA^8 Vps74$ OE with Gea2 (early) and Sec7 (late) marker.

Student t-test. S.E.M (Standard Error Mean). **p=0.0059, ****p<0.0001.

D) Double knock out of *ARF1* and *VPS74*:

Observed alteration in Golgi cisterna size in case of single knock out of genes *VPS74* (Fig: 5.14, 5.15 & 5.16) and *ARF1*. Double knock out of *VPS74* and *ARF1* is not lethal, but its effect on Golgi size was not known. In the case of $\Delta arf1$, early and late cisterna size is affected [87], while $\Delta vps74$ altered only the late cisterna size. We created endogenous $\Delta vps74$ using URA3 selection cassette in the mother strain with $\Delta arf1$.

Created double knock out in Gea2-Sec7 epitope tag (Golgi cisterna marked) two-color system. PCR confirmed the deletion of *VPS74* gene. In case of double knock out $\Delta arf1$ - $\Delta vps74$ the large cisterna phenotype persisted (Fig 5.23). However, the quantification of average volume showed that the late cisterna volume had increased significantly in a double knock out compared to single knock out $\Delta vps74$ (Fig 5.24). The cisterna size was also quantified (Fig 5.24). The cisternal volume and size alteration in a double knock out as compared to null mutant *arf1* was not significant.

Figure 5.23: Panel shows wild-type, $\Delta vps74$, $\Delta arf1$, and $\Delta arf1$ - $\Delta vps74$ with Gea2 and Sec7 marker

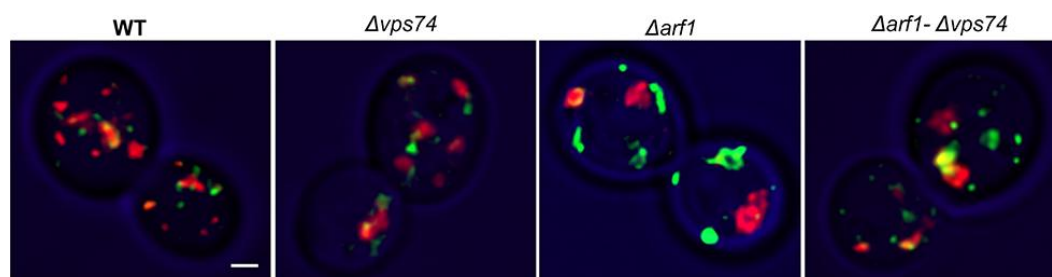
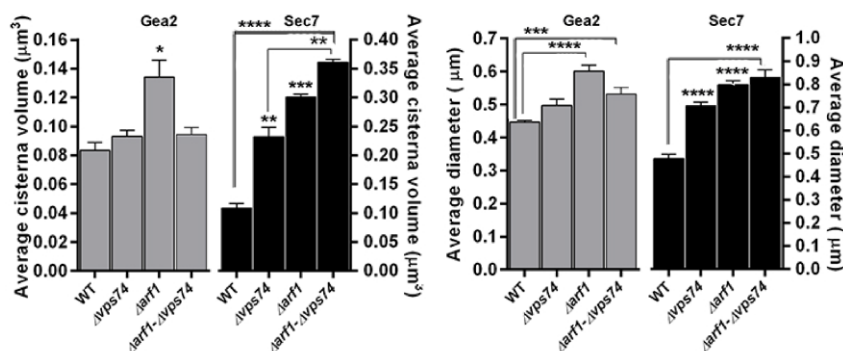


Figure 5.24: Graphical plot for average cisterna volume (N=60 cells) and diameter (N=10 cells) for wild-type, $\Delta vps74$, $\Delta arf1$, and $\Delta arf1$ - $\Delta vps74$ with Gea2 (early) and Sec7 (late) marker.

Student t-test. *p=0.0225, **p=0.0024, ***p=0.005, ****p<0.0001



The effect of $\Delta arf1$ - $\Delta vps74$ DKO gave enhanced Golgi size phenotype compared to $vps74$ null mutant. We further checked whether the enlarged Golgi phenotype is altered if one of the proteins Arf1 or Vps74 is overexpressed in the deletion background of $\Delta vps74$ or $\Delta arf1$ respectively.

E) Effect of overexpression of Arf1 in $vps74$ null mutant:

Deletion of *ARF1* interacting domain of Vps74 altered the Golgi cisterna size. Double knock out of $\Delta arf1$ - $\Delta vps74$ caused enhanced enlarged late cisterna phenotype. To further characterize the role of Vps74 and Arf1, we overexpressed one protein in the absence of other. Transformed YEplac195 *ARF1* plasmid (overexpresses Arf1) in the $vps74$ null mutant. There was phenotype reversion of enlarged late cisterna to wild-type (Fig 5.25). The average volume and size of cisterna were also quantified (Fig 5.26).

Figure 5.25: Panel shows wild-type, $\Delta vps74$ and $\Delta vps74$ / *ARF1* OE with Gea2 and Sec7 marker

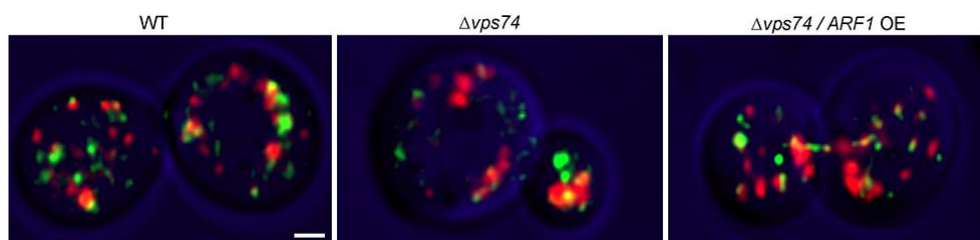
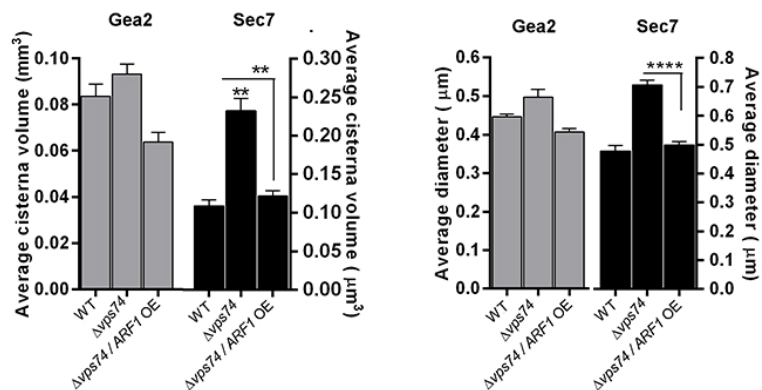


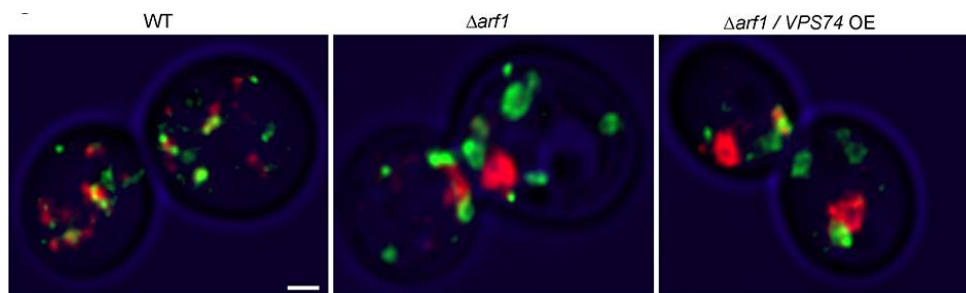
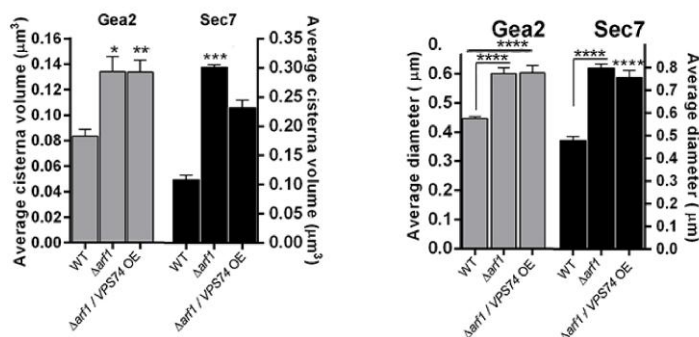
Figure 5.26: Graphical plot for average cisterna volume (N=60 cells) and diameter (N=10 cells) for wild-type, $\Delta vps74$, and $\Delta vps74 / ARF1 OE$. Student t-test. ****p<0.0001, **p=0.0024



We see the rescue of phenotype when Arf1 is overexpressed in the *vps74* null mutant (Fig 5.26). $\Delta vps74$ resulted in enlarged late Golgi cisterna is evident from this study. $\Delta arf1$ delayed the recruitment of clathrin coat at TGN [116]. We believe the Arf1 overexpression might enhance the recruitment of clathrin coat on the enlarged phenotype of $\Delta vps74$ and hence the recovery of Golgi size is observed.

F) Effect of overexpression of Vps74 in *arf1* null mutant:

Transformed YEplac195 *VPS74* plasmid (overexpresses Vps74) into the *arf1* null mutant. There was no change in the phenotype (Fig 5.27). The late cisterna size was as enlarged as in $\Delta arf1$ strain. The average cisterna size and volume was also quantified (Fig 5.28).

Figure 5.27: Panel shows wild-type, $\Delta arf1$ and $\Delta arf1 / VPS74 OE$ with Gea2 and Sec7 marker**Figure 5.28:** Graphical plot for average cisterna volume (N=60 cells) and diameter (N=10 cells) for wild-type, $\Delta arf1$ and $\Delta arf1 / VPS74 OE$. Student t-test. *p=0.0173, ***p=0.0005, ****p<0.0001

ARF1 is pre-dominant in regulating Golgi size in comparison to *VPS74* as the volume and number of cisterna affected in $\Delta arf1$ is greater [87] compared to $\Delta vps74$. Hence *Arf1* overexpressed in $\Delta vps74$ rescued the enlarged cisterna phenotype. *Arf1* is required for the clathrin coat recruitment on TGN. Thus the enhanced clathrin coat recruitment in $\Delta vps74$ might have rescued the enlarged phenotype. Deletion of *arf1* delays the clathrin recruitment [116] and also alters the maturation kinetics [87]. Thus in $\Delta arf1$, the enlarged phenotype could not be recovered to wild type when *Vps74* is overexpressed; although *Vps74* helps retrograde transport from TGN [7,8].

It is also essential to know the effect on Golgi size if Arf1 or Vps74 is overexpressed in wild-type.

G) Arf1 overexpression in WT does not alter Golgi cisterna size

YEplac195 *ARF1* (overexpresses Arf1) was transformed into JK9 Gea2-Sec7 (WT) dual color strain. There is no effect on Golgi cisterna size, if Arf1 is overexpressed in WT (wherein *VPS74* is functional).

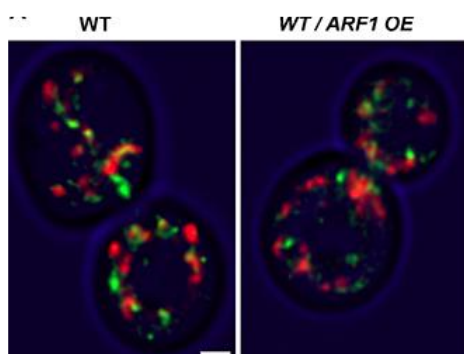


Figure 5.29: Panel shows wild-type, WT/ *ARF1* OE with Gea2 and Sec7 marker

There was no alteration in early or late cisterna after overexpressing Arf1 in WT (Fig 5.29). Quantified the average volume and diameter of cisterna (Fig 5.30) and confirmed the observation.

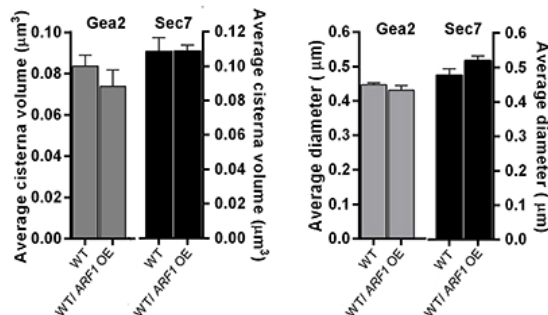


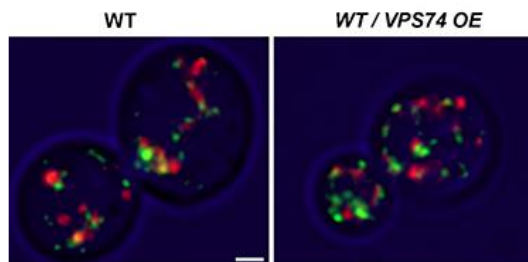
Figure 5.30: Graphical plot for average cisterna volume (N=60 cells) and diameter (N= 10 cells) for wild-type and WT/ *ARF1 OE*. Analysed statistically using Student t-test.

This result gives evidence for the critical role of *ARF1* and *VPS74* interaction in the regulation of Golgi cisterna size. These proteins are linked to regulating Golgi cisterna size.

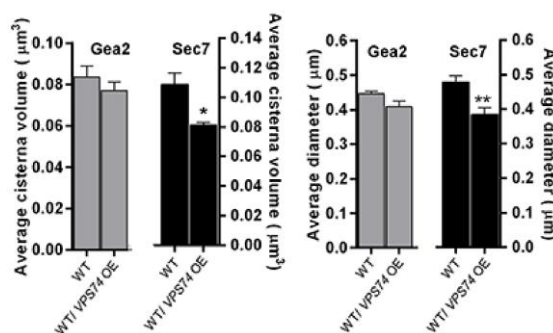
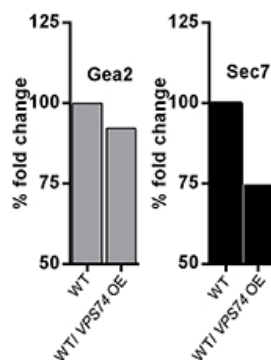
H) *Vps74* overexpression in WT alters late Golgi cisterna size:

$\Delta arf1$ or $\Delta vps74$ or both $\Delta arf1$ - $\Delta vps74$ deletions affect the late Golgi cisterna size. *Arf1* is speculated to be pre-dominant over *Vps74* in functionally controlling Golgi cisterna size (mentioned in sub point E). Overexpression of *Vps74* in wild-type represented in Fig 5.31 does not clearly distinguish the altered Golgi cisterna size, but significant number of cisterna was smaller. This difference in reduced average volume and diameter were quantified (Fig 5.32).

When *Vps74* was overexpressed in JK9 Gea2- Sec7 strain (WT), a slight reduction in the late cisterna size and volume was observed while there was no change in early cisterna size and volume (Fig 5.32). The percent graph plot represents a 25% reduction in volume compared to that of WT (Fig 5.33).

Figure 5.31: Panel shows wild-type, WT/ *Vps74* OE with *Gea2* and *Sec7* marker**Figure 5.32:** Graphical plot for average cisterna volume (N=60 cells) and diameter (N=10 cells) for wild-type and WT/ *Vps74* OE. Analysed statistically using Student t-test. *p=0.0268,

**p=0.0024.

**Figure 5.33:** Graphical plot for percent fold change of average cisterna volume for wild-type and WT/ *Vps74* OE

I) Overexpression of Arf1 and Vps74 in wild-type dual color strain Rer1- Sec7

Arf1 and Vps74 were overexpressed separately in JK9 Rer1- Sec7 dual color strain. 2D projection of the strains is represented along (Fig 5.34 & 5.35).

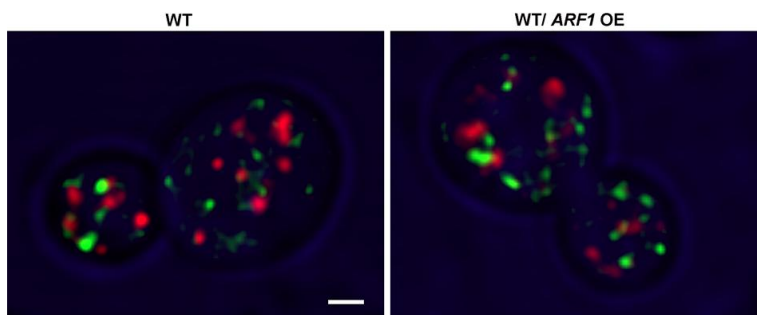


Figure 5.34: Panel shows wild-type and WT/ Arf1 OE with Rer1 and Sec7 marker

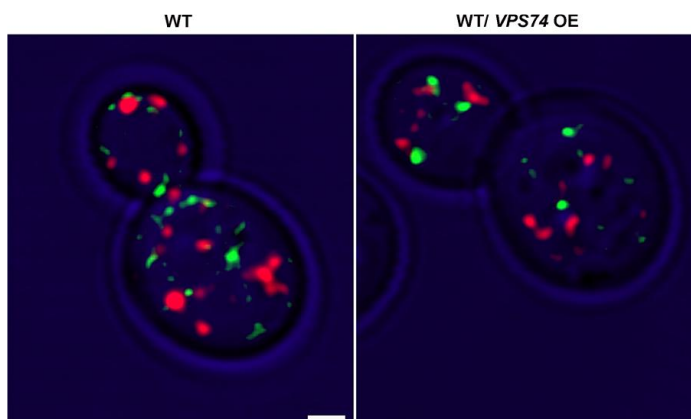


Figure 5.35: Panel shows wild-type and WT/ VPS74 OE with Rer1 and Sec7 marker

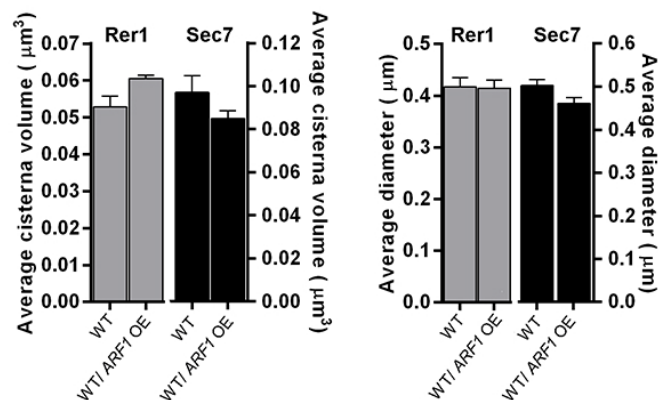


Figure 5.36: Graphical plot for average cisterna volume (N=60 cells) and diameter (N= 10 cells) for wild-type and WT/ *ARF1* OE with Rer1 and Sec7 marker. Statistically non-significant. Used

Student t-test.

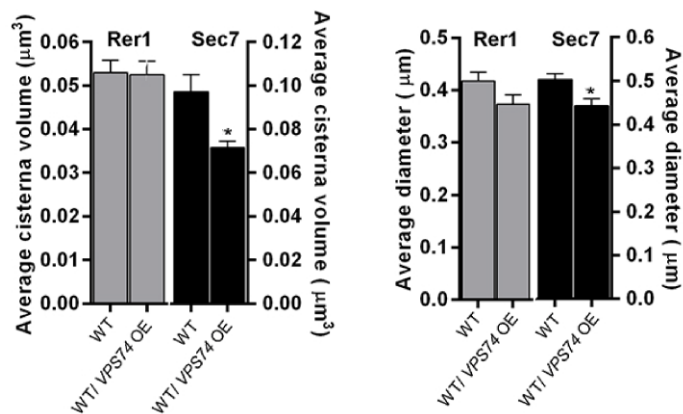


Figure 5.37: Graphical plot for average cisterna volume (N=60 cells) and diameter (N=10 cells) for wild-type and WT/ *VPS74* OE with Rer1 and Sec7 marker. Performed Student-t test.

*p=0.0372 (average volume), *p=0.0116 (average diameter)

The average diameter and volume of Golgi cisterna were quantified (Fig: 5.36 and 5.37). Arf1 overexpression and Vps74 overexpression in the wild-type strain independently did

not alter the early marker Rer1 cisterna size and volume. Vps74 overexpression in wild-type slightly decreased the late marker Sec7 cisterna volume and diameter.

5.2.4 How the cisterna maturation parameters differ for WT, null mutants and overexpressing strain?

We quantified the cisterna maturation parameters for other null mutants and overexpressing (OE) strains like $\Delta arf1$, $\Delta arf1 / VPS74 OE$, $\Delta vps74 / ARF1 OE$, $VPS74 OE$ and $ARF1 OE$ expressing cisterna markers Gea2-3X- GFP and Sec7 6XD_sRed. Parameters were quantified from mother cell acquired with N=10 movies for each strain.

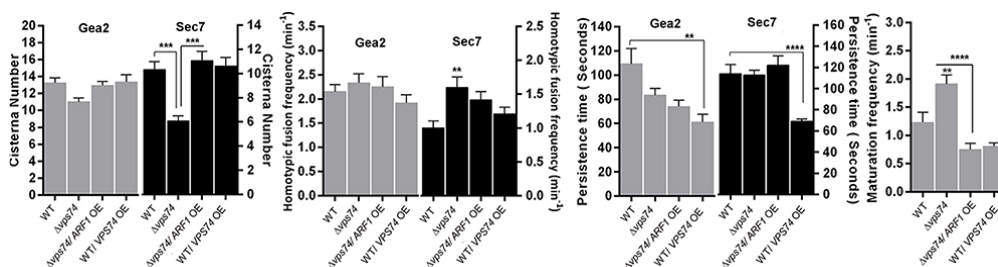


Figure 5.38: Cisterna maturation parameter comparison for WT, $\Delta vps74$, $\Delta vps74 / ARF1 OE$ and WT / $VPS74 OE$. Performed Student-t test. **** $p < 0.0001$, ** $p = 0.0090$ (homotypic fusion frequency graph, ** $p = 0.0027$ (persistence time graph) and ** $p = 0.0086$ (maturation frequency graph). Error bar represents S.E.M (Standard error mean).

In the case of $\Delta vps74$ (Gea2- Sec7 dual color strain), maturation frequency is more as compared to WT (Fig 5.38). We should have observed more late cisterna, but due to high late fusion frequency (Fig 5.38), we see a reduction in late cisterna number (Fig 5.38), and thereby it also caused an increase in the late cisterna size and volume (Fig 5.38).

In the case of Vps74 overexpression in WT, maturation frequency shows a non-significant reduction as compared to WT (Fig 5.38). Homotypic fusion rate of early and late has not altered significantly (Fig 5.38). The persistence time of late cisterna is reduced considerably (Fig 5.38). Vps74 is required for budding at trans Golgi [6]. Thus overexpression of Vps74 in WT might have increased the budding reaction, which is supported by the observed reduction in persistence time of late cisterna and thereby accounts for the reduced late cisterna size and volume (Fig 5.38).

In the case of Arf1 overexpression in $\Delta vps74$, the number of late cisternae has increased significantly (Fig 5.38) as compared to *vps74* null mutant. We observe rescue of enlarged late cisterna size to WT. Late cisterna fusion frequency has reduced slightly in comparison to $\Delta vps74$ strain (Fig 5.38). Maturation frequency has been lowered significantly. Almost all the parameters are reversed to that of the wild-type.

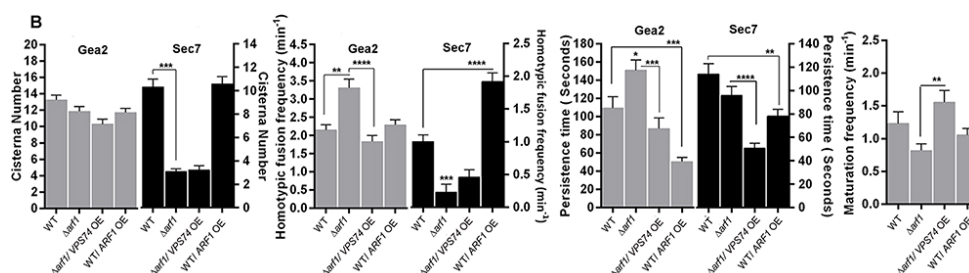


Figure 5.39: Cisterna maturation parameter comparison for WT, *arf1Δ*, $\Delta arf1$ /Vps74 OE and WT/Arf1 OE. Performed Student-t test. **** p<0.0001, *** p<0.0001 (cisterna number graph), **p=0.0012(homotypic fusion frequency graph), ***p=0.0002 (homotypic fusion frequency graph), ***p=0.0007 and 0.0004 (Persistence time graph), **p= 0.0028 (persistence time graph) *p=0.225(persistence time graph). Error bar represents S.E.M (Standard error mean).

In case of ARF1 deletion (Gea2-Sec7 strain), persistence time of early cisterna is increased significantly (Fig 5.39) that leads to significant increase in the early fusion frequency and drop in the maturation frequency (Fig 5.39). $\Delta arf1$ cells show significantly reduced late fusion frequency and reduced late cisterna number (Fig 5.39).

In the case of Arf1 overexpression in WT, the persistence time of early and late cisterna has reduced significantly (Fig 5.39) compared to that of WT. However, it has not altered maturation frequency and cisterna number (Fig 5.39). The fusion frequency of late cisterna has increased significantly (Fig 5.39).

In the case of Vps74 overexpression in $\Delta arf1$ strain, the persistence time of early and late cisterna has reduced significantly (Fig 5.39) compared to that of $\Delta arf1$ strain, and the maturation frequency has increased (Fig 5.39). However, the cisterna number has not shown much deviation from $\Delta arf1$ (Fig 5.39). Early cisterna homotypic fusion has reduced significantly compared to $\Delta arf1$.

5.2.5 ARF1 deletion can alter the Vps74 gradient

Vps74 has a gradient lower towards late cisterna and higher towards early cisterna [110]. Vps74 is of 345 amino acid length. The region 67-345 of Vps74 interacts with Arf1 [85]. To validate whether Arf1 is required for the localization of Vps74, we showed that in *arf1* null mutant 3X GFP- Vps74 localizes to the Golgi membrane tagged with Sec7-6XDsRed (Fig: 5.40).

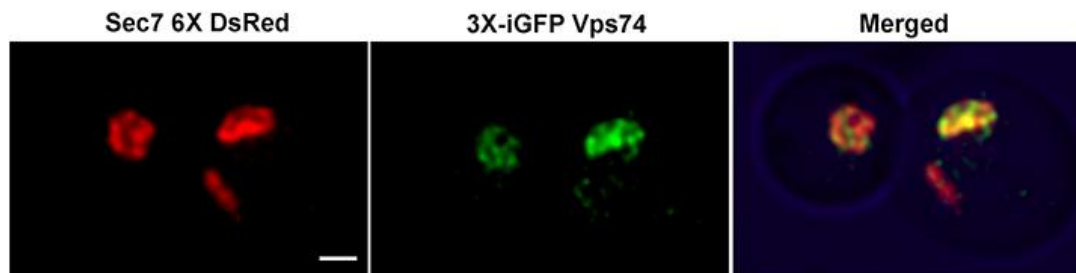


Figure 5.40: Representative image of localization of Vps74 in $\Delta arf1$

However, in the presence of Arf1 (in WT) a clear non-overlap of signals of Sec7 and Vps74 was observed (Fig: 5.2). The Golgi cisterna coalesces into few and larger cisternae in $arf1\Delta$. We also found the localization of Vps74 in Sec7 cisterna has increased in $\Delta arf1$ compared to that of wild-type. To confirm this observation, we quantified the Pearson's coefficient for colocalization of Vps74 with Sec7 in wild-type and $arf1\Delta$ (N=25 cells).

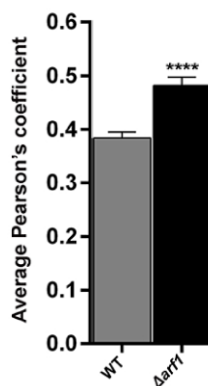


Figure 5.41: Average Pearson's coefficient plot obtained for colocalization of Vps74 with Sec7 cisterna in wild-type and $\Delta arf1$ (N=25 cells). Student t-test. ****p<0.0001

The average Pearson's coefficient obtained for colocalization of Vps74 with Sec7 is higher in $\Delta arf1$ than in wild-type (Fig: 5.41). This result suggests that *ARF1* deletion destroys the Vps74 distribution pattern throughout the Golgi. Alternatively, in other

words, Arf1 possibly is responsible for Vps74 gradient along the Golgi, suggesting that size regulation by Vps74 is Arf1 dependent. Vps74 and PI4P have an opposite gradient maintained along Golgi cisterna stack [110]. If $\Delta arf1$ disturbs the Vps74 gradient, we speculated it might also upset the PI4P gradient. Since Vps74 is one of the effectors of PI4P, the PI4P gradient might also be affected in $\Delta vps74$.

5.2.6 PI4P gradient is disturbed in Golgi compartments of *vps74* and *arf1* null mutants:

Phospholipids PI4P is abundant in Golgi, and it has a gradient which is higher towards trans Golgi and reduces towards early Golgi. Pik1 kinase required for phosphorylation of PtdIns is also abundant in trans Golgi. Vps74 mediated retrograde transport of specific Golgi resident enzymes in COPI vesicles also carry along PI4P towards early cisterna [6, 110]. However, Vps74 has a gradient opposite to PI4P. In *vps74* null mutants, we observed enlarged late cisterna phenotype (Section 5.2.3), and we correlated the observation with cisterna maturation parameters (Section 5.2.4). Vps74 is an effector of PI4P and exhibits gradient opposite to PI4P. This result led us to know the connecting link between the enlarged Golgi cisterna and the PI4P gradient across the Golgi compartment. To demonstrate the PI4P levels across the Golgi compartment in wild-type versus null mutants, we created strains with late Golgi cisterna Sec7-6XmCherry and PI4P marker GFP-PH^{OSH1} (Fig: 5.42). We observed PI4P marker and late Golgi cisterna overlap as yellow color in the merged panel (Fig: 5.42). Similarly, we also checked the PI4P marker mCherry-PH^{OSH1} along the early Golgi cisterna Gea2-3XGFP (Fig: 5.43).

Here, we could observe the localization of PI4P marker with Golgi cisterna Gea2 (Fig: 5.43) is not as overlapping as the one with Sec7 (Fig: 5.42).

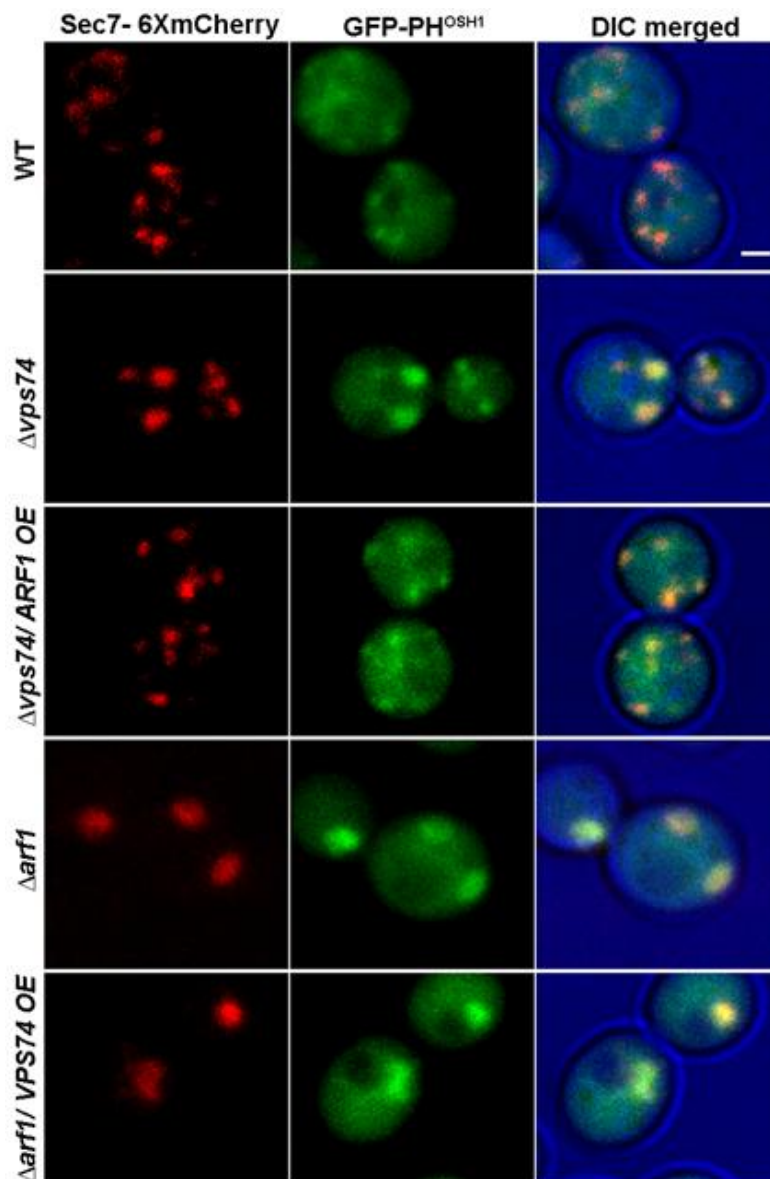


Figure 5.42: Figure panel represents localization of PI4P marker GFP-PH^{OSH1} along late Golgi cisterna Sec7-6XmCherry in wild-type, $\Delta vps74$, $\Delta vps74/ARF1OE$, $\Delta arf1$, $\Delta arf1/ VPS74 OE$

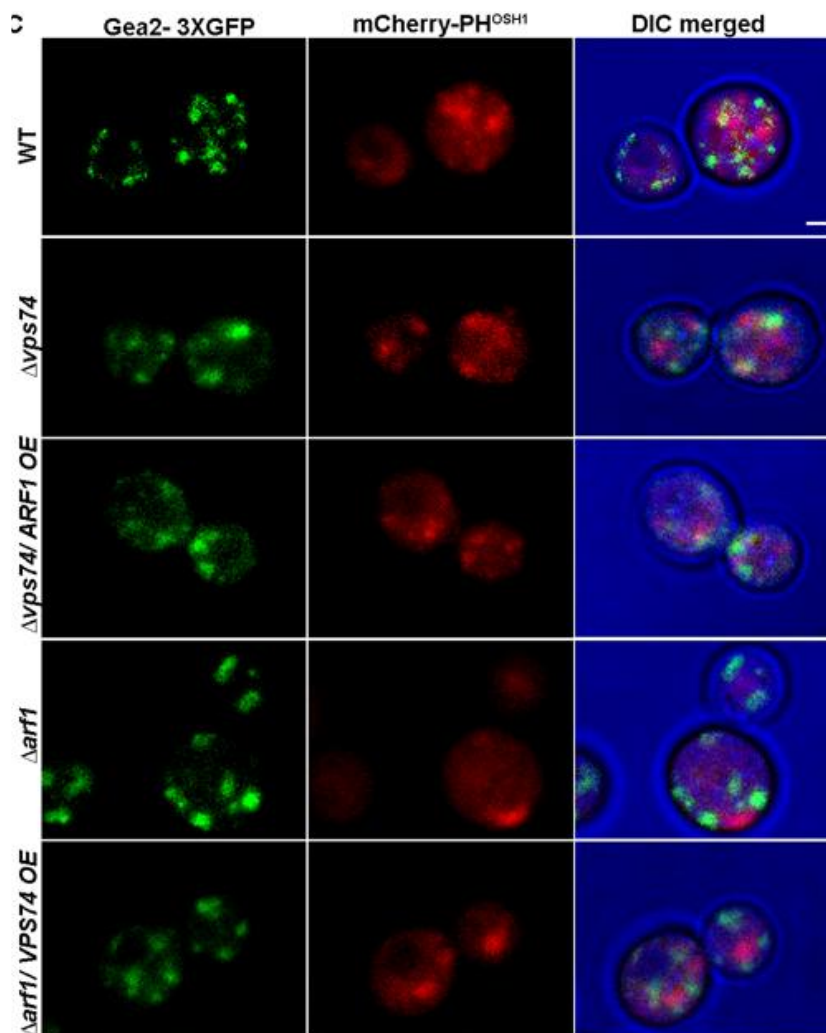


Figure 5.43: Figure panel represents localization of PI4P marker mCherry-PH^{OSH1} along early Golgi cisterna Gea2-3X GFP in wild-type, $\Delta vps74$, $\Delta vps74/ARF1$ OE, $\Delta arf1$, $\Delta arf1/VPS74$ OE

To analyze the levels of PI4P along the Golgi compartment Sec7 and Gea2 in wild-type and mutants, colocalization of the two markers were quantified using Coloc tool of Imaris software. Average Pearson's coefficient was plotted.

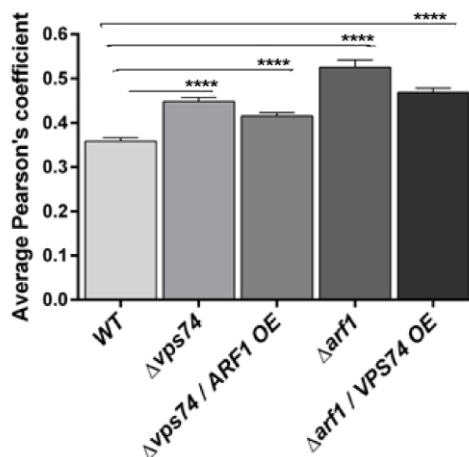


Figure 5.44: Average Pearson's coefficient plot showing colocalization of PI4P with Sec7 Golgi cisterna (N=30 cells). Student t-test. S.E.M (Standard Error Mean). ****p<0.0001

We observed that the average Pearson's coefficient in case of null mutant $\Delta vps74$ and $\Delta arf1$ had increased in comparison to wild-type (Fig: 5.44). Neither overexpression of Vps74 in $\Delta arf1$ nor overexpression of Arf1 in $\Delta vps74$ had altered the PI4P levels compared to null mutants.

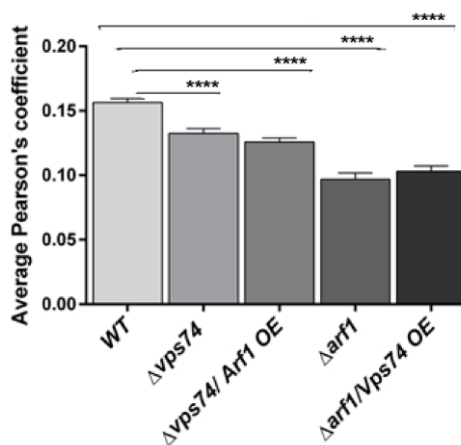


Figure 5.45: Average Pearson's coefficient plot showing colocalization of PI4P with Gea2 Golgi cisterna (N=30 cells). Student t-test. S.E.M (Standard Error Mean). ****p<0.0001

The average Pearson's coefficient of PI4P with Gea2 cisterna had reduced slightly in mutants compared to wild-type (Fig: 5.45).

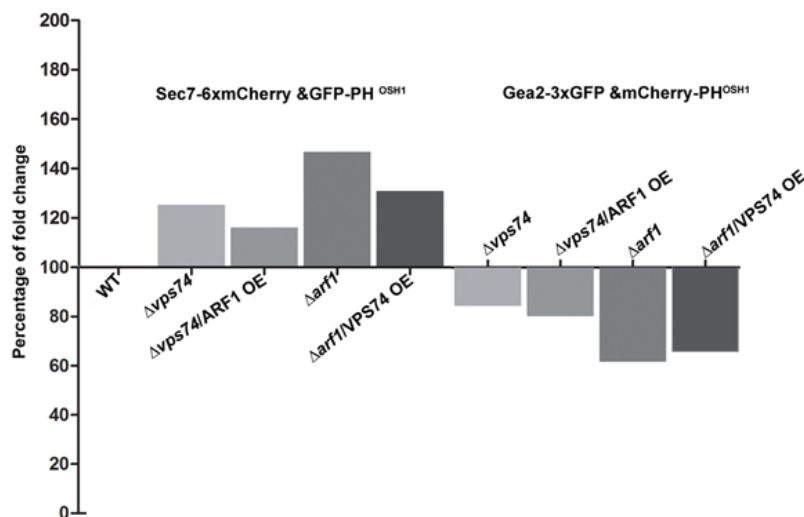


Figure 5.46: The graph represents the percent fold change of average Pearson's coefficient in mutants compared to wild-type. Wild-type is considered as 100

The percent fold graph (Fig: 5.46) represents the PI4P localization along the early and late Golgi compartments. It demonstrates PI4P levels with late cisterna Sec7 had increased while it decreased with early cisterna Gea2 in mutants.

5.2.7 Effect of *pik1^{ts}* mutation on Golgi cisterna

Earlier we had demonstrated PI4P levels in *Δarf1* and *Δvps74*. Golgi associated PI4P in yeast is generated by a conserved type IIIβ PI4-kinase, Pik1. Pik1 is required for secretion and Golgi integrity [111, 112]. Conditional *pik1^{ts}* mutations can disturb the phospholipid pool, PI4P [113] which is required for regulation of budding vesicle machinery and membrane dynamics at Golgi [86]. We observed that deletion of Vps74

affects Golgi cisterna size and PI4P gradient. We checked whether reduction of PI4P levels affects Golgi morphology. Hence we demonstrated the effect of the *pik1-83^{ts}* mutation on Sec7 and Vrg4 cisterna at permissive (22°C) and non-permissive conditions (37°C). We made separate strains of *pik1-83^{ts}* with early cisterna GFP- Vrg4 and late cisterna Sec7-3XGFP.

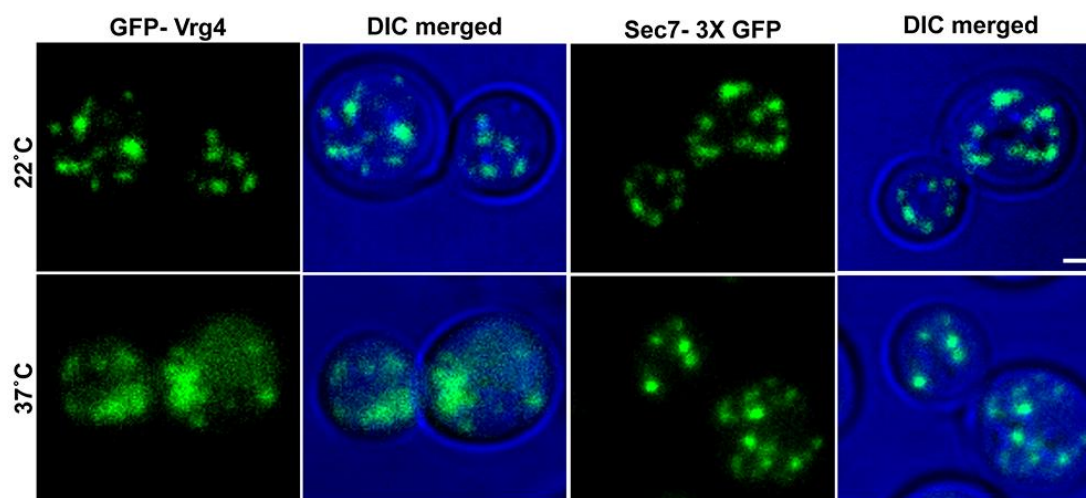


Figure 5.47: Representative image of the effect of *pik1-83^{ts}* on Vrg4 and Sec7 Golgi cisterna at the permissive and non-permissive condition

At non-permissive condition, we observed altered Vrg4 cisterna while no such prominent effect was found on Sec7 cisterna.

5.3: Discussion:

The COPII vesicles that exit from ER exit sites is small, about 30-50nm. This size is beyond the resolution limit of the confocal microscope. These vesicles undergo

homotypic fusion to form bigger cisterna of size 200 to 250nm and higher which is clearly detected by the confocal microscope. Amongst the well-known marker for cis, medial and trans-Golgi compartment; the markers have a hierarchy of appearing on the temporal scale of maturation. The fusion frequency amongst the very early marker to form big sized cisterna should be higher. From our studies on fusion frequency for the different Golgi tag (Part 5.2.2 of result section), we have proved that the homotypic fusion rate for the early marker is relatively higher. We have shown Gea2 labeled compartment can mature to both Vrg4 (Fig: 5.4) and also to Sec7 labeled compartments (Fig: 5.5). These results elucidate that Gea2 is an early Golgi protein as compared to either of Vrg4 and Sec7 in the temporal scale of cisternal maturation. Rer1 is a well known early marker. We could establish the fact that fusion frequency amongst very early marker Rer1 and Gea2 before Vrg4 on the temporal scale is very higher (Fig 5.7 & 5.12).

Reports are stating Vps74 has a role in the retrograde transport of certain Golgi associated glycosyltransferases from trans to early Golgi compartments [7]. However, there is no study available that revealed the role of yeast homolog Vps74 in maintaining Golgi size. This study establishes the function of *VPS74* in regulating Golgi size (Part 5.2.3 of result section). Deletion of *VPS74* altered the late Golgi size tagged with Sec7 6X DsRed while it did not change the early cisterna size marked with 3X-iGFP Rer1 or Gea2-3X-GFP. We found that deletion of *VPS74* alters the localization of an early cisterna marker GFP-Vrg4. Vrg4 is a mannosyltransferase. Vps74 is reported to be required to retain certain Golgi associated glycosyltransferase [7]. Might be on a similar

way Vps74 is also needed to maintain the Vrg4 on Golgi membrane. *VPS74* overexpression in the wild-type strain (Gea2-Sec7) was quantified to show a slight reduction in the late Golgi volume and size. Since Vps74 protein is required for budding of vesicles at trans Golgi [6], hence we hypothesize that (Fig: 5.48) deletion of *VPS74* gene might result in reduced trans Golgi budding thus resulting in increased size or volume while overexpression of *VPS74* in wild-type causes increased budding reaction at trans Golgi leading to a slight reduction in its size or volume (Fig: 5.32, 5.33 & 5.37).

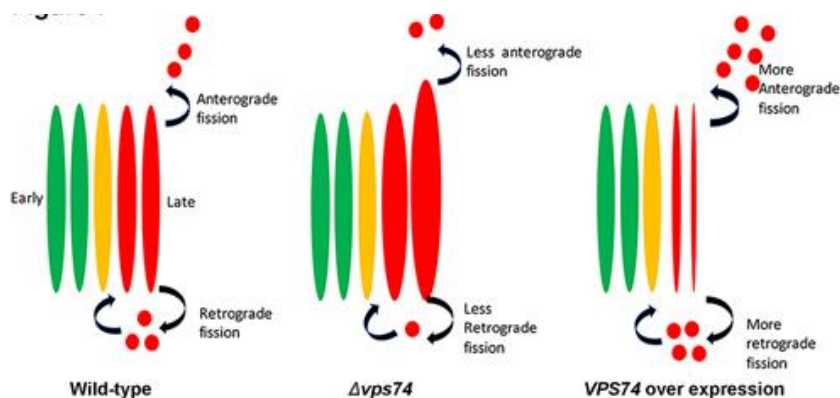


Figure 5.48: A hypothetical model explaining the role of Vps74 in Golgi size regulation

The other reason for the increase in the late Golgi cisterna size of $\Delta vps74$ is due to an increase in the maturation frequency event that adds on to the available late cisterna for homotypic fusion. Enhanced homotypic fusion frequency observed (Fig: 5.17) also caused a decrease in late cisterna count. However, the persistence time is unaffected. Observed reduced persistence time in the case of Vps74 overexpressed in the wild-type

strain. Reduction in persistence time of late cisterna might be due to increased budding reaction at the trans cisterna as explained by the hypothetical model (Fig: 5.48).

Vps74 has an interacting domain for protein Arf1 and COPI [85]. We have demonstrated that the deletion of Arf1 interacting domain of *VPS74* results into the same phenotype of $\Delta vps74$. We tried to analyze further the link between Vps74 and Arf1 in regulating Golgi size. In the case of double knock out $\Delta arf1-\Delta vps74$, we observed that the phenotype for late enlarged Golgi is enhanced as compared to $\Delta vps74$. Overexpression of Arf1 in $\Delta vps74$ strain rescued the enlarged late Golgi to wild-type, while overexpression of Vps74 in $\Delta arf1$ strain did not recover the enlarged phenotype. Arf1 is a master regulator of cisternal size. Arf1 required for clathrin coat assembly from the TGN membrane is a PI4P dependent process [114-119]. Assembly of clathrin adaptors in $\Delta arf1$ was delayed [116]. Probably Arf1 overexpression in $\Delta vps74$ might have increased this process of clathrin-associated budding dynamics which in turn may rescue the large late cisterna size phenotype of $\Delta vps74$.

Along with size rescue, we also observed the maturation frequency is almost similar to that of wild-type. When Vps74 is overexpressed in $\Delta arf1$, the enlarged Golgi cisterna is still observed. However, fewer and larger Golgi cisterna seen in $\Delta arf1$ phenotype [87, 105] is dominant and probably for that reason overexpression of Vps74 fails to rescue $\Delta arf1$ phenotype. The fusion frequency and the persistence time of early cisterna are reduced. The maturation frequency has increased to that of WT. However, there is no rescue of pre-dominant enlarged late cisterna exhibited by $arf1\Delta$.

In the case of $\Delta arf1$ (Gea2-Sec7 strain), we observed enhanced late Golgi size which confirms with the earlier study [87, 105] as well. Persistence time of early cisterna has increased, and the maturation frequency has reduced (Fig: 5.39). When Arf1 is overexpressed in wild-type, we do not observe any alterations of Golgi cisterna size. Persistence time of early has reduced than WT. Though we see increased late cisterna fusion events, late cisterna size has not increased. It is because the persistence time of the late cisterna is lowered. Thereby parameters like maturation freq, size and number are the same as that of WT.

Vps74 and Arf1 both alter Golgi cisterna size and maturation. *VPS74* deletion shows increased maturation frequency, and hence more late cisterna is available for fusion. The observed increase in the fusion frequency of late cisterna has resulted in enlarged late cisterna size. The $\Delta arf1$ results in increased persistence time of early Golgi cisterna that also increases their fusion probability. As a result, early cisterna size has increased that matures to enlarged late cisterna. Due to an increase in the persistence time of early cisterna, maturation frequency has also reduced. Though we observe enlarged late Golgi phenotype in $\Delta arf1$ and $\Delta vps74$, they have an antagonistic effect on maturation frequency. In the absence of one, when other gene is overexpressed, it balances and tries to maintain maturation frequency similar to that of WT. Arf1 may be a dominant regulator of Golgi cisterna size; hence overexpression of Vps74 did not alter the enlarged Golgi size in $\Delta arf1$ strain. However, overexpression of Arf1 in $\Delta vps74$ could rescue the enlarged late Golgi phenotype. We have demonstrated that Vps74 regulates Golgi size in an Arf1 dependent manner.

Vps74 has a gradient distribution along Golgi cisterna which is opposite to the PI4P gradient [110]. We had also shown Vps74 that show non-overlap along Sec7 Golgi cisterna in wild-type (Fig: 5.2) had almost accumulated in the enlarged Sec7 cisterna in case of $\Delta arf1$ (Fig: 5.40). To verify the colocalization of Vps74 with Sec7, average Pearson's coefficient was quantified. Average Pearson's coefficient obtained for colocalization of Vps74 with Sec7 cisterna is higher in $\Delta arf1$ compared to wild-type (Fig: 5.41). It demonstrated that Vps74 is an effector of Arf1, and its distribution is altered in the absence of Arf1.

PtdIns4-kinase Pik1 recruitment requires Arf1, and lack of Arf1 affects PI4P levels [111, 120]. Alteration of Vps74 localization in the absence of Arf1 might also have altered PI4P levels. To validate the Golgi PI4P levels, we analyzed PI4P marker GFP-PH^{OSH1} along with Golgi cisterna Sec7-6X DsRed (Fig: 5.42) and quantified the average Pearson's coefficient in $\Delta vps74$ and $\Delta arf1$ (Fig: 5.44). We demonstrated enhanced colocalization of PI4P marker with Sec7 cisterna in case of $\Delta vps74$ or $\Delta arf1$. Further, the localization of mCherry-PH^{OSH1} with Gea2-3XGFP was also analyzed (Fig: 5.43). In the case of wild-type itself, lower overlap of PI4P marker with Gea2 cisterna was observed compared to Sec7 cisterna (Fig: 5.44, 5.45, and 5.46). The extent of non-overlap of PI4P marker with Gea2 in $arf1$ and $vps74$ mutants was more prominently visible. The average Pearson's coefficient detailing colocalization of PI4P marker with Gea2 in $\Delta arf1$ and $\Delta vps74$ was slightly less compared to wild-type (Fig: 5.45, 5.46). Thus, we showed that the PI4P levels along the Golgi compartment are altered in case of mutant $\Delta vps74$ and

Δarf1. This altered PI4P levels could not be rescued if Vps74 is overexpressed in *Δarf1* or Arf1 is overexpressed in *Δvps74* (Fig: 5.44).

We had demonstrated in detail the role of Vps74 and Arf1 in regulating the Golgi size, maturation kinetics and altering the PI4P levels along Golgi. Pik1 kinase generates PI4P . Pik1 is essential to maintain Golgi function and levels of PI4P. In the case of *pik1-83^{ts}* subjected to the non-permissive condition, we observed altered localization of the Vrg4 protein while Sec7 cisterna is not prominently altered (Fig 5.47).

Chapter 6

Study Golgi size regulation in budding yeast

***S. cerevisiae* by mathematical simulation**

6.1: Introduction:

Every eukaryotic organelle obtains its membrane composition, lipids, and proteins through the vesicular traffic mediated exchange. Golgi is one of the essential organelles of membrane trafficking, and the widely accepted cisterna maturation model explains its function [49, 121, 122]. Golgi complex is divided functionally into a cis, medial and trans compartment which is formed by cisterna maturation. Formation of new Cis Golgi compartment happens via budding and homotypic fusion of COPII vesicles that exit at ER-Golgi intermediate compartments (ERGIC) [123]. Further dissipation of cisterna is observed at the trans end as cargo carriers [124, 125], coupled with retrograde recycling of Golgi and ER resident proteins move towards newly formed cisterna at ERGIC [126]. Golgi organelle also contains phospholipid marker PtdIns4-P at trans Golgi, as a signaling molecule for its downstream effectors that regulate the membrane dynamics of the trafficking network [86]. It explains the well-planned processing unit of the endomembrane system. There exist proteins like COPI, COPII, SNAREs, GTPases, and others, essential in maintaining the trafficking network in Golgi.

Traffic rules of Golgi complex:

Following steps maintains the structure of vesicle traffic:

- a) GTPase of Arf and other Rab families assist in membrane curvature [127, 128].
- b) Coats and adaptors load and ferry cargoes and ER- Golgi resident proteins to their target organelle [129].

- c) SNARES and tethers help transport and fusion of vesicles [130-132].

Cisterna maturation model of the Golgi is widely accepted. The maturation process is well established in *S.cerevisiae* [28, 58]. To understand the maturation kinetics and its role in cisterna size control, we resorted to developing a mathematical model. To include all the details of the different functional proteins involved in the dynamics of cisterna maturation of Golgi would be very complicated.

We demonstrated the *in-silico* model, for studying cisterna maturation kinetics with respect to *S.cerevisiae* using coarse-grained density-dependent model. It is primarily essential to understand the membrane trafficking genes involved in the regulation of Golgi size and dynamics. Such a broad study of dynamics expands to know the kinetics of the Golgi cisterna maturation as well. We had basically done a classic knock out and overexpression study of several genes involved in membrane trafficking using experimental model organism *S.cerevisiae*. Many of the critical findings of cisterna maturation parameters in the experiment drew our focus to know the key trigger that each gene regulates and thereby maintains Golgi cisterna size. The question to be addressed was to understand the physical quantity (size, time, specific protein) that plays a vital role in the in-vivo dynamics of Golgi cisterna maturation. We believe this physical quantity is altered as per the absence of certain significant membrane traffic governing genes.

6.1.1 Rationale for the in-silico study

In a previous study from our lab, we have elucidated that *ARF1* controls Golgi size by altering cisterna maturation kinetics [87]. We hypothesized a simple mathematical, empirical equation (Fig: 6.1) to explain the cisterna maturation process.

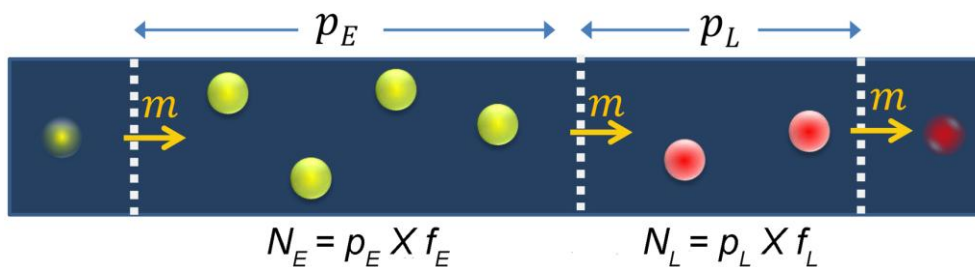


Figure 6.1: Illustration diagram of the empirical mathematical equation

Description of the terms used in Fig: 6.1: E = average number of early Golgi cisternae (shown as green-colored sphere) per cell, L = average number of late Golgi cisternae (shown as red-colored sphere) per cell, m = average maturation frequency, pE = average persistence time of early Golgi cisternae, pL = average persistence time of late Golgi cisternae. In steady state, the average number of early or late Golgi cisternae should be equal to the frequency of appearance multiplied by the persistence time.

Thus: $E=pE \times m$ and $L=pL \times m$

	E	L	m (per minute)	p_E (seconds)	p_L (seconds)	$m \times p_E$	$m \times p_L$
Wild type	9.2±0.7	7.0±0.4	3.0±0.2	103±8	113±10	5.2	5.7
<i>arf1</i> Δ	5.2±0.3	2.0±0.3	1.2±0.2	185±19	101±7	3.7	2.0

Figure 6.2: Maturation parameters for wild-type and $\Delta arf1$ cells [87]. The red rectangular box marks the parameter value obtained for cisterna number and product of maturation frequency and persistence time

The predicted cisterna number from this steady state kinetics failed to match with the experimental data set (Fig: 6.2). This disproved our assumption. The factor that was not considered in the empirical equation was homotypic fusion. We were able to observe these homotypic fusions in 4D imaging captured for *in vivo* experiments.

Demonstration of maturation process involving the transition of early Golgi cisterna to late Golgi cisterna is easier in *S.cerevisiae*. 4D imaging and the analysis of different parameters described in chapter 5 also enabled us to determine the homotypic fusion frequency. Several findings of the Golgi cisterna size in yeast with enhanced resolution of cellular structure also gave the more delicate details of the compartment dimensions. The changes obtained in *arf1* mutants will allow estimation and confirmation of kinetics regulated or affected by these proteins. Thus we developed a coarse-grained computational model with a more precise detailing of Golgi size regulation and its dynamics.

We developed an in-silico cisterna maturation process for *S.cerevisiae*. Since many vital proteins are involved in *in-vivo* cisterna maturation and Golgi dynamics, representing all

of them in the proposed simulation model would make it more complicated. So we resorted to neglect fine scales while still making it an efficient one to compute the large-scale events such as maturation dynamics of Golgi vesicles in terms of rates they appear or disappear [133]. We have assumed values based on existing knowledge for specific input parameters (Refer to Table 6.1) in our minimalistic model.

We considered a three dimension spheroid cell with a randomly positioned spherical nucleus. In *S.cerevisiae* the ER exit sites, from which Golgi vesicles emerge is distributed throughout the cytoplasm. To include this factor, we assumed early Golgi vesicles of mean size $\text{Size}_{\text{denovo}}$ appear randomly within the cytoplasm with a rate K_{denovo} . These Golgi vesicles move randomly. To control the maturation of Golgi vesicles we included two rates- K_{early} and K_{late} . The early Golgi vesicles emerging from ER exit sites has its early protein density set at a maximum value (1) while late protein density at a minimum value (0) (Fig:6.3).

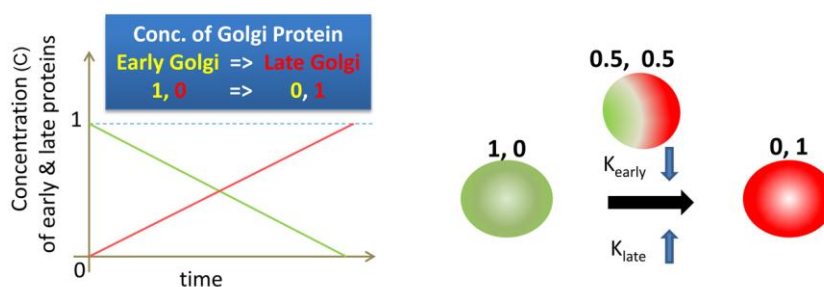


Figure 6.3: Graph representing the concentration of early and late proteins with respect to time

In figure 6.3 identity of cisterna as early or late is marked by the level of early or late proteins respectively. These are represented by rates K_{early} and K_{late} , which are inversely

related as the cisterna matures. As the cisterna develops the value of K_{early} tends to zero, while the value of K_{late} tends to one

Eventually, observed the vesicle transformation or maturation by the altered early and late protein density. Rate K_{early} and K_{late} governed early and late protein densities. So the maturation process from early to late cisterna involved alteration of these two rates that decreased the early protein density (towards 0) and increased the late protein density (towards 1). Assumed homotypic fusion event between similar types of vesicles in close proximity [28, 87] (Fig: 6.4).

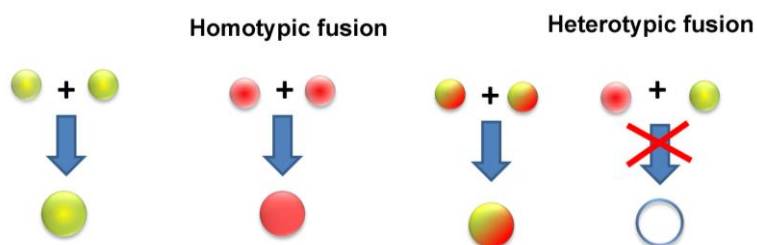


Figure 6.4: Fusion between similar kinds of vesicles was only allowed

Considered a repulsive potential and avoided fusion between different types of vesicle. Maintained a repulsive potential between Golgi vesicles, cell, and nuclear periphery. Matured Golgi cisterna then disappears through fission. In our model, we assumed the fission process is an instantaneous process. A random force (F_{random}) acts on the Golgi vesicles that move through the cytoplasm in a Brownian trajectory path. Collectively all these factors were assumed, and the simulation was carried out using parameters listed in the table (Result section IV).

Result section comprises of six parts. Firstly we describe that **cisterna volume is conserved before and after fusion (6.2.1)**. Volume quantified from 4D imaging of experimental data supports this description. The mathematical model for cisterna maturation and dynamics in *S.cerevisiae* is monitored using four parameters K_{denovo} , $\text{Size}_{\text{denovo}}$, K_{early} , and K_{late} . We had tried to see the **effect on cisterna size and number by modulating two parameters (6.2.2)**. Vesicles in the *insilico* model experience an absolute magnitude of force while moving in Brownian trajectory path. We tuned **the random force (in simulation) with an experimentally measured velocity of the cisterna (6.2.3)**. **The values used for all four parameters differ with strains. The values are tabulated (6.2.4) in Table 6.1.** Detailed discussion of **rationales for attribution of absolute values to four parameters (6.2.5)**. Further once the simulation is done based on values attributed to different strains we had made **comparative analysis for experimental and simulation data (6.2.6)**.

6.2: Results:

6.2.1 The cisterna volume is conserved before and after fusion

We analyzed the volume of cisterna *in vivo* before and after fusion. We quantified the volume of fusing vesicles (V_1 and V_2) and the volume of vesicle after fusion (V_{fused}). The volumes are additive, and they remain conserved during the fusion event (Fig 6.5).

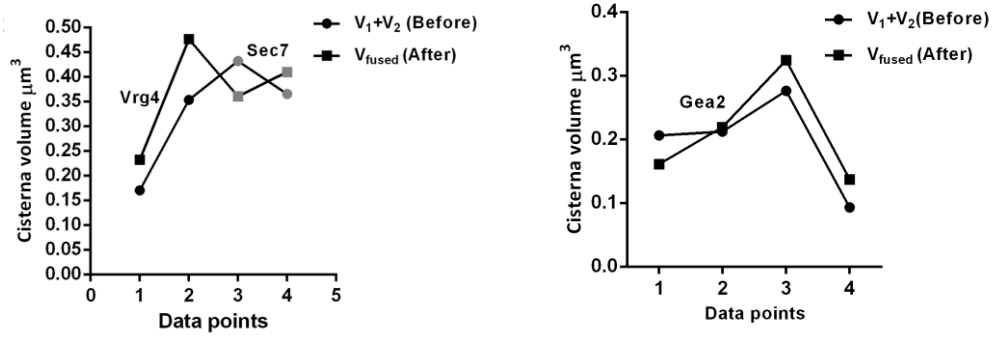


Figure 6.5: Volume of cisterna before and after fusion

We quantified the cisterna volume for Vrg4, early marker (black round and square) and Sec7, late marker (grey round and square). The graph plot (Fig 6.1) represents cumulative cisterna volume of V_1 and V_2 vesicles (round shaped label) fusing and the volume of the new cisterna V_{fused} (square shaped label) obtained after fusion. The following equation thereby maintains the density of proteins (early and late) present on the newly formed vesicle:

$$D_{new} = (D_i V_i + D_j V_j) / V_{new}$$

Here D and V denote the density and volume of two merging Golgi vesicles. Volume conservation in the simulation was assumed based on the experimental measurements (Fig 6.5). Did quantification of the volume of cisterna before and after fusion for the Gea2 marker.

6.2.2 Tuning of parameters:

Our model has four free parameters $Size_{denovo}$, K_{denovo} , K_{early} , and K_{late} wherein the value of $Size_{denovo}$ is 50-100nm. We have scanned the remaining three-parameter space and

optimized their range which reproduced experimental data satisfactorily. Detailed range of parameters is as follows:

6.2.2A. The rates K_{early} and K_{late} parameters studied with respect to Golgi vesicle size and number

We assumed vesicle of size 50-100nm ($\text{Size}_{\text{denovo}}$) appear at a rate K_{denovo} from the ER exit sites and gets distributed randomly within a cell. Table 6.1 discuss these values for the WT and mutant strains. We tuned the rates K_{early} and K_{late} keeping a constant value for $\text{Size}_{\text{denovo}}$ (75nm) and K_{denovo} (30/sec). The rates K_{early} and K_{late} define the persistence time of Golgi vesicles, and for *in vivo* dynamics, they represent the retrograde flow of the Golgi resident proteins. If the value of K is less, it means the persistence time is high and vice versa.

We made a heatmap plot (Fig 6.6) for the tuning of rates K_{early} and K_{late} when the other two parameters $\text{Size}_{\text{denovo}}$ and K_{denovo} are kept constant and monitors the number and size of Golgi vesicles. If the rate value K_{early} and K_{late} are small (both $<2 \times 10^{-3}/\text{s}$) their respective persistence time is high that increases the probability of fusion events, thereby forming larger sized early vesicles (as shown by the red/orange color at the left corner in plot ii) and reduced number of early vesicles (blue/violet at the left edge of plot i). From this, we can infer that higher fusion events reduce the number of early vesicles and increase the size of early vesicles.

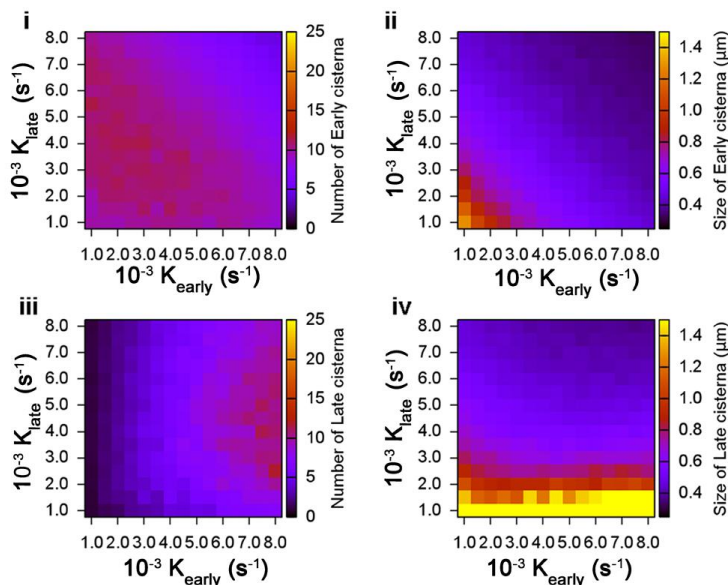


Figure 6.6: Heatmap plot for distribution of number and size of cisterna based on parameter space K_{early} and K_{late}

For same reason even we see the reduction in the number of the late vesicles (blue/violet at the left corner of plot iii) an increase in the size of the late vesicle (as shown by the red/orange color at the left corner in scheme iv). If the rate values K_{early} and K_{late} are high (both $>7 \times 10^{-3}/\text{s}$), then it reduces the number and size of vesicles because the vesicles mature quickly before reaching the microscopic limit.

6.2.2B. The parameter $\text{Size}_{\text{denovo}}$ and K_{denovo} studied with respect to Golgi vesicle size and number

In a similar kind of approach (Fig 6.7) we kept the rates K_{early} and K_{late} constant (both 0.006/sec) and the other parameters $\text{Size}_{\text{denovo}}$ and K_{denovo} were tuned to see the variations in number and size of Golgi vesicles (early and late). If the appearance rate K_{denovo} is assumed to be very small (i.e., >5) the density of early vesicles existing in the system will

be minimal that in turn reduces the chance of fusion (fusion probability increases with the vesicle density and size), and we observe small sized early vesicle maturation. Capturing these events is beyond microscopic resolution ($\sim 250\text{nm}$). Hence we see a small number of early vesicles for a low value of K_{denovo} (dark bar at the left corner in plot i and ii). If the persistence time of late vesicle is not very small (in this case $\sim 100\text{sec}$), then these tiny matured cisternae (beyond the microscopic limit) will fuse with other matured cisterna and increase the size and number of late cisterna (as in plot iii).

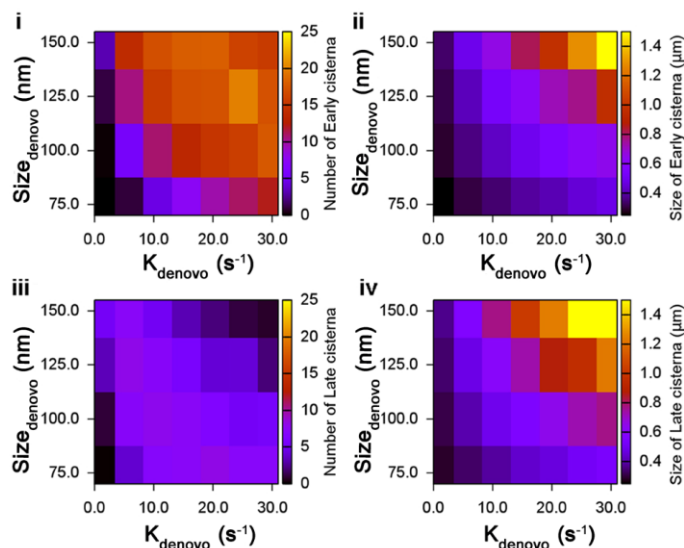


Figure 6.7: Heatmap plot for distribution of number and size of cisterna based on parameter space K_{denovo} and $\text{Size}_{\text{denovo}}$

While for higher values of $K_{\text{denovo}} (>10)$ with the increase in the density of early vesicles the chance of increased fusion event leads to an increasing early vesicle size beyond the microscopic limit and also increased number of early vesicles (orange/red colors in plot i). However, in this case, the early vesicle will mature at a bigger size and the matured/late vesicle will have a high probability to fuse with existing late vesicle

resulting into reduced late vesicle number (blue/violet in plot iii compared to the red/orange in plot i) compared to the early vesicle count.

After giving the apt input of parameters, we checked the size distribution of Golgi vesicle for WT Vrg4- Sec7 and *arf1* Δ Vrg4- Sec7. We made a comparative graphical plot for early cisterna size obtained in the experiment and after simulation. We confirmed to obtain a good overlap for experimental and simulation data and thereby assumed the input parameters for different strains and performed simulation (Fig 6.8).

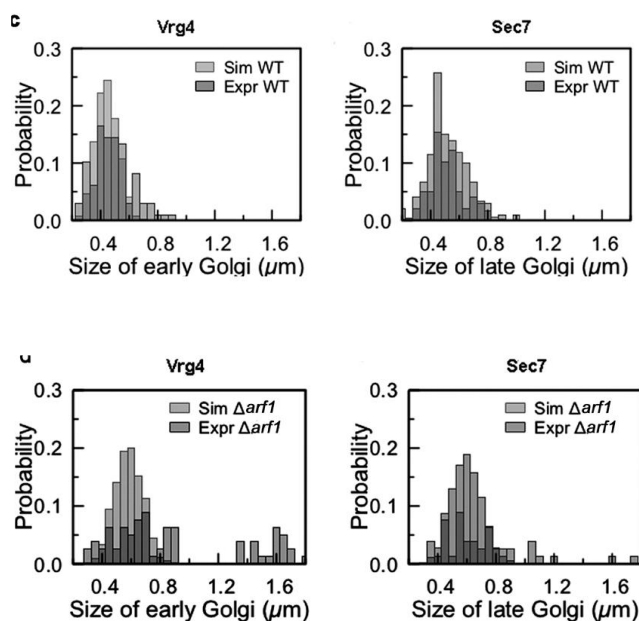


Figure 6.8: The cisterna size distribution probability plots for experimental (dark grey shaded bar) and simulation data (light grey shaded bar) of wild-type showed a matching overlap for early marker Vrg4 and late marker Sec7

6.2.3 Magnitude of force exerted is tuned to match the velocity of cisterna

Within the cytosolic environment, the randomly moving Golgi cisterna experiences a random force. Apart from the thermal noise, an active random force acting on the vesicles arising from the interactions between Golgi membrane and cytoskeletal filaments move Golgi vesicles intermittently over short distances through the cytoplasm. The magnitude of the random force is tuned to match the velocity distribution of the vesicles obtained from our experimental measurements [101]. The movement of Golgi vesicles following Brownian dynamics is simplified as follows, i.e., the position of the i^{th} vesicle is updated after time δt according to:

$$\vec{X}_i(t+\delta t) = \vec{X}_i(t) + \vec{\beta}_i + \vec{F}_i^{\text{conserved}} \delta t / \xi \quad \text{Eq.1}$$

$\vec{X}_i(t)$ is the position vector of the i^{th} vesicle in the 3-dimensional time t . $\vec{\beta}_i$ represents the displacement due to active force plus thermal noise and is drawn from a Gaussian distribution with 0 mean and variance $2D\delta t$. Here D ($\sim 0.25 \mu\text{m}^2/\text{s}^2$) is the diffusion constant and $\vec{F}_i^{\text{conserved}}$ is the conserved force on the i^{th} vesicle due to repulsion from other types of vesicles, nucleus, and cell membrane; ξ represents the viscous drag and δt (~ 10 ms) is the time increment in the simulation.

The overlap between early and late Golgi vesicles is avoided using a steric repulsion. If R_{ij} denotes the center-to-center distance between i^{th} (early) and j^{th} (late) vesicles and \vec{e}_{ij} denotes the unit vector pointing from i to j , the repulsive force on i^{th} vesicle is given by:

$$\vec{F}_i^{\text{rep}} = F^0 \vec{e}_{ij} (1 - R_{ij}/(R_i + R_j)), \quad \text{if } R_{ij} < (R_i + R_j) \quad \text{Eq.2}$$

Where F^0 is the maximal repulsion force and R_i and R_j are the radii of the i^{th} and j^{th} vesicles. Considered a similar expression for the repulsive force between Golgi vesicles and cell or nuclear periphery. Integrating all repulsive forces, one can obtain the total conserved force $\underline{F}_i^{\text{conserved}}$.

The velocity of cisterna from 4D imaging data was measured using the measurement tool in Imaris software. Plotted the velocity of cisterna obtained for the experiment against the force exerted on the cisterna in the simulation.

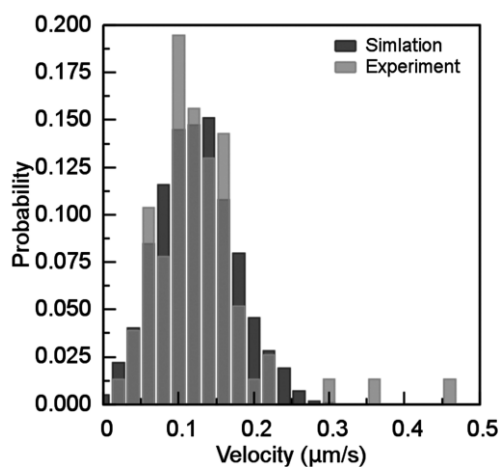


Figure 6.9: Plot for random Force (simulation) and velocity of cisterna (experiment)

Magnitude and distribution of the random force are tuned to match the velocity distribution of the vesicles obtained from our experimental measurements (Fig 6.9).

6.2.4 Tabulation of parameters for simulating different strains

Table 6.1: Parameter value for different strains

Strain	Size _{denovo}	K _{denovo}	K _{early}	K _{Late}	Rational
WT Vrg4-Sec7	75nm	30/sec	0.0006/sec	0.0006/sec	Initial size is taken from <i>Bigay et. al</i> [134], For the other three parameters, we scanned the parameter space and chose the values that corroborate well with the experiments.
<i>arf1</i> Δ	125nm	5/sec	0.003/sec	0.003/sec	Arf1 that induces membrane curvature [107] maintains the size and rate of budding and size of the vesicle at trans Golgi and helps the retrograde flow of different resident proteins [103-105, 108], and hence we used bigger <i>Size_{denovo}</i> and a slower rate of rate resident protein flow.
WT <i>Gea2-Sec7</i>	75nm	30/sec	0.0065/sec	0.0006/sec	We used the hypothesis that <i>Gea2</i> marker marks very early resident proteins and decays slightly quicker than <i>Vrg4</i> marker.
<i>vps74</i> Δ	75nm	30/sec	0.0065/sec	0.003/sec	We consider that <i>Vps74</i> helps to create budding of the late Golgi vesicle/TGN [6, 86] to maintain a level of late resident protein flow to the early/medial vesicles.
<i>arf1</i> Δ/ <i>VPS74</i> OE	125nm	5/sec	0.003/sec	0.0045/sec	ARF1 deletion nucleates bigger vesicle and decreases both early and late protein flow. However, overexpression of <i>Vps74</i> increases the late resident protein flow.

<i>vps74Δ/ARF1</i> OE	50nm	60/sec	0.0075/sec	0.0045/sec	<i>VPS74</i> deletion perturbs the rate of late resident protein flow, and on the other hand, Arf1 overexpression rescues the enlarged late cisterna phenotype along with an increment in the early resident flow.
WT/ <i>ARF1</i> OE	50nm	60/sec	0.0075/sec	0.0075/sec	In Arf1 overexpression, there is an increment in early resident flow compared to the WT scenario and hence the size of vesicles is lowered as compared to WT.
WT/ <i>VPS74</i> OE	75nm	30/sec	0.0065/sec	0.0075/sec	Overexpression of Vps74 increases the late resident protein flow compared to the WT case.

6.2.5 Rationale for parameter values used in different strains

Difference between WT Vrg4-Sec7 and WT Gea2-Sec7: We have used two wild-type strains. The only difference in the wild-type strain is they have different early marker Gea2 or Vrg4, while the late marker is Sec7. Gea2 marks the cisterna earlier than Vrg4. Gea2 matures into Vrg4 (Fig 5.4). So the decay rate of Gea2 cisterna is higher than Vrg4 cisterna. Hence the rate K_{early} for Gea2 (0.0065) is high than Vrg4 (0.0006). Kept remaining three parameters constant (Table 6.1).

1) Difference between WT and *arf1Δ*: We have considered in the model that Arf1 maintains

i. the rate of budding from late Golgi &

ii. Helps in retrograde flow of different resident proteins to maintain faithful maturation dynamics [103-105, 108].

Hence we assumed reduced K_{denovo} (reason i), K_{early} and K_{late} (reason ii)

Since experimentally we observe enlarged cisterna in $\text{arf1}\Delta$, initial vesicle size is considered more than WT.

2) Difference between WT and ARF1 OE: the rate of creation K_{denovo} is more compared to WT, and even the flow of resident proteins is also high leading to increased K_{early} and K_{late} compared to that of WT. Initial vesicle size in ARF1 OE is less as compared to WT.

3) Difference between WT and $\text{vps74}\Delta$: We considered VPS74 helps to bud at the late Golgi vesicle/TGN [6, 86] to maintain a level of late resident protein flow to the early/medial vesicles. Hence the $\text{vps74}\Delta$ leads to smaller K_{late} as compared to WT. Remaining 3 parameters are the same as WT.

4) Difference between WT and VPS74 OE: When Vps74 is provided in a high amount to WT, it alters K_{late} considering more budding reaction at trans-Golgi. Here K_{late} is higher compared to WT. Other 3 parameters are constant.

5) Difference between $\text{vps74}\Delta$ and $\text{vps74}\Delta / \text{ARF1}$ OE: The rates like K_{denovo} , K_{early} and K_{late} is increased in $\text{vps74}\Delta / \text{ARF1}$ OE as compared to only $\text{vps74}\Delta$. We experimentally see that Arf1 overexpression in $\text{vps74}\Delta$ cause shrinking of the enlarged late cisterna, hence the initial size of vesicles is considered small in $\text{vps74}\Delta / \text{ARF1}$ OE as compared to only $\text{vps74}\Delta$.

6) Difference between *arf1Δ* and *arf1Δ/VPS74* OE: Considering Vps74 helps in the budding reaction at trans Golgi [6]. Increased Vps74 in *arf1Δ* has led to increased K_{late} compared to only *arf1Δ*. Remaining other 3 parameters are the same as *arf1Δ*.

6.2.6 Comparative plot for experiment and simulation:

The computational model built on these assumptions aimed to quantify the number of early and late Golgi vesicles, maturation frequency, the size distribution of the Golgi vesicles, and persistence time of early and late Golgi for wild-type, null mutants and other overexpressing strains. After accounting homotypic fusion our *insilico* prediction corroborated well with the experimental results. In sync with the experiment, the following was considered while doing the measurement:

- 1) We have only counted those vesicles, which are above the microscopic resolution (~250 nm).
- 2) We have recorded model outputs at 4 seconds each (same as experiments) to count the cisterna number, persistence time, maturation frequency, etc.
- 3) Before recording the data, we simulated our model for ~15 minutes to allow the system to attain a steady state. We have simulated 50 independent samples, and each sample is simulated for 30 minutes to collect the data.

We compared the simulation data with experimental data for each strain. For calculating the parameters *in vivo*, we did 4D imaging for each strain with a time interval of 4-5 seconds in Leica SP8 confocal platform. Movies taken were processed in Image J as

mentioned in the materials and method section and further analyzed for different cisterna maturation parameters.

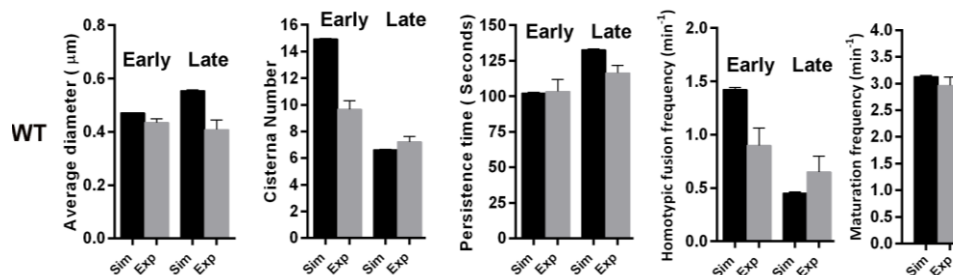


Figure 6.10: Experiment and simulation comparison of cisterna maturation parameters for wild-type Vrg4-Sec7 strain

Fig: 6.10 is a comparative graph of WT Vrg4-Sec7 strain for experimental and simulation data. We compared the cisterna maturation parameters like average diameter, cisterna number, persistence time, homotypic fusion frequency and maturation frequency. There exists an overlap between experimental and simulation data.

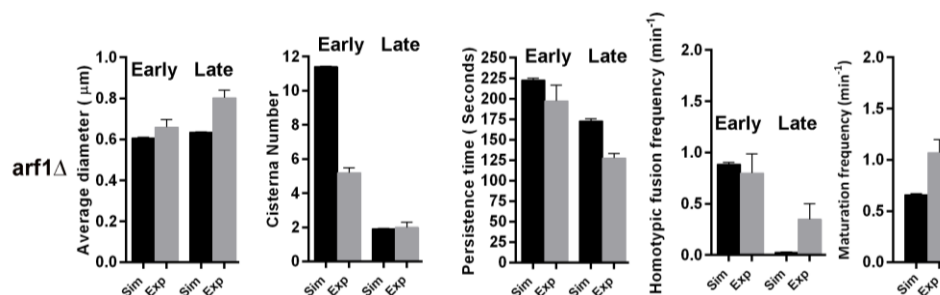


Figure 6.11: Experiment and simulation comparison of cisterna maturation parameters for *arf1Δ* Vrg4-Sec7 strain

Fig: 6.11 is a comparative graph of *arf1Δ* Vrg4-Sec7 strain for experimental and simulation data. We were able to develop the simulation model for WT and $\Delta arf1$ (Vrg4-

Sec7) that matched with the outcome of *in-vivo* experiments. Further, we also demonstrated the simulation for WT (Gea2-Sec7) and other null mutants. Table 6.1 mentions the parameter value chosen in each case.

Experimentally, Vrg4 marker gets delocalized on deletion of Vps74 gene. Calculating these maturation parameters in the strain *vps74Δ* Vrg4-Sec7 was difficult. However, we could make *vps74* null mutant in Gea2- Sec7 strain. So simulation was also carried out for another WT strain with Gea2-Sec7 cisterna marker (Fig 6.12).

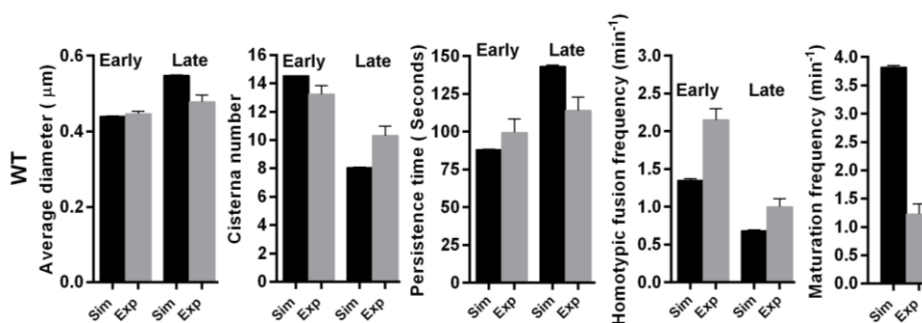


Figure 6.12: Experiment and simulation comparison of cisterna maturation parameters for wild-type Gea2-Sec7 strain

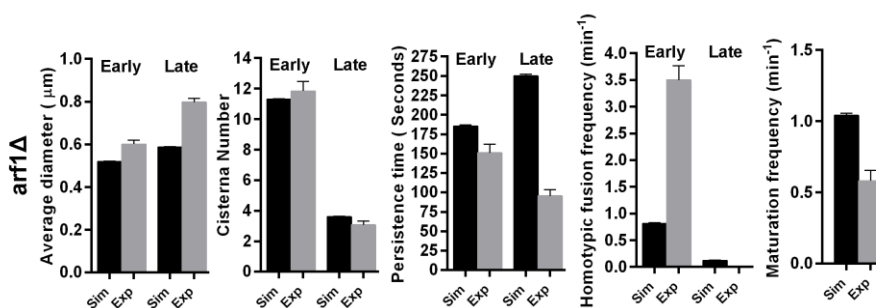


Figure 6.13: Experiment and simulation comparison of cisterna maturation parameters for *arf1Δ* Gea2-Sec7 strain

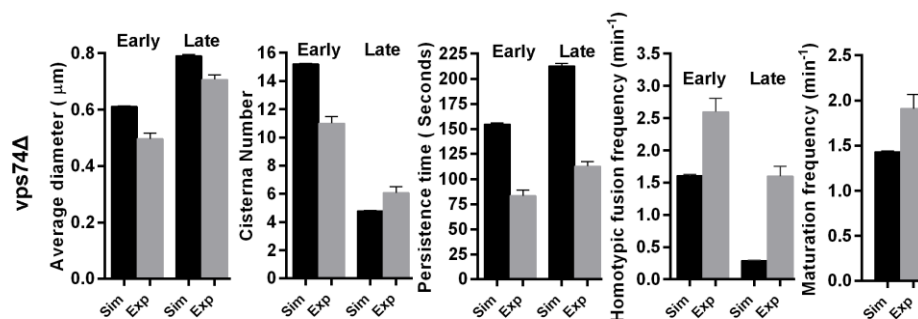


Figure 6.14: Experiment and simulation comparison of cisterna maturation parameters for *vps74Δ* Gea2-Sec7 strain

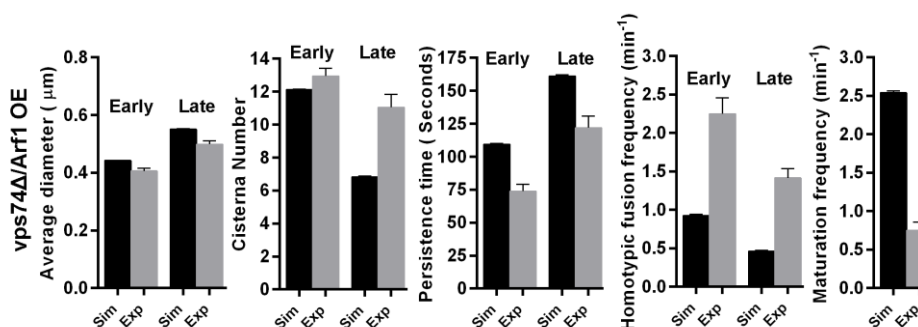


Figure 6.15: Experiment and simulation comparison of cisterna maturation parameters for *vps74Δ/ARF1* OE Gea2-Sec7 strain

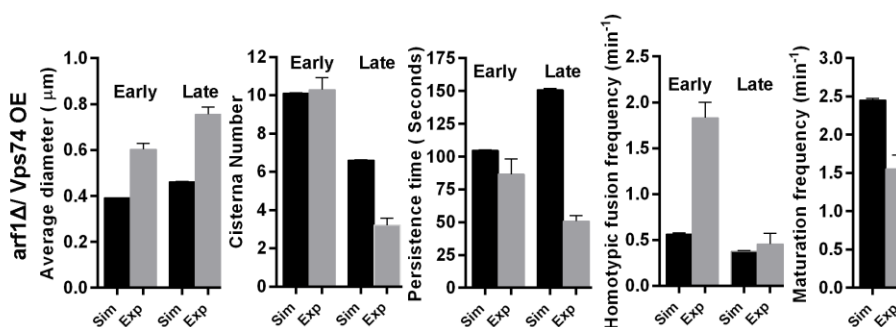


Figure 6.16: Experiment and simulation comparison of cisterna maturation parameters for *arf1Δ/VPS74* OE Gea2-Sec7 strain

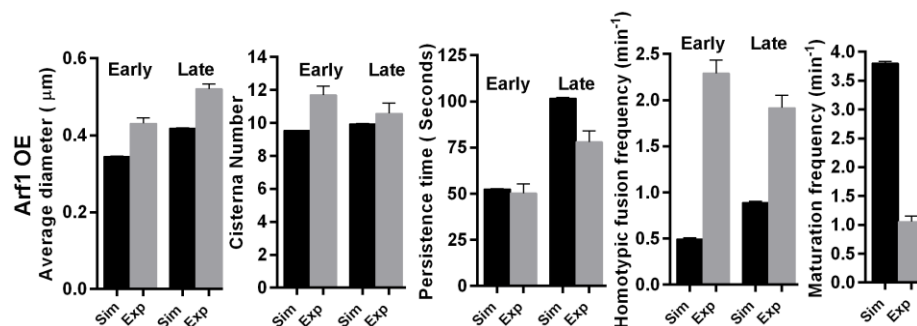


Figure 6.17: Experiment and simulation comparison of cisterna maturation parameters for WT/

ARF1 OE Gea2-Sec7 strain

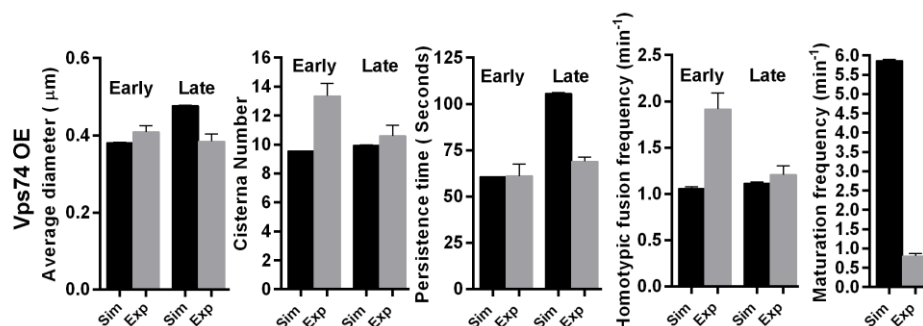


Figure 6.18: Experiment and simulation comparison of cisterna maturation parameters for WT/

VPS74 OE Gea2-Sec7 strain

In-silico mathematical simulation preliminarily outlined the four parameters ($\text{Size}_{\text{denovo}}$, K_{denovo} , K_{early} , and K_{late}) in case of $\Delta arf1$ and its respective wild-type. We were able to demonstrate that the parameter value chosen for WT and *arf1* null mutant gave a good overlap of maturation parameters (Fig: 6.10 & 6.11) obtained in simulation and experiment. We further enhanced this approach to the function of other gene null mutants and overexpressing strains (Fig: 6.12 to 6.18) studied in the lab. Although experimental and simulation data for most of the cisterna maturation parameters matched, few maturation parameters does not give an approximate match. Since microscopic resolution

limits the visualization of only 300nm structures and above, there is the possibility of error in the experimental data by being incapable of accounting small sized Golgi vesicles. We had tuned the mathematical parameters as much as possible to get an approximate match with the experimental data. Maybe the parameter values could be tweaked with different combinations for *vps74Δ* and other overexpressing mutants.

6.3: Discussion:

Membrane trafficking involves not only the modification of secretory proteins but also ferry the cargo to the destined organelle in a cell, and retain the ER and Golgi resident proteins. Golgi being a membrane-bound organelle comprises of lipids, that form its structure, and proteins that monitor the post-translational modification of secreted proteins. This function involves an enormous amount of exchange of materials through fusion and fission process, which includes proteins functional in the budding and scission process, and also proteins that recognize the target organelle before fusion. To represent all these proteins in an *in-silico* model would be very complex. We demonstrated the mathematical model for cisterna maturation in *S.cerevisiae* using different rates representing the function of proteins involved in regulating the size of vesicles, the rate of vesicle formation, and maturation of Golgi compartments. Cisterna maturation is a very dynamic process [28], and its regulation is poorly understood. In previous work from our lab, we have shown *arf1* deletion alters the maturation kinetics by an increase in the persistence time of early cisterna [87]. The empirical mathematical equation framed for steady state (Fig: 6.1) cisterna number (E or L) equaled the product of persistence time (P_E or P_L) and maturation frequency (m) but did not include the experimentally observed

homotypic fusion frequency. It prompted us to develop a simulation model of cisterna maturation considering different factors in the form of rates. We combined information from 4D imaging and mathematical simulation to get insight into the modes and factors affecting Golgi cisterna size. We tried to develop a model to validate the functions of potential Golgi size regulators. We were able to corroborate our data by studying null mutant *arf1*. The optimized parameters for simulation resulted in a good overlapping match with the experimental maturation parameters. Based on these assumptions though Arf1 is the protein that helps in membrane curvature [107] and controls the rate of vesicle exit from ERES while for ferrying Golgi resident proteins from trans to early Golgi compartment required Vps74 [6] thus maintaining Golgi size in their specific way. The ability to incorporate experimental input in terms of the trajectories of the early Golgi particles and prediction of outcome as a functional two effective rates justifies the clarity of the model. In our coarse-grained computational model, we had introduced four parameters with fixed value for specific strain as per the functional knowledge existing about the protein that was either deleted or overexpressed. Based on the heatmap diagram for tuning rates k_{early} , k_{late} governing the size and number of cisterna (Fig 6.6 and 6.7) we could simulate an in-silico Golgi cisterna maturation process of *S.cerevisiae* and arrive at the proximity of experimental key parameters measured.

Golgi biogenesis and structure maintenance involves tight regulation of anterograde and retrograde transport between ER- Golgi, intra-Golgi compartments and the Golgi-endosome network. Lowered rate of retrograde transport from late to early Golgi causes enhanced late Golgi formation, seen in the case of *vps74* deletion. Our study emphasizes

the role of transport rate alterations on Golgi morphology and dynamics by monitoring maturation parameters of null mutant like *arf1*. It is a unique study wherein we had put forth the modes of Golgi size regulation by different membrane trafficking proteins. This study could significantly help in deciphering regulatory functions of other potential regulatory factors of Golgi size control mechanism through our proposed mathematical model. This study could be further used to validate other membrane trafficking proteins and their role in the regulation of cisterna maturation and dynamics.

Chapter 7

CRISPR mediated gene knock out in mammalian cells

7.1: Introduction

Golgi apparatus plays an integral role in the secretory system. Although the function of Golgi is evolutionarily conserved throughout the eukaryotes, yet there is variation in Golgi structure amongst organisms. Dispersed Golgi stacks are present throughout the cytoplasm in protozoa, fungi, plants, and invertebrates. The Golgi ribbon in mammalian cells comprises of two coupled features: structural continuity and its perinuclear localization. This complex ribbon-shaped structure of Golgi possibly has a purpose of easing protein modification and secretion. Some factors take care of its disassembly [135-138] and distribution [139] during cell division like mitosis. It explains the morphological changes observed in Golgi during mitosis.

Phosphatidylinositol-4-phosphate (PI4P) is a hallmark feature, which serves as a Golgi associated marker, and regulates several downstream effectors like GOLPH3/Vps74. We focused our work on studying the role of PtdIns4P effector- Vps74 in regulating Golgi size using *S.cerevisiae* (Chapter 5) as our model system. The mammalian orthologue, GOLPH3 is a potent oncogene reported to be a candidate gene of 5p13 amplification in several cancers like breast, prostate, oral and ovarian [4]. Being a potent oncogene, GOLPH3 also has a role in maintaining Golgi morphology. shRNA mediated knockdown of GOLPH3 results into compact Golgi [5], and also blocks the anterograde transport from Trans Golgi. Another paralog of protein GOLPH3, known as GOLPH3L is shown to have the opposite effect on Golgi morphology. shRNA mediated knock out of GOLPH3L results into dispersed Golgi [78].

GTPases of Arf family, COPI, COPII, clathrin-mediated vesiculation, and cargo transport regulate uninterrupted trafficking. Arf1 helps in the recruitment of various signaling molecules onto the Golgi membrane. Arf1 is pre-requisite for coatamer associated intra-Golgi retrograde transport of vesicles, and for inducing membrane curvature. Membrane-bound phospholipids and proteins of Golgi serve a vital function to maintain membrane trafficking and also its morphology. The membrane-bound trimeric G proteins assemble cytosolic proteins Arf1 or β -COP onto Golgi membranes. Studying the maintenance of the tubular-vesiculated structure of Golgi is essential. BFA inhibits the association of Arf1 or β -COP onto Golgi membrane by inhibiting the activity of G protein or coupling of G-protein effectors [140]. The enhanced retrograde flow of Golgi membrane to ER and tight block of export from ER was observed.

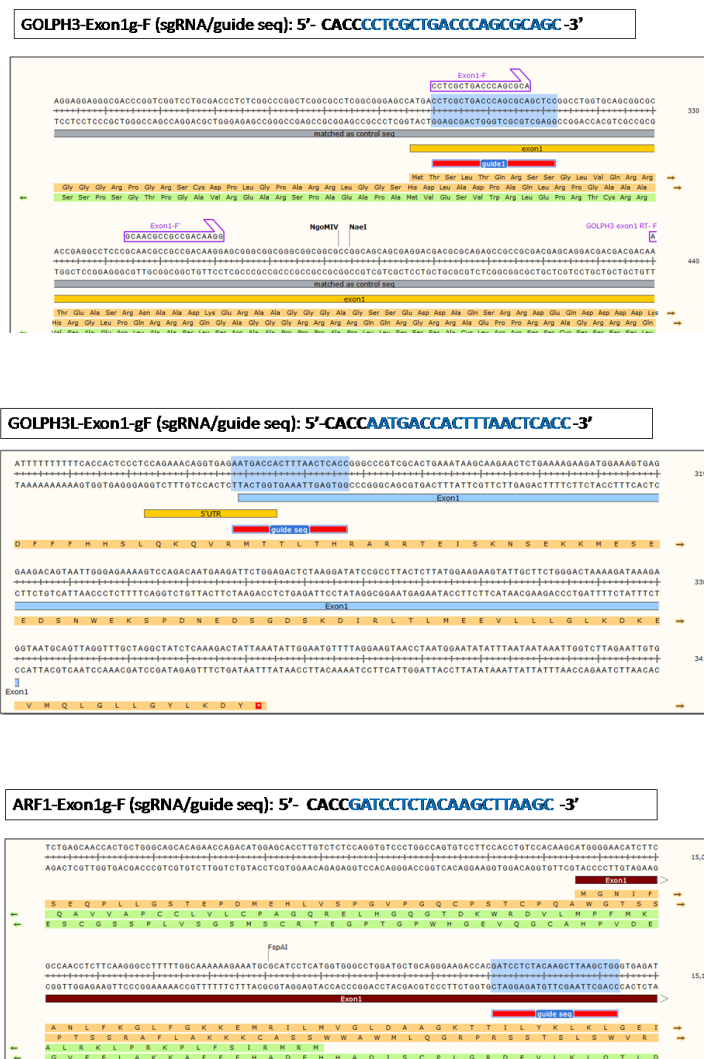
We tried to demonstrate the role of GOLPH3L, GOLPH3, and ARF1 KO on Golgi morphology and quantified the changes observed. We used CRISPR mediated knock out strategy in U2-OS cell line to make the stable knock out clones. Along with the morphological changes observed using a confocal microscope, we put forth different parameters to understand the morphological changes in the knock out compared to control cells. In our study, we also proposed a simple method to analyze the morphology based on 3D imaging and analysis. In ARF1 and GOLPH3L CRISPR KO, we observed dispersed phenotype. However, the extent of dispersion and size of Golgi surfaces varied in morphology. We used 3D reconstruction module of Imaris to quantify the total Golgi volume. To measure the compactness or fragmentation phenotype of Golgi we put forth another parametric measurement, no. of fragmented Golgi surfaces in knockouts and

control cells. These different parametric measurement scales enabled us to classify the various phenotype of Golgi shape observed. This study will allow us to understand the spatial dimension of the Golgi organelle within a cell. We could know the different parameters like total Golgi volume and no. of fragmented Golgi surfaces in a highly complex tubular-vesicular structure of Golgi.

7.2: Results

7.2.1 Transient knockout of GOLPH3, GOLPH3L, and ARF1:

The guide sequence specifically targeting the desired gene (Fig 7.1) was designed as per the protocol from the Zhang lab [141-144]. Annealing of the complementary oligonucleotide sequence and ligation of the guide sequence in the CRISPR vector backbone is detailed in Appendix section 10.7, 10.8 and 10.9.

Figure 7.1: Guide sequence for GOLPH3, GOLPH3L, and ARF1 designed in exon1

In U2OS cell line, transient transfection of BFP tagged CRISPR plasmid targeting genes GOLPH3, GOLPH3L and ARF1 separately gave varied effect on Golgi morphology (Fig 7.2), marked by the co-transfected GalNacT2-GFP Golgi marker. CRISPR plasmid positive cells were marked with BFP tag. We found that in the case of GOLPH3 KO, the Golgi morphology had become compact while in case of both ARF1 and GOLPH3L KO the Golgi had become dispersed. Since we observed a polyclonal population of cells with

different Golgi morphology, we resorted making a stable clone using puromycin selection. In case of control empty CRISPR BFP plasmid is transfected. The co-transfected GalNacT2-GFP plasmid determines Golgi morphology. Scale bar is 5 μ m.

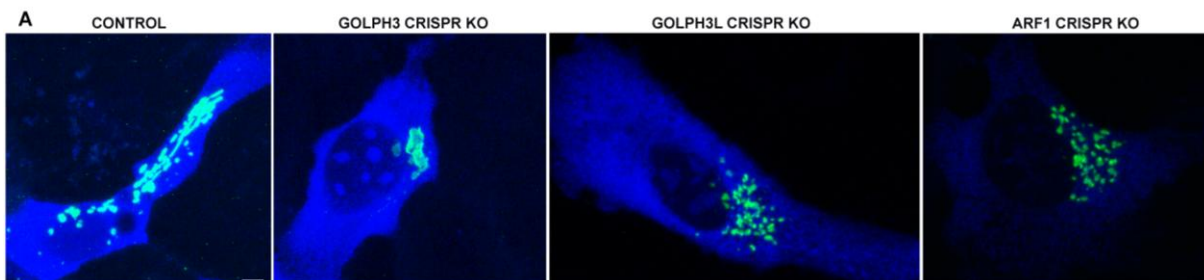


Figure 7.2: Representative U2OS cell line with the CRISPR BFP plasmid having guide sequence targeting GOLPH3, GOLPH3L, and ARF1 genes

7.2.2 Stable clone development for ARF1, GOLPH3, and GOLPH3L knock out:

We tried to make a stable clone for GOLPH3, GOLPH3L and ARF1 knock out in U2-OS cell line using puromycin selection based CRISPR plasmid. After screening many clones for the desired knock out we were able to make GOLPH3L and ARF1 knock out in U2-OS cell line. The representative image GOLPH3L and ARF1 knock out (Fig 7.3) shows that the Golgi gets dispersed into many small vesicles.

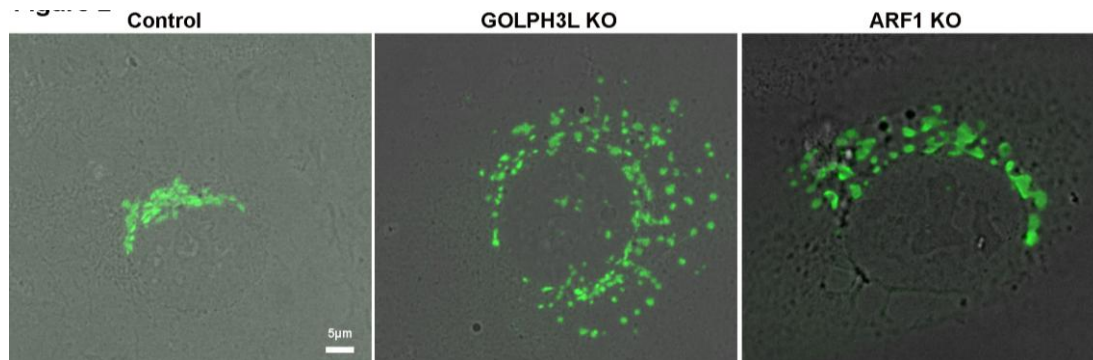
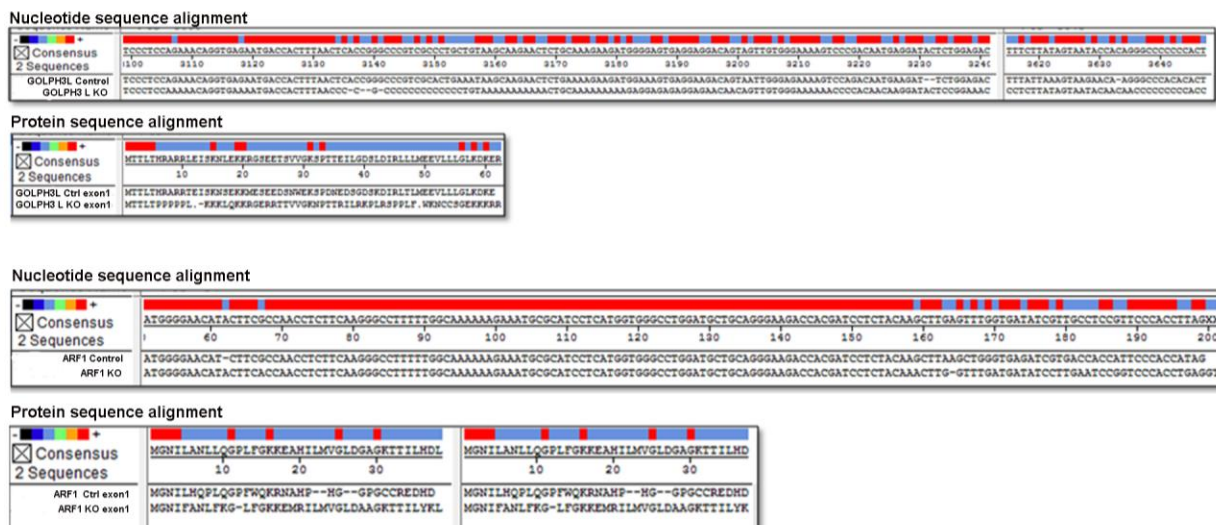


Figure 7.3: Representative Golgi morphology in control, GOLPH3L, and ARF1 KO cells

Further for confirming the gene knock out we did sequencing and compared the Knockout sequence with control (Fig 7.4). The comparison of the sequence around exon 1 of GOLPH3L and ARF1 gene was aligned using the Mega line (Laser gene) software.

7.2.3 Sequence analysis of knock out clones



Red color codes full alignment. Blue color codes misalignment. - represents deletion & . denotes stop codon

Figure 7.4: The upper two panels compare the nucleotide and protein sequence for GOLPH3L

KO with control while the bottom two sequence alignments are for ARF1 KO with control

Megaline (laser gene) software was used for sequence comparison. The color code red states full alignment while blue represents misalignment. '-' means deletion, while '.' represents stop codon.

We could not make stable GOLPH3 KO clones. The sequencing data analyzed using the BLAST tool do not show any deletion or insertion of nucleotides in the target region or guide region designed for GOLPH3.

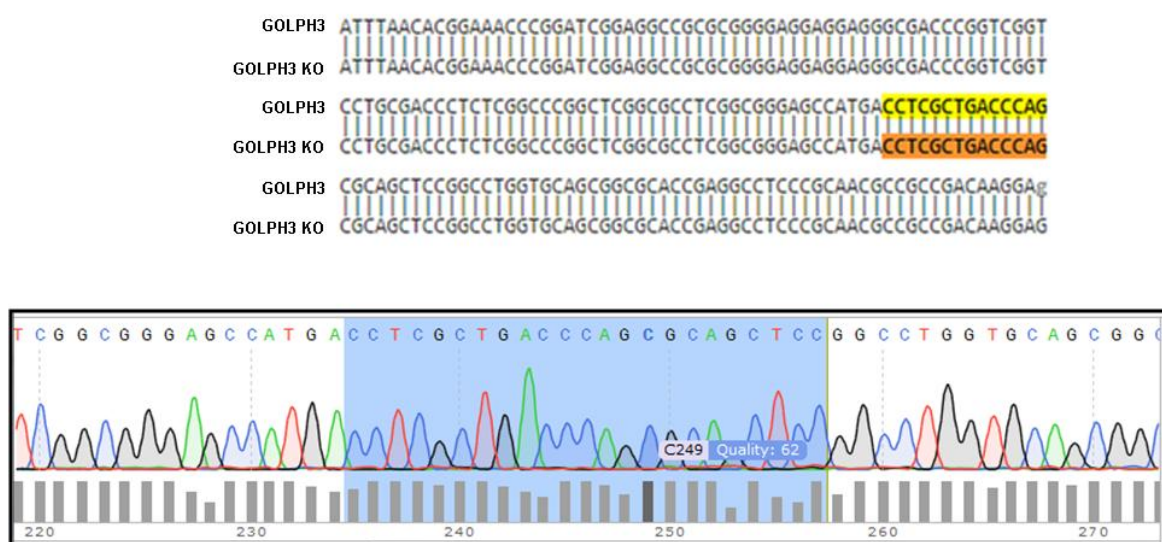


Figure 7.5: Blast sequence comparison for GOLPH3 in the clones and control

The orange highlighted sequence in Figure 7.5 is the target region used to design the guide sequence. The knockout sequence read was the same as the control at the guide region of the target explaining that the clone is not a knockout. In the Chromatogram, blue color highlights the target guide sequence.

7.2.4: T7 endonuclease test

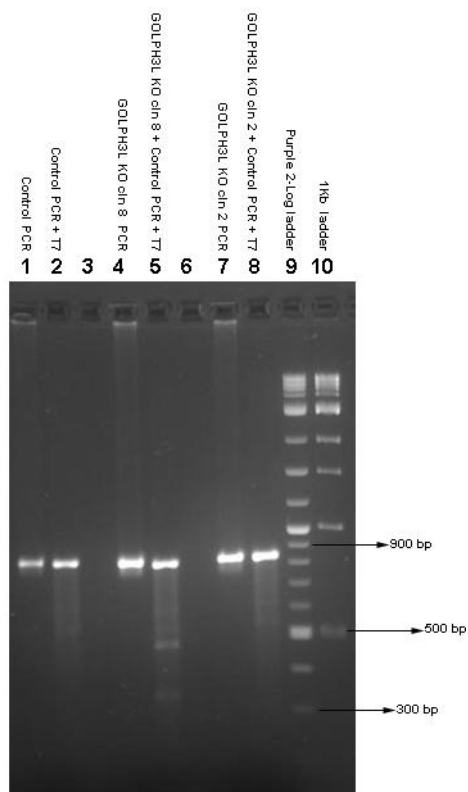


Figure 7.6: T7 micronuclease assay for the stable clone of U2OS GOLPH3L knock out

To confirm the alterations in sequence in the knock out strains, we also did T7 micronuclease assay. The total length of the PCR for the primers designed for sequence around GOLPH3L exon1 is 844bp. If there are any alterations near the desired guide region, T7 nuclease cut will generate two fragments of 346 and 498 bp.

Positive clone PCR sample for GOLPH3L KO clone 8 gave two bands approximately of 500bp and 346bp (lane 5, Fig 7.6). Negative clone in lane 8, clone 2 does not show any band release (lane 8, Fig 7.6). It is giving band size the same as control treated with T7 shown in lane 5.

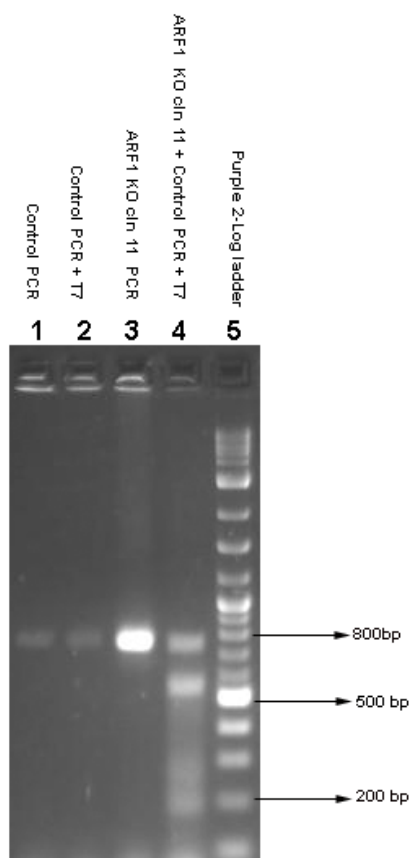


Figure 7.7: T7 micronuclease assay for the stable clone of U2OS ARF1 knock out

The ARF1 KO clones obtained were confirmed using T7 nuclease assay. The total amplicon length spanning the target region around ARF1 exon1 is 725bp. If the target region exhibited deletion or insertion of nucleotide, T7 nuclease cut would generate two fragments of length 190 and 535 bp. The clones screened by T7 nuclease assay for the ARF1 knock out gave the desired fragment release (lane 4, Fig 7.7). PCR fragment from control cells gave a single band even after treatment with the T7 nuclease (lane 2, Fig 7.7).

We confirmed that the GOLPH3 KO clones obtained are not showing alterations like deletion or insertion at the target sequence from T7 nuclease assay. The total amplicon length spanning the target region is 703bp. If the target region exhibited deletion or addition of a nucleotide, T7 nuclease cut would generate two fragments of length 278 and 425 bp. However, the clones screened by T7 nuclease assay for the GOLPH3 knock out did not give the desired fragment release (lane 4 and 6, Fig 7.7). Instead it was similar to the control lane (lane 2, Fig 7.7).

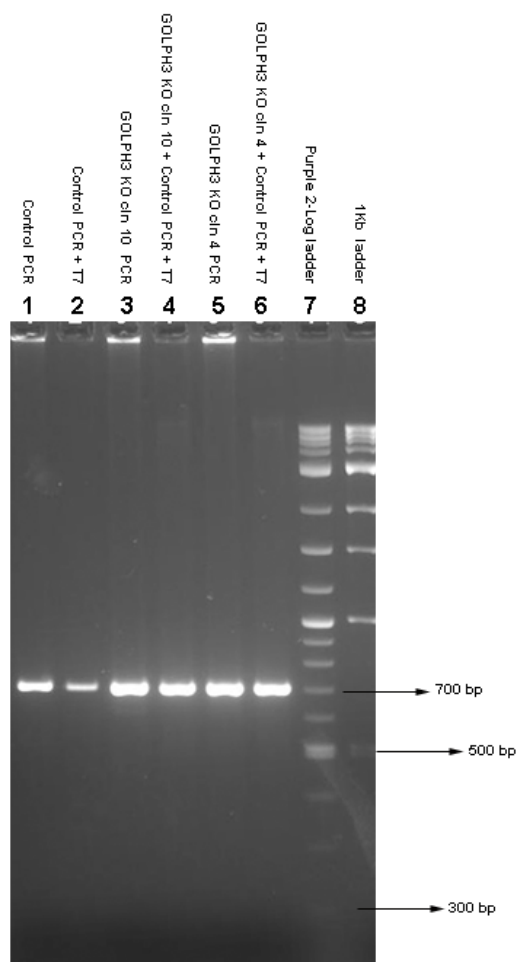


Figure 7.8: T7 micronuclease assay for the stable clone of U2OS GOLPH3 knock out

The lane no. 4 and 6 in the gel shows that the clone screened for GOLPH3 KO is not giving the desired two fragment release after T7 treatment. They resemble the control lane 5.

7.2.5 Quantitative measure of the Golgi morphology changes in the stable GOLPH3L KO:

We measured the parameters like total volume and no. of disconnected Golgi surfaces for the GOLPH3L and ARF1 stable clone.

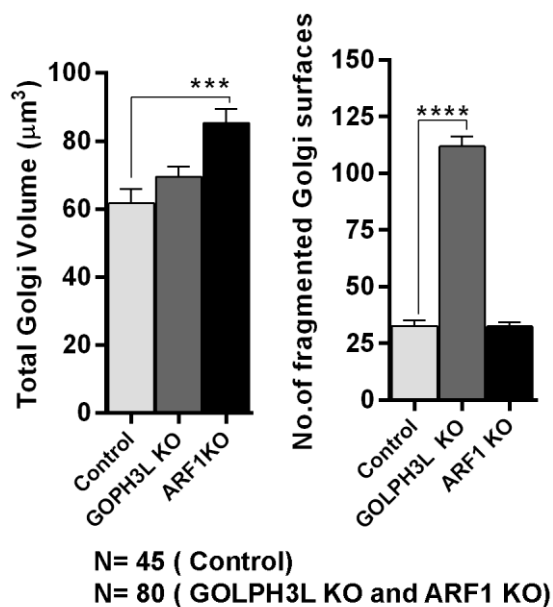


Figure 7.9: Graph for parameters, total Golgi volume and no. of disconnected Golgi surfaces is compared for the GOLPH3L knock out strains and ARF1 KO with control cells

The Golgi organelle was dispersed in case of GOLPH3L KO (Fig 7.3) the total volume quantified was similar to that in control cells. The Golgi dispersed into a large number of fragments in case of GOLPH3L KO (Fig 7.3). The number of disconnected Golgi

surfaces counted in case of GOLPH3L KO was significantly high ($p < 0.0001$) as compared to control cells. In the case of ARF1 KO cells, total Golgi volume was substantially higher compared to control cells. However, the number of fragmented Golgi surfaces did not differ from control cells. This data analyzed is based on N=45 cells for control cells and N= 80 for KO cells. The statistical analysis is done using students' unpaired t-test.

7.3: Discussion

Morphology of Golgi changes during cell division and later distributed into daughter cells. The factors involved in bringing morphological changes are essential to be studied. Golgi disassembles into ER on treatment with BFA drug. Golgi enzymes return to their original position in Golgi after washing out of BFA drug. Golgi rebuilds back to its original ribbon-shaped morphology. It is interesting to study the mechanism of dispersed Golgi determining its structure architect and how it undergoes self-organization. It is important to know specific genes that monitor the organelle size and the mechanism if any. BFA drug inhibits ARF1 activity. ARF1 KO showed dispersed and bulky Golgi. The stable clone for GOLPH3L CRISPR KO also resulted in dispersed Golgi phenotype. Phenotypes of such altered Golgi morphology in case of GOLPH3 and GOLPH3L knockdown is reported [5, 78]. Although the knockdown studies already had detailed the morphology changes in Golgi, we showed the phenotype for GOLPH3L and ARF1 KO using CRISPR technology, and also measured the Golgi morphology parameters like total Golgi volume and number of fragmented Golgi surfaces.

Golgi dispersed upon GOLPH3L KO. GOLPH3L has been shown to interact with Arf1 [85], a protein that helps in vesiculation reaction. We observed dispersal of Golgi when ARF1 or GOLPH3L is knocked out. The dispersed phenotype amongst GOLPH3L and ARF1 KO also vary. The number of fragmented Golgi surfaces generated in the case of GOLPH3L KO was significantly high, while total Golgi volume for ARF1 KO was significantly high compared to control cells. The dispersed Golgi surface in ARF1 KO is bulkier as compared to GOLPH3L KO. There is enlargement in Golgi size in case of ARF1 KO, which is in concordance with the phenotype observed in case of $\Delta arf1$ in *S. cerevisiae*.

Normal Golgi contains both vesicular and tubular structures. Vesiculation process needs both membrane curvature inductions (usually mediated by different GTPases) as well as the pinching off mechanism (normally mediated by dynamin-like proteins). It suggests the balances of such processes along with GTPases and dynamin may also be involving other genes like GOLPH3, GOLPH3L, and ARF1. The ratio of tubular and vesicular structures in Golgi perturbed may thereby alter Golgi morphology. Alterations in the membrane trafficking transport in the anterograde or retrograde direction may also affect the homeostasis of resident Golgi enzymes. The membrane system showing various modifications of vesiculation and tubulation is hypothesized and pictorially represented (Fig 7.10). Extensive vesiculation may cause fragmentation of Golgi structures (Fig: 7.10C), while lower abundance cause tubulation (Fig: 7.10B) and complete elimination of vesiculation and tubulation (Fig: 7.10D) may render the Golgi into more compact structure such as we see in case of GOLPH3 knock out condition (Fig: 7.1). In short, we

are observing the variable degree of vesiculation for GOLPH3L and ARF1 knock out, while compact Golgi reported in the GOLPH3 knockdown [5] may be due to the absence of any vesicular or tubular structure.

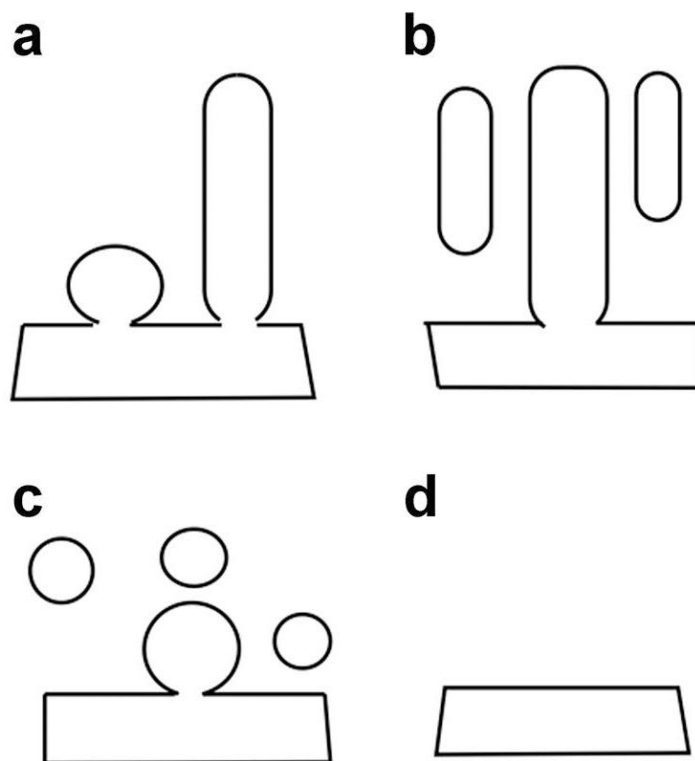


Figure: 7.10: Hypothetical diagram explaining membrane undergoing vesiculation and tubulation at different conditions

We speculate that GOLPH3, GOLPH3L, and ARF1 may cooperatively or antagonistically regulate the tubulation and vesiculation process of Golgi membrane along with GTPases, and especially the dynamins. Such regulation is also strengthened by a previous report stating that overexpression of GOLPH3 causes dispersion while overexpression of GOLPH3L causes compact Golgi formation. Possibly GOLPH3 cooperatively works with or regulates dynamin-like proteins to control Golgi shape. Role

of GOLPH3L and ARF1 could also be determined with dynamins. Synaptojanin works cooperatively with dynamin in neurons [145]. Synaptojanin is a homolog of yeast protein SacI. SacI phosphatase maintains the lower gradient of PI4P towards early cisterna. It works in conjunction with Vps74, a yeast homolog of GOLPH3 and maintains its reverse gradient to that of PI4P. However, there are still a few unanswered questions. Role of dynamins in the knock out cells could be studied.

Mammalian Golgi apparatus is a dynamic organelle which possibly maintains and dynamically regulates its morphology. Golgi is dispersed and distributed in daughter cells during mitosis. It is possible that the gene knockout that disperses the Golgi somehow also plays a crucial role in the case of cell division. One of the potential regulators of Golgi size and shape may be regulating the critical balance of tubular and vesicular structures. It is possibly manifested by fine-tuning the ratio of abundances of membrane curvature inducing GTPases and dynamins. There are likely several factors which directly or indirectly regulate this ratio, and GOLPH3, GOLPH3L, and ARF1 are few of them. This study clearly emphasizes the probable link of these proteins in the regulation of Golgi morphology and the parameters measured can be well accounted for the variation in the Golgi morphology observed.

Chapter 8:

Summary

We speculate both Arf1 and Vps74 both affects the cisterna size. Vps74 and Arf1 regulate the maturation kinetics differently. Increased persistence time of early cisterna and fusion frequency had resulted in an enhanced early Golgi phenotype that matures to few and larger late cisternae in *arf1* Δ . Whereas, in Δ *vps74* the increased homotypic fusion frequency of late cisterna has resulted in a few enlarged late cisterna. This study reveals that Vps74 protein alters the Golgi cisterna size. We could demonstrate the role of Vps74 protein in Golgi maturation using *S. cerevisiae* as a model system (Chapter 5). We have shown the combined role of Vps74 and Arf1 in regulating Golgi cisterna size and maturation kinetics. Arf1 has a dominant role in regulating Golgi cisterna size than Vps74. Arf1 regulates PI4P dependent Clathrin associated vesicle formation. Thus overexpression of Arf1 in Δ *vps74* might have enhanced the amount of clathrin-associated budding from late cisterna and thereby rescued the enlarged phenotype to that of wild-type. Thus Vps74 regulates Golgi cisterna size in an Arf1 dependent manner. Arf1 can alter the distribution of Vps74 along Sec7 cisterna. We had also shown deletion of *ARF1* or *VPS74* changes PI4P gradient along the Golgi compartment. Reduction of PI4P in conditional mutant *pik1-83^{ts}* prominently changed the early cisterna Vrg4 localization.

We have demonstrated the *in-silico* model (Chapter 6) for the cisternal maturation kinetics of *S.cerevisiae* system. The cisterna maturation parameters for WT and Δ *arf1* obtained after simulation was comparable to the experimentally obtained data. The coarse grain model developed using simple rate parameters like $\text{Size}_{\text{denovo}}$ (it decides the size of the cisterna that exit from ER exit sites), K_{denovo} (rate of appearance of cisterna from ER exit site), K_{early} (early Golgi resident protein density) and K_{late} (late Golgi resident protein

density) were demonstrated. Based on the rationale assumption for different Golgi size regulators, this model could be further modified and their role in Golgi cisternal dynamics and maturation could be studied. Studies based on genes involved in anterograde and retrograde transport between ER- Golgi, intra-Golgi and its role in Golgi size could also be added on to the model.

We had demonstrated the effect of GOLPH3L and ARF1 KO in Golgi morphology using CRISPR mediated gene knockout technology (Chapter 7). We observed the Golgi becomes fragmented in the KO versions. We were able to distinguish the dispersed phenotype seen in two different gene mutants with the parameters: total Golgi volume and no. of fragmented Golgi surfaces. GOLPH3L KO cells show numerous and small dispersed Golgi surfaces, while ARF1 KO cells show large and dispersed Golgi surfaces. The number of fragmented Golgi surfaces in case of GOLPH3L KO is significantly high as compared to control U2OS cells. Though the number of Golgi surfaces in ARF1 KO is almost similar to control U2OS cells, their total Golgi volume is significantly higher than control U2OS cells. We speculate GOLPH3, GOLPH3L or ARF1 might have a role in the regulation of Golgi morphology by maintaining tubulation and vesiculation processes. Function of these proteins with other dynamin like proteins and other GTPases could be further elaborated.

Chapter 9

Bibliography

References

1. Kellokumpu, S., R. Sormunen, and I. Kellokumpu, *Abnormal glycosylation and altered Golgi structure in colorectal cancer: dependence on intra-Golgi pH*. FEBS Lett, 2002. **516**(1-3): p. 217-24.
2. Petrosyan, A., *Onco-Golgi: Is Fragmentation a Gate to Cancer Progression?* Biochem Mol Biol J, 2015. **1**(1).
3. Bekier, M.E., 2nd, et al., *Knockout of the Golgi stacking proteins GRASP55 and GRASP65 impairs Golgi structure and function*. Mol Biol Cell, 2017. **28**(21): p. 2833-2842.
4. Scott, K.L., et al., *GOLPH3 modulates mTOR signalling and rapamycin sensitivity in cancer*. Nature, 2009. **459**(7250): p. 1085-90.
5. Dippold, H.C., et al., *GOLPH3 bridges phosphatidylinositol-4- phosphate and actomyosin to stretch and shape the Golgi to promote budding*. Cell, 2009. **139**(2): p. 337-51.
6. Wood, C.S., et al., *PtdIns4P recognition by Vps74/GOLPH3 links PtdIns 4-kinase signaling to retrograde Golgi trafficking*. J Cell Biol, 2009. **187**(7): p. 967-75.
7. Tu, L., et al., *Signal-mediated dynamic retention of glycosyltransferases in the Golgi*. Science, 2008. **321**(5887): p. 404-7.
8. Marshall, W.F., *Organelle size control systems: from cell geometry to organelle-directed medicine*. Bioessays, 2012. **34**(9): p. 721-4.
9. Hollmann, K.H., *A morphometric study of sub-cellular organization in mouse mammary cancers and normal lactating tissue*. Z Zellforsch Mikrosk Anat, 1968. **87**(2): p. 266-77.
10. Koning, A.J., et al., *DiOC6 staining reveals organelle structure and dynamics in living yeast cells*. Cell Motil Cytoskeleton, 1993. **25**(2): p. 111-28.
11. Prinz, W.A., et al., *Mutants affecting the structure of the cortical endoplasmic reticulum in Saccharomyces cerevisiae*. J Cell Biol, 2000. **150**(3): p. 461-74.
12. Palade, G., *Intracellular aspects of the process of protein synthesis*. Science, 1975. **189**(4206): p. 867.
13. Hobman, T.C., et al., *Immunoisolation and characterization of a subdomain of the endoplasmic reticulum that concentrates proteins involved in COPII vesicle biogenesis*. Mol Biol Cell, 1998. **9**(6): p. 1265-78.
14. Staehelin, L.A., *The plant ER: a dynamic organelle composed of a large number of discrete functional domains*. Plant J, 1997. **11**(6): p. 1151-65.
15. Cosson, P. and F. Letourneur, *Coatamer interaction with di-lysine endoplasmic reticulum retention motifs*. Science, 1994. **263**(5153): p. 1629-31.
16. Gaynor, E.C. and S.D. Emr, *COPI-independent anterograde transport: cargo-selective ER to Golgi protein transport in yeast COPI mutants*. J Cell Biol, 1997. **136**(4): p. 789-802.
17. Lewis, M.J. and H.R. Pelham, *SNARE-mediated retrograde traffic from the Golgi complex to the endoplasmic reticulum*. Cell, 1996. **85**(2): p. 205-15.
18. Palmer, D.J., et al., *Binding of coatamer to Golgi membranes requires ADP-ribosylation factor*. J Biol Chem, 1993. **268**(16): p. 12083-9.
19. Serafini, T., et al., *ADP-ribosylation factor is a subunit of the coat of Golgi-derived COP-coated vesicles: a novel role for a GTP-binding protein*. Cell, 1991. **67**(2): p. 239-53.
20. Donaldson, J.G., D. Finazzi, and R.D. Klausner, *Brefeldin A inhibits Golgi membrane-catalysed exchange of guanine nucleotide onto ARF protein*. Nature, 1992. **360**(6402): p. 350-2.
21. McMahon, H.T. and I.G. Mills, *COP and clathrin-coated vesicle budding: different pathways, common approaches*. Curr Opin Cell Biol, 2004. **16**(4): p. 379-91.

22. Pagano, A., et al., *Sec24 proteins and sorting at the endoplasmic reticulum*. J Biol Chem, 1999. **274**(12): p. 7833-40.
23. Miller, E.A., et al., *Multiple cargo binding sites on the COPII subunit Sec24p ensure capture of diverse membrane proteins into transport vesicles*. Cell, 2003. **114**(4): p. 497-509.
24. Bielli, A., et al., *Regulation of Sar1 NH2 terminus by GTP binding and hydrolysis promotes membrane deformation to control COPII vesicle fission*. J Cell Biol, 2005. **171**(6): p. 919-24.
25. Sato, K. and A. Nakano, *Dissection of COPII subunit-cargo assembly and disassembly kinetics during Sar1p-GTP hydrolysis*. Nat Struct Mol Biol, 2005. **12**(2): p. 167-74.
26. Mellman, I. and K. Simons, *The Golgi complex: in vitro veritas?* Cell, 1992. **68**(5): p. 829-40.
27. Griffiths, G., et al., *Exit of newly synthesized membrane proteins from the trans cisterna of the Golgi complex to the plasma membrane*. J Cell Biol, 1985. **101**(3): p. 949-64.
28. Losev, E., et al., *Golgi maturation visualized in living yeast*. Nature, 2006. **441**(7096): p. 1002-6.
29. Farquhar, M.G. and G.E. Palade, *The Golgi apparatus (complex)-(1954-1981)-from artifact to center stage*. J Cell Biol, 1981. **91**(3 Pt 2): p. 77s-103s.
30. Rothman, J.E., *The golgi apparatus: two organelles in tandem*. Science, 1981. **213**(4513): p. 1212-9.
31. Dunphy, W.G. and J.E. Rothman, *Compartmental organization of the Golgi stack*. Cell, 1985. **42**(1): p. 13-21.
32. Farquhar, M.G., *Progress in unraveling pathways of Golgi traffic*. Annu Rev Cell Biol, 1985. **1**: p. 447-88.
33. Rothman, J.E. and F.T. Wieland, *Protein sorting by transport vesicles*. Science, 1996. **272**(5259): p. 227-34.
34. Orci, L., et al., *Exclusion of golgi residents from transport vesicles budding from Golgi cisternae in intact cells*. J Cell Biol, 2000. **150**(6): p. 1263-70.
35. Pelham, H.R. and J.E. Rothman, *The debate about transport in the Golgi--two sides of the same coin?* Cell, 2000. **102**(6): p. 713-9.
36. Dahan, S., et al., *Concentration of intracellular hepatic apolipoprotein E in Golgi apparatus saccular distensions and endosomes*. J Cell Biol, 1994. **127**(6 Pt 2): p. 1859-69.
37. Martinez-Menarguez, J.A., et al., *Peri-Golgi vesicles contain retrograde but not anterograde proteins consistent with the cisternal progression model of intra-Golgi transport*. J Cell Biol, 2001. **155**(7): p. 1213-24.
38. Gilchrist, A., et al., *Quantitative proteomics analysis of the secretory pathway*. Cell, 2006. **127**(6): p. 1265-81.
39. Bannykh, S.I. and W.E. Balch, *Membrane dynamics at the endoplasmic reticulum-Golgi interface*. J Cell Biol, 1997. **138**(1): p. 1-4.
40. Mironov, A.A., et al., *ER-to-Golgi carriers arise through direct en bloc protrusion and multistage maturation of specialized ER exit domains*. Dev Cell, 2003. **5**(4): p. 583-94.
41. Glick, B.S. and V. Malhotra, *The curious status of the Golgi apparatus*. Cell, 1998. **95**(7): p. 883-9.
42. Rabouille, C. and J. Klumperman, *Opinion: The maturing role of COPI vesicles in intra-Golgi transport*. Nat Rev Mol Cell Biol, 2005. **6**(10): p. 812-7.
43. Weidman, P.J., *Anterograde transport through the Golgi complex: do Golgi tubules hold the key?* Trends Cell Biol, 1995. **5**(8): p. 302-5.
44. Mironov, A.A., P. Weidman, and A. Luini, *Variations on the intracellular transport theme: maturing cisternae and trafficking tubules*. J Cell Biol, 1997. **138**(3): p. 481-4.
45. Marsh, B.J., et al., *Direct continuities between cisternae at different levels of the Golgi complex in glucose-stimulated mouse islet beta cells*. Proc Natl Acad Sci U S A, 2004. **101**(15): p. 5565-70.

46. Trucco, A., et al., *Secretory traffic triggers the formation of tubular continuities across Golgi sub-compartments*. Nat Cell Biol, 2004. **6**(11): p. 1071-81.
47. San Pietro, E., et al., *Group IV phospholipase A(2)alpha controls the formation of inter-cisternal continuities involved in intra-Golgi transport*. PLoS Biol, 2009. **7**(9): p. e1000194.
48. Patterson, G.H., et al., *Transport through the Golgi apparatus by rapid partitioning within a two-phase membrane system*. Cell, 2008. **133**(6): p. 1055-67.
49. Emr, S., et al., *Journeys through the Golgi--taking stock in a new era*. J Cell Biol, 2009. **187**(4): p. 449-53.
50. Bonfanti, L., et al., *Procollagen traverses the Golgi stack without leaving the lumen of cisternae: evidence for cisternal maturation*. Cell, 1998. **95**(7): p. 993-1003.
51. Mironov, A.A., et al., *Small cargo proteins and large aggregates can traverse the Golgi by a common mechanism without leaving the lumen of cisternae*. J Cell Biol, 2001. **155**(7): p. 1225-38.
52. Eggeling, C., et al., *Direct observation of the nanoscale dynamics of membrane lipids in a living cell*. Nature, 2009. **457**(7233): p. 1159-62.
53. Rambourg, A. and Y. Clermont, *Three-dimensional electron microscopy: structure of the Golgi apparatus*. Eur J Cell Biol, 1990. **51**(2): p. 189-200.
54. Kondylis, V. and C. Rabouille, *The Golgi apparatus: lessons from Drosophila*. FEBS Lett, 2009. **583**(23): p. 3827-38.
55. Melkonian, M., B. Becker, and D. Becker, *Scale formation in algae*. J Electron Microsc Tech, 1991. **17**(2): p. 165-78.
56. Kang, B.H. and L.A. Staehelin, *ER-to-Golgi transport by COPII vesicles in Arabidopsis involves a ribosome-excluding scaffold that is transferred with the vesicles to the Golgi matrix*. Protoplasma, 2008. **234**(1-4): p. 51-64.
57. Yelinek, J.T., C.Y. He, and G. Warren, *Ultrastructural study of Golgi duplication in Trypanosoma brucei*. Traffic, 2009. **10**(3): p. 300-6.
58. Matsuura-Tokita, K., et al., *Live imaging of yeast Golgi cisternal maturation*. Nature, 2006. **441**(7096): p. 1007-10.
59. Clermont, Y., A. Rambourg, and L. Hermo, *Trans-Golgi network (TGN) of different cell types: three-dimensional structural characteristics and variability*. Anat Rec, 1995. **242**(3): p. 289-301.
60. Wang, Y.J., et al., *Phosphatidylinositol 4 phosphate regulates targeting of clathrin adaptor AP-1 complexes to the Golgi*. Cell, 2003. **114**(3): p. 299-310.
61. Farhan, H., et al., *MAPK signaling to the early secretory pathway revealed by kinase/phosphatase functional screening*. J Cell Biol, 2010. **189**(6): p. 997-1011.
62. Rossanese, O.W., et al., *Golgi structure correlates with transitional endoplasmic reticulum organization in Pichia pastoris and Saccharomyces cerevisiae*. J Cell Biol, 1999. **145**(1): p. 69-81.
63. Kurokawa, K., et al., *Live cell visualization of Golgi membrane dynamics by super-resolution confocal live imaging microscopy*. Methods Cell Biol, 2013. **118**: p. 235-42.
64. Yang, W., et al., *Modification of the cytoplasmic domain affects the subcellular localization of Golgi glycosyl-transferases*. Eur J Cell Biol, 1996. **71**(1): p. 53-61.
65. Barr, F.A., et al., *GRASP65, a protein involved in the stacking of Golgi cisternae*. Cell, 1997. **91**(2): p. 253-62.
66. Shorter, J., et al., *GRASP55, a second mammalian GRASP protein involved in the stacking of Golgi cisternae in a cell-free system*. EMBO J, 1999. **18**(18): p. 4949-60.
67. Wang, Y., A. Satoh, and G. Warren, *Mapping the functional domains of the Golgi stacking factor GRASP65*. J Biol Chem, 2005. **280**(6): p. 4921-8.
68. Puthenveedu, M.A., et al., *GM130 and GRASP65-dependent lateral cisternal fusion allows uniform Golgi-enzyme distribution*. Nat Cell Biol, 2006. **8**(3): p. 238-48.

69. Feinstein, T.N. and A.D. Linstedt, *GRASP55 regulates Golgi ribbon formation*. Mol Biol Cell, 2008. **19**(7): p. 2696-707.
70. Xiang, Y. and Y. Wang, *GRASP55 and GRASP65 play complementary and essential roles in Golgi cisternal stacking*. J Cell Biol, 2010. **188**(2): p. 237-51.
71. Sinka, R., et al., *Golgi coiled-coil proteins contain multiple binding sites for Rab family G proteins*. J Cell Biol, 2008. **183**(4): p. 607-15.
72. Hayes, G.L., et al., *Multiple Rab GTPase binding sites in GCC185 suggest a model for vesicle tethering at the trans-Golgi*. Mol Biol Cell, 2009. **20**(1): p. 209-17.
73. Boehm, J., et al., *Sec12p requires Rer1p for sorting to coatomer (COPI)-coated vesicles and retrieval to the ER*. J Cell Sci, 1997. **110 (Pt 8)**: p. 991-1003.
74. Fullekrug, J., et al., *Human Rer1 is localized to the Golgi apparatus and complements the deletion of the homologous Rer1 protein of Saccharomyces cerevisiae*. Eur J Cell Biol, 1997. **74**(1): p. 31-40.
75. Sato, K., M. Sato, and A. Nakano, *Rer1p as common machinery for the endoplasmic reticulum localization of membrane proteins*. Proc Natl Acad Sci U S A, 1997. **94**(18): p. 9693-8.
76. Richardson, B.C., et al., *The Sec7 N-terminal regulatory domains facilitate membrane-proximal activation of the Arf1 GTPase*. Elife, 2016. **5**.
77. Tokuda, E., et al., *Phosphatidylinositol 4-phosphate in the Golgi apparatus regulates cell-cell adhesion and invasive cell migration in human breast cancer*. Cancer Res, 2014. **74**(11): p. 3054-66.
78. Ng, M.M., et al., *GOLPH3L antagonizes GOLPH3 to determine Golgi morphology*. Mol Biol Cell, 2013. **24**(6): p. 796-808.
79. Buschman, M.D., M. Xing, and S.J. Field, *The GOLPH3 pathway regulates Golgi shape and function and is activated by DNA damage*. Front Neurosci, 2015. **9**: p. 362.
80. Ali, M.F., et al., *Golgi phosphoprotein 3 determines cell binding properties under dynamic flow by controlling Golgi localization of core 2 N-acetylglucosaminyltransferase 1*. J Biol Chem, 2012. **287**(47): p. 39564-77.
81. Isaji, T., et al., *An oncogenic protein Golgi phosphoprotein 3 up-regulates cell migration via sialylation*. J Biol Chem, 2014. **289**(30): p. 20694-705.
82. Eckert, E.S., et al., *Golgi phosphoprotein 3 triggers signal-mediated incorporation of glycosyltransferases into coatomer-coated (COPI) vesicles*. J Biol Chem, 2014. **289**(45): p. 31319-29.
83. Schmitz, K.R., et al., *Golgi localization of glycosyltransferases requires a Vps74p oligomer*. Dev Cell, 2008. **14**(4): p. 523-34.
84. Hsu, J.W., et al., *The N-terminus of Vps74p is essential for the retention of glycosyltransferases in the Golgi but not for the modulation of apical polarized growth in Saccharomyces cerevisiae*. PLoS One, 2013. **8**(9): p. e74715.
85. Tu, L., L. Chen, and D.K. Banfield, *A conserved N-terminal arginine-motif in GOLPH3-family proteins mediates binding to coatomer*. Traffic, 2012. **13**(11): p. 1496-507.
86. Graham, T.R. and C.G. Burd, *Coordination of Golgi functions by phosphatidylinositol 4-kinases*. Trends Cell Biol, 2011. **21**(2): p. 113-21.
87. Bhave, M., et al., *Golgi enlargement in Arf-depleted yeast cells is due to altered dynamics of cisternal maturation*. J Cell Sci, 2014. **127**(Pt 1): p. 250-7.
88. Farber-Katz, S.E., et al., *DNA damage triggers Golgi dispersal via DNA-PK and GOLPH3*. Cell, 2014. **156**(3): p. 413-27.
89. Cervigni, R.I., et al., *JNK2 controls fragmentation of the Golgi complex and the G2/M transition through phosphorylation of GRASP65*. J Cell Sci, 2015. **128**(12): p. 2249-60.

90. Inoue, H., H. Nojima, and H. Okayama, *High efficiency transformation of Escherichia coli with plasmids*. *Gene*, 1990. **96**(1): p. 23-8.
91. Liu, H. and J.H. Naismith, *An efficient one-step site-directed deletion, insertion, single and multiple-site plasmid mutagenesis protocol*. *BMC Biotechnol*, 2008. **8**: p. 91.
92. Higuchi, R., et al., *A general method for cloning eukaryotic structural gene sequences*. *Proc Natl Acad Sci U S A*, 1976. **73**(9): p. 3146-50.
93. Sherman, F., *Getting started with yeast*. *Methods Enzymol*, 2002. **350**: p. 3-41.
94. Kawai, S., W. Hashimoto, and K. Murata, *Transformation of Saccharomyces cerevisiae and other fungi: methods and possible underlying mechanism*. *Bioeng Bugs*, 2010. **1**(6): p. 395-403.
95. Harju, S., H. Fedosyuk, and K.R. Peterson, *Rapid isolation of yeast genomic DNA: Bust n' Grab*. *BMC Biotechnol*, 2004. **4**: p. 8.
96. Looke, M., K. Kristjuhan, and A. Kristjuhan, *Extraction of genomic DNA from yeasts for PCR-based applications*. *Biotechniques*, 2011. **50**(5): p. 325-8.
97. Guldener, U., et al., *A new efficient gene disruption cassette for repeated use in budding yeast*. *Nucleic Acids Res*, 1996. **24**(13): p. 2519-24.
98. Guldener, U., et al., *A second set of loxP marker cassettes for Cre-mediated multiple gene knockouts in budding yeast*. *Nucleic Acids Res*, 2002. **30**(6): p. e23.
99. Boeke, J.D., F. LaCroute, and G.R. Fink, *A positive selection for mutants lacking orotidine-5'-phosphate decarboxylase activity in yeast: 5-fluoro-orotic acid resistance*. *Mol Gen Genet*, 1984. **197**(2): p. 345-6.
100. Suda, Y. and A. Nakano, *The yeast Golgi apparatus*. *Traffic*, 2012. **13**(4): p. 505-10.
101. Moseley, J.B. and B.L. Goode, *The yeast actin cytoskeleton: from cellular function to biochemical mechanism*. *Microbiol Mol Biol Rev*, 2006. **70**(3): p. 605-45.
102. Lundmark, R., et al., *Arf family GTP loading is activated by, and generates, positive membrane curvature*. *Biochem J*, 2008. **414**(2): p. 189-94.
103. Krauss, M., et al., *Arf1-GTP-induced tubule formation suggests a function of Arf family proteins in curvature acquisition at sites of vesicle budding*. *J Biol Chem*, 2008. **283**(41): p. 27717-23.
104. Kondo, Y., et al., *ARF1 and ARF3 are required for the integrity of recycling endosomes and the recycling pathway*. *Cell Struct Funct*, 2012. **37**(2): p. 141-54.
105. Gaynor, E.C., et al., *ARF is required for maintenance of yeast Golgi and endosome structure and function*. *Mol Biol Cell*, 1998. **9**(3): p. 653-70.
106. Donaldson, J.G., *Arfs and membrane lipids: sensing, generating and responding to membrane curvature*. *Biochem J*, 2008. **414**(2): p. e1-2.
107. Beck, R., et al., *Membrane curvature induced by Arf1-GTP is essential for vesicle formation*. *Proc Natl Acad Sci U S A*, 2008. **105**(33): p. 11731-6.
108. Nakai, W., et al., *ARF1 and ARF4 regulate recycling endosomal morphology and retrograde transport from endosomes to the Golgi apparatus*. *Mol Biol Cell*, 2013. **24**(16): p. 2570-81.
109. Ettinger, A. and T. Wittmann, *Fluorescence live cell imaging*. *Methods Cell Biol*, 2014. **123**: p. 77-94.
110. Wood, C.S., et al., *Local control of phosphatidylinositol 4-phosphate signaling in the Golgi apparatus by Vps74 and Sac1 phosphoinositide phosphatase*. *Mol Biol Cell*, 2012. **23**(13): p. 2527-36.
111. Audhya, A., M. Foti, and S.D. Emr, *Distinct roles for the yeast phosphatidylinositol 4-kinases, Stt4p and Pik1p, in secretion, cell growth, and organelle membrane dynamics*. *Mol Biol Cell*, 2000. **11**(8): p. 2673-89.
112. Walch-Solimena, C. and P. Novick, *The yeast phosphatidylinositol-4-OH kinase pik1 regulates secretion at the Golgi*. *Nat Cell Biol*, 1999. **1**(8): p. 523-5.

113. Ghugtyal, V., et al., *Phosphatidylinositol-4-phosphate-dependent membrane traffic is critical for fungal filamentous growth*. Proc Natl Acad Sci U S A, 2015. **112**(28): p. 8644-9.
114. Bonifacino, J.S., *The GGA proteins: adaptors on the move*. Nat Rev Mol Cell Biol, 2004. **5**(1): p. 23-32.
115. Carlton, J.G. and P.J. Cullen, *Coincidence detection in phosphoinositide signaling*. Trends Cell Biol, 2005. **15**(10): p. 540-7.
116. Daboussi, L., G. Costaguta, and G.S. Payne, *Phosphoinositide-mediated clathrin adaptor progression at the trans-Golgi network*. Nat Cell Biol, 2012. **14**(3): p. 239-48.
117. Demmel, L., et al., *The clathrin adaptor Gga2p is a phosphatidylinositol 4-phosphate effector at the Golgi exit*. Mol Biol Cell, 2008. **19**(5): p. 1991-2002.
118. Traub, L.M., *Common principles in clathrin-mediated sorting at the Golgi and the plasma membrane*. Biochim Biophys Acta, 2005. **1744**(3): p. 415-37.
119. Wang, J., et al., *PI4P promotes the recruitment of the GGA adaptor proteins to the trans-Golgi network and regulates their recognition of the ubiquitin sorting signal*. Mol Biol Cell, 2007. **18**(7): p. 2646-55.
120. Godi, A., et al., *ARF mediates recruitment of PtdIns-4-OH kinase-beta and stimulates synthesis of PtdIns(4,5)P2 on the Golgi complex*. Nat Cell Biol, 1999. **1**(5): p. 280-7.
121. Luini, A., *A brief history of the cisternal progression-maturation model*. Cell Logist, 2011. **1**(1): p. 6-11.
122. Glick, B.S. and A. Luini, *Models for Golgi traffic: a critical assessment*. Cold Spring Harb Perspect Biol, 2011. **3**(11): p. a005215.
123. Nakano, A. and A. Luini, *Passage through the Golgi*. Curr Opin Cell Biol, 2010. **22**(4): p. 471-8.
124. Bard, F. and V. Malhotra, *The formation of TGN-to-plasma-membrane transport carriers*. Annu Rev Cell Dev Biol, 2006. **22**: p. 439-55.
125. De Matteis, M.A. and A. Luini, *Exiting the Golgi complex*. Nat Rev Mol Cell Biol, 2008. **9**(4): p. 273-84.
126. Papanikou, E., et al., *COPI selectively drives maturation of the early Golgi*. Elife, 2015. **4**.
127. D'Souza-Schorey, C. and P. Chavrier, *ARF proteins: roles in membrane traffic and beyond*. Nat Rev Mol Cell Biol, 2006. **7**(5): p. 347-58.
128. Stenmark, H., *Rab GTPases as coordinators of vesicle traffic*. Nat Rev Mol Cell Biol, 2009. **10**(8): p. 513-25.
129. Bonifacino, J.S. and J. Lippincott-Schwartz, *Coat proteins: shaping membrane transport*. Nat Rev Mol Cell Biol, 2003. **4**(5): p. 409-14.
130. Jahn, R. and R.H. Scheller, *SNAREs--engines for membrane fusion*. Nat Rev Mol Cell Biol, 2006. **7**(9): p. 631-43.
131. Wickner, W. and R. Schekman, *Membrane fusion*. Nat Struct Mol Biol, 2008. **15**(7): p. 658-64.
132. Yu, I.M. and F.M. Hughson, *Tethering factors as organizers of intracellular vesicular traffic*. Annu Rev Cell Dev Biol, 2010. **26**: p. 137-56.
133. Kuhnle, J., et al., *A modeling approach to the self-assembly of the Golgi apparatus*. Biophys J, 2010. **98**(12): p. 2839-47.
134. Bigay, J., et al., *Lipid packing sensed by ArfGAP1 couples COPI coat disassembly to membrane bilayer curvature*. Nature, 2003. **426**(6966): p. 563-6.
135. Farmaki, T., et al., *Forward and retrograde trafficking in mitotic animal cells. ER-Golgi transport arrest restricts protein export from the ER into COPII-coated structures*. J Cell Sci, 1999. **112** (Pt 5): p. 589-600.
136. Kano, F., et al., *Cdc2 kinase-dependent disassembly of endoplasmic reticulum (ER) exit sites inhibits ER-to-Golgi vesicular transport during mitosis*. Mol Biol Cell, 2004. **15**(9): p. 4289-98.

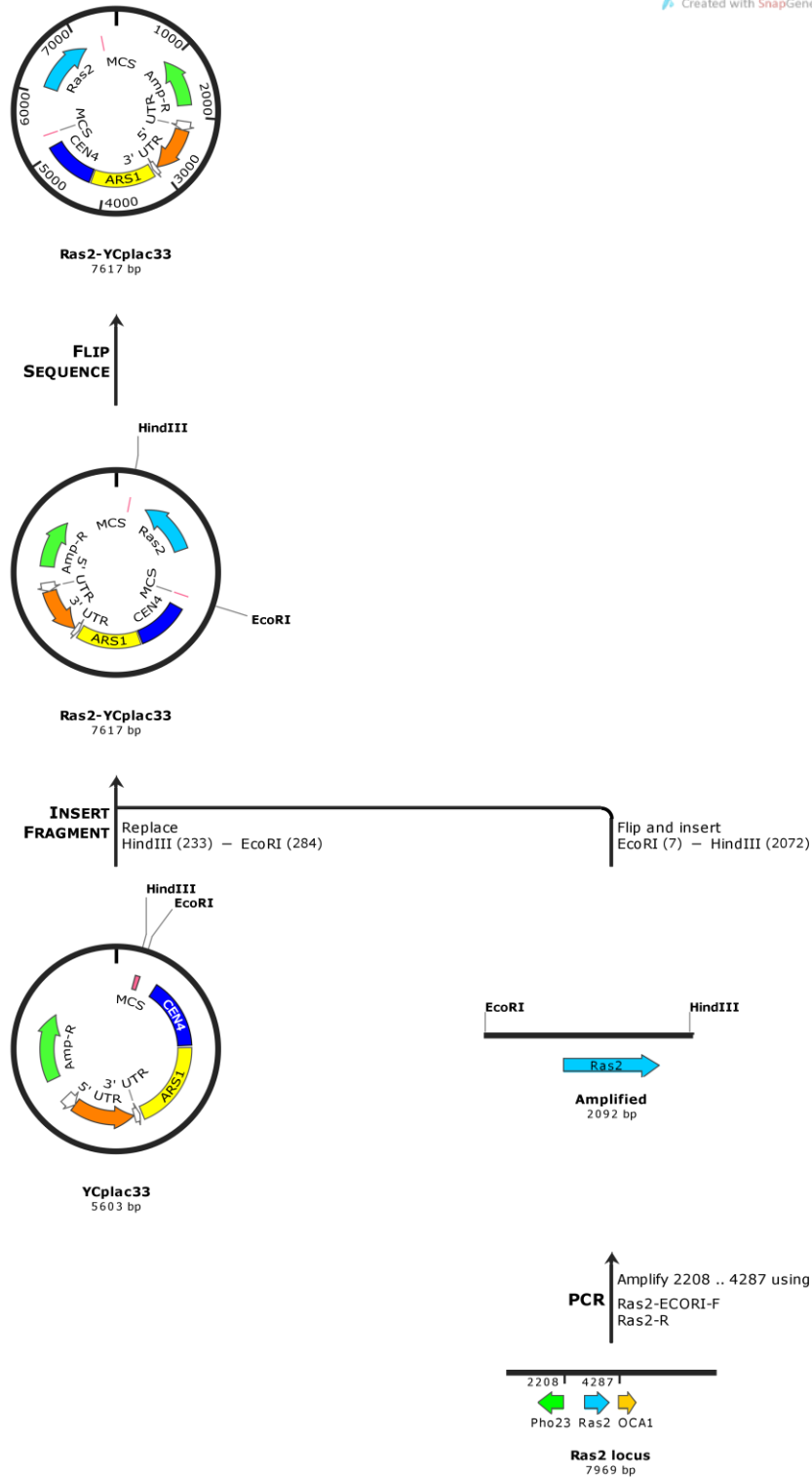
137. Lowe, M., et al., *Cdc2 kinase directly phosphorylates the cis-Golgi matrix protein GM130 and is required for Golgi fragmentation in mitosis*. Cell, 1998. **94**(6): p. 783-93.
138. Wang, Y., et al., *Golgi cisternal unstacking stimulates COPI vesicle budding and protein transport*. PLoS One, 2008. **3**(2): p. e1647.
139. Wei, J.H. and J. Seemann, *Mitotic division of the mammalian Golgi apparatus*. Semin Cell Dev Biol, 2009. **20**(7): p. 810-6.
140. Sciaky, N., et al., *Golgi tubule traffic and the effects of brefeldin A visualized in living cells*. J Cell Biol, 1997. **139**(5): p. 1137-55.
141. Yang, L., et al., *CRISPR/Cas9-Directed Genome Editing of Cultured Cells*. Curr Protoc Mol Biol, 2014. **107**: p. 31 1 1-17.
142. Yang, L., et al., *CRISPR-Cas-mediated targeted genome editing in human cells*. Methods Mol Biol, 2014. **1114**: p. 245-67.
143. Zhou, Y., H. Zhang, and W. Wei, *Simultaneous generation of multi-gene knockouts in human cells*. FEBS Lett, 2016. **590**(23): p. 4343-4353.
144. Zhang, Y., et al., *Efficient and transgene-free genome editing in wheat through transient expression of CRISPR/Cas9 DNA or RNA*. Nat Commun, 2016. **7**: p. 12617.
145. McPherson, P.S., et al., *A presynaptic inositol-5-phosphatase*. Nature, 1996. **379**(6563): p. 353-7.

Chapter 10

Appendix

Appendix 10.1: The cloning strategy for mCherry- Ras2

Created with SnapGene®

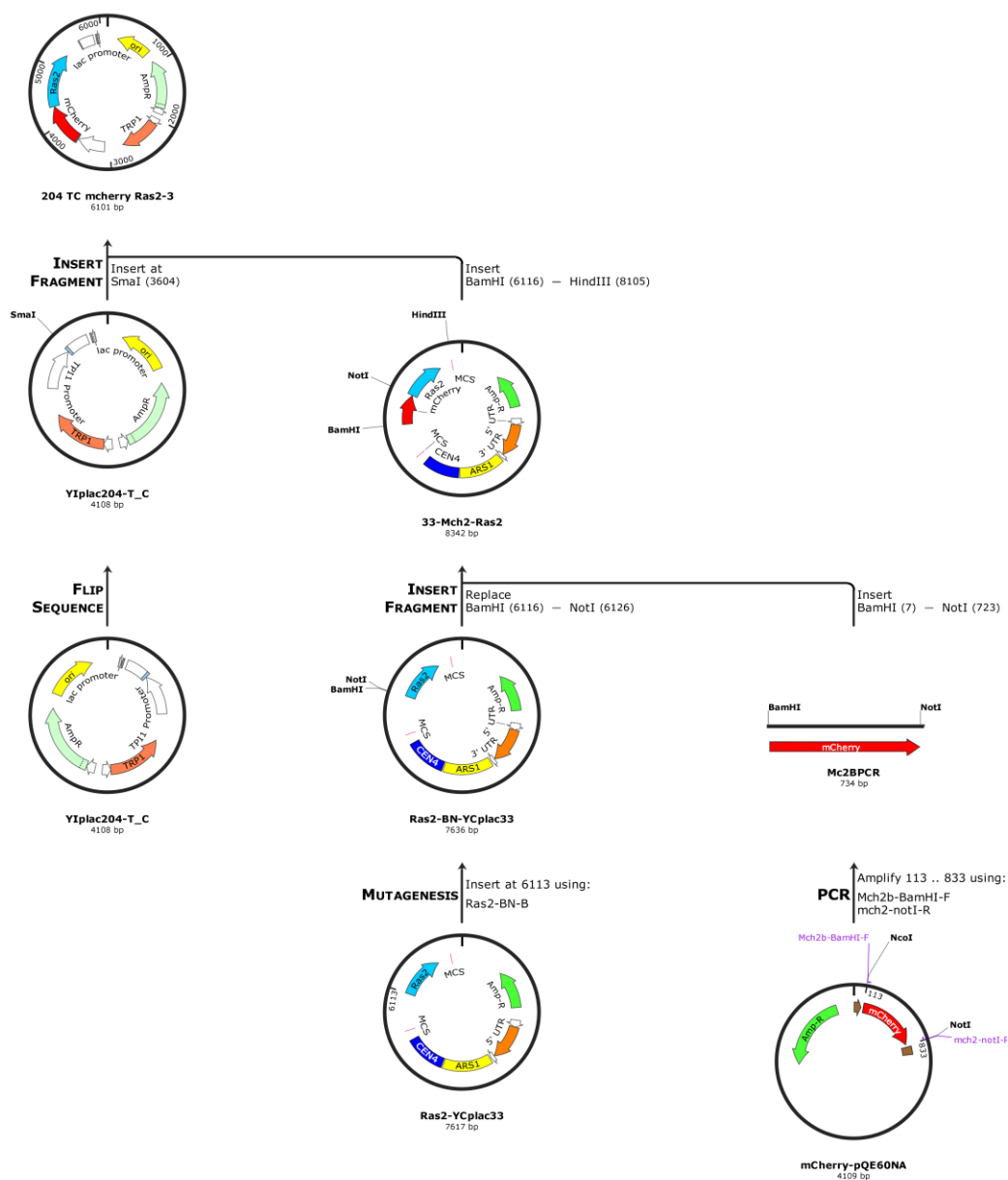


- 1) Endogenous Ras2 gene was amplified using JK9 genomic DNA as template (appx. Fig.10.1A) Primers used were: Ras2- EcoRI-F and Ras2-R. Amplicon size - 2092bp. Annealing temperature- $T_m = 59^\circ\text{C}$ and extension time 4 min at 72°C . The buffer used is GC Phusion buffer with DMSO (added separately).

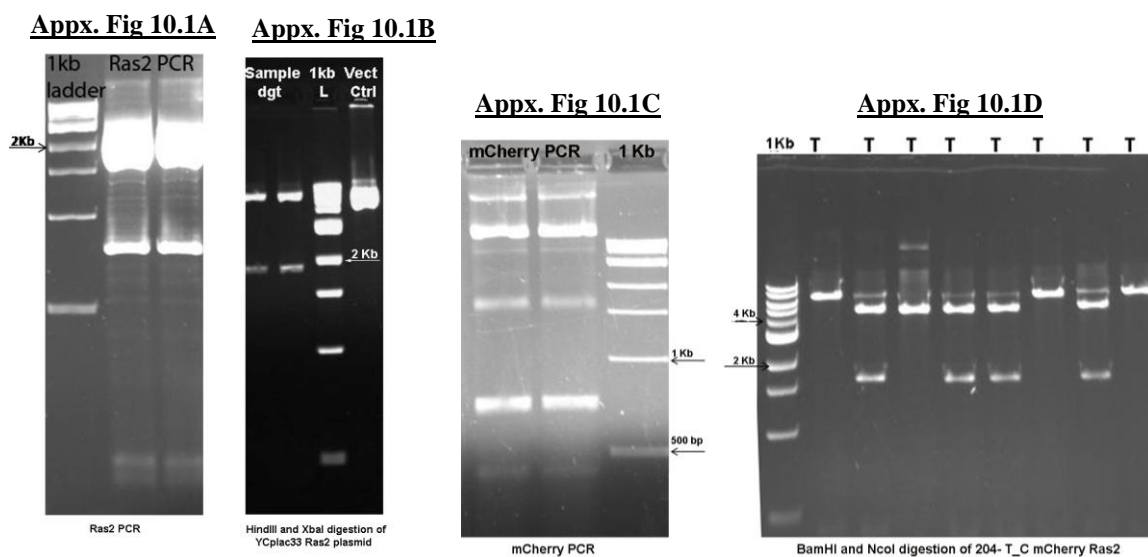
Table 10.1: Ras2 gene PCR cycle

1	98°C	30s
2	98°C	10s
	59°C	30s
	72°C	4min Go to Step 2--- 10X
3	98°C	10s
	59°C	30s
	72°C	4min Go to Step 3----20X Extend 20 sec/cycle
4	72°C	8min
5	25°C	forever

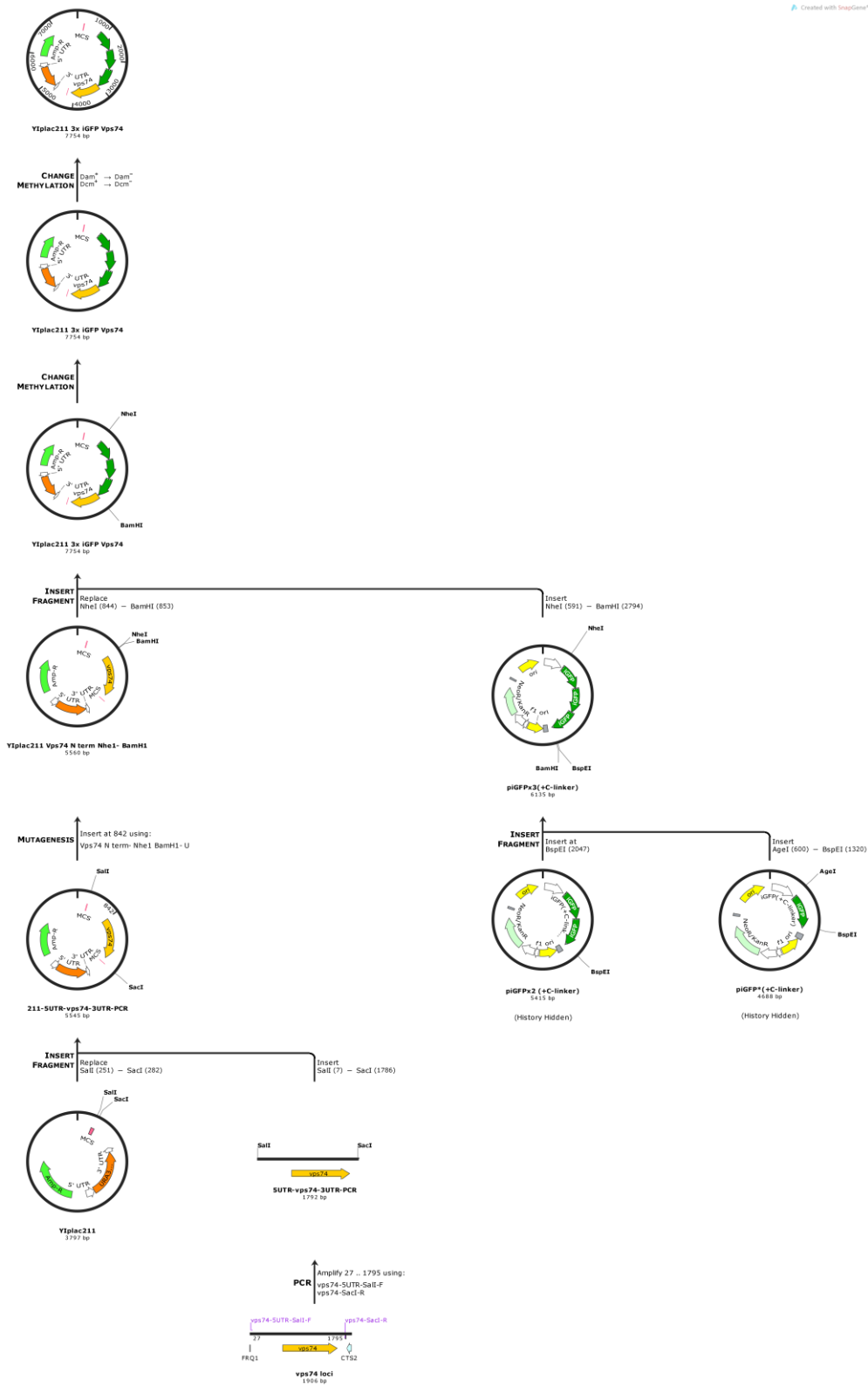
- 2) The resulting PCR product was digested with EcoRI and HindIII enzyme and subcloned in the vector YCplac33 (centromeric Yeast plasmid with Ura3 selection).
- 3) For the diagnosis of the clone Ras2- YCplac33 plasmid, few clones was digested with HindIII and XbaI (appx. Fig 10.1B). Expected band release is near 5kb and 2kp. Bam-Not cassette was introduced at N-termini of Ras2 by site-directed mutagenesis. Primers used were Ras2-BN-B and Ras2-BN-T



- 4) PCR of the mCherry tag from plasmid mCherry- PQE60NA was done (appx. Fig 10.1C) using primers Mch2b-BamHI-F and mch2-notI-R. Used Pfu Turbo enzyme with annealing temperature 77°C. Desired amplicon size is 736bp. The PCR reaction cycle is same as mentioned in Step 1, except annealing T_m= 77°C and extension done for 30sec initially and was extended 20 sec/cycle later. The amplicon of the mCherry tag was digested with BamHI and NotI and subcloned at N-termini of Ras2 in the clone Ras2-YCplac33. The plasmid obtained is 33-Mch2- Ras2. YIplac204-T_C was digested with SmaI while fragment mCherry-Ras2 from clone 33-Mch2- Ras2 was digested with BamHI and HindIII and treated with lg klenow to blunt the overhangs. Subcloned the fragment mCherry- Ras2 in plasmid YIplac204-T_C. It was diagnosed by using restriction enzyme BamHI and NcoI (appx. Fig 10.1D) that gave two bands of size 4.1kb and 1.9kb.

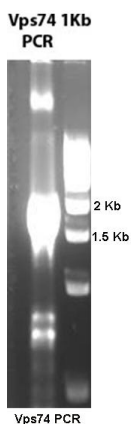
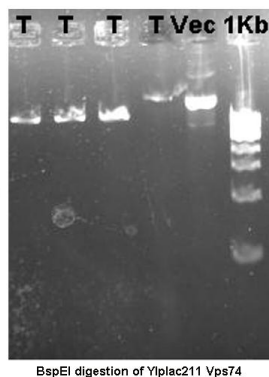
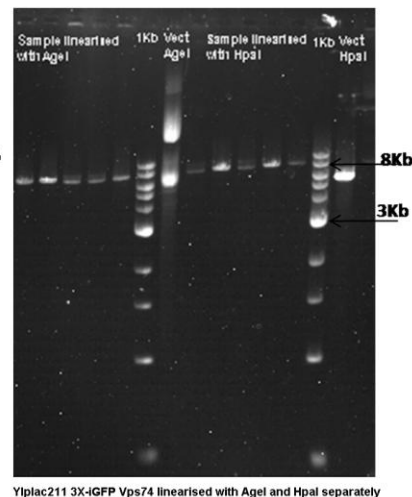


Appendix 10.2: The cloning strategy for 3X-iGFP Vps74



- 1) Endogenous Vps74 gene was amplified (appx. Fig 10.2A) using JK9 genomic DNA as a template. Primers used were: vps74-5UTR-SalI-F and vps74-SacI-R. Amplicon size - 1792bp. Annealing temperature- $T_m = 49^\circ\text{C}$ and extension time 1 min at 72°C . PCR cycle used is the standard one mentioned in Materials and method section. The resulting positive clone 211-5UTR- vps74-3UTR-PCR plasmid was digested with SalI and SacI and subcloned in the yeast vector YIplac211 (an integrative vector with Ura3 selection). The positive clone was confirmed by digesting the plasmid with BspEI resulting in a linearized band (appx. Fig 10.2B). The parent vector does not have restriction site BspEI.

- 2) Further at the N-termini of Vps74 BamHI- NheI cassette was introduced by site-directed mutagenesis. Primers used were Vps74 N term- NheI BamHI- U and Vps74 N term- NheI BamHI-B. The standard PCR protocol was followed for site-directed mutagenesis as mentioned in Materials and method section. The clone obtained was YIplac211 Vps74 N term NheI-BamHI. The positive clone was diagnosed by separately digesting with enzyme BamHI and NheI (Appx. Fig 10.2C).

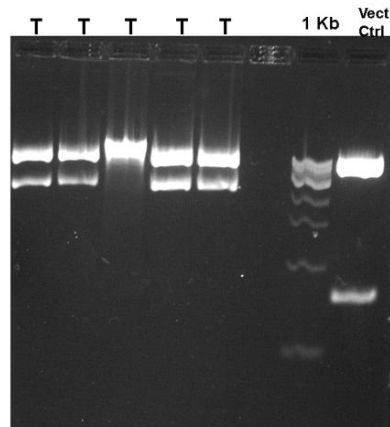
Appx. Fig 10.2A**Appx. Fig 10.2B****Appx. Fig 10.2C****Appx. Fig 10.2D**

- 3) The tag 3X-iGFP from plasmid piGFPx3- (+ C-linker) was removed by restriction digestion with BamHI and NheI and subcloned at N-termini of Vps74 in plasmid Yiplac211 Vps74 N term NheI-BamHI. The resulting final clone Yiplac211- 3X-iGFP Vps74 was diagnosed by linearising with restriction enzyme AgeI and HpaI (Fig 10.2D). We passed the positive plasmid through Dcm-Dam- strain to change the methylation status of BCI enzyme.

Appendix 10.3: The cloning strategy for 3X-iGFP RerI

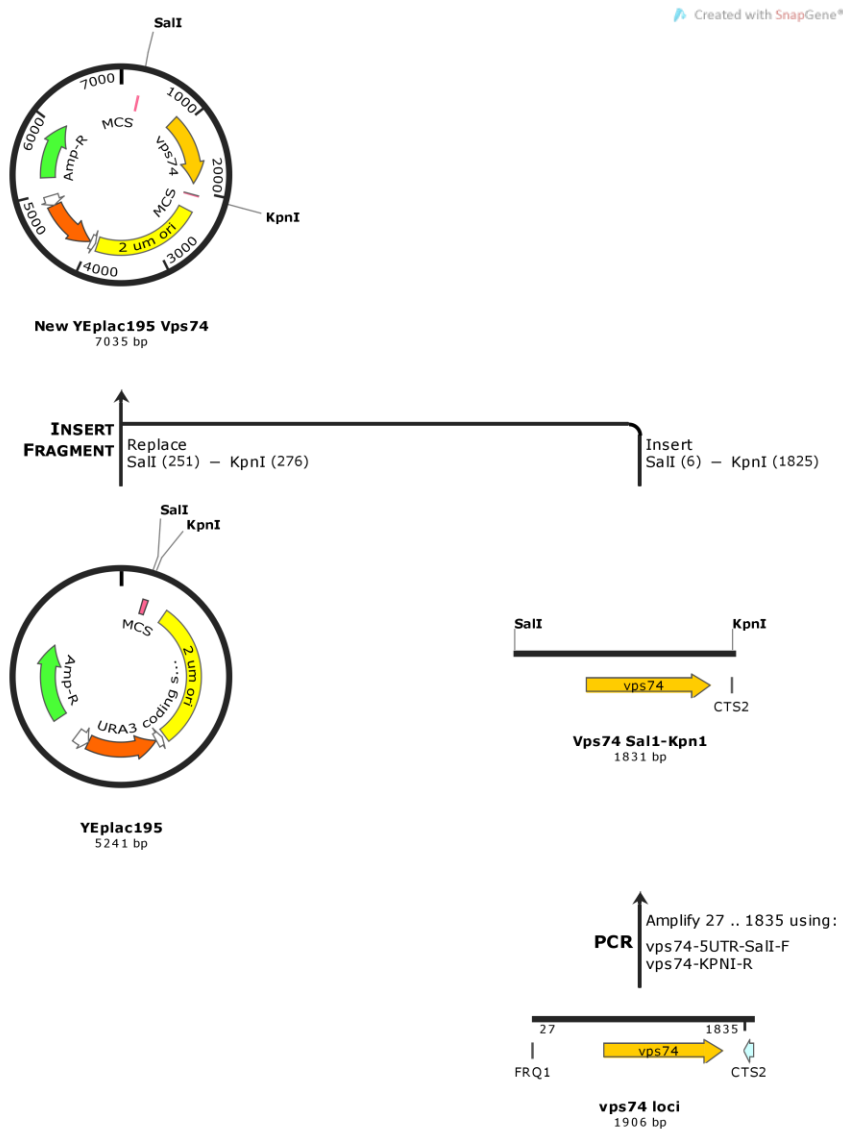


- 1) The earlier clone made in the lab for tagging RerI was not giving the appropriate signal. So the cloning strategy was modified to clone three tandem repeat of GFP at N-termini of RerI gene.
- 2) The starting clone for this strategy used was Rer1 Nterm lms GFP. msGFP was tagged at N-termini of Rer1 protein. It was digested with BamHI and NheI to swap msGFP epitope with 3X-iGFP epitope. The resulting fragment that lacked msGFP was cut from the gel and purified.
- 3) The tag 3X-iGFP from plasmid piGFPx3- (+ C-linker) was removed by restriction digestion with BamHI and NheI and dropped at the same site for the fragment lacking msGFP obtained in step 2.

Appx. Fig 10.3**BamHI and NheI digestion of Ylplac211- 3X-iGFP Rer1**

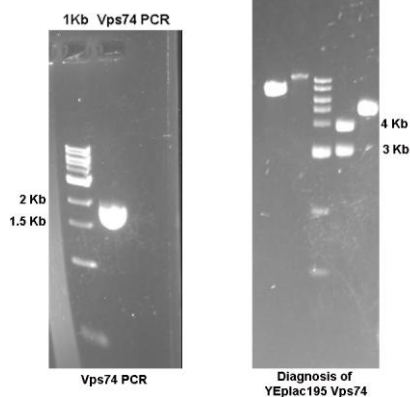
- 4) The final clone obtained 3X-iGFP- RerI was diagnosed by restriction digestion with the same enzyme used for cloning BamHI and NheI (appx. Fig 10.3). The positive clone gave band release of 5.1kb and 2.2kb.

Appendix 10.4: The cloning strategy for YEplac195 Vps74:



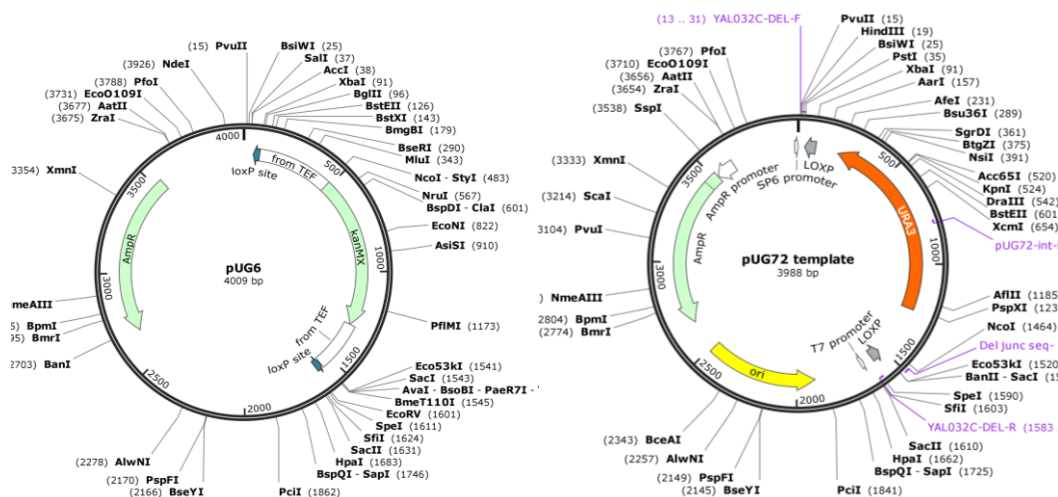
- 1) Endogenous *VPS74* gene was amplified (appx. Fig 10.4A) using JK9 genomic DNA as a template. Primers used were: vps74-5UTR-SalI-F and vps74-KPNI-R. Amplicon size - 1831bp. Annealing temperature- $T_m = 51^\circ\text{C}$ and extension time 1 min at 72°C . PCR cycle used is the standard one mentioned in Materials and method section.

- 2) The desired PCR product of *VPS74* gene was digested with SalI and KpnI and subcloned at the same site in the yeast vector YEplac195 (an episomal vector with Ura3 selection). The positive clone was diagnosed using restriction enzyme BspEI and EcoRV (appx. Fig 10.4B) that gave band release of approximate 3kb and 4kb.

Appx.Fig 10.4B**Appx. Fig10.4A**

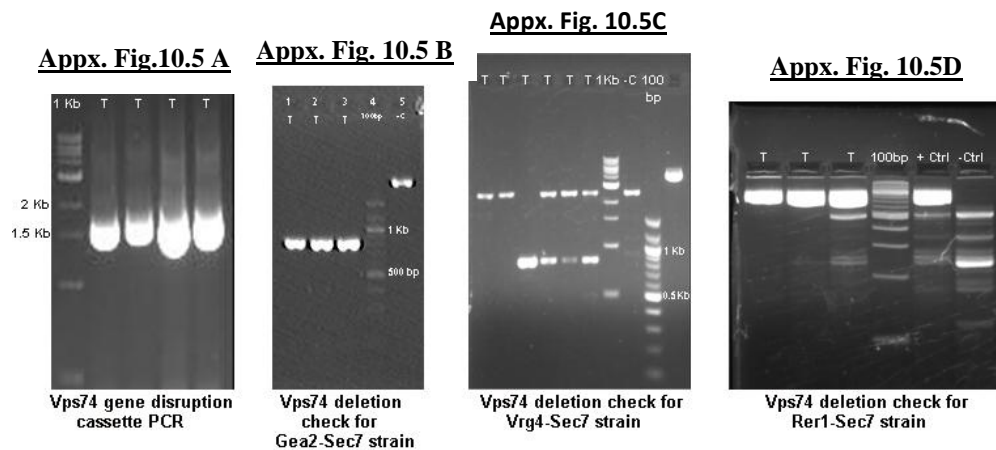
- 3) Note: for introducing alanine residue at position 6-8 and replace the amino acid arginine present in WT *VPS74* gene, site-directed mutagenesis was done using primers -Vps74 6-AAA-8 up and Vps74 6-AAA-8 bottom

Appendix 10.5: Making gene disruption cassette for deleting *VPS74* gene:



- 1) Used the plasmid pUG6 containing Kanamycin cassette or pUG72 containing Uracil as the template. Primers used Vps74 Kan Fw, and Vps74 Kan Rv had flanking homologous region to Vps74 with few bp homologous to the template. Set annealing temperature $T_m = 61^\circ\text{C}$ and extension time 1min. The gene disruption cassette produced was approximately 1600bp (appx. Fig 10.5A). The PCR product obtained was purified using nucleotide removal kit (Qiagen) and transformed in the wild-type *S.cerevisiae* strain JK9 with early and late Golgi marked (two color strain).
- 2) We used three different two-color strain namely JK9 GFP **Vrg4-Sec7** 6X DsRed, JK9 **Gea2** 3XGFP- **Sec7** 6X DsRed and JK9 3X iGFP **RerI**- **Sec7** 6X DsRed.
- 3) Confirmatory PCR was done to determine the swapping of the endogenous gene with the Kanamycin or Uracil cassette thereby resulting in *VPS74* gene deletion. Primers used for checking was vps74-5UTR-SalI-F and Kan RV (for Kanamycin cassette) or pUG72-int-R

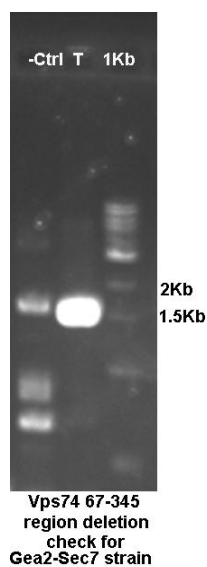
(for Uracil cassette). Used annealing temperature $T_m = 51^\circ\text{C}$ with extension time 1 min for detecting clone with Kanamycin cassette while extension time 2 min was used for detecting clone with Uracil cassette. The positive clone with Kanamycin cassette gave amplicon at nearly 800bp (appx. Fig 10.5 B, C, and D) while the one with Uracil cassette gave 1300bp band size.



Appendix 10.6: Making gene disruption cassette for deleting the 67-345 region of *VPS74* gene:

- 1) The plasmid pUG72 containing Uracil was used as the template. Primers Vps74 -67 LEU DEL F and Vps74 Kan Rv with annealing temperature $T_m = 61^\circ\text{C}$ and extension time 1min.
- 2) Confirmed PCR for determining swap of endogenous *VPS74* with Uracil cassette with primers vps74-5UTR-SalI-F and pUG72-int-R. The desired band obtained was 1600bp (appx. Fig 10.6).

Appx. Fig.10.6



Appendix 10.7: Annealing of complementary oligonucleotide guide sequence:

1) The following components enlisted in the table were mixed:

Table 10.2: Annealing protocol for guide sequence

sgRNA top guide sequence (100 μ M)	1 μ l
sgRNA bottom guide sequence (100 μ M)	1 μ l
T4 DNA ligase buffer 10X	1 μ l
T4 PNK enzyme	1 μ l
MiliQ	6 μ l –Volume make up to 10 μ l

2) Kept the annealing mix at 22°C for 3-4hrs.

3) Dilluted the resultant mix to 1: 200 and 2 μ l of the dilution was used as the insert to clone at BbsI site generated in CRISPR vector BFP- mut PX458 and PX459 (puromycin selection).

Appendix 10.9: PCR for checking integration of guide sequence in CRISPR vector:

- 1) Primers used were the reverse oligo used for guide sequence annealing and U6-promoter primer as a forward primer with annealing temperature $T_m = 61^\circ\text{C}$ and extension time of 30sec. Followed standard PCR protocol. Band size of 273bp confirms the clone to be positive.
- 2) Following (Appx. Fig 10.9 A, B, C & D) is the representation of a positive clone for guide sequence cloned in CRISPR vector Px458 BFP mut and Px459 (puromycin)

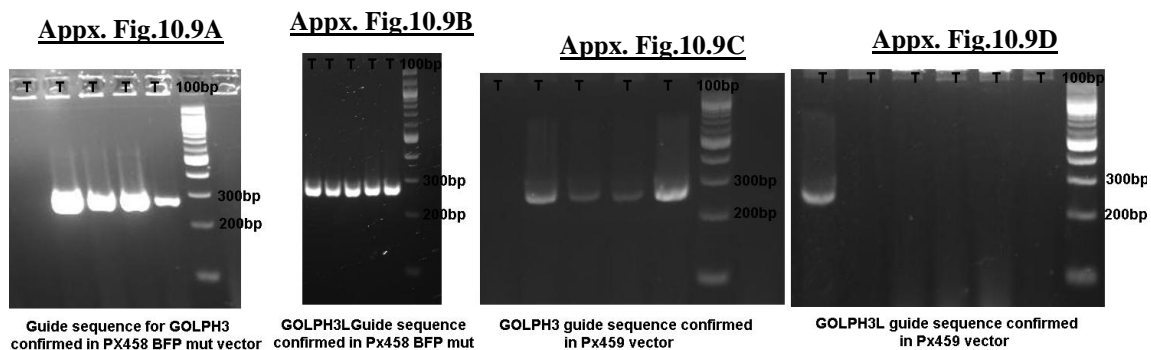


Table 10.4: List of primers

Sr. no	Name of primer	Sequence 5'-3'
1	Ras2-EcoRI-F	TCGATGAATTCTAGCTCTCGGGCGAATATC
2	Ras2-R	TCTAAGGGGAAAGAGAAGCTTG
3	Mch2b-BamHI-F	TGGTAGGATCCATGGTGAGCAAGGGCGAGGA
4	mch2-notI-R	TGTTTCGCGGCCCGCACTTGTACAGCTCGTCCATGC
5	Ras2-BN-B	TTATGTTTCGACTTGTTCAAAGGCATgCGGCCGCTAGGG ATCCCCTTTTTTTTCTGTATATCTCCTTTCA
6	Ras2-BN-T	TGAAAGGAGATATACAGAAAAAAAAGGGGATCCCTA GCGGCCGcATGCCTTTGAACAAGTCGAACATAA
7	vps74-5UTR-SalI-F	GCTAAGTCGACAATCAAAAACAGTTTTCAAG
8	vps74-SacI-R	GCTTGGAGCTCGTTTGGTCTATTTATTATCC
9	Vps74 N term- NheI BamHI- U	AAACAAAACTATCTAAAAAAATACGCTAGCcatGGAT CCAAAGCAAAAATCATGTCTACTTTAC
10	Vps74 N term- NheI BamHI- B	GTAAAGTAGACATGATTTTTGCTTTGGATCCATGGCTA GCGTATTTTTTAGATAGTTTTTGTTT
11	vps74-KPNI-R	ACGAAGGTACCAAGCAATGAATACGAATGTGG
12	Vps74 6-AAA-8 up	AGCAAAAATCATGTCTACTTTACAAGCTGCTGCTGTCA ATAGGGCGGATTCTGGAGATA
13	Vps74 6-AAA-8 botom	TATCTCCAGAATCCGCCCTATTGACAGCAGCAGCTTGT AAAGTAGACATGATTTTTGCT
14	Kan RV	GGATGTATGGGCTAAATG
15	pUG72-int-R	AGGGTACTGTCGTTCCAT
16	Vps74 -67 LEU DEL F	GACCCAGAAGAATCGAAATTGAGAGACAACATCAATA TCCCTACGCAGCTGAAGCTTCGTACGC
17	Vps74 Kan Rv	AAAGCTTGACTTTTCCTTATGTTTCAAAGAGAGGATTT TTGTTGTGCATAGGCCACTAGTGGATCTG
18	Vps74 Kan Fw	CGTAAAAGAATTCAAACAAAACTATCTAAAAAATA CAAAGCAACAGCTGAAGCTTCGTACGC
19	GOLPH3L-Exon1-gF	CACCAATGACCACTTTAACTCACC
20	GOLPH3L-Exon1-gR	AAACGGTGAGTTAAAGTGGTCATT
21	ARF1-Exon1g-F	CACCGATCCTCTACAAGCTTAAGC
22	ARF1-Exon1g-R	AAACGCTTAAGCTTGTAGAGGATC
23	u6-F	GAGGGCCTATTTCCCATG
24	GOLPH3L Ex1-Fw	GAGCAAGACTCCCTCTCAAGAAAAG
25	GOLPH3L Ex1- Rv	GGGCCCTTGTCTTACTTTAATAAA
26	Arf1 CrKO- Fw	GCAGCACAGAACCAGACATGGAGCA
27	Arf1 CrKO- Rv	GAACCCACACTGGCTCCTCACATTC
28	GOLPH3- EXON1g-F	CACCCCTCGCTGACCCAGCGCAGC
29	GOLPH3- EXON1g-R	AAACGCTGCGCTGGGTGAGCGAGG
30	GOLPH3-new-F	CTTGGAGCTCGGGGTGTTTCGGGGACTG
31	GOLPH3new-R	CAAGCCATCTCTACGGGGAGGATCCAGAAAG

Table 10.5: List of strains

Sr. no.	Strain name	Genotype
1	<i>JK9-3d</i>	<i>Mat a, leu 2-3, 112 ura -52 rme1 trp1 his4</i>
2	<i>JK9-GFP Vrg4-Sec7 6X Ds Red</i>	<i>Mat a, leu 2-3, 112 ura -52 rme1 his4 Sec7 6X Ds Red :: TRP GFP-Vrg4 pop out</i>
3	<i>JK9-Gea2-3XGFP-Sec7 6X Ds Red</i>	<i>Mat a, leu 2-3, 112 ura -52 rme1 his4 Sec7 6X Ds Red :: TRP Gea2-3XGFP pop out</i>
4	<i>JK9-Gea2-3XGFP-Sec7 6X Ds Red- vps74Δ</i>	<i>Mat a, leu 2-3, 112 rme1 his4 Sec7 6X Ds Red :: TRP Gea2-3XGFP pop out vps74Δ :: kanMX6</i>
5	<i>JK9-Gea2-3XGFP-Sec7 6X Ds Red- arf1Δ</i>	<i>Mat a, leu 2-3, 112 rme1 his4 Sec7 6X Ds Red :: TRP Gea2-3XGFP pop out arf1Δ :: kanMX6</i>
6	<i>JK9-Gea2-3XGFP-Sec7 6X Ds Red- arf1Δ- vps74Δ</i>	<i>Mat a, leu 2-3, 112 rme1 his4 Sec7 6X Ds Red :: TRP Gea2-3XGFP pop out arf1Δ :: kanMX6 vps74Δ:: URA3</i>
7	<i>JK9-Gea2-3XGFP-Sec7 6X Ds Red- vps74 67-345Δ</i>	<i>Mat a, leu 2-3, 112 rme1 his4 Sec7 6X Ds Red :: TRP Gea2-3XGFP pop out vps74 67-345Δ :: URA3</i>
8	<i>JK9-Gea2-3XGFP-Sec7 6X Ds Red- vps74Δ- YEplac195- Vps74</i>	<i>Mat a, leu 2-3, 112 rme1 his4 Sec7 6X Ds Red :: TRP Gea2-3XGFP pop out vps74Δ :: kanMX6 [YEplac195- Vps74]</i>
9	<i>JK9-Gea2-3XGFP-Sec7 6X Ds Red- vps74Δ- YEplac195- Vps74- 6AAA8</i>	<i>Mat a, leu 2-3, 112 rme1 his4 Sec7 6X Ds Red :: TRP Gea2-3XGFP pop out vps74Δ :: kanMX6 [YEplac195- Vps74- 6AAA8]</i>

10	<i>JK9-Gea2-3XGFP-Sec7 6X Ds Red- YEplac195 Vps74</i>	<i>Mat a, leu 2-3, 112 rme1 his4 Sec7 6X Ds Red :: TRP Gea2-3XGFP pop out [YEplac195 Vps74]</i>
11	<i>JK9-Gea2-3XGFP-Sec7 6X Ds Red- YEplac195 Arf1</i>	<i>Mat a, leu 2-3, 112 rme1 his4 Sec7 6X Ds Red :: TRP Gea2-3XGFP pop out [YEplac195 Arf1]</i>
12	<i>JK9-Gea2-3XGFP-Sec7 6X Ds Red- vps74Δ- YEplac195- Arf1</i>	<i>Mat a, leu 2-3, 112 rme1 his4 Sec7 6X Ds Red :: TRP Gea2-3XGFP pop out vps74Δ :: kanMX6 [YEplac195- Arf1]</i>
13	<i>JK9-Gea2-3XGFP-Sec7 6X Ds Red- arf1Δ- YEplac195- Vps74</i>	<i>Mat a, leu 2-3, 112 rme1 his4 Sec7 6X Ds Red :: TRP Gea2-3XGFP pop out arf1Δ :: kanMX6 [YEplac195- Vps74]</i>
14	<i>JK9-Rer1-3X-iGFP-Sec7 6X Ds Red</i>	<i>Mat a, leu 2-3, 112 ura -52 rme1 his4 Sec7 6X Ds Red :: TRP Rer1-3X-iGFP pop out</i>
15	<i>JK9-Rer1-3X-iGFP-Sec7 6X Ds Red vps74Δ</i>	<i>Mat a, leu 2-3, 112 ura -52 rme1 his4 Sec7 6X Ds Red :: TRP Rer1-3X-iGFP pop out vps74Δ :: URA3</i>
16	<i>JK9-Rer1-3X-iGFP-Sec7 6X Ds Red- YEplac195- Vps74</i>	<i>Mat a, leu 2-3, 112 rme1 his4 Sec7 6X Ds Red :: TRP Rer1-3X-iGFP pop out [YEplac195 Vps74]</i>
17	<i>JK9-Rer1-3X-iGFP-Sec7 6X Ds Red- YEplac195-Arf1</i>	<i>Mat a, leu 2-3, 112 rme1 his4 Sec7 6X Ds Red :: TRP Rer1-3X-iGFP pop out [YEplac195 Arf1]</i>
18	<i>Pik1-83^{ts}</i>	Source: Benjamin Glick (University of Chicago, IL)

Publication

Vps74p controls Golgi size in an Arf1-dependent manner

Prasanna Iyer^{1,2}, Madhura Bhawe^{1,2}, Bhawik Kumar Jain^{1,2}, Sudeshna RoyChowdhury^{1,2} and Dibyendu Bhattacharyya^{1,2} 

¹ Advanced Centre for Treatment Research & Education in Cancer (ACTREC), Tata Memorial Centre, Kharghar, Navi Mumbai, India

² Homi Bhabha National Institute, Training School Complex, Anushakti Nagar, Mumbai, India

Correspondence

D. Bhattacharyya, Advanced Centre for Treatment Research & Education in Cancer (ACTREC), Tata Memorial Centre, Kharghar, Navi Mumbai 410210 MH, India
Fax: +91 22 2740 5085
Tel: +91 22 2740 5025
E-mail: dbhattacharyya@actrec.gov.in

(Received 10 May 2018, revised 26 September 2018, accepted 1 October 2018)

doi:10.1002/1873-3468.13266

Edited by Felix Wieland

The oncogene GOLPH3 is implicated in Golgi size regulation, a function yet to be experimentally linked to its PI4P effector function or the Golgi cisternal maturation in general. Moreover, its yeast homolog, Vps74p is not yet implicated in Golgi size regulation. Our results indicate that *VPS74* deletion increases the late Golgi cisternal size and the cisternal maturation frequencies, and destabilizes the Golgi PI4P gradient in budding yeast. Overexpression of Arf1 can suppress this cisternal enlargement and increased maturation frequency phenotype of $\Delta vps74$. $\Delta arf1$ alters Vps74p and PI4P distribution along the Golgi stacks. We conclude that Vps74p, the downstream effector of Arf1, regulates Golgi size by altering its cisternal maturation frequency and by maintaining the PI4P distribution along the Golgi compartments.

Keywords: Golgi; organelle; size regulation; Vps74

The exact mechanisms that regulate size and shape of intracellular organelles are poorly understood. Few recent studies have tried to understand the underlying mechanisms involved in organelle size regulation [1–6]. Usually, an organelle can alter its size in either of the two ways. One, the organelle can adjust the amount of its internal content. For example, nuclear size can be influenced by alteration of nucleo-cytoplasmic transport [2]. Alternatively, the organelle can change its surface area by forming vesicles or tubules at the bordering membrane. Golgi being a dynamic organelle may fit into the latter category.

The Golgi apparatus is composed of several independent membrane-bound structures called cisternae that show evidence of lateral interconnections, fenestrations, and tubulation [7,8]. This complex architecture poses a challenge to find a simplistic hypothetical solution for its size regulation. At present, the well-accepted model for Golgi biogenesis supports the continuous formation of Golgi cisternae from endoplasmic reticulum (ER) exit sites by cisternal maturation [9,10].

Previously, we have shown that a Golgi-resident GTPase, Arf1 can regulate the Golgi maturation rate and thereby possibly control Golgi size [1]. However, the exact mechanism by which Arf1 controls cisternal maturation is still unknown. Arf1 is known to be a multifunctional protein and has many effector molecules [11]. So, it is possible that Arf1 can regulate Golgi size in multiple ways through different effectors. To explore this issue, we need to find first such additional factors that regulate the Golgi size and further investigate their relation to Arf1.

Arf1 can induce membrane curvature [12–14], a function may depend on the membrane limitation, that in turn might play a vital role in organelle size regulation. Limiting the phospholipid pool by decreasing PI4KII α expression shows expanded Golgi phenotype [15]. PI4K regulates budding of vesicles while PtdIns4P binding effector proteins mediate Golgi membrane dynamics [16]. Being a primary effector of PI4P [16,17], Vps74p restrict PI4P to trans Golgi network (TGN) and copackage it with early Golgi-resident

Abbreviations

ER, endoplasmic reticulum; TGN, trans Golgi network.

proteins into COPI-coated retrograde vesicles. Thus, Vps74p is known to be directly involved in sorting COPI cargos [18–20], while COPI function requires Arf1. Arf1 and COPI are also known to regulate cisternal maturation [1,21]. Based on this, one may conclude that Arf1 and Vps74 must ‘function in coordination’ to regulate cisternal maturation rate as well as the Golgi size. For verification of such a statement, we first experimentally need to show that Vps74 indeed regulates Golgi size.

Although the oncogene GOLPH3, the human homolog of *VPS74* [22,23] was implicated in Golgi size control [24], the attempt to associate Vps74p to the Golgi size regulation was unsuccessful [16]. Moreover, the proposed mechanism of GOLPH3 for regulation of Golgi size was not linked either to its PI4P effector function or the Golgi cisternal maturation. Instead, a complex mechanism was reported involving myosins and cytoskeleton structures [24,25].

Arf1 is requisite for recruitment of PI4 kinase to the Golgi membrane and also essential for the synthesis of PI4P [26]. The ultrastructure of Golgi morphology observed in the case of the *pik1^{ts}* mutant was similar to that of *arf1* mutant [27]. We can hypothesize that Arf1 may regulate the Golgi size through such PI4P effectors, like Vps74p which itself may control the machinery of vesicle budding at Golgi [16]. If this hypothesis is correct, then deletion of *VPS74* should also cause alteration of Golgi cisternal size in the same way as *ARF1* deletion [1,28]. We found that deletion of *VPS74* causes large cisterna phenotype in the two-color Golgi strain that harbors early and late cisterna marked with green and red fluorescent fusions.

We showed that deletion of *VPS74* increases late cisternal size, maturation frequencies, and homotypic fusion of late cisterna. Arf1 overexpression in the Δ *vps74* strain can suppress this phenotype, but it fails to affect the Golgi size in the wild-type strain. On the other hand, overexpression of Vps74p in the wild-type strain can reduce the Golgi cisternal size to some extent. *VPS74* deletion also destabilizes the PI4P gradient in Golgi. Since Vps74 is one of the PI4P effectors [16] and PI4P synthesis is Arf1 dependent [26], we hypothesize that Arf1 and Vps74p probably function in the same pathway to regulate the Golgi size, while Vps74p possibly functions downstream of Arf1.

Our results support the fact that multifunctional Arf1 can regulate Golgi size in many different ways through its different effectors. Vps74p being one of such effectors controls the Golgi size by namely two mechanisms: regulating cisternal maturation and maintaining the PI4P gradient in Golgi by restricting PI4P in TGN directly or indirectly.

Materials and methods

Yeast strains and plasmids

All the primers that were used are listed in Table 1. All the strains were derived or created from parent wild-type haploid *Saccharomyces cerevisiae* strain, JK9-3d and are listed in Table 2. GFP-tagged Vrg4 and 6XDsRed-tagged Sec7 were used for gene replacement to make JK9-GFP Vrg4-Sec7 6XDsRed, while Gea2-3XGFP and Sec7-6XDsRed were used to make JK9-Gea2-3XGFP-Sec7-6XDsRed. Endogenous Vps74 gene or region 67-345 of Vps74 was replaced with either KanMx6 or URA3 cassette. All wild-type and mutant yeast strains were maintained in YPD media at 30 °C/200 rpm in the baffled flask. Primer-Vps74-Kan-Fw and Vps74-Kan-Rv were used to generate Vps74 gene disruption cassette. For deleting a 67-345 region of Vps74, primer Vps74-67-Leu Del- F and Vps74-Kan-Rv were used. pUG6 (Kan⁺) or pUG72 (Ura⁺) was used as a template for PCR-based generation of the gene disruption cassette. This cassette was then transformed into appropriate strains, and subsequently, the transformants were screened by G418 (200 µg·mL⁻¹) or SD Ura⁻ selection.

Gea2 was tagged at its C terminus with 3XGFP. *RER1* was tagged at N terminus with 3XGFP. The endogenous *RER1* was replaced with 3XGFP-RER1 by homologous recombination, and the additional homologous fragment of *RER1* was then cured by plating on SD plate containing 5-Fluoroorotic acid. A strain containing 3XGFP Rer1 as the early marker was grown at 23 °C and this temperature was also maintained while acquiring images.

YIplac204-T/C-iGFP-PH (OSH1) plasmid and the *pik1-83^{ts}* strain was a kind gift from Benjamin Glick (University of Chicago, IL).

Episomal copy of wild-type *VPS74* and mutant Vps74-6AAA8 was prepared as follows: Endogenous *VPS74* gene was amplified using primer vps74-5UTR-SalI-F and vps74-KpnI-R. It was digested at flanking SalI and KpnI site and subcloned in the YEplac195 vector at the same site. Episomal copy of *VPS74* gene with mutation AAA at the 6–8th position was created in clone YEplac195 Vps74 by site-directed mutagenesis using primers Vps74 6-AAA-8 up and Vps74 6-AAA-8 bottom. When required, overexpressing plasmid was cured of the strain by plating on 5-Fluoroorotic acid. 3XGFP epitope was used to tag endogenous Vps74.

Imaging

3D imaging: Cells were mounted on glass coverslips treated with concanavalin-A (2 mg·mL⁻¹) using SD as a mounting medium. Imaging for Gea2-Sec7 dual color strain was done at 30 °C using Leica SP8 confocal microscope. Cells were imaged using 63X objective with a scan frame of 256 × 150, pinhole 1 A.U., and galvo scanner enabled in

Table 1. Primers used in the study.

Sr. no.	Primer name	Primer sequence 5'-3'
1	Vps74- Kan- Fw	CGTAAAAGAATTCAAACAAAACTATCTAAAAAATACAAAAGCAACAGCTGAAGCTTCGTACGC
2	Vps74- Kan -Rv	AAAGCTTGACTTTTCCTTATGTTTTCAAAGAGAGGATTTTTGTTGTGCATAGGCCACTAGTGGATCTG
3	Vps74-67-Leu Del- F	GACCCAGAAGAATCGAAATTGAGAGACAACATCAATATCCCTACGCAGCTGAAGCTTCGTACGC
4	Gea2- Pst1- Fw	ACACAGCTGCAGGACACACAATCTGTCTATG
5	Gea2- EcoRI- Rv	TTCGAAGAATTCAGCTTTTATGGACCCTGA
6	Gea2-BN-Fw	GAAGTTATCTGATGTAGAAAAGGATAGGGATCCCTAGCGGCCGCAGATGCTAAGAGATAGTGATGATAT
7	Gea2-BN-Rv	ATATCATCACTATCTCTTAGCATCTGCGGCCGCTAGGGATCCCTATCCTTTTCTACATCAGATAACTTC
8	Rer1 Fw- Hind3-new	CGCCTAAGCTTCAATATAATTGCTTCG
9	Rer1-SacI- Rv	TTGAAGAGCTCAAGTTGACGAATCAACGT
10	Rer1-Nterm BN-U	TAGAGTATCAAAAAAGGAAGCAAGGCTAGCCTAAAGGATCCATGGATTACGATAGCTCTGATACAA
11	Rer1-Nterm BN-B	TTGTATCAGAGCTATCGTAATCCATGGATCCTTTAGGCTAGCCTTGCTTCCTTTTTTTGATACTCTA
12	Vps74-5UTR- Sall- F	GCTAAGTCGACAATCAAAAACAGTTTTCAAG
13	Vps74-KPNI-R	ACGAAGGTACCAAGCAATGAATACGAATGTGG
14	Vps74 6-AAA-8 Up	AGCAAAAATCATGTCTACTTTTACAAGCTGCTGCTGTCAATAGGGCGGATTTCTGGAGATA
15	Vps74 6-AAA-8 bottom	TATCTCCAGAATCCGCCTATTGACAGCAGCAGCTTGTAAGTAGACATGATTTTTTGCT
16	Vps74 N term- Nhe 1 BamH1- U	AAACAAAACTATCTAAAAAATACGCTAGCCATGGATCCAAAGCAAAAATCATGTCTACTTTAC
17	Vps74 N term- Nhe1 BamH1- B	GTAAAGTAGACATGATTTTTGCTTTGGATCCATGGCTAGCGTATTTTTTTAGATAGTTTTTTGTTT
18	Kan-Rv	GGATGTATGGGCTAAATG
19	pUG72-int-R	AGGGTACTGTCGTTCAT

the bidirectional mode having the speed of 700 Hz. Line averaging 2, 10X zoom, and a 0.3 μm optical section was maintained. Imaging for RER1- Sec7 dual color strain was done at 23 $^{\circ}\text{C}$, with 100X Objective, 1.2 AU pinhole, Galvo scanner in bidirectional mode at 400 Hz, averaging 2 and zoom 6.5X. 15–20 optical sections were captured at 6–8 s. For *pik1-83^{ts}* imaging, a permissive temperature of 22 $^{\circ}\text{C}$ was maintained, while 37 $^{\circ}\text{C}$ for the nonpermissive condition.

4D imaging was done using a Leica SP8 with frame 512 \times 128, 63X objective, scan speed 1400 Hz, zoom 5, line averaging 2 and pixel size 70 nm. For all live cell movies, each Z stack was captured with time frame 4–5 s. For Jk9 Gea2 -6X DsRed GFP-Vrg4 strain (Fig. S1B), frame 512 \times 512 was used with zoom 4, line averaging 2, and pixel size 70 nm in LSM 710.

Image analysis

Images captured were opened in Imaris software, and the 3D surface was rendered for early and late cisterna by

surface fill tool with an average diameter of 0.5 μm . Smoothing was done using a filter of radius 0.07 μm and enabled 0.5 μm split for touching surfaces. This step enabled quantification of the volume of cisterna signal captured. Twenty cells were imaged and quantified in a triplicate set.

The major X-Y plane of each early and late cisterna were measured in surpass mode of Imaris for randomly 10 cells of all strains to measure the size of cisterna. 4D images were opened in Image J and passed through a plug-in 3D hybrid median filter to remove background noise and further bleach corrected.

Quantitative analysis of maturation parameters

All the quantification of maturation parameters was done using ten movies each of wild-type and Δvps74 with Gea2-3XGFP and Sec7-6XDsRed marker. Maturation parameters were quantified for mother cell. Cisterna number counted for 10 frames in a movie were averaged. Homotypic fusion frequency counted for 1–3 min (total 2 min) of the movie was converted to fusion event per minute. For persistence time

Table 2. Yeast strains used in the study.

Sr. no.	Strain name	Genotype
1	<i>JK9-3d</i>	<i>Mat a, leu 2-3, 112 ura -52 rme1 trp1 his4</i>
2	<i>JK9-GFP Vrg4-Sec7 6X DsRed</i>	<i>Mat a, leu 2-3, 112 ura -52 rme1 his4 Sec7 6X DsRed :: TRP GFP-Vrg4 pop out</i>
3	<i>JK9-Gea2-3XGFP-Sec7 6X DsRed</i>	<i>Mat a, leu 2-3, 112 ura -52 rme1 his4 Sec7 6X DsRed :: TRP Gea2-3XGFP pop out</i>
4	<i>JK9-Gea2-3XGFP-Sec7 6X DsRed-vps74Δ</i>	<i>Mat a, leu 2-3, 112 rme1 his4 Sec7 6X DsRed :: TRP Gea2-3XGFP pop out vps74Δ :: kanMX6</i>
5	<i>JK9-Gea2-3XGFP-Sec7 6X DsRed-arf1Δ</i>	<i>Mat a, leu 2-3, 112 rme1 his4 Sec7 6X DsRed :: TRP Gea2-3XGFP pop out arf1Δ :: kanMX6</i>
6	<i>JK9-Gea2-3XGFP-Sec7 6X DsRed-arf1Δ-vps74Δ</i>	<i>Mat a, leu 2-3, 112 rme1 his4 Sec7 6X DsRed :: TRP Gea2-3XGFP pop out arf1Δ :: kanMX6 vps74Δ:: URA3</i>
7	<i>JK9-Gea2-3XGFP-Sec7 6X DsRed-vps74 67-345Δ</i>	<i>Mat a, leu 2-3, 112 rme1 his4 Sec7 6X DsRed :: TRP Gea2-3XGFP pop out vps74 67-345Δ :: URA3</i>
8	<i>JK9-Gea2-3XGFP-Sec7 6X DsRed-vps74Δ- YEplac195- Vps74</i>	<i>Mat a, leu 2-3, 112 rme1 his4 Sec7 6X DsRed :: TRP Gea2-3XGFP pop out vps74Δ :: kanMX6 [YEplac195- Vps74]</i>
9	<i>JK9-Gea2-3XGFP-Sec7 6X DsRed-vps74Δ- YEplac195- Vps74- 6AAA8</i>	<i>Mat a, leu 2-3, 112 rme1 his4 Sec7 6X DsRed :: TRP Gea2-3XGFP pop out vps74Δ :: kanMX6 [YEplac195- Vps74-6AAA8]</i>
10	<i>JK9-Gea2-3XGFP-Sec7 6X DsRed- YEplac195 Vps74</i>	<i>Mat a, leu 2-3, 112 rme1 his4 Sec7 6X DsRed :: TRP Gea2-3XGFP pop out [YEplac195 Vps74]</i>
11	<i>JK9-Gea2-3XGFP-Sec7 6X DsRed- YEplac195 Arf1</i>	<i>Mat a, leu 2-3, 112 rme1 his4 Sec7 6X DsRed :: TRP Gea2-3XGFP pop out [YEplac195 Arf1]</i>
12	<i>JK9-Gea2-3XGFP-Sec7 6X DsRed-vps74Δ- YEplac195- Arf1</i>	<i>Mat a, leu 2-3, 112 rme1 his4 Sec7 6X DsRed :: TRP Gea2-3XGFP pop out vps74Δ :: kanMX6 [YEplac195- Arf1]</i>
13	<i>JK9-Gea2-3XGFP-Sec7 6X DsRed-arf1Δ- YEplac195- Vps74</i>	<i>Mat a, leu 2-3, 112 rme1 his4 Sec7 6X DsRed :: TRP Gea2-3XGFP pop out arf1Δ :: kanMX6 [YEplac195- Vps74]</i>
14	<i>JK9-Rer1-3X-iGFP-Sec7 6X DsRed</i>	<i>Mat a, leu 2-3, 112 ura -52 rme1 his4 Sec7 6X DsRed :: TRP Rer1-3X-iGFP pop out</i>
15	<i>JK9-Rer1-3X-iGFP-Sec7 6X DsRed vps74Δ</i>	<i>Mat a, leu 2-3, 112 ura -52 rme1 his4 Sec7 6X DsRed :: TRP Rer1-3X-iGFP pop out vps74Δ :: URA3</i>
16	<i>JK9-Rer1-3X-iGFP-Sec7 6X DsRed- YEplac195-Vps74</i>	<i>Mat a, leu 2-3, 112 rme1 his4 Sec7 6X DsRed :: TRP Rer1-3X-iGFP pop out [YEplac195 Vps74]</i>
17	<i>JK9-Rer1-3X-iGFP-Sec7 6X DsRed- YEplac195-Arf1</i>	<i>Mat a, leu 2-3, 112 rme1 his4 Sec7 6X DsRed :: TRP Rer1-3X-iGFP pop out [YEplac195 Arf1]</i>
18	<i>pik1-83^{ts}</i>	Benjamin Glick (University of Chicago, IL)

calculations, the time point from which green signal appears (that marks the birth of a new early cisterna) was chased until it partially converts to a red signal (which is the formation of new late cisterna) and disappears. Cisterna undergoing fusion was excluded while calculating persistence time. Further, the late cisterna was chased until it disappears from the cell. The number of maturation events for 1–4 min (total 3 min) was viewed and converted to the number of events occurring per minute.

Colocalization measurement

‘Coloc’ tool in Imaris was used to determine the Pearson’s coefficient. It was calculated using the threshold method for $N = 30$ cells.

Statistical measurement

Statistical analysis was done using the unpaired Student t -test. All graphs are plotted using GRAPHPAD PRISM.

Results

Golgi cisterna size increases in the *vps74* deletion mutant

GOLPH3, a potential oncogene has been associated with abnormal Golgi morphology [24]. *VPS74* is the yeast homolog of GOLPH3. Although *VPS74* share sequence homology with its mammalian counterpart, its functional homology concerning Golgi size regulation has not been reported yet.

In our previous study [1], we have described several maturation parameters of Golgi that are affected when Golgi size is altered. Maturation frequency (number of early cisternae get converted to late cisternae per minute), persistence time (lifetime of early or late cisterna), and homotypic fusion frequencies (fusion events per minute for early or late cisterna) are such parameters. Together with Golgi cisternal volume and cisterna numbers, these

parameters represent the status of Golgi size regulation.

To validate whether Vps74p can regulate the Golgi size, we used a knockout method [29,30] to study the effect of *VPS74* deletion on Golgi. In our previous work, we have used Vrg4 as an early Golgi marker that did show homotypic fusion both in wild-type as well as in the $\Delta arf1$ background [1]. When we deleted *VPS74* in a two-color Golgi strain labeled with GFP-Vrg4 and Sec7-6XDsRed, we observed that Vrg4 localization is dramatically altered (Fig. S1A). It is possible that *VPS74* deletion is affecting normal localization of Vrg4. So, for Vps74p studies, we concluded that we need to use different markers suitable to label earlier Golgi compartments; we selected Gea2 and Rer1 to do so.

Rer1 is well established as an early marker [31]. When we deleted Vps74 in this dual color strain expressing 3XGFP-Rer1 and Sec7-6XDsRed, we see Sec7-labeled compartments become much larger as evidenced by both average cisternal volumes and average cisternal diameter measurements (Fig. 1A,B). We got similar results with Gea2-3XGFP and Sec7-6XDsRed

strain (Fig. 2). The result shows that *VPS74* deletion causes an increase in late cisternal size (Fig. 2A–C), but a decrease in the number of late cisternae (Fig. 2D).

We noted that Gea2-labeled domain matures into Vrg4 domain in a Gea2 Vrg4 double-labeled strain (S1B) which suggests that Gea2 is an earlier marker than Vrg4 regarding temporal maturation scale. However, some groups suggested that Gea2 labels the medial compartments. We have also observed that the Gea2-labeled domain mature into Sec7 domains in a Gea2 Sec7 double-labeled strain (Fig. 2H). Taken all these into account, we realized that Gea2 at least can be safely used to mark earlier Golgi compartments that mature into Sec7-labeled compartments. It is to be noted that though, the use of any compartment marker which is not an integral membrane protein is associated with one risk: acquisition or loss of these markers might not reflect a complete maturation process. However, it is of general concern for all such markers so far used for cisternal maturation studies [9,10]. Gea2 signal was much brighter and long-lived than Rer1, a criterion crucial for

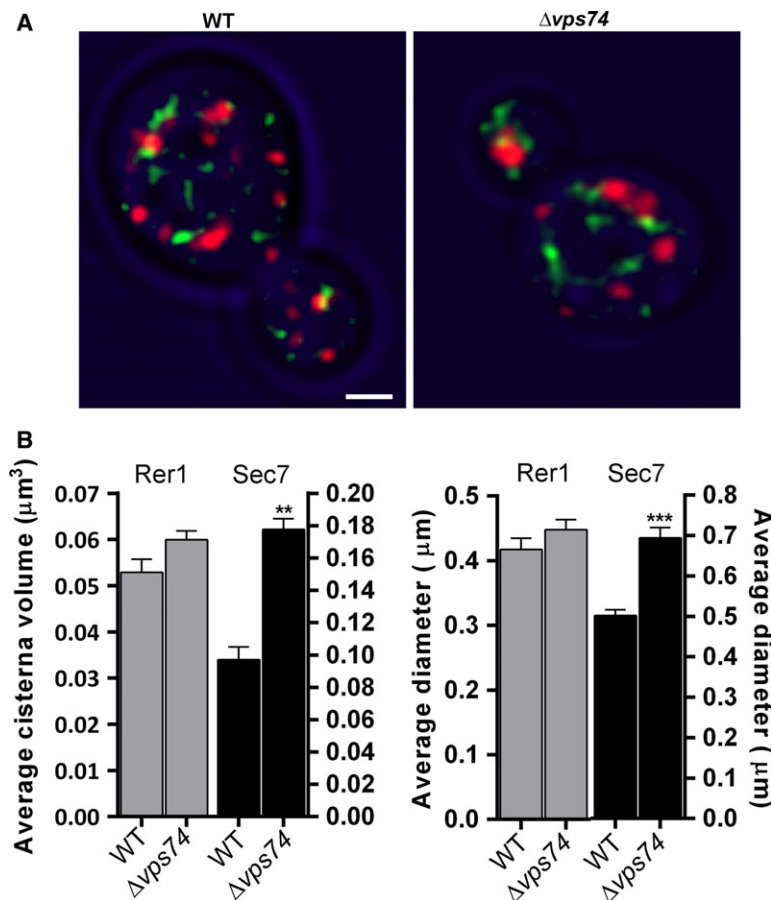


Fig. 1. Deletion of oncogene homolog *VPS74* causes an increase in cisterna size.

(A) Cells expressing 3XGFP-Rer1 and Sec7-6XDsRed in wild-type and $\Delta vps74$ strains were grown at 23 °C until log phase. Confocal images were captured using a Leica SP8 microscope under 100X objective with zoom factor 6.5 and single optical Z spacing of 0.3 μm . Images were deconvoluted by Huygens pro, projected by IMAGEJ (U. S. National Institutes of Health, Bethesda, MD, USA). Representative image of the strains is shown. Scale bar is 1 μm . (B) Imaris Bitplane software was used to render the 3D surface to quantify cisterna volume ($N = 60$), and the diameter was measured using a line tool in slice mode ($N = 10$). The graphs represent the average cisternal volume and diameter of 3XGFP-Rer1 and Sec7-6XDsRed. Values represent mean \pm SEM. Student *t*-test was performed ****P*-value < 0.05.

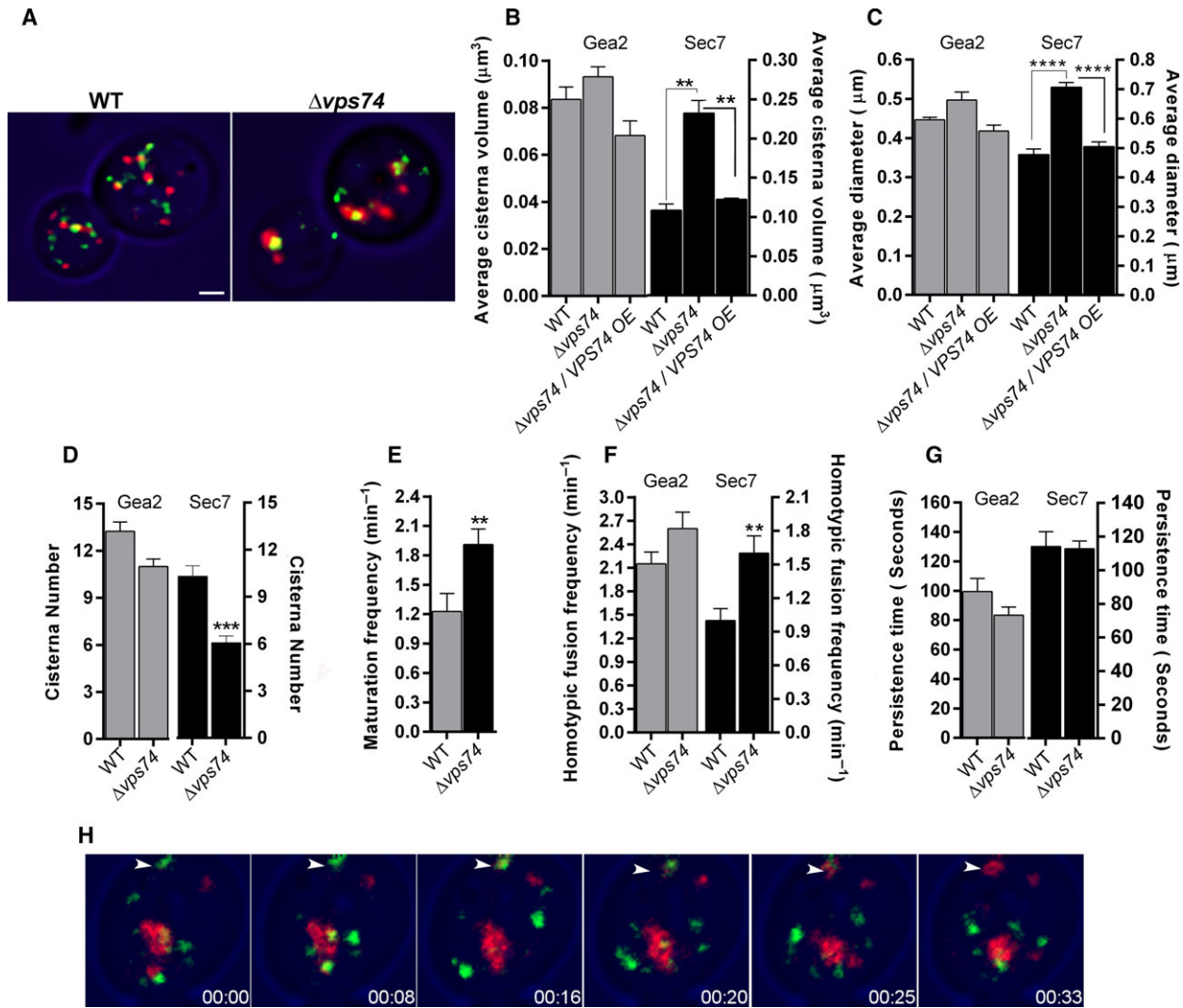


Fig. 2. Effect of *VPS74* deletion on *Gea2* and *Sec7* cisterna size and maturation parameters. (A) Wild-type and $\Delta vps74$ strains expressing *Gea2*-3X GFP and *Sec7*-6XDsRed were grown at 30 °C until log phase. Confocal images were captured using a Leica SP8 microscope under 63X objective with zoom factor 10 and single optical Z spacing of 0.3 μm. Images were deconvoluted by Huygens pro, projected by IMAGEJ. Representative images are shown. Scale bar is 1 μm. (B) The 3D surface was rendered using Imaris tool to quantitate volume. Average volume ($N = 60$) and average X-Y diameter (C) were plotted ($N = 10$). There is a significant increase in *Sec7* volume ($P = 0.0024$) and diameter ($P < 0.0001$), which was restored to wild-type by expression of the YEp Δ 195 *Vps74* plasmid in the *vps74* null mutant. Error bar indicates SEM (standard error mean). (D) Wild-type and $\Delta vps74$ strains were grown at 30 °C till log phase and 4D movies were taken using Leica SP8 under 63X objective with scan frame 512 × 128 and zoom factor 5. The early cisterna and late cisterna number were counted in wild-type and $\Delta vps74$ cells for ten frames and averaged. Values represent mean \pm SEM ($N = 10$ movies), Student *t*-test was performed *** P -value < 0.0001. (E) 4D movies were analyzed for a time frame of 1–4 min. The number of maturation events were observed and rounded off to events occurring per min for 10 movies. The maturation frequency of $\Delta vps74$ strain was increased ($P = 0.0086$) compared to wild-type. (F) The fusion events for time frame 1–3 min were converted to the number of events per minute. Thus, the average homotypic fusion frequency event for *Gea2* and *Sec7* cisterna in wild-type and $\Delta vps74$ cells were calculated. $N = 10$ movies. There was a significant increase in late cisterna fusion frequency ($P = 0.0090$) in $\Delta vps74$ compared to wild-type. (G) The persistence time of *Sec7* and *Gea2* cisterna for WT and $\Delta vps74$ was calculated using 4D movies, which was found to be unchanged for $\Delta vps74$ and wild-type. (H) Cisternal maturation event marked by *Gea2*-3XGFP converting into *Sec7*-6X DsRed is denoted in the movie panel. The arrowhead indicates *Gea2* cisterna (green) getting converted to *Sec7* (red). The time stamp is in min: s.

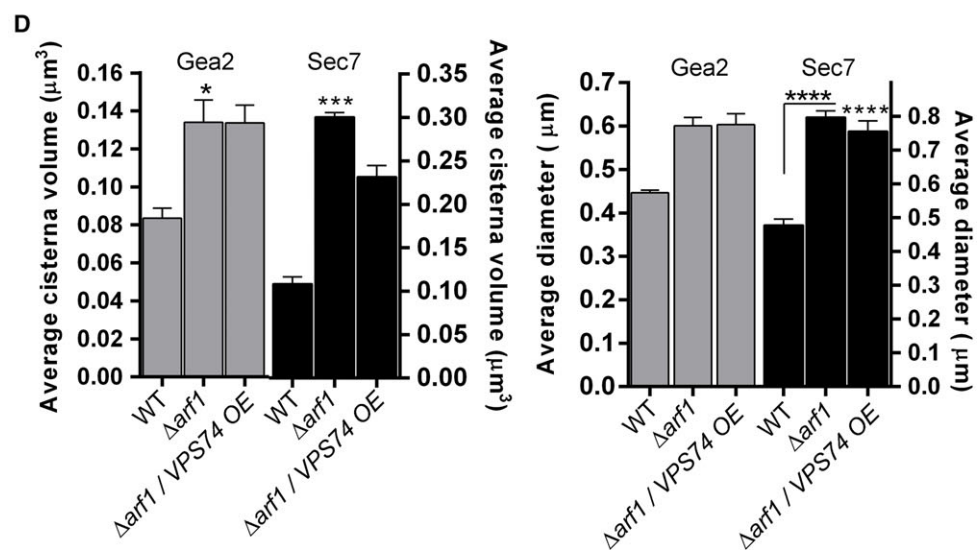
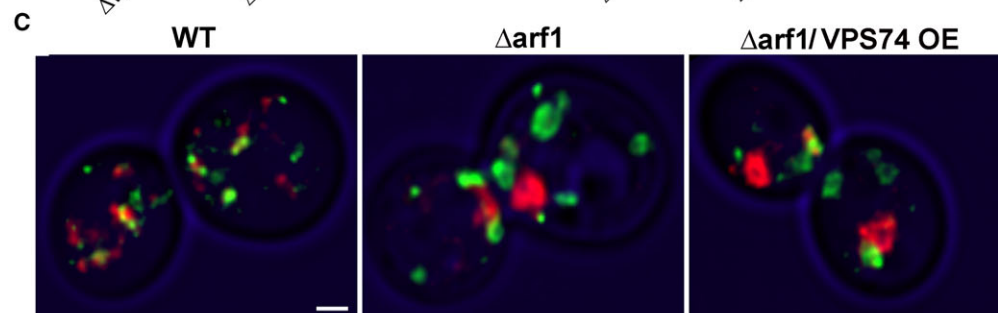
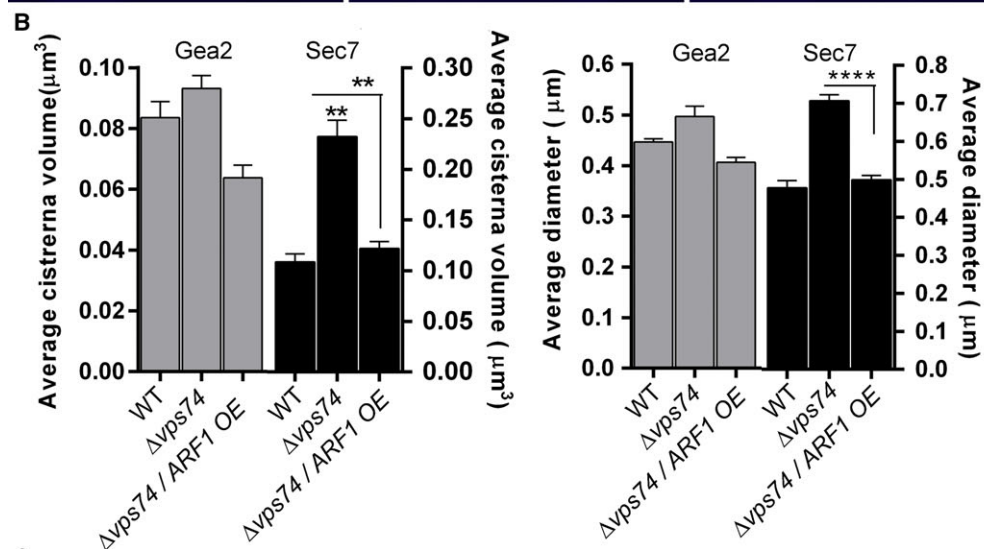
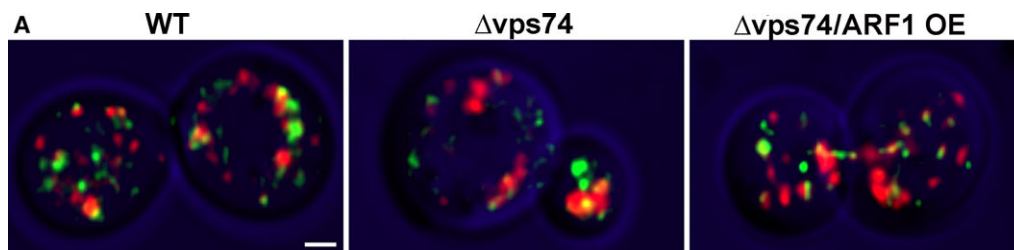


Fig. 3. Arf1 can suppress *vps74* null phenotype, but Vps74 cannot suppress *arf1* null phenotype. (A) Wild-type, $\Delta vps74$, and $\Delta vps74/ARF1$ overexpression strains expressing Gea2-3XGFP and Sec7-6XDsRed were grown at 30 °C until log phase. Confocal images were captured using a Leica SP8 microscope under 63X objective with zoom factor 10 and single optical Z spacing of 0.3 μm . Images were deconvoluted by Huygens pro, projected by IMAGEJ. Representative image of the strains is shown. Scale bar is 1 μm . (B) The average volume ($N = 60$) and diameter ($N = 10$) of early cisterna Gea2-3XGFP and Sec7-6XDsRed in wild-type, $\Delta vps74$, and $\Delta vps74/ARF1$ overexpression were compared quantitatively. Error bar indicates SEM (standard error mean). The Sec7 cisterna volume and diameter in $\Delta vps74/ARF1$ overexpression was reduced prominently ($P = 0.0033$ for volume and $P < 0.0001$ for diameter) to wild-type. (C) Wild-type, $\Delta arf1$, and $\Delta arf1/VPS74$ overexpression strains expressing Gea2-3XGFP and Sec7-6XDsRed were grown at 30 °C until log phase. Confocal images were captured using a Leica SP8 microscope under 63X objective with zoom factor 10 and single optical Z spacing of 0.3 μm . Images were deconvoluted by Huygens pro, projected by IMAGEJ. Representative images of the strains are shown. Scale bar is 1 μm . (D) The graph is plotted for average volume ($N = 60$) and diameter ($N = 10$) of Gea2 and Sec7 cisterna in wild-type, $\Delta arf1$, and $\Delta arf1/VPS74$ overexpression. Error bar indicates SEM.

live imaging to determine maturation parameters. For this reason, we decided to proceed further with Gea2 as a marker to label compartments earlier than that are marked by Sec7.

Maturation frequency and homotypic fusion rate increased in the *vps74* deletion mutant

The larger cisterna phenotype caused by $\Delta vps74$ can be rescued by overexpression of Vps74p (Fig. 2B,C) suggesting the expression of Vps74p can functionally complement the deletion phenotype. When we measured the maturation parameters, we observed an increase of maturation frequencies (Fig. 2E). Although we see a significant increase in late cisternal homotypic fusion (Fig. 2F), change in persistence time was not observed (Fig. 2G). Changes in early cisterna parameters were nonsignificant.

Deletion of the Arf1-binding site of Vps74 increases the Golgi size

We analyzed the importance of Arf1 or COPI to Vps74p by creating the deletion of these specific domains of Vps74p that bind Arf1 or COPI. Vps74p exhibit COPI-interacting arginine residues at position 6–8 and an Arf1-interacting region at 67–345 positions [32](Fig. S1C). To understand the role of COPI-interacting domain of Vps74p in Golgi size regulation, we created a strain which was overexpressing *VPS74*, harboring a mutation in the putative COPI-interacting domain (with alanine residues at 6–8 positions instead of arginine) in $\Delta vps74$ strain (Fig. S2B). The cisterna size is increased as compared to wild-type, suggesting the importance of the COPI interaction (Fig. S2C). To understand the role of Arf1-interacting domain of Vps74p in Golgi size regulation, we deleted Arf1-interacting region from endogenous *VPS74*, and created $\Delta(67-345)vps74$ strain in Gea2-3XGFP and Sec7-

6XDsRed background (Fig. S2A) and measured the cisterna size (Fig. S2C). The result indicates a double fold increase in late cisterna size suggesting the importance of Vps74 and Arf1 interaction.

ARF1 deletion alters Vps74 distribution along Golgi stacks

However, since the Arf1-binding domain encompasses almost the entire protein, one may argue such an experimental result is not conclusive. To validate whether Arf1 is required to localize Vps74p to the Golgi membrane, we demonstrated that in the absence of Arf1, 3XGFP-Vps74p localizes entirely to the Golgi membrane tagged with Sec7-6XDsRed (Fig. S3B). While in the presence of Arf1, clear nonoverlap of Vps74 and Sec7 signals were visible (Fig. S3A). Pearson's coefficient for colocalization of Vps74 with Sec7 cisterna compartment in $\Delta arf1$ is more as compared to the wild-type (Fig. S3C). In addition to Sec7-labeled late cisternal spots coalescing into fewer and larger spots in $\Delta arf1$, we observed an increase in localization of Vps74 in these Sec7 cisternae as compared to the wild-type. These results suggest that *ARF1* deletion destroys the Vps74p distribution pattern throughout the Golgi. Alternatively, in other words, Arf1 possibly is responsible for Vps74p gradient along the Golgi, suggesting that size regulation by Vps74p is Arf1-dependent.

Arf1 can suppress cisternal enlargement phenotype of $\Delta vps74$, but Vps74p cannot suppress the cisternal enlargement phenotype of $\Delta arf1$

To see whether Arf1 and Vps74p function in coordination to regulate the Golgi size, we created a double knockout for Arf1 and Vps74p. Representative images

of wild-type, $\Delta vps74$, $\Delta arf1$, and double knockout mutant $\Delta arf1 \Delta vps74$ shows that late cisterna size was prominently bigger in the double mutant as compared to single knockout $\Delta vps74$ (Fig. S6). In the ($\Delta arf1 \Delta vps74$) double knockout strain, a twofold increase of late cisterna size was observed as compared to $\Delta vps74$ (Fig. S6B). However, there was no significant change in cisternae size and volume between $\Delta arf1 \Delta vps74$ and $\Delta arf1$.

We have previously shown that *ARF1* knockout alone also results in increased cisternal size [1]. Between *ARF1* and *VPS74*, when we deleted only one of them and overexpressed the other to check for any phenotypic suppression, we found quite opposing results. Overexpression of Arf1 protein in $\Delta vps74$ strain could rescue the enlarged Golgi phenotype to

wild-type (Fig. 3A,B). $\Delta arf1$ exhibit fewer and larger Golgi cisterna [1,28] and delayed clathrin adaptor formation [33]. The cisterna volume and size in $\Delta arf1$ is higher than $\Delta vps74$ (Fig. S4). The enlarged phenotype of Golgi cisterna is predominant and thereby Vps74p overexpression fails to restore the Golgi phenotype in $\Delta arf1$ strain (Fig. 3C,D). Overexpression of Arf1 also can suppress the increase in maturation frequency caused by $\Delta vps74$ (Fig. 5A). However, overexpression of Vps74p can suppress the decrease of maturation frequency observed in $\Delta arf1$ strain as well (Fig. 5B). These results suggest that Vps74p possibly function downstream to Arf1 in the pathway of Golgi cisternal size regulation and it possibly exerts such regulation through controlling the rate of cisternal maturation itself.

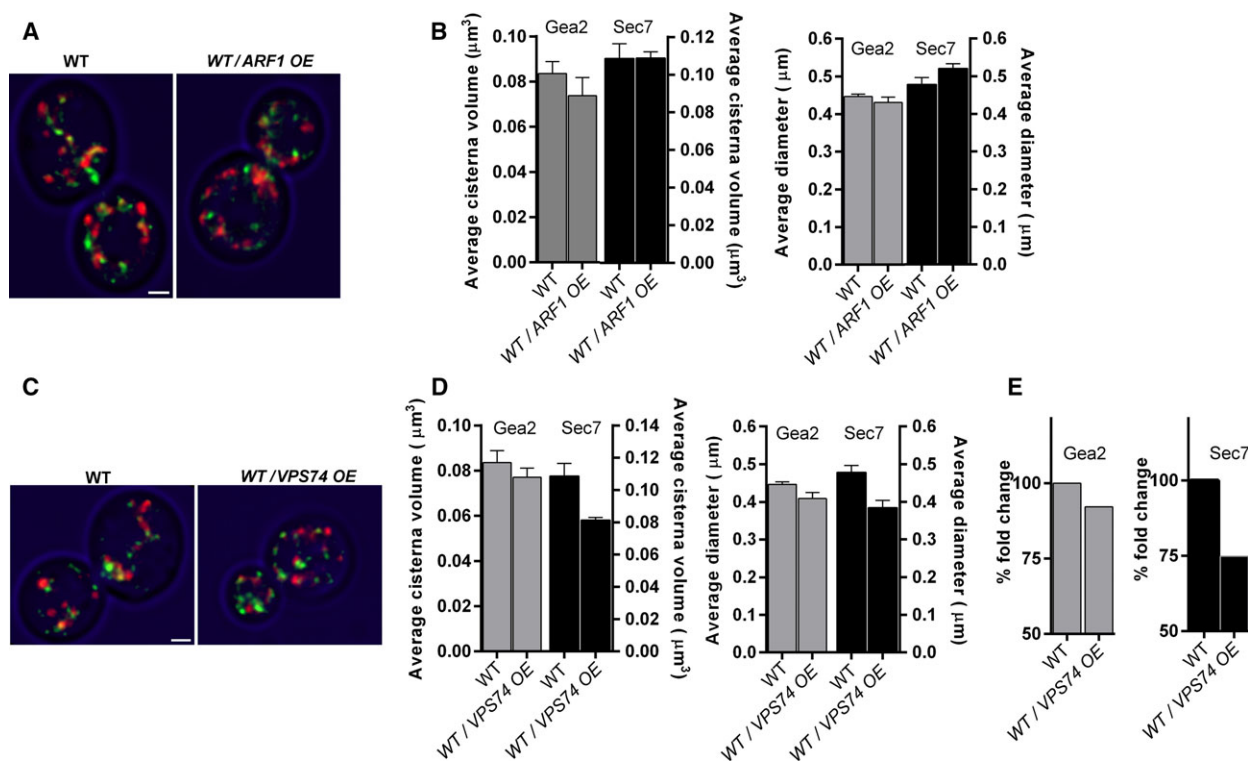


Fig. 4. Effect of overexpressing Arf1 and Vps74 in the wild-type strain. (A) Wild-type and WT/*ARF1* overexpression plasmid strain expressing Gea2-3XGFP and Sec7-6XDsRed were grown at 30 °C until log phase. Confocal images were captured using a Leica SP8 microscope under 63X objective with zoom factor 10 and single optical Z spacing of 0.3 μm . Representative images of the strains are shown. Scale bar is 1 μm . (B) The average volume ($N = 60$) and diameter ($N = 10$) of Gea2 and Sec7 cisterna for wild-type and WT/*ARF1* overexpression strains were quantified. Error bar is SEM (standard error mean). (C) Wild-type and WT/*VPS74* overexpression strain expressing Gea2-3XGFP and Sec7-6XDsRed were grown at 30 °C until log phase. Confocal images were captured using a Leica SP8 microscope under 63X objective with zoom factor 10 and single optical Z spacing of 0.3 μm . Images were deconvoluted by Huygens pro, projected by IMAGEJ. Representative images of the strains are shown. Scale bar is 1 μm . (D) The average volume ($N = 60$) and diameter ($N = 10$) of early and late Golgi marker for wild-type and WT/*VPS74* overexpression strains were quantified. Error bar is SEM (standard error mean). (E) The percentage fold graph for average cisterna volume of wild-type and WT/*VPS74* overexpression strains were calculated. It illustrates a 25% reduction of Sec7 cisterna volume in WT/*VPS74* overexpression. WT is considered 100%.

Overexpression of Vps74p in wild-type causes Golgi to shrink while overexpression of Arf1 does not affect wild-type Golgi size

Arf1 overexpression suppressed the large Golgi phenotype observed in $\Delta vps74$ strain (Fig. 3A,B). We found that Arf1 overexpression in wild-type strain did not alter the early or late Golgi cisterna size (Fig. 4A,B).

However, the overexpression of Vps74p in wild-type strain had shown a slight decrease in the late Golgi cisternal size as compared to wild-type (Fig. 4C–E). It shows congruency with observations in dual color strain labeled with Rer1 and Sec7 cisterna as well (Fig. S4 and S5).

Overexpression of Vps74 or Arf1 in wild-type did not significantly alter maturation frequency (Fig. 5A, B).

Deletion of ARF1 alter PI4P distribution along Golgi stacks

The ultrastructure of Golgi morphology obtained for $pik1^{ts}$ was reported to be similar to $\Delta arf1$ [27]. Recruitment of PtdIns 4-kinase to Golgi membrane is Arf1-dependent [26], while Vps74 is an effector of

PI4P. It is reported that lack of Arf1 results in slow accumulation of PI4P in the large coalesced Golgi elements [33].

All this information suggests that it is possible that lack of Arf1 affects the distribution of Golgi associated PI4P. To investigate whether $\Delta arf1$ indeed altered the PI4P distribution across the Golgi compartment, we performed colocalization studies of PI4P marker and Golgi marker. Colocalization of PI4P marker, GFP-PH^{OSH1} with Sec7-6XmCherry, and mCherry-PH^{OSH1} with Gea2-3XGFP was analyzed. The lack of Arf1 showed an increased accumulation of PI4P marker PH^{OSH1} with Sec7 cisterna as compared to wild-type (Fig. 6A). Average Pearson's coefficient for colocalization of PI4P and Sec7 in $\Delta arf1$ was observed to be higher than in wild-type (Fig. 6B). However, there was no such colocalization observed for PH^{OSH1} with Gea2 cisterna (Fig. 6C). It is also reported that most of the Sec7 and PI4P are located in compartments other than Gea2 [34]. PI4P is located in a different compartment other than Gea2 [34] which is also supported from our observation of reduced average Pearson's coefficient between PI4P and Gea2 than with Sec7 (Fig. 6B,D). The colocalization between PH^{OSH1} and Gea2 in $\Delta arf1$ was

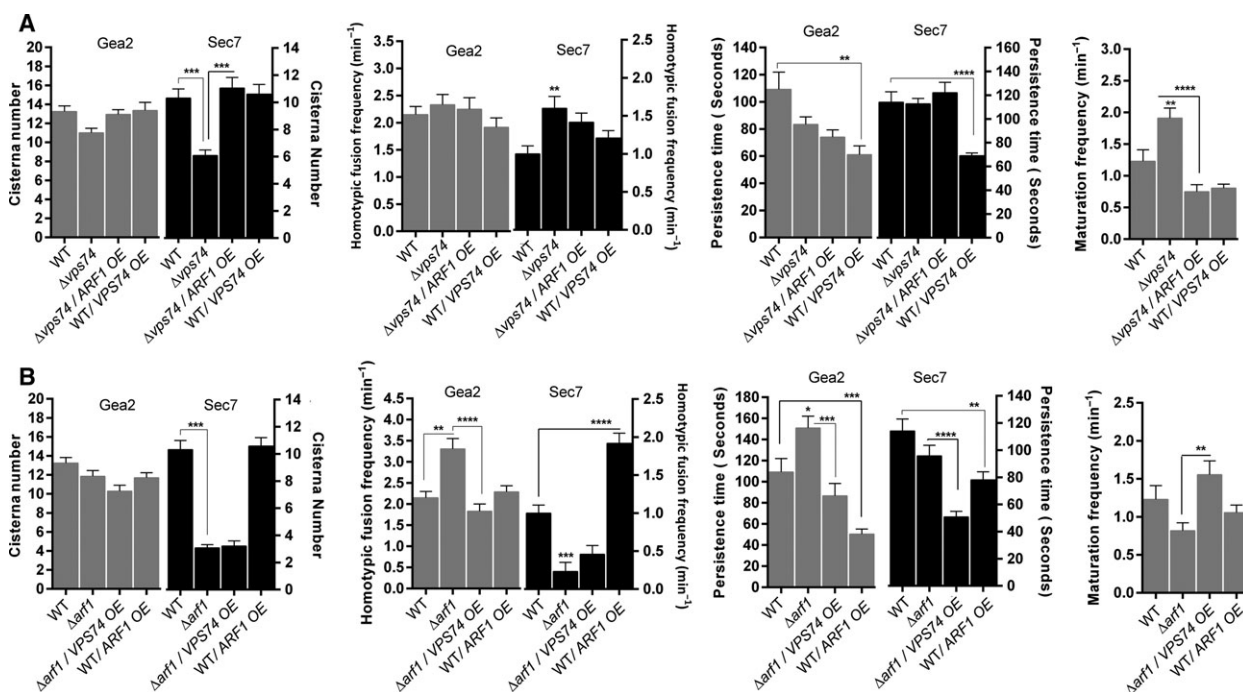


Fig. 5. Cisterna maturation parameters of mutants compared with wild-type. (A) The comparative plot for cisterna maturation parameters like cisterna number, homotypic fusion frequency, persistence time, and maturation frequency are represented for strains wild-type, $\Delta vps74$, $\Delta vps74/ARF1$ overexpression, WT/*VPS74* overexpression and in (B) for wild-type, $\Delta arf1$, $\Delta arf1/VPS74$ overexpression, WT/*ARF1* overexpression. Overexpression is denoted by OE. 4D movies were taken using Leica SP8 using 100X objective with scan frame 512×128 and zoom factor 5. $N = 10$ movies.

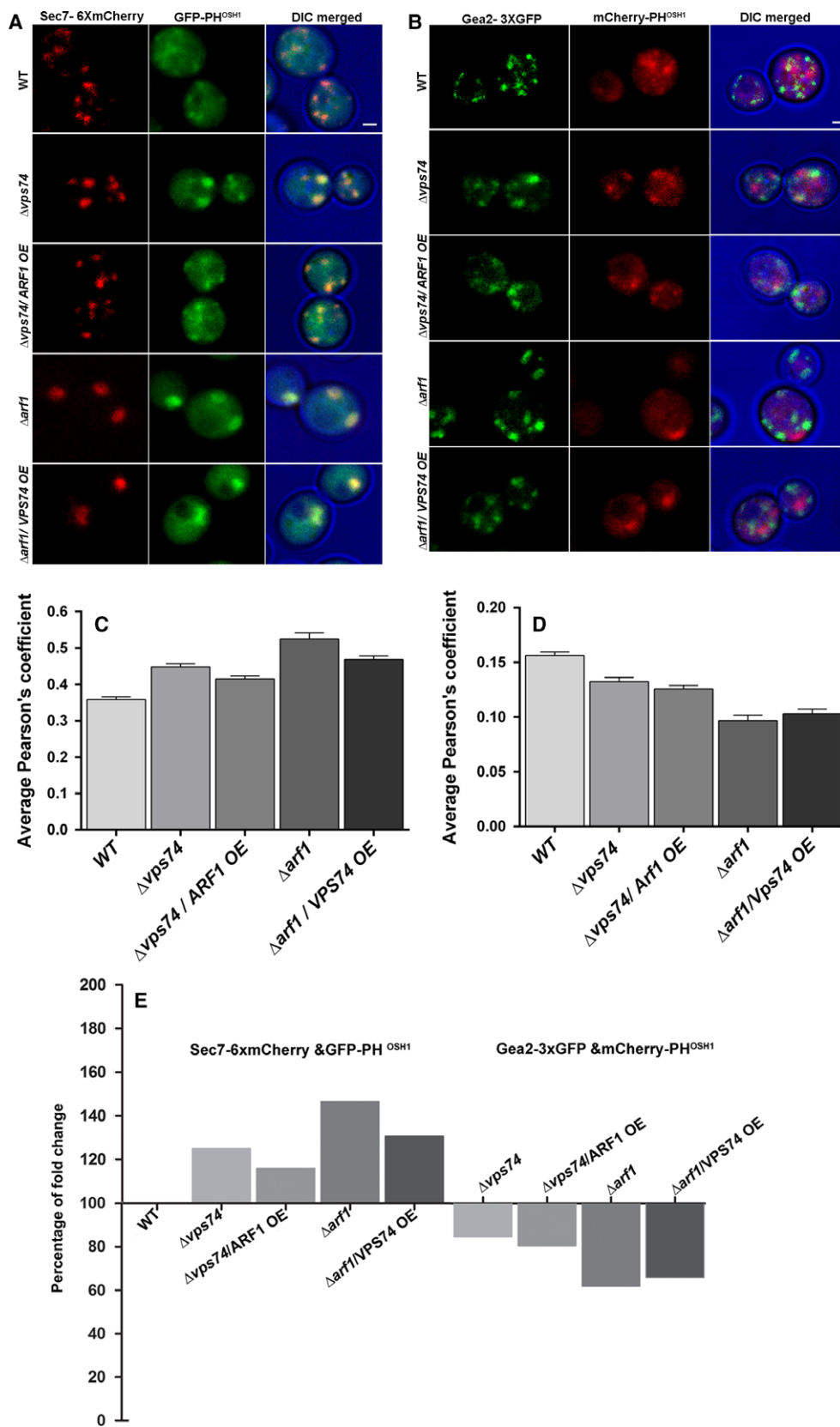


Fig. 6. Correlation of PI4P levels along Golgi cisterna compartments. (A) Wild-type, $\Delta vps74$, $\Delta vps74/ARF1$ OE, $\Delta arf1$, and $\Delta arf1/VPS74$ OE strains expressing PI4P marker GFP-PH^{OSH1} and Sec7-6XmCherry were grown at 30 °C until log phase. Confocal images were captured using a Leica SP8 microscope under 100X objective with zoom factor 6.5 and single optical Z spacing of 0.3 μ m. Scale bar is 1 μ m. Representative images of in wild-type, $\Delta vps74$, $\Delta vps74/ARF1$ OE, $\Delta arf1$, and $\Delta arf1/VPS74$ OE strains are shown. (B) Average Pearson's coefficient was quantified for PI4P marker GFP-PH^{OSH1} and Sec7-6XmCherry for $N = 30$ cells using the coloc tool of Imaris Bitplane software. (C) Wild-type, $\Delta vps74$, $\Delta vps74/ARF1$ OE, $\Delta arf1$, and $\Delta arf1/VPS74$ OE strains expressing PI4P marker mCherry-PH^{OSH1} and Gea2-3XGFP were grown at 30 °C until log phase. Confocal images was captured using Leica SP8 microscope under 100X objective with zoom factor 6.5 and single optical Z splicing of 0.3 μ m. Image panel represents PI4P marker mCherry-PH^{OSH1} and Gea2-3XGFP in wild-type, $\Delta vps74$, $\Delta vps74/ARF1$ OE, $\Delta arf1$, and $\Delta arf1/VPS74$ OE strains. Scale bar is 1 μ m. (D) Average Pearson's coefficient was quantified for PI4P marker mCherry-PH^{OSH1} and Gea2-3X GFP for $N = 30$ cells using the coloc tool of Imaris software. (E) The graph represents percent fold change for colocalization of PI4P marker PH^{OSH1} with Sec7 and Gea2 cisterna. WT is considered as 100%.

also reduced as compared to wild-type (Fig. 6D). Percent fold change (Fig. 6E) for average Pearson's coefficient also represents the increased localization of PI4P with late Golgi in the mutants. PtdIns 4-kinase recruitment to Golgi membrane is Arf1-dependent [26]. The Vps74p level has been reported to follow a gradient being highest in early Golgi and lowest in late Golgi [35]. In case of $\Delta arf1$, we observed increased colocalization of PI4P with late cisterna (Fig. 6A,B), and may be due to this disturbed PI4P gradient Vps74 colocalizes more with Sec7 cisterna in $\Delta arf1$ (Fig. S3) in order to maintain Golgi homeostasis. These results suggest Arf1 possibly is directly or indirectly responsible for maintaining such a distribution gradient of Vps74p in Golgi.

Deletion of VPS74 alter PI4P distribution along the Golgi stacks

PI4P colocalization with Sec7 had also increased in $\Delta vps74$ (Fig. 6A,B). Vps74 regulates PI4P-dependent retrograde transport of specific Golgi-resident enzymes [20]. The plausible reason for the increase in PI4P colocalization is probably due to the absence of functional Vps74 in case of $\Delta vps74$. The colocalization of PI4P with Gea2 in $\Delta vps74$ was lesser than with Sec7 (Fig. 6B,D). The colocalization of PI4P and Gea2 in $\Delta vps74$ is relatively lower as compared to wild-type (Fig. 6C,D). This result demonstrates that the PI4P distribution along the Golgi compartments changes in $\Delta vps74$ mutant as compared to the wild-type. A previous study [35] had reported no effect of *VPS74* depletion on PI4P in the Sec7-positive compartments. We believe the difference in methodology could be the primary reason for the difference in data for the PI4P level in the Sec7-positive compartment. However, the same study [35] did report an increase of PI4P level in medial Golgi compartments, and a slight decrease in the early compartment, an observation similar to our

results—alteration of PI4P distribution along the Golgi compartments.

Concerning PI4P levels, we observed that the levels of PI4P colocalization with Sec7 or Gea2 in $\Delta vps74/ARF1$ overexpression and $\Delta arf1/VPS74$ overexpression are almost similar to the mutants $\Delta vps74$ and $\Delta arf1$, respectively (Fig. 6).

Golgi PI4P pool in yeast is generated by a conserved type III β PI4-kinase, Pik1. It is required for secretion and Golgi integrity [27,36]. Earlier we demonstrated PI4P levels in $\Delta arf1$ and $\Delta vps74$. Conditional mutation of *PIK1* can disturb the phospholipid pool, PI4P [37] which is required for regulation of vesicle budding machinery and membrane dynamics at Golgi [16]. Thus, the effect of the *pik1-83^{ts}* mutation on Sec7 and Vrg4 cisterna was observed in permissive and nonpermissive conditions. We observed that *pik1-83^{ts}* mutants on subjection to nonpermissive condition altered Vrg4-labeled cisterna. (Fig. S7). However, prominent alteration on Sec7 cisterna was not observed in nonpermissive conditions (Fig. S7).

Discussion

In the present study, we for the first-time reporting that Vps74p regulates Golgi size by regulating Golgi cisternal maturation and homotypic fusions, maintaining PI4P distribution and effectively regulating retrograde fission efficiency. In our study, we have shown that *VPS74* deletion caused an increase in trans cisterna size, cisternal maturation frequencies, as well as late cisterna homotypic fusion frequencies. However, its function in regulating maturation frequencies seems redundant since its absence does not jeopardize the maturation process, and cells are also viable. Overexpression of Arf1 can suppress the increase in cisternal size and maturation frequency in $\Delta vps74$, but overexpression of Vps74p fails to suppress cisternal size enlargement of $\Delta arf1$. Overexpression of Vps74p

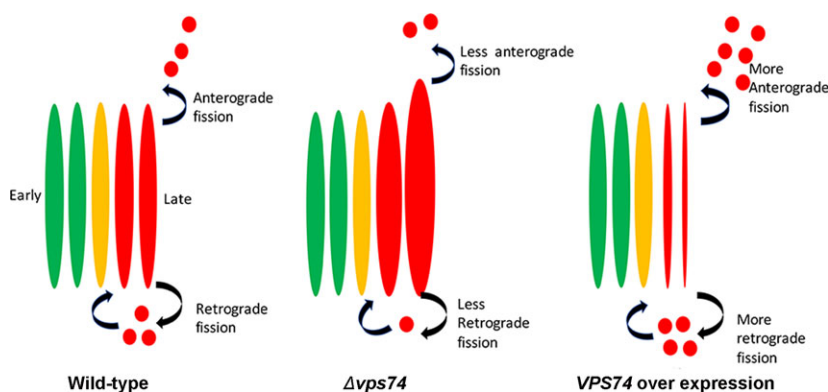


Fig. 7. A hypothetical model explaining the role of Vps74 in regulating Golgi Size. The early, medial, and late Golgi compartment is depicted by green, yellow, and red oval compartments. The lower curved black arrow represents Vps74-mediated retrograde transport, while upper curved black arrow shows the anterograde transport. In $\Delta vps74$, the amount of retrograde transport decreases, causing enlarged late cisterna. In the case of Vps74 overexpression in the wild-type strain, the enhanced fission events might cause a slight reduction in the late cisterna.

caused a slight reduction in the trans cisterna size in the wild-type strain.

Probably Arf1 overexpression in $\Delta vps74$ might have increased the process of clathrin-associated budding dynamics which in turn may rescue the large late cisterna size phenotype of $\Delta vps74$. Arf1 is required for clathrin coat assembly from the TGN [33,38–42]. Assembly of clathrin adaptors in $\Delta arf1$ was delayed [33]. Clathrin adaptor recruitment on TGN is Arf1- and PI4P-dependent process. However, fewer and larger Golgi cisternae observed in $\Delta arf1$ phenotype [1,28] is dominant and probably for that reason overexpression of Vps74p fails to rescue $\Delta arf1$ phenotype.

We found that $\Delta arf1$ deletion alters Vps74p distribution along Golgi stacks suggesting that Arf1 regulates Vps74 gradient along Golgi. Arf1 is required for recruitment of PtdIns4-kinase Pik1, and lack of Arf1 affects total cellular PI4P levels [26,27]. We also observed an increased localization of PI4P marker PH^{OSH1} with Sec7 cisterna in case of $\Delta arf1$. Probably this alteration of PI4P distribution in $\Delta arf1$ is a direct result or cause for alteration of Vps74p distribution along Golgi in $\Delta arf1$ cells. It is to be noted that both $\Delta arf1$ deletion and $\Delta vps74$ causes alteration of PI4P distribution along Golgi stacks. We found the localization of PI4P marker PH^{OSH1} had slightly increased with Sec7 cisterna in $\Delta vps74$. This result suggests both Arf1 and Vps74p regulate PI4P gradient although the former may function quite upstream than the latter in such regulatory pathway. Pik1 associates functionally for production of Golgi associated PI4P in yeast. The $pik1^{ts}$ mutation affects secretion and Golgi integrity [27,36]. We did observe enlargement of early cisterna for $pik1-83^{ts}$ at the nonpermissive condition.

It appears that multifunctional Arf1 can regulate Golgi size in multiple ways through its various effectors, Vps74p being one of them. Our result shows Arf1 maintains the gradient of Vps74p. It is already known that Arf1 recruits Pik1 [27] which along with Vps74p and Sac1 maintains the gradient of PI4P along the Golgi. Our result confirms that Vps74p maintains the gradient of PI4P along Golgi. Pik1 mutation alters the PI4P gradient and affects the Golgi morphology. All these observations suggest that Vps74p, being an Arf1 effector, functions downstream of Arf1 in the pathway of Golgi size regulation.

Vps74p regulates Golgi size by maintaining PI4P gradient and effectively promoting retrograde fission of PI4P vesicles from TGN. In normal condition, Vps74p and Sac1 distribution along Golgi stacks follow a gradient diminishing in the direction of maturation, i.e., higher at early cisterna and lowest at TGN. Pik1 forms a gradient against the direction of maturation, i.e., highest at TGN and lowest at early cisterna. These two opposing distribution gradients maintain phosphorylation and dephosphorylation level of PI4P. PI4P is found highest at TGN, and lowest in the opposing direction. Vps74p remains in complexed form with Sac1 mostly in the early cisterna and the uncomplexed form mostly at TGN. Vps74-Sac1 complex dephosphorylates the PI4P, and Pik1 phosphorylates PtdIns to create PI4P. Uncomplexed Vps74 can recruit these PI4Ps at TGN to budding vesicles in the retrograde direction, thereby promoting fission. A well-balanced ratio of amounts of complexed (with Sac1) and uncomplexed Vps74p, controls the dephosphorylation and phosphorylation balance of PI4P and thereby control PI4P level at TGN and retrograde fission efficiency.

In $\Delta vps74$ condition, dephosphorylation of PI4P by Vps74-SacI complex is expected to stop, recruitment of PI4P by uncomplexed Vps74p in budding vesicles are expected to stop, thereby retrograde fission is diminished. The PI4P gradient is collapsed, and TGN gets saturated with unused PI4P. The absence of Vps74p decreases the number of budding reactions so as the fission at TGN [16]. Due to lack of fission, we experimentally observe the enlarged TGN (Fig. 7). A question may arise why do we see an increase in maturation frequency in $\Delta vps74$. In addition to the previously published reports, our results suggest that Vps74p is a critical player in regulating the retrograde traffic. By controlling PI4P vesicles budding, it controls the retrograde traffic rate. The net effect of retrograde and anterograde traffic rate determines the maturation rate. Maturation frequencies reflect the combinatorial net effect of these two opposing trafficking rates. In the absence of Vps74p, retrograde traffic rate dramatically diminishes, while anterograde traffic rate remains unchanged, as evidenced by somewhat increased homotypic fusions. As a result, early compartments mature faster, hence the increase in the maturation frequencies. Our model suggests that Vps74p regulate cisternal maturation by maintaining the PI4P distribution and regulating retrograde fission efficiency.

Our model (Fig. 7) also suggests a stoichiometric amount of Vps74p in Golgi is vital for its size regulation and is inversely proportional to the cisternal size to some extent. The overexpression of Vps74p in wild-type increases the amount of uncomplexed Vps74p at TGN, causing the higher budding efficiency of PI4P vesicles at TGN. That results in the observed decrease in the size of Sec7 marked compartments (Fig. 7). This view is also supported by the observation that for the wild-type strain overexpressing Vps74p, persistence time of late cisterna is also reduced (Fig. 5A), suggesting a faster budding rate at TGN.

Overexpression of Arf1 in $\Delta vps74$ can rescue the size phenotype primarily recruiting a combination of other effectors, possibly as suggested before, by increasing the process of clathrin-associated budding dynamics or even partially restoring the PI4P gradient by other redundant effectors. However, it cannot restore the function of Vps74p completely to maintain the PI4P gradient, as Vps74p is one of the essential factors for maintaining the PI4P gradient. So, it cannot restore the gradient as like normal condition. However, it can restore the cisternal size through some other unknown effectors through their unknown mechanism. That is what we observed experimentally.

Taken all together into account, we can conclude these: Multifunctional Arf1 can regulate Golgi size in multiple ways through its many effectors. Vps74p, being one such effector, regulates the PI4P distribution along Golgi stacks. This function, in turn, regulates the retrograde traffic rate which in turn controls the maturation frequencies and the homotypic fusion. Through this cascade of chain events, Vps74p regulates the Golgi size, all along functioning downstream of Arf1.

Acknowledgements

This work was supported by DBT grant 102/IFD/SAN/2282/2012-2013 (to D.B), an ACTREC doctoral fellowship through HBNI (to P.I.). We thank Benjamin Glick for sharing the PI4P marker GFP-PH^{OSH1} plasmid construct and the *pik1-83^{ts}* strain used for our studies. We thank Bhattacharyya lab members for critically reviewing the manuscript.

Author contributions

PI carried out most of the experiments, helped to draft the manuscript. MB created original Gea2 strains and captured 4D movies showing Gea2 maturation to Vrg4. BJ cloned mCherry-PHOSH1 construct, helped in drafting the manuscript. SRC helped in the analysis of 4D movies. DB lead the entire project, conceived all experiments and wrote the manuscript.

References

- 1 Bhave M, Papanikou E, Iyer P, Pandya K, Jain BK, Ganguly A, Sharma C, Pawar K, Austin J 2nd, Day KJ *et al.* (2014) Golgi enlargement in Arf-depleted yeast cells is due to altered dynamics of cisternal maturation. *J Cell Sci* **127**, 250–257.
- 2 Ganguly A, Bhattacharjee C, Bhave M, Kailaje V, Jain BK, Sengupta I, Rangarajan A and Bhattacharyya D (2016) Perturbation of nucleo-cytoplasmic transport affects size of nucleus and nucleolus in human cells. *FEBS Lett* **590**, 631–643.
- 3 Goehring NW and Hyman AA (2012) Organelle growth control through limiting pools of cytoplasmic components. *Curr Biol* **22**, R330–R339.
- 4 Levy DL and Heald R (2012) Mechanisms of intracellular scaling. *Annu Rev Cell Dev Biol* **28**, 113–135.
- 5 Marshall W (2002) Size control in dynamic organelles. *Trends Cell Biol* **12**, 414–419.
- 6 Sengupta D and Linstedt AD (2011) Control of organelle size: the Golgi complex. *Annu Rev Cell Dev Biol* **27**, 57–77.

- 7 Ladinsky MS, Mastronarde DN, McIntosh JR, Howell KE and Staehelin LA (1999) Golgi structure in three dimensions: functional insights from the normal rat kidney cell. *J Cell Biol* **144**, 1135–1149.
- 8 Rambourg A and Clermont Y (1990) Three-dimensional electron microscopy: structure of the Golgi apparatus. *Eur J Cell Biol* **51**, 189–200.
- 9 Losev E, Reinke CA, Jellen J, Strongin DE, Bevis BJ and Glick BS (2006) Golgi maturation visualized in living yeast. *Nature* **441**, 1002–1006.
- 10 Matsuura-Tokita K, Takeuchi M, Ichihara A, Mikuriya K and Nakano A (2006) Live imaging of yeast Golgi cisternal maturation. *Nature* **441**, 1007–1010.
- 11 Beck R, Sun Z, Adolf F, Rutz C, Bassler J, Wild K, Sinning I, Hurt E, Brugger B, Bethune J *et al.* (2008) Membrane curvature induced by Arf1-GTP is essential for vesicle formation. *Proc Natl Acad Sci USA* **105**, 11731–11736.
- 12 Beck R, Adolf F, Weimer C, Bruegger B and Wieland FT (2009) ArfGAP1 activity and COPI vesicle biogenesis. *Traffic* **10**, 307–315.
- 13 Lee SY, Yang JS, Hong W, Premont RT and Hsu VW (2005) ARFGAP1 plays a central role in coupling COPI cargo sorting with vesicle formation. *J Cell Biol* **168**, 281–290.
- 14 Lundmark R, Doherty GJ, Vallis Y, Peter BJ and McMahon HT (2008) Arf family GTP loading is activated by, and generates, positive membrane curvature. *Biochem J* **414**, 189–194.
- 15 Wang YJ, Wang J, Sun HQ, Martinez M, Sun YX, Macia E, Kirchhausen T, Albanesi JP, Roth MG and Yin HL (2003) Phosphatidylinositol 4 phosphate regulates targeting of clathrin adaptor AP-1 complexes to the Golgi. *Cell* **114**, 299–310.
- 16 Graham TR and Burd CG (2011) Coordination of Golgi functions by phosphatidylinositol 4-kinases. *Trends Cell Biol* **21**, 113–121.
- 17 Wood CS, Schmitz KR, Bessman NJ, Setty TG, Ferguson KM and Burd CG (2009) PtdIns4P recognition by Vps74/GOLPH3 links PtdIns 4-kinase signaling to retrograde Golgi trafficking. *J Cell Biol* **187**, 967–975.
- 18 Eckert ES, Reckmann I, Hellwig A, Rohling S, El-Battery A, Wieland FT and Popoff V (2014) Golgi phosphoprotein 3 triggers signal-mediated incorporation of glycosyltransferases into coatomer-coated (COPI) vesicles. *J Biol Chem* **289**, 31319–31329.
- 19 Schmitz KR, Liu J, Li S, Setty TG, Wood CS, Burd CG and Ferguson KM (2008) Golgi localization of glycosyltransferases requires a Vps74p oligomer. *Dev Cell* **14**, 523–534.
- 20 Tu L, Tai WC, Chen L and Banfield DK (2008) Signal-mediated dynamic retention of glycosyltransferases in the Golgi. *Science* **321**, 404–407.
- 21 Papanikou E, Day KJ, Austin J and Glick BS (2015) COPI selectively drives maturation of the early Golgi. *Elife* **4**, pii: e13232.
- 22 Abraham RT (2009) GOLPH3 links the Golgi network to mTOR signaling and human cancer. *Pigment Cell Melanoma Res* **22**, 378–379.
- 23 Scott KL, Kabbarah O, Liang MC, Ivanova E, Anagnostou V, Wu J, Dhakal S, Wu M, Chen S, Feinberg T *et al.* (2009) GOLPH3 modulates mTOR signalling and rapamycin sensitivity in cancer. *Nature* **459**, 1085–1090.
- 24 Dippold HC, Ng MM, Farber-Katz SE, Lee SK, Kerr ML, Peterman MC, Sim R, Wiharto PA, Galbraith KA, Madhavarapu S *et al.* (2009) GOLPH3 bridges phosphatidylinositol-4-phosphate and actomyosin to stretch and shape the Golgi to promote budding. *Cell* **139**, 337–351.
- 25 Buschman MD and Field SJ (2018) MYO18A: An unusual myosin. *Adv Biol Regul* **67**, 84–92.
- 26 Godi A, Pertile P, Meyers R, Marra P, Di Tullio G, Iurisci C, Luini A, Corda D and De Matteis MA (1999) ARF mediates recruitment of PtdIns-4-OH kinase-beta and stimulates synthesis of PtdIns(4,5)P2 on the Golgi complex. *Nat Cell Biol* **1**, 280–287.
- 27 Audhya A, Foti M and Emr SD (2000) Distinct roles for the yeast phosphatidylinositol 4-kinases, Stt4p and Pik1p, in secretion, cell growth, and organelle membrane dynamics. *Mol Biol Cell* **11**, 2673–2689.
- 28 Gaynor EC, Chen CY, Emr SD and Graham TR (1998) ARF is required for maintenance of yeast Golgi and endosome structure and function. *Mol Biol Cell* **9**, 653–670.
- 29 Gueldener U, Heinisch J, Koehler GJ, Voss D and Hegemann JH (2002) A second set of loxP marker cassettes for Cre-mediated multiple gene knockouts in budding yeast. *Nucleic Acids Res* **30**, e23.
- 30 Gueldener U, Heck S, Fielder T, Beinbauer J and Hegemann JH (1996) A new efficient gene disruption cassette for repeated use in budding yeast. *Nucleic Acids Res* **24**, 2519–2524.
- 31 Sato K, Ueda T and Nakano A (1999) The Arabidopsis thaliana RER1 gene family: its potential role in the endoplasmic reticulum localization of membrane proteins. *Plant Mol Biol* **41**, 815–824.
- 32 Tu L, Chen L and Banfield DK (2012) A conserved N-terminal arginine-motif in GOLPH3-family proteins mediates binding to coatomer. *Traffic* **13**, 1496–1507.
- 33 Daboussi L, Costaguta G and Payne GS (2012) Phosphoinositide-mediated clathrin adaptor progression at the trans-Golgi network. *Nat Cell Biol* **14**, 239–248.
- 34 Gloor Y, Schone M, Habermann B, Ercan E, Beck M, Weselek G, Muller-Reichert T and Walch-Solimena C (2010) Interaction between Sec7p and Pik1p: the first clue for the regulation of a coincidence detection signal. *Eur J Cell Biol* **89**, 575–583.

- 35 Wood CS, Hung CS, Huoh YS, Mousley CJ, Stefan CJ, Bankaitis V, Ferguson KM and Burd CG (2012) Local control of phosphatidylinositol 4-phosphate signaling in the Golgi apparatus by Vps74 and Sac1 phosphoinositide phosphatase. *Mol Biol Cell* **23**, 2527–2536.
- 36 Walch-Solimena C and Novick P (1999) The yeast phosphatidylinositol-4-OH kinase pik1 regulates secretion at the Golgi. *Nat Cell Biol* **1**, 523–525.
- 37 Ghugtyal V, Garcia-Rodas R, Seminara A, Schaub S, Bassilana M and Arkowitz RA (2015) Phosphatidylinositol-4-phosphate-dependent membrane traffic is critical for fungal filamentous growth. *Proc Natl Acad Sci USA* **112**, 8644–8649.
- 38 Bonifacino JS (2004) The GGA proteins: adaptors on the move. *Nat Rev Mol Cell Biol* **5**, 23–32.
- 39 Carlton JG and Cullen PJ (2005) Coincidence detection in phosphoinositide signaling. *Trends Cell Biol* **15**, 540–547.
- 40 Demmel L, Gravert M, Ercan E, Habermann B, Muller-Reichert T, Kukhtina V, Haucke V, Baust T, Sohrmann M, Kalaidzidis Y *et al.* (2008) The clathrin adaptor Gga2p is a phosphatidylinositol 4-phosphate effector at the Golgi exit. *Mol Biol Cell* **19**, 1991–2002.
- 41 Traub LM (2005) Common principles in clathrin-mediated sorting at the Golgi and the plasma membrane. *Biochem Biophys Acta* **1744**, 415–437.
- 42 Wang J, Sun HQ, Macia E, Kirchhausen T, Watson H, Bonifacino JS and Yin HL (2007) PI4P promotes the

recruitment of the GGA adaptor proteins to the trans-Golgi network and regulates their recognition of the ubiquitin sorting signal. *Mol Biol Cell* **18**, 2646–2655.

Supporting information

Additional supporting information may be found online in the Supporting Information section at the end of the article.

Fig. S1. (A) Vrg4 localization is altered in *vps74* null mutant. (B) Gea2-labeled cisterna mature into Vrg4-labeled cisterna. (C) Model depicting the interaction of *VPS74* with Arf1 and COPI.

Fig. S2. Arf1-interacting domain of Vps74 is more important for Golgi size.

Fig. S3. Localization of Vps74.

Fig. S4. Overexpression of Vps74 in wild-type with Rer1-labeled cisterna.

Fig. S5. Effect of Arf1 on overexpression on Rer1-labeled cisterna.

Fig. S6. Effect of *arf1* and *vps74* double knockout on Golgi cisterna size.

Fig. S7. Effect of *pik1-83^{ts}* mutation on Golgi compartment Vrg4 and Sec7.